UNIVERSITY OF OULU

FACULTY OF TECHNOLOGY

GEOLOGICAL CHARACTERIZATION OF ANORTHOSITIC ROCKS IN THE OTANMÄKI INTRUSION, CENTRAL FINLAND: CONSTRAINTS ON MAGMA EVOLUTION AND Fe-Ti-V OXIDE ORE GENESIS

Anssi Johannes Mäkisalo

MASTER'S PROGRAMME IN GEOSCIENCES

Master's thesis

2019

TIIVISTELMÄ OPINNÄYTETYÖSTÄ

Oulun yliopisto Teknillinen tiedekunta

Koulutusohjelma (kandidaatintyö, diplomityö) Geologian ja mineralogian koulutusohjelma		Pääaineopintojen ala (lisensiaatintyö)	
Tekijä Mäkisalo, Anssi Johannes		Työn ohjaaja yliopistolla Kärenlampi, K., tohtorikoulutettava, Hanski, E., professori emeritus	
Työn nimi Otanmäen intruusion anortosiittisten kivien geologinen karakterisointi ja merkitys magmaattisessa evoluutiossa sekä Fe-Ti-V-oksidimalmin synnyssä			
Opintosuunta Geotieteet	Työn laji Pro gradu	Aika Maaliskuu 2019	Sivumäärä 128 s., 6 liitettä

Tiivistelmä

Kainuussa sijaitseva Otanmäen intruusio on differentioitunut mafinen intruusio, jossa esiintyy kerrosmyötäistä Fe-Ti-V-oksidimalmia. Malmi ilmenee <1–200 metriä leveinä linsseinä heterogeenisessä vyöhykkeessä, joka koostuu eri gabrotyypeistä sekä anortosiitista. Anortosiitti muodostaa muutamia metrejä halkaisijaltaan olevia runsaslukuisia, muodoltaan vaihtelevia sulkeumia. Sulkeumat ovat merkittävä komponentti intruusion malmia sisältävässä osassa, mutta niitä ei ole tutkittu tarkasti ja niiden merkitys intruusion geologisessa historiassa on osin epäselvä. Tämän pro gradu- tutkielman tarkoitus on karakterisoida anortosiittiset kivet geologisen kartoituksen sekä kokokivi- ja mineraalikemiallisten menetelmien avulla, verrata niitä intruusion muihin mafisiin kiviin sekä vastaaviin intruusioihin globaalisti ja tutkia niiden merkitystä magmaattisen evoluution ja Fe-Ti-V-oksidimalmin synnyn kannalta. Työtä varten valmistettiin 20 ohuthiettä, joista tehtiin mikroskooppisten tutkimusten lisäksi 64 elektronimikroanalyysiä plagioklaasin koostumuksen selvittämiseksi. Geokemiallinen aineisto sisältää 18 ICP-OES/ICP-MS analyysiä sekä 58 kannettavalla XRF-analysaattorilla tehtyä koostumusmittausta. Lisäksi hyödynnettiin aikaisempien tutkimusten aineistoja, joihin kuuluu 941 kallioperähavaintopistettä, 139 ohuthiettä, 197 kokokivigeokemiallista analyysia, 110 elektronimikroanalyysia sekä Rautaruukki Oy:n laatimia karttoja ja kairasydänraportteja.

Otanmäen intruusiosta laadittiin vuosina 2017–18 suoritetun kartoitustyön perusteella 20 km^2:n kattava, 1:50 000-mittakaavainen geologinen kartta sekä stratigrafiapylväs. Lisäksi laadittiin 1:200-mittakaavassa yksityiskohtaisia geologisia karttoja anortosiittisia sulkeumia sisältäviltä alueilta hyödyntäen drone-ilmakuvausta. Työssä esitetään uusi, yhtenäistetty nimistö Otanmäen intruusiolle. Intruusio jaetaan kolmeen tektoniseen lohkoon: Otanneva, Otanmäki ja Vuorokas. Intruusiolohkot sisältävät kolme magmaattisen stratigrafian pääyksikköä: alavyöhyke, malmivyöhyke ja ylävyöhyke. Lisäksi intruusion reunoilla esiintyy kahdessa kohtaa hienorakeisia amfiboliittisia kiviä.

Mineralogisten havaintojen sekä pää- ja hivenalkuainekoostumuksen perusteella anortosiittiset kivet ovat voimakkaasti differentioituneita plagioklaasiadkumulaatteja, jotka ovat syntyneet samasta magmasta muiden intruusion kivien kanssa. Malmi- ja ylävyöhykkeiden kiteytymisen aikana plagioklaasi on ainakin ajoittain kellunut magmassa. Tämä on mahdollistanut plagioklaasikiteiden kasautumisen magmasäiliön yläosaan. Osa tästä yläosan massiivisesta anortosiitista upposi takaisin magmasäiliön alempiin osiin vaihtelevasti kiinteytyneinä autoliitteina, jotka kerrostuivat osin jähmettyneeseen kumulaattikerrokseen. Oksidimalmin kiteytyminen ja siitä seurannut tiheyden lasku jäännössulassa ovat todennäköisesti vaikuttaneet autoliittien uppoamiseen. Fe-Ti-V-oksidimalmin syntyyn on vaikuttanut osittain kiteytyneiden kumulaattien valuminen kohti magmasäiliön vajonnutta keskustaa. Malmivyöhykkeessä tapahtuneet magmaattiset liikunnot ovat tapahtuneet ainakin osittain anortosiittisten autoliittien kerrostumisen jälkeen. Autoliittien osalta Otanmäen intruusiolla on merkittäviä yhteneväisyyksiä Skaergaardin ja Sept Ilesin intruusioihin.

Muita tietoja

Asiasanat: Otanmäki, intruusio, anortosiitit, Fe-Ti-V-malmit, magmaattinen evoluutio, paleproterotsooinen

ABSTRACT
FOR THESIS

University of Oulu Faculty of Technology

Degree Programme (Bachelor's Thesis, Master's Thesis) Degree Programme in Geology and Mineralogy		Major Subject (Licentiate Thesis)	
Author Mäkisalo, Anssi Johannes		Thesis Supervisor Kärenlampi, K., Doctoral student, Hanski, E., Professor emeritus	
Title of Thesis Geological characterization of anorthositic rocks in the Otanmäki intrusion, central Finland: constraints on magma evolution and Fe-Ti-V oxide ore genesis			
Major Subject Geosciences	Type of Thesis Master's Thesis	Submission Date March 2019	Number of Pages 128 p., 6 App.

Abstract

The 2.06 Ga Otanmäki intrusion in central Finland is a differentiated mafic intrusion hosting stratabound Fe-Ti-V oxide ore. The ore occurs as <1–200-m-wide lenses in a heterogeneous zone comprising different gabbro varieties and anorthosite. Anorthosite forms ubiquitous amoeboid-shaped inclusions a few meters in diameter, constituting a significant component in the ore-bearing part of the intrusion. The anorthositic rocks have not been studied earlier in detail and their role in the geological history of the intrusion is not well understood. The purpose of this Master's thesis is to characterize the anorthositic rocks by means of mapping and geochemical and minerochemical methods, compare them to other mafic rocks in the Otanmäki intrusion and corresponding mafic intrusions globally and study their role in the magmatic evolution and Fe-Ti-V oxide ore genesis. A total of 20 thin sections were prepared for petrographic microscopy and 64 EPMA analyses were made to determine the plagioclase composition. The geochemical data include 18 ICP-OES/ICP-MS analyses and 58 portable XRF measurements. Pre-existing data, which include 941 bedrock observation points, 139 thin sections, 197 geochemical analyses and 110 electron microanalyses, were utilized as well as historical maps and drill core logs by the mining company Rautaruukki Oy.

Based on the mapping campaign carried out in 2017–2018, a 1:50 000 geological map of the Otanmäki intrusion covering 20 km^2 and a related stratigraphical column are presented. Detailed maps in 1:200 scale, which are based on aerial drone photography from anorthosite-bearing areas, were also compiled. A revised nomenclature for the Otanmäki intrusion is presented, in which the intrusion is divided into three tectonic blocks: Otanneva, Otanmäki, and Vuorokas. All these blocks comprise three major stratigraphical units: the Lower Zone, Ore Zone and Upper Zone. Furthermore, fine-grained marginal amphibolites are reported from two locations.

Based on the mineralogical observations and major and trace element data, the anorthositic rocks represent strongly differentiated plagioclase adcumulates and are cognate to the Otanmäki intrusion. Crystallization of the Ore and Upper Zones has likely included one or several periods of plagioclase buoyancy, enabling accumulation of plagioclase crystals in the roof part of the magma chamber. Parts of the massive roof anorthosite sank gravitationally into the lower parts of the magma chamber as variably solidified autoliths and were deposited on a semi-solidified substratum. The sinking was likely affected by Fe-Ti-oxide crystallization and subsequent decrease in the density of the residual melt. The genesis of the Fe-Ti-V oxide ore is suggested to have been affected by gravitational movements of partially solidified cumulate slurry towards a subsided magma chamber center. At least parts of these movements postdate the deposition of the anorthositic autoliths. The occurrence of anorthositic autoliths bears many similarities with the Skergaard and Sept Iles mafic intrusions.

Additional Information

Keywords: Otanmäki, mafic intrusion, anorthosite, Fe-Ti-V mineralization, magmatic evolution, Paleoproterozoic

CONTENTS

1 INTRODUCTION 1
2 THEORETICAL CONSIDERATIONS 4
2.1 Mafic magmatism 4
2.1.1 Layered mafic intrusions 5
2.1.2 Origin of layering in mafic intrusions 5
2.1.3 Mafic pegmatites 7
2.2 Magmatic Fe-Ti-V oxide deposits 8
2.2.1 Deposit types 8
2.2.2 Genesis 9
2.2.3 Mineralogy 11
2.3 Anorthosites 12
2.3.1 Definition 12
2.3.2 Anorthosite occurrences 13
2.3.3 Anorthosite autoliths and xenoliths in mafic intrusions 14
2.3.4 Genesis and the anorthosite problem 15
3 REGIONAL GEOLOGICAL SETTING 16
3.1 Archean complexes 16
3.2 The Kainuu belt 18
3.3 Tectonic evolution 20
4 PREVIOUS STUDIES OF THE OTANMÄKI Fe-Ti-V DEPOSIT AND RELATED ROCKS 21
4.1 Geological studies of the Otanmäki intrusion 21
4.2 Fe-Ti-V oxide ores 24
5 METHODS 28
5.1 Geological mapping 28
5.1.1 Field observations 28
5.1.2 Other material 29
5.2 Sample collection 29
5.3 Sample preparation 30
5.4 Petrographic microscopy 31
5.5 Electron microprobe analysis 31
5.5.1 Plagioclase analyses 31
5.5.2 Previously published data 32

5.6 Geochemical analyses 32
5.6.1 ICP-OES and ICP-MS 32
5.6.2 Portable XRF 33
5.6.3 Previously published data 33
6 GEOLOGY OF THE OTANMÄKI INTRUSION 36
6.1 Country rocks 40
6.1.1 Archean rocks 40
6.1.2 Katajakangas metaturbidite 40
6.1.3 Otanmäki suite A-type granites and intermediate rocks 40
6.1.4 Kajaani granite suite 40
6.1.5. Mafic rocks 41
6.2 Otanmäki intrusion 41
6.2.1 Marginal amphibolites 41
6.2.2 Lower Zone gabbros 44
6.2.3 Lower Zone vari-textured gabbros (VTG) 45
6.2.4 Ore Zone and Fe-Ti-V oxide ore 50
6.2.5 Upper Zone 55
6.2.6 Mafic and felsic dikes 57
6.3 Deformation and metamorphism 58
7 ANORTHOSITIC AUTOLITHS 62
7.1 Position in the stratigraphy 62
7.2 Descriptions of autoliths and their contact relations 65
7.3. Textures and mineralogy 69
8 GEOCHEMISTRY 72
8.1 Major elements 72
8.2 Trace elements 84
9 PLAGIOCLASE COMPOSITIONS 93
10 DISCUSSION 99
10.1 Magmatic emplacement 99
10.2 Structure of the intrusion 100
10.2.1 Marginal amphibolites 100
10.2.2 Lower Zone 101
10.2.3 Ore Zone 102
10.2.4 Upper Zone 105
10.2.5 A layered intrusion? 105
10.3 Satellite intrusions 106

10.4 Anorthositic autoliths 106
10.4.1 Contacts to country rocks 107
10.4.2 Composition of the autoliths 108
10.4.3 Formation of roof anorthosite and sinking of autoliths in the magma chamber 109
10.4.4 Factors affecting plagioclase buoyancy 110
10.4.5 Genesis of the anorthositic autoliths in the Otanmäki magma chamber 111
10.5 Magmatic evolution 112
10.6 Deformation and metamorphism 114
10.7 Suggestions for follow-up research 115
11 CONCLUSIONS 118
12 ACKNOWLEDGEMENTS 121
13 LITERATURE 122
APPENDICES

1 INTRODUCTION

The Otanmäki Fe-Ti-V oxide ore deposit was discovered in 1938 when the Geological Survey of Finland was carrying out an exploration campaign to search for the provenance of two magnetite- and ilmenite-rich boulders discovered in Sukeva, central Finland. The exploration area was soon narrowed down to a location known as Otanmäki, where a strong magnetic anomaly had been found 37 km southwest from the city of Kajaani (Paarma, 1954). Targeted field work led to a discovery of an oxide ore body associated with gabbroic rocks at Otanmäki. Similar occurrence of ore at Vuorokas, about four kilometers east of Otanmäki, was discovered by the Geological Survey in 1939. Later several satellite intrusions with similar magnetite-ilmenite mineralization were discovered within a 15-kilometer radius from the main deposit (Pääkkönen, 1956).

Underground mining operations commenced at Otanmäki in 1953 and at Vuorokas in 1979 and the mines were closed in 1985. The historical production was 31 Mt of ore grading 32–34 wt% Fe, 6–8 wt% Ti, 0.26 wt% V and minor pyrite (Sarapää et al., 2015). The Otanmäki mine was historically the largest iron mine in Finland and an important global producer of vanadium (Sarapää et al., 2015). Remaining resources at Otanmäki and Vuorokas are indicated to be 17 Mt of ore (Otanmäki Mine Oy, 2017).

The oxide ore is present as irregular lenses in a heterogenous zone of gabbroic and anorthositic rocks. “Anorthositic rocks” refer to variously shaped, plagioclase-rich bodies of meters to tens of meters in diameter. The anorthositic rocks were first described by Paarma (1954). They are a voluminous component in the area of oxide ore occurrence and are mentioned by many researchers (Pääkkönen, 1956; Kerkkonen, 1979; Talvitie and Paarma, 1980). These enigmatic rocks have, however, been largely overlooked as the focus of previous studies has been on the ore mineralogy and genesis. As a result, the nomenclature of the rocks which host the oxide ore has been diverse. The host rocks have been referred to as amphibolite with gabbro and anorthosite lenses (Paarma, 1961), gabbro-anorthosite series (Kerkkonen, 1979), heterogenous zone of metagabbros, gabbros and anorthosites (Lindholm and Anttonen, 1980), anorthosites (Nykänen, 1995) and layered gabbro anorthosite (Sarapää et al., 2015).

Anorthosite is a rock consisting of 90 % or more plagioclase (Streckeisen, 1976). Anorthosites occur predominantly as Proterozoic anorthosite massifs and as a component in layered mafic complexes (Ashwal, 1993, 2010). Only one massif anorthosite is known to occur in Finland, the Angeli anorthosite in Lapland (Vartiainen 1989, Rask and Vartiainen 1989). Many layered mafic intrusions contain anorthositic rocks as continuous layers or inclusions, and anorthosite can make up to 6–21 % of the total intrusion volume, providing essential insight into the magmatic evolution of the intrusions (Ashwal, 1993, 2010; Irvine et al., 1998; Namur et al., 2015). Furthermore, anorthosite makes up approximately 83 % of the lunar crust, forming the so-called lunar highlands, and hence the study of terrestrial anorthosites contributes to the understanding of the lunar geology (Wood et al., 1970; Warren, 1990; Namur et al., 2011).

The purpose of this study is to characterize the leucocratic rocks within the mafic intrusive rocks at Otanmäki and Vuorokas. Previous studies have not specified whether the plagioclase-rich rocks originated from the same magma as the gabbros and the oxide ore, or represent an exotic component in the intrusion. This question can be addressed by means of mapping and geochemical and minerochemical methods. The leucocratic rocks are a volumetrically important component in the ore-bearing part of the intrusive bodies and spatially closely linked to the oxide ore. Whether or not they are cognate with the mafic intrusive rocks, their chemical composition and position in the intrusion should yield constraints to understanding the magmatic evolution and ore genesis in the intrusion.

The terminology used for the mafic rocks in the Otanmäki area has been problematic. Terms such as *Otanmäki intrusion*, *Vuorokas intrusion*, *Otanmäki association* and *Otanmäki intrusion complex* have been used all together and sometimes interchangeably (e.g. Talvitie and Paarma, 1980; Nykänen, 1995; Hokka and Torppa, 2016; Huhma et al., 2018). In a tectonostratigraphic division the mafic intrusive rocks at Otanmäki are classified by Luukas et al. (2017) as *Otanmäki suite*, a term which is in turn also used for the A-type rocks at Otanmäki by Kärenlampi et al. (2019). Different nomenclature has also been applied to the five satellite intrusions, e.g. Honkamäki, Isoaho and Koski satellite intrusions have been referred to as Hautakangas, Isokivenkangas and Itäranta, respectively.

To unify the wide and sometimes misleading terminology for the mafic rocks at Otanmäki, an updated terminology is proposed and used in this study (Fig. 1.1). With a very high probability the ore-bearing mafic intrusive bodies at Vuorokas and Otanmäki represent the same magmatic event and are developed in one magma chamber. They are therefore collectively referred to as the *Otanmäki intrusion*. The Otanmäki intrusion is split by later tectonic movements into three major *tectonic blocks* (or *blocks* for short) which are, from east to west, Otanneva, Otanmäki and Vuorokas. The term *Otanmäki intrusive complex* is used to cover the Otanmäki intrusion and the five satellite intrusions which likely represent the same magmatic event.

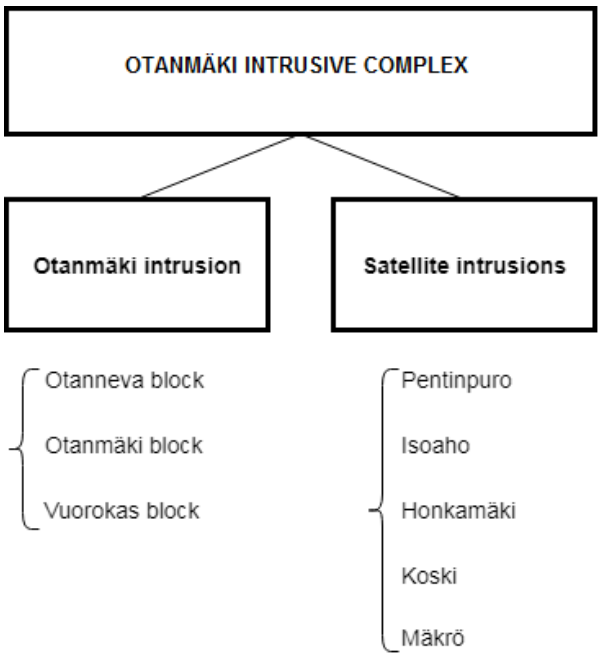

Figure 1.1. Terminology used in this study for the mafic intrusive rocks at Otanmäki.

2 THEORETICAL CONSIDERATIONS

2.1 Mafic magmatism

Basaltic melts are partial melts of peridotitic mantle rocks (Kushiro, 2001). Their genesis is often linked to an extensional tectonic setting and mantle plumes. The majority of basaltic magmatism occurs in mid-ocean ridges, but mafic magmas are also generated in continental environments (Robb, 2005). The chemical composition of mafic melt depends on the source rock composition, P-T conditions, and the extent of partial melting (Grove, 2000). It can further change when rising magma undergoes fractional crystallization with or without crustal assimilation. Magma can be referred to as "primary" when its composition is controlled solely by the mineralogic and chemical content of the source and the extent of melting but not by differentiation processes upon ascend to shallower depths (Winter, 2001).

Examples of manifestations of continental mafic magmatism include potassic and sodic alkali basalts, continental flood basalts and layered mafic intrusions (Farmer, 2003). Most of the mafic magmas generated under continents likely do not rise to surface levels because of their high density (c. 2600 kgm^{-3} at 10^{-4}Gpa, Spera, 2000). This is especially likely if the magma is anhydrous (Farmer, 2004). Mafic magmas tend to pool in the crust and form (layered) mafic intrusions, sills or extensive dike swarms. As demonstrated by Rudnick (1992), most of the lower continental crust is globally mafic in composition, and mafic intrusive rocks may contribute greatly to continental growth (Johnson, 1991).

Mafic-ultramafic igneous intrusions are met in all continents and throughout the geologic time. They are important hosts for many types of ore deposits, such as those of Ni, Cu, Co and PGE, Cr and apatite (Robb, 2005; Maier, 2015). They are also the dominant host of magmatic Fe-Ti-V deposits (Gross, 1996).

2.1.1 Layered mafic intrusions

Layered mafic intrusions are differentiated igneous bodies that have intruded into continental crust. They have a gabbroic, noritic or troctolitic bulk composition and show well-developed layering (Ashwal, 1993).

Cumulate refers to an igneous rock comprising minerals formed by accumulation of crystals from a magma through gravitational settling, flotation or flow segregation (Blatt et al., 2006). The composition of cumulate rocks differs from that of the magma from which they crystallized. They display an interlocking fabric of sub- to euhedral minerals, which are in contact with each other. The interstitial space between cumulus minerals is filled with intercumulus liquid, which crystallizes into postcumulus crystals of other minerals. The cumulate terminology is used only in a descriptive sense without reference to genesis (Irvine, 1982). Cumulate rocks can be named with different prefixes after their texture based on the proportions of cumulus and intercumulus material orthocumulates have 25–50% of intercumulus material, mesocumulates 7–25 % and adcumulates 0–7 %.

2.1.2 Origin of layering in mafic intrusions

Magmatic layering is a commonplace feature in igneous bodies, especially in mafic-ultramafic intrusions (Wager and Brown, 1968; Irvine et al., 1998; Namur et al., 2015). It is formed by sets of individual layers with different grain sizes, mineral modes or textures. Layering can also be cryptic, which means that it is observed in variations in the chemical composition of cumulus minerals with respect to stratigraphic height (Irvine, 1982). Layering can be distinct or poorly defined and it can be horizontal or form different structures, such as inch-scale layering and convoluted layering (Namur et al., 2015).

Layering is a general structure of cumulates: each of the individual layers forms a sheet like cumulate unit and a distinctive entity in terms of composition (whole rock or mineral) and/or textural features (e.g., grain size) (Irvine, 1982; Naslund and McBirney, 1996).

Igneous layers are commonly planar, but more complex morphologies are observed in some layered intrusions. The layer thickness and lateral continuity, homogeneity and sharpness of contacts to surrounding layers vary considerably between intrusions or even within one intrusion (Namur et al., 2015). Layers having a thickness of less than 2.5 cm and sharp contacts are referred to as lamina (Irvine, 1982). Igneous lamination refers similarly to pervasive planar structures that extent through cumulates on a scale similar to their grain size.

Traditionally, layering in mafic intrusions has solely been attributed to fractional crystallization and crystal settling (Wager et al., 1960). Minerals in a silicate melt settle gravitationally with a velocity which depends on the density contrast between the crystal and liquid, crystal radius and viscosity of the liquid. Settling velocity (V) is expressed by the Stokes law (Equation 2.1):

$$V = 2r^2 g(\rho_1 - \rho_2) / 9\eta \qquad (2.1)$$

where r is crystal radius, g gravitational constant, ρ_1 and ρ_2 crystal and liquid densities and η is viscosity of the liquid.

Minerals with different densities and crystal sizes settle at different velocities, which may or may not result in igneous layering. The process results in mineral sorting because of contrasts in the density between the solid phases and melt. Gravitational crystal settling is comparable to sedimentation, and igneous layers can portray pseudo-sedimentary structures, such as cross bedding or flow structures. Due to the broad range of layer types and features, it is considered unlikely that a single process, such as gravitational settling, could be the driving factor for all the different occurrences of layering. Also, experiments and modelling have shown that plagioclase may be buoyant in basaltic melts (Campbell et al., 1978; Scoates, 2000), especially in those rich in iron, and does not inevitably accumulate on the floor of a magma chamber. In some cases, plagioclase is abundant in cumulate layers in the upper part of a mafic intrusion as the crystals have floated upwards in a dense, Fe-rich residual magma. This kind of process can produce anorthosite layers in upper parts of mafic intrusions (Ashwal, 2010; Namur et al., 2015).

Most well-known examples of layering cannot be attributed to a single process; the Skaergaard intrusion, for example, portrays several different types of layering (McBirney and Noyes, 1979). Currently, layering is understood to be a result of a combination of igneous processes involving complex density and chemical diffusive controls (Namur et al., 2015). Generally, layering processes are driven by dissipation of energy and the attempt of a magmatic system to reach thermodynamic equilibrium. Layering may originate from fractional crystallization, settling of phenocrysts, convection, thermal diffusion and wall rock assimilation (Namur et al., 2015). Crystallization processes producing layering also include in-situ crystallization of magma at the slightly undercooled chamber margins (McBirney and Noyes, 1979; Naslund and McBirney, 1996; Namur et al., 2015).

Processes generating igneous layering can be divided into dynamic and non-dynamic (Irvine, 1982; Boudreau and McBirney, 1997; Namur et al., 2015). Processes during the filling and crystallization of a magma chamber are referred to as dynamic layering processes involving gravitational or flotational settling of crystals with different densities and sizes, flow-segregation of partially crystallized magma, segregation of crystals during convective liquid movements, magma injection and mixing, and liquid immiscibility (Namur et al., 2015). Non-dynamic layering processes originate principally from drastic changes in the crystallization conditions (pressure, temperature and oxygen fugacity) which destabilize the stable liquid assemblages, and do not require large-scale movements of material in the magma chamber (Namur et al., 2015).

2.1.3 Mafic pegmatites

Pegmatite is an igneous rock which has an extremely coarse and/or variable grain size. The large grain size is, however, not the sole prerequisite for a rock to be called pegmatitic, as the term also covers other characteristics. According to London (2008), any of the following textural attributes should be considered when categorizing an igneous rock as pegmatitic:

1. Extremely coarse grain size in comparison to normal igneous rock of similar composition
2. Large variations in grain size with increase from margins towards the center of a distinct igneous body
3. Sharply bounded spatial zonation of mineral assemblages
4. Skeletal crystal habit or graphic crystal intergrowths

Pegmatites occur in igneous or metamorphic host rocks with sharply bounded to zoned contacts. Pegmatite textures are found throughout the spectrum of igneous rock compositions (Blatt et al., 2006; London, 2008), but most pegmatites are granitic in composition. Mafic pegmatites are generally rare.

London (2008) classifies gabbro pegmatites in layered mafic intrusions into two types: in-situ pegmatites and intrusive pegmatites. In-situ pegmatites are more common and consist of spatially limited pegmatitic segregations dispersed in the main gabbro body. The segregations may show normal zoning with borders richer in mafic minerals and cores in plagioclase – or reverse. Intrusive pegmatites often show a pipe-like shape and cut their hosts at a high angle. These pegmatites are chemically different from their host gabbros and likely represent late differentiates intruding the cognate gabbros.

In general, magma must be supersaturated and undercooled to facilitate crystal nucleation and growth. The genesis of pegmatites is traditionally associated with slow cooling rates and/or abundant volatiles (e.g., Blatt et al., 2006). Slow cooling rates are enabled by a low thermal gradient and high wall rock temperatures whereas volatiles enhance diffusivity and contribute to a large crystal growth (London, 2008). Other factors, such as a high concentration of chemical compounds acting as fluxes and high water pressures, may also advance pegmatite formation.

2.2 Magmatic Fe-Ti-V oxide deposits

2.2.1 Deposit types

Magmatic Fe-Ti-V oxide ores are typically hosted by massif anorthosite complexes or mafic intrusions where mineralization occurs in stratiform or stratabound horizons

(Gross, 1996; Gross et al., 1997; Maier, 2015). The richest and most continuous deposits are found in the most voluminous intrusions, such as the Bushveld Igneous Complex, which hosts approximately 70% of the world's vanadium resources (Crowson, 2001).

Magmatic Ti ores can be classified into ilmenite ores and titaniferous magnetite ores (Gross et al., 1997). Ilmenite ores are exclusively associated with anorthositic massifs. Titaniferous magnetite ores are hosted by gabbroic intrusions with titaniferous magnetite as the main ore mineral.

The occurrences of Fe-Ti-V mineralization are generally characterized by complex textural and field relations in both massif anorthosite complexes and mafic intrusions (Gross, 1996). Fe-Ti-V oxide ore can be present in concordant layered units produced by fractional crystallization as well as irregular, discordant masses. Mineralization can also be disseminated or vein-type. In large intrusions, the ore reefs can be laterally continuous up to 100 km (Maier, 2015). Magnetite is a low-T phase, and magnetite mineralizations occur typically in upper parts of intrusions. This is the case with Bushveld (e.g. Maier et al., 2013) and Skaergaard (McBirney, 1996), for example.

2.2.2 Genesis

Magmatic Fe-Ti-V ores originate from a variety of igneous processes. Important petrogenetic features for ore formation in igneous intrusions include the following (Robb, 2005):

1. Crystal fractionation and gravity induced crystal settling
2. Density stratification of magma chambers and the ability of magmas to undergo density changes as crystallization proceeds
3. Repeated recharge of chambers by injection of fresh magma
4. The ability of fresh magma to find its own density level and turbulently mix with the residual magma
5. The existence of transient periods of crystallization when only a single phase is in the liquidus

Furthermore, oxide-silicate liquid immiscibility, i.e. the segregation of iron-rich and silica-rich paired melts, have been recognized as a major differentiation process in the Sept Iles layered intrusion and Skaergaard intrusion (Jakobsen et al., 2005; Charlier et al., 2011; Veksler and Charlier, 2015). Factors controlling the formation of Fe-Ti mineralization include temperature, the amount of water in the magma and Fe^{3+}/Fe^{2+} ratio, which is in turn controlled by the oxygen fugacity (Reynolds, 1985).

Maier et al. (2013) suggest that the formation of oxide reefs in large intrusions may include subsidence of intrusions centers due to crystal loading resulting in the slumping of semi-solidified cumulate slurries towards intrusion center. This is witnessed in the Kemi layered intrusion where the chromitite ore is only a few cm in thickness at the flanks of the intrusion but more than 70 m in its central part (Alapieti et al., 1989; Huhtelin, 2015; Maier and Hanski, 2017). The PGE reefs and oxide layers in the Bushveld complex also become thicker and higher in grade towards the center (Maier et al., 2013). The model of slumping of oxide slurry is applicable especially to large layered intrusions (Maier et al., 2013). In smaller intrusions where cooling is faster and subsidence less prominent, the process may result in less continuous, wider reefs (Maier, 2015). A simplified illustration of oxide ore genesis including crystal fractionation, gravity-induced crystal settling and slumping of oxide cumulates is presented in Fig. 2.1.

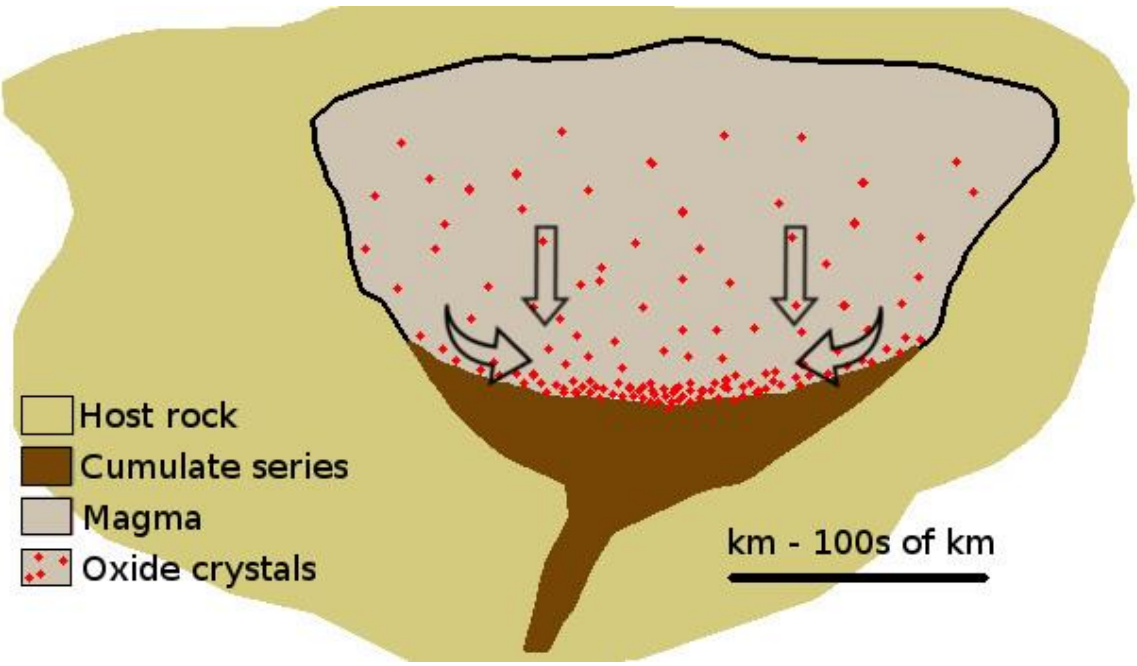

Figure 2.1. Schematic illustration of oxide ore formation in a large mafic intrusion. Oxide minerals crystallize from a Fe-Ti-V-saturated magma and segregate gravitationally on the cumulate rocks. Magma loading may cause the central part of the intrusions to subside, and semiconsolidated oxide cumulate mush concentrates in the central part of the magma chamber. Modified after Maier (2015).

2.2.3 Mineralogy

Titaniferous magnetite layers are often mineralogically straightforward: massive layers are monomineralic, whereas poorer reefs contain intercumulus silicates, such as pyroxene, amphibole and plagioclase or their alteration products (Maier, 2015). Vanadium is compatible into magnetite, and therefore the magnetite-bearing layers lower in the stratigraphy are usually more enriched in V.

Compositions of Fe-Ti oxides can be illustrated with the Fe-Ti-O ternary system (Fig. 2.2). Titanomagnetite, or titaniferous magnetite, belongs to the magnetite–ulvöspinel (Fe_3O_4–Fe_2TiO_4) solid solution.

Titanomagnetite is stable under conditions of low oxygen fugacity but under oxidizing conditions, it commonly undergoes oxy-exsolution that produces magnetite-ilmenite lamellae according to the following equation (Reynolds, 1985):

$$3\ Fe_2TiO_4 + 1/2\ O_2 \rightarrow 3\ FeTiO_3 + Fe_3O_4 \qquad (2.2)$$

(ulvospinel) (ilmenite) (magnetite)

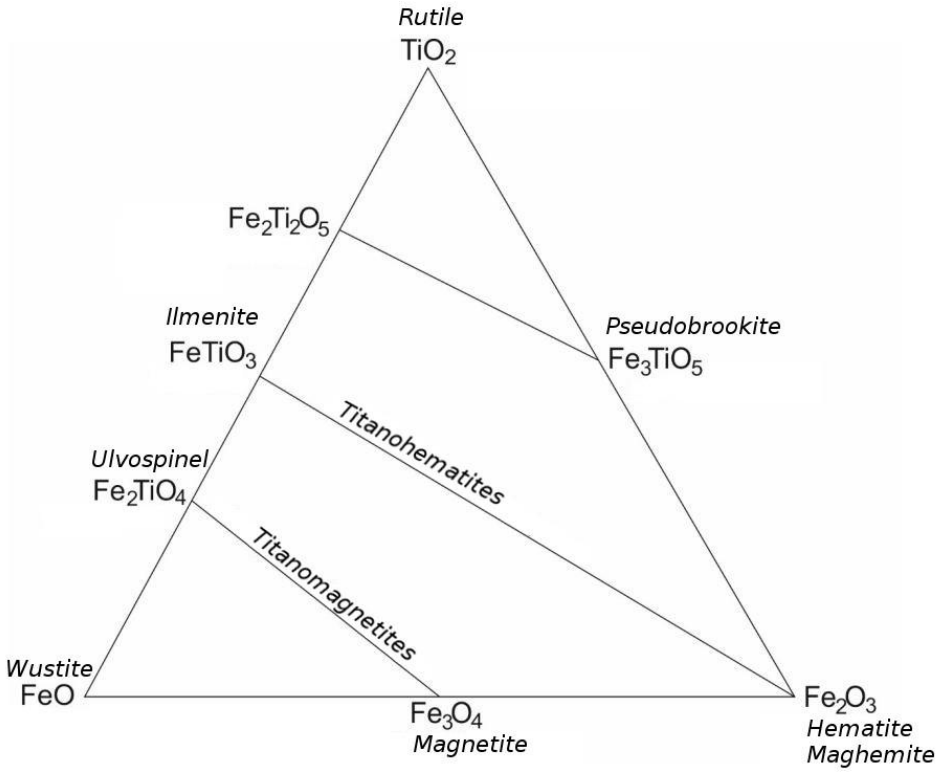

Figure 2.2. Ternary diagram of the Fe-Ti-O system with important iron oxide minerals, titanomagnetite and titanohematite solid solution series.

2.3 Anorthosites

2.3.1 Definition

Anorthosite is a leucocratic igneous rock consisting of 90 % or more of plagioclase as defined by the IUGS Subcomission on the Systematics of Igneous Rocks (Fig 2.3; Streckeisen, 1976). Ashwal (1993) further classifies leucogabbroids after Buddington (1939) into gabbroic anorthosites (10–22.5 % mafic minerals) and anorthositic gabbros (22.5–35 % mafic minerals). The most common mafic minerals are pyroxenes, olivine

and Fe-Ti oxides (e.g., Hamilton et al., 2010). The prefix "oxide-rich" should be used when the magnetite and ilmenite content is more than 10% (Ashwal, 1993). The anorthite content of plagioclase in anorthosites can be anything between An_{20} and An_{100} (Ashwal, 1993).

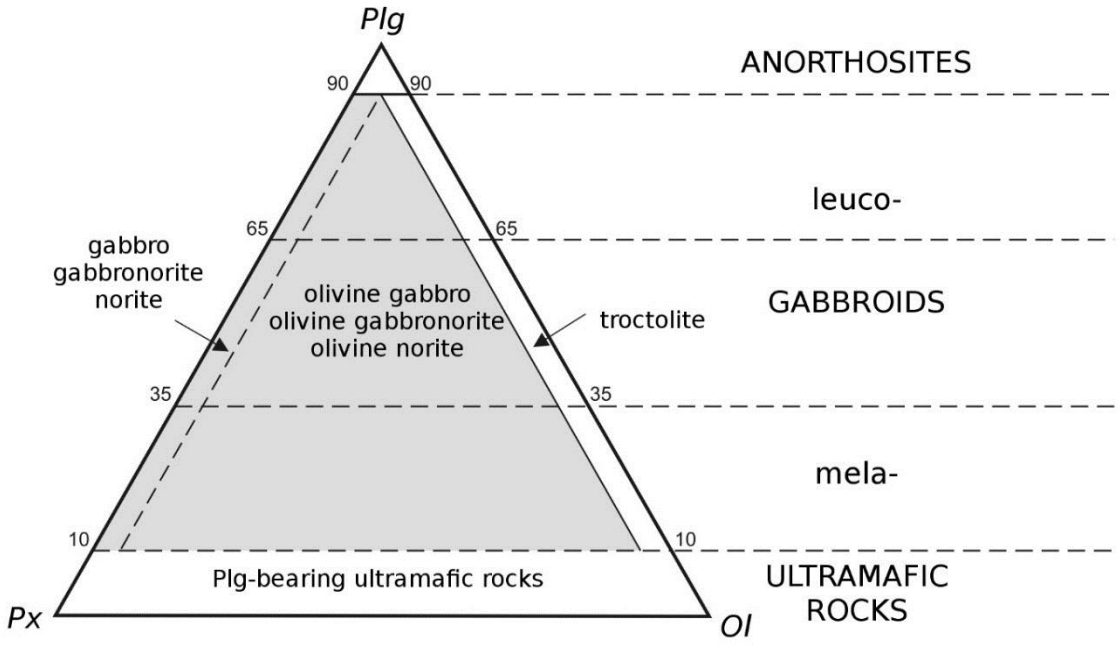

Figure 2.3. Classification of gabbroic rocks based on normative mineral proportions of plagioclase (Plg), pyroxene (Px) and olivine (Ol) after Streckeisen (1976).

2.3.2 Anorthosite occurrences

Ashwal (1993) categorizes anorthosites into six occurrences: Archean anorthosites, Proterozoic massif-type anorthosites, anorthosites of oceanic settings, anorthosite inclusions in other igneous rocks, extraterrestrial anorthosites and anorthosites of layered mafic complexes. All massif anorthosites are Proterozoic in age, possibly owing to abnormally high crustal temperatures during the eon (Arndt, 2013). Anorthosites in ophiolites and layered mafic intrusions occur throughout the geological history (Ashwal, 1993, 2010).

Globally, massif anorthosite associations are important sources of Ti and favorable geological environments for Fe and V (Laznicka, 2006). The world-class Tellnes Ti deposit in Norway, for example, occurs in the Rogaland anorthosite province (Korneliussen et al., 2000).

In anorthosite-bearing layered mafic intrusions, anorthosite makes up typically from 3 to 18% of their total volume (Ashwal, 1993). Anorthosite can be present as laterally continuous, thick layers, potholes, or different types of inclusions (Ashwal, 1993, Namur et al., 2011; Maier et al., 2016). Similarly to massif anorthosites, this geological environment favors Fe, Ti and V mineralization (Laznicka, 2006).

Anorthosite in layered series is most commonly present as layers from a few cm to m in thickness (Namur et al., 2015). Layers can be laterally extensive but are not typically thick. In the Bushveld complex, for example, the anorthosite layers are less than 50 meters in thickness.

Anorthosites can become more voluminous in higher parts of magmatic stratigraphy: The Sept Iles intrusion in Canada portrays an up to 500-m-thick anorthositic upper border series. The upper parts of the Kemi layered intrusion, northern Finland, have leucogabbroic-anorthositic layers tens to hundreds of meters in thickness, though the topmost rocks of the intrusion have been eroded away (Alapieti et al., 1989; Huhtelin, 2015).

In layered mafic intrusions, anorthosites are also present as anorthositic potholes, i.e., subcircular-irregular cavities, which vary from a few meters to hundreds of meters in diameter. Potholes occur as hole-like structures in the cumulate series and originate possibly from tectonically mobilized, semi-solidified anorthositic slurry moving gravitationally and filling tectonic pull-apart structures (Maier et al., 2016).

2.3.3 Anorthosite autoliths and xenoliths in mafic intrusions

Layered inclusions can have anorthositic rocks as fragments or blocks of varying sizes (Ashwal, 1993; Namur et al., 2011; Krause et al., 1985). In the Skaergaard intrusion, angular to subrounded blocks of anorthosite are up to 500 m in diameter (Naslund, 1986). Host rocks of the Tellnes Ti deposit also portray anorthosite xenoliths brecciated from the anorthositic host rock by a later noritic intrusion (Krause et al., 1985). Anorthosite inclusions can be cognate or xenolithic in nature, i.e. they can derive from the magma itself or from the host rocks (Krause et al., 1985; Ashwal, 1993; Namur, 2011).

Anorthosite blocks may represent rocks from the upper series sunk due to a density decrease in the melt by fractionation (Irvine, 1987; Namur et al., 2011). Structural relationships in the Bushveld intrusion suggest that anorthositic blocks sank through the magma and were emplaced on the incompletely consolidated cumulate pile of the Layered Series (Ashwal, 1993). The provenance of anorthositic autoliths, i.e., a compositionally corresponding unit higher in the magmatic stratigraphy, is not necessarily known. In the case of Sept Iles intrusion, the anorthositic autoliths of the layered series have a known mineralogical and textural counterpart in the massif anorthosites of the uppermost part of the intrusion, which is regarded to be their source (Namur et al., 2011).

2.3.4 Genesis and the anorthosite problem

The origin of anorthosites is not completely understood (Ashwal, 1993; Maier et al., 2016). Especially, the genesis of massif anorthosites have unanswered questions in terms of the origin and composition of the parental magma (Ashwal, 1993).

Anorthosites are regarded as cumulates, because a purely anorthositic magma would have a too high solidus temperature for the magma to remain liquid in crustal environment temperatures. On the other hand, formation of monomineralic anorthosite massifs through fractional crystallization would require vast amounts of basaltic magma and voluminous mafic series are not typically associated with massif anorthosites. The absence of mafic residual may originate from segregation and downward migration of the dense residual magma from the chamber, as suggested by Arndt (2013).

For the origins of stratiform anorthosites in layered intrusions, accumulation of plagioclase during fractional crystallization seems the most probable answer (Namur et al., 2015). Anorthositic upper border series, such as that in the Sept Iles intrusion, are probably caused by plagioclase flotation in the magma chamber (Namur et al., 2011). A similar path of fractional crystallization and plagioclase flotation in a magma ocean is suggested for the genesis of lunar anorthosites (Namur et al., 2011; Arai and Maruyama, 2017).

3 REGIONAL GEOLOGICAL SETTING

The Otanmäki intrusive complex is located between Archean TTG-gneiss complexes and the A-type rocks of the Otanmäki-Kuluntalahti nappe near the western margin of the Archean Karelia craton (Luukas et al., 2017; Huhma et al., 2018; Kärenlampi et al., 2019). The Otanmäki intrusion represent a pulse of tholeiitic magmatism which was related to a rifting event of the Archean basement at 2.06 Ga (Huhma et al., 2018). The intrusion is of the same age with the Kevitsa intrusion in northern Finland (Mutanen and Huhma, 2001) and the Bushveld Igneous Complex in South Africa (Hamilton, 1977).

At the time of the emplacement of the Otanmäki intrusion, the Archean craton had already undergone several rifting events from 2.5 Ga onward with concurrent volcanic activity and sedimentation (Laajoki, 1998; 2005). Rifting gradually led to the break-up of the craton and the formation of MORB-type volcanic rocks of the 1.95 Ga Jormua ophiolite (Kontinen, 1986, 1987; Peltonen et al., 1998). The Archean basement, enclosed intrusions and supracrustal rocks were metamorphosed and deformed in the Svecofennian orogeny over a time period of 1.92–1.77 Ga (Nironen, 2017).

A geological map of the Kainuu area is presented in Fig. 3.1. where the study area is shown with a black rectangle. The geological evolution of the Kainuu region is summarized in Table 3.1.

3.1 Archean complexes

The study area is located at the northern margin of the Rautavaara (<2.75 Ga) complex, close to the tectonic boundaries of the Rautavaara, Iisalmi (2.7–3.2 Ga) and Manamasalo (2.6–2.7 Ga) complexes (Hölttä et al., 2012). Apart from their northern side, the Otanmäki and Vuorokas intrusion blocks are in contact with Archean rocks of the Rautavaara complex. Whether the Rautavaara complex represents a younger part of the Iisalmi complex or is a separate tectonic terrain, is still unclear (e.g., Vaasjoki et al., 2001; Hölttä et al., 2012; Huhma et al., 2018).

The rocks of the Rautavaara complex are predominantly tonalite-trondhjemite-granodiorite series gneisses (TTG's), which contain amphibolite mesosomes (Hölttä et

al., 2012). Only few age determinations have been reported from the complex, recording maximum ages of ca. 2.75 Ga (Hölttä et al., 2012).

Table 3.1. Timing of major geological events in the Kainuu area.

Age (Ga)	*Event*
<2.7	Formation of the Archean Rautavaara complex (Hölttä et al., 2012)
2.68–2.1	Cratonic stage with intermittent extensional episodes (Nironen, 2017)
2.3–2.06	Jatulian sedimentation: fluvial and shallow marine sandstones and shelf dolomites (Laajoki, 2015; Hanski and Melezhik, 2013)
2.1–1.9	Kalevian sedimentation: turbiditic sandstones, pelites and black schists (Lahtinen et al., 2010, 2015)
2.06	Emplacement of the Otanmäki intrusion (Huhma et al., 2018)
2.05	Intrusion of the Otanmäki suite A-type granites and intermediate rocks (Kärenlampi et al., 2019)
1.92	First Svecofennian thrusting at the Kainuu belt (Lahtinen et al., 2015)
1.88–1.79	Svecofennian greenschist to amphibolite facies metamorphism (Hölttä and Heilimo, 2017)
~1.86– 1.80	Svecofennian granitoid magmatism (Kontinen et al., 2013b)

3.2 The Kainuu belt

The Paleoproterozoic Kainuu belt is a N-S-oriented, 200-km long and 40-km wide schist belt located between the Archean Rautavaara, Pudasjärvi and Lentua complexes (Peltonen and Kontinen, 2004; Laajoki, 2005; Huhma et al., 2018). It consists of a relatively thin (2–3 km thick) sequence of faulted and folded, allochtonous and autochtonous supracrustal rocks (e.g., Laajoki, 2005). The Otanmäki intrusion is in contact with A-type granitoids and intermediate rocks of the Otanmäki-Kuluntalahti nappe (Kärenlampi et al., 2019).

The Kainuu belt records supracrustal successions, deposited between 2500–1900 Ma (Laajoki, 2005), which are divided into several tectofacies: volcanic and sedimentary rocks ("Sumi-Sariola"), fluvial to shallow marine sandstones ("Jatuli"), shelf dolomites ("Marine Jatuli") and turbiditic sandstones and pelites ("Lower Kaleva") (Laajoki, 1998; 2005). The youngest tectofacies, deep marine sediments ("Upper Kaleva"), are considered to be allochthonous (Laajoki, 2005; Kontinen and Hanski, 2015). The traditional tectofacies nomenclature (Sumi-Sariola, Jatuli…) is here used as broad terms without reference to exact sedimentary facies, chronostratigraphic units or lithostratigraphic groups. The latest tectonostratigraphic division for all Karelian supracrustal rocks in Finland is presented in Luukas et al. (2017) and is based on decreasing epoch ages.

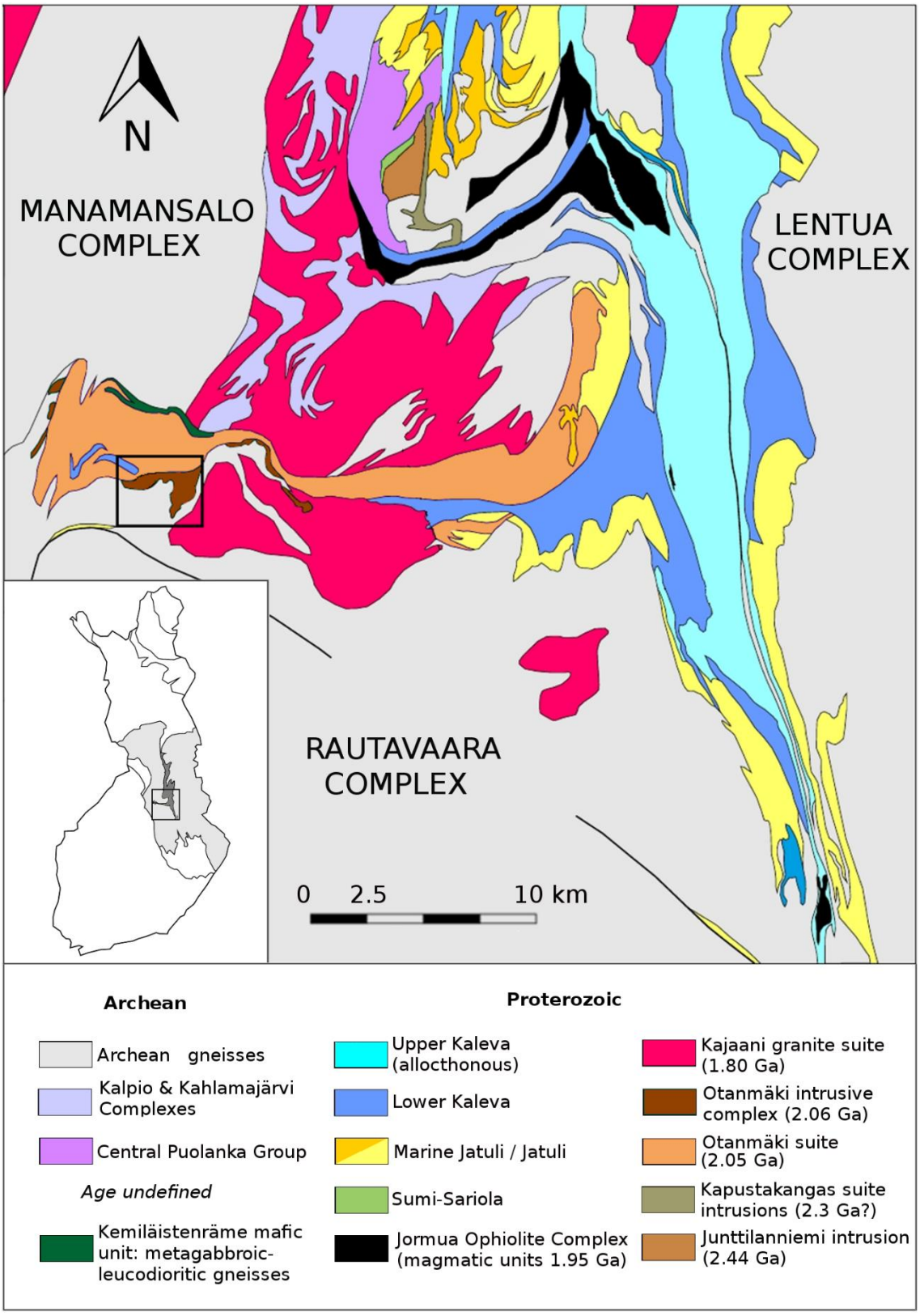

Figure 3.1 Simplified geological map of the central part of the Kainuu belt located between Archean complexes. The location of the study area is shown by a small rectangle. The small inset map shows the location of NW-SE oriented craton margin and the location of Archean craton in central Finland (light grey) with the enclosed Kainuu belt (dark grey). Modified from Huhma et al. (2018). Published with permission from the GTK.

3.3 Tectonic evolution

The major phases in the tectonic evolution of the Kainuu area are the amalgamation, attenuation and rifting of the Archean craton followed by convergent tectonics of the Svecofennian orogenic events (Nironen et al., 2016). The Archean Karelia domain is thought to have formed by accretion of diverse crustal fragments in continent-continent type collisions at ca. 2.70 Ga (e.g., Mänttäri and Hölttä, 2002; Kontinen and Paavola, 2006). The craton is regarded to have been tectonically stabilized and cratonized before 2680 Ma (Nironen, 2017). The period between 2680 and 2100 Ma is characterized by a relative tectonic stability with smaller rifting events marked by volcanic rocks and sediments (Strand, 1988; Laajoki, 1998, Nironen, 2017). Subsequently, the basement underwent rifting in many separate tectonic events involving (mafic) igneous activity. The Otanmäki intrusion and the 2.06 Ga Kevitsa mafic intrusion in northern Finland represent magmatism of one of the extensional phases between 2.05 and 2.1 Ga. Coeval Fetholeiitic mafic dikes are also reported from the Archean Lentua complex and Central Lapland greenstone belt (Vuollo and Huhma, 2005).

Final break-up of the Archean craton took place at ca. 2.1–2.05 Ga (Nironen, 2017). The 2.05 Ga Otanmäki suite granitoids and intermediate rocks represent magmatism that is likely associated with further rifting of the craton margin (Kärenlampi et al., 2019). Rifting culminated in the initiation of oceanic crust formation and deep-sea sedimentation at ca. 1.95 Ga as established by the age of the magmatic units of the Jormua ophiolite (Kontinen, 1986, 1987; Peltonen et al., 1998).

In the Svecofennian orogeny, the Archean foreland and the enclosed intrusions were buried under nappe units, which created low- to high-amphibolite facies metamorphic conditions in the Paleoproterozoic supracrustal rocks of the Kainuu belt (Kontinen et al., 1992; Hölttä and Heilimo, 2017). The Rautavaara complex was deformed to some extent in the Paleoproterozoic and underwent retrograde metamorphism under conditions of around 600 °C and 5–6 kbar at 1.89 Ga (Paavola 1999; Mänttäri and Hölttä 2002; Hölttä and Heilimo, 2017).

4 PREVIOUS STUDIES OF THE OTANMÄKI Fe-Ti-V DEPOSIT AND RELATED ROCKS

4.1 Geological studies of the Otanmäki intrusion

The first geological map sheet, which includes the Otanmäki area, and its explanation were compiled by Wilkman (1929, 1931), who noted that there are gabbros at the Pikku Otanmäki hill. After the discovery of the Fe-Ti-V deposit in 1938, the mafic intrusive rocks of the area have been a subject of many research papers and theses including Paarma (1954), Pääkkönen (1956), Kerkkonen (1979), Lindholm and Anttonen (1980), Jaanus-Järkkälä (1989), and Nykänen (1995). The previous studies have largely focused on the mineralogy and genesis of the oxide ore bodies.

The Otanmäki and Vuorokas blocks are composed mostly of gabbroic rocks with a highly variable grain size, composition and color index. In describing the rock types, various names have been used, including magnetite gabbro, gabbro, anorthosite, leucogabbro, (gabbro)amphibolite, ortoamphibolite, etc. (Paarma, 1961; Kerkkonen, 1979; Talvitie and Paarma, 1980; Nykänen, 1995) The mining company used its own nomenclature for the classification of the rock types in the area. Different lithological names used by researchers over time are summarized and presented together with the terms used in this study in Chapter 6.

As seen in Fig. 4.1, the gabbroic bodies at both Otanmäki and Vuorokas comprise two dominant parts: a gabbroic southern part and a more heterogeneous gabbroic-anorthositic northern part, with the latter hosting iron oxide ore bodies (Kerkkonen, 1979; Lindholm and Anttonen, 1980; Nykänen, 1995). Pegmatitic gabbro occurrences and marginal amphibolites are also reported to exist both in the Otanmäki and Vuorokas blocks (Talvitie and Paarma, 1980). However, the orthoamphibolitic-metagabbroic layer shown in Rautaruukki Oy's maps at the SE flank of the Vuorokas block does not have a counterpart in other studies. Nykänen (1995) describes olivine-bearing layers in the SE part of the Vuorokas block. Similarly, Havola (1997) reports olivine gabbros from the S part of the Vuorokas block. The ore zones at Otanmäki and Vuorokas are similar in terms of their ore geometry and mineralogy but differ in the proportions of rock types and the degree of tectonic strain (Kerkkonen, 1979; this study). The ore zones are not

uniform layers but heterogenous regions composed of lenticular bodies of massive to semi-massive magnetite-ilmenite ore within gabbroic to anorthositic host rocks (Paarma, 1961; Kerkkonen, 1979). Mineable oxide ore lenses are 20–200 meters in length and follow leucogabbroic-anorthositic inclusions of roughly the same size. The semi-circular form and steep dip of the ore zone are of tectonic origin. The main rock type in the ore zone is gabbro amphibolite, i.e. recrystallized and hydrated gabbro (Paarma, 1961; Kerkkonen, 1979; Lindholm and Anttonen, 1980).

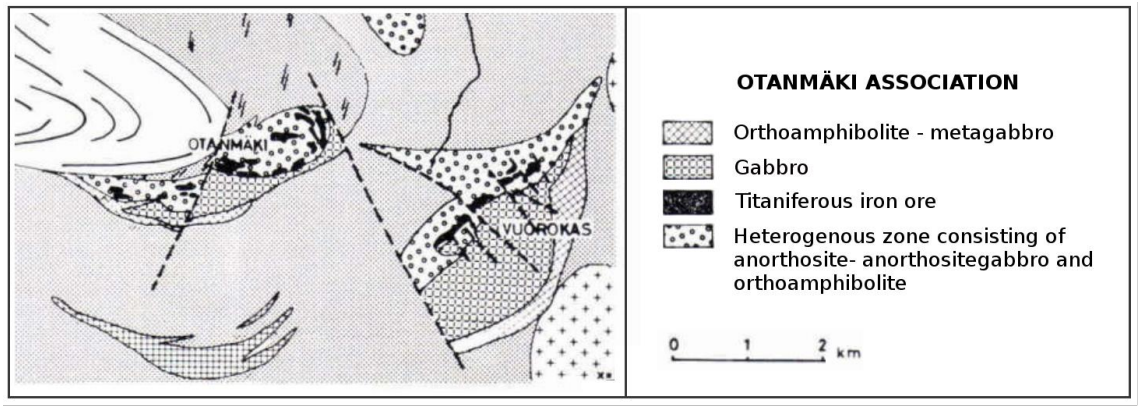

Figure 4.1. Historical map of the Otanmäki intrusion with the subdivision of the gabbroic rocks used by mining company Rautaruukki Oy. Map shows the division of the bodies into gabbroic lower part and ore- and anorthosite-bearing upper part. Modified after Lindholm and Anttonen (1980). Published with permission from the Geological Survey of Finland.

The first age determination of the mafic intrusive rocks at Otanmäki was published by Talvitie and Paarma (1980). A U-Pb zircon TIMS age of 2065 ± 4 Ma was obtained for zircon separated from mafic pegmatoid samples collected from Otanmäki and Vuorokas. Using the current regression algorithm and the isotope data from Talvitie and Paarma (1980), Huhma et al. (2018) calculated an upper intercept age of 2058 ± 13 Ma. On the other hand, Sm-Nd analyses of hand-picked mineral fractions define an isochron with an age of 2043 ± 19 Ma (Huhma et al., 2018), being consistent, within error, with the results of the U-Pb dating. The parental magma of both the Otanmäki and Vuorokas blocks has been suggested to be tholeiitic in composition with enrichment in Fe, Ti and V (Kerkkonen, 1979; Nykänen, 1995). The hafnium isotope study by Patchett et al. (1981) implies minimal crustal contamination of the magma. According to Nykänen (1995), cooling and crystallization of the magma in the lower parts of the magma chamber enabled cumulus growth and gravitational settling of plagioclase, which resulted in the residual melt to become enriched in volatiles, Fe, Ti and V.

Kerkkonen (1979) and Nykänen (1995) constructed magmatic cross sections for parts of the Otanmäki and Vuorokas blocks, respectively. Kerkkonen (1979) separated five magmatic "macrorhytmic" ore layers from the eastern part of the ore zone at Otanmäki (Fig. 4.2A). Layering is present as horizontal, slightly convoluted bands from few meters to 20 meters in thickness. Modal layering of gabbro in a cm-scale has also been reported from outcrops south of the Otanmäki ore zone. According to Kerkkonen (1979), the lower sections of the stratigraphy are located in the southern part of the Otanmäki block. Nykänen (1995) presented a stratigraphical column for the Vuorokas block based on drill core and outcrop data and regarded the (olivine) gabbronoritic SE part of the intrusion block as the lowermost unit in the magmatic stratigraphy (Fig. 4.2B). Above the more primary parts lies a voluminous unit of gabbro norite with a varying cumulate mineralogy and sporadic interlayers of bronzite and websterite. The oxide ore in the upper part is reported to be sandwiched between two anorthositic layers.

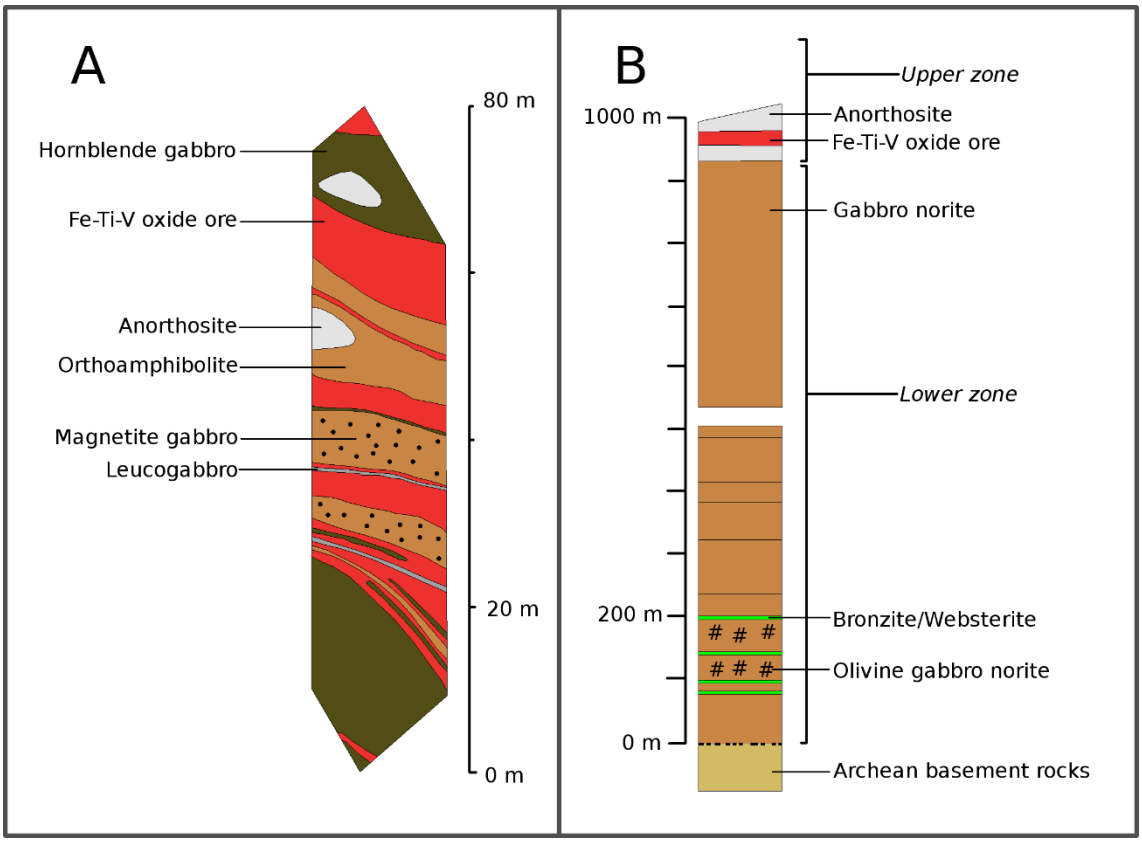

Figure 4.2. Stratigraphic columns for parts of the Otanmäki and Vuorokas blocks. A. Simplified cross section from the ore zone in the Otanmäki underground mine after Kerkkonen (1979), showing five "macrorhytmic" oxide ore layers. B. Simplified stratigraphic column from Vuorokas after Nykänen (1995). Note the different scales.

The presence of light-colored, plagioclase-rich inclusions in the Otanmäki and Vuorokas ore zones and gabbros immediately north of them has been mentioned by many researchers (Paarma, 1954, 1961; Kerkkonen, 1979; Lindholm and Anttonen, 1980; Nykänen, 1995). The inclusions are present as lenticular bodies or fragments from few meters to up to 200 meters along their longitudinal axis and are usually anorthositic to leucogabbroic in composition (Paarma, 1954, 1961; Kerkkonen, 1979). Kerkkonen (1979) also reports gabbroic inclusions in the ore zone, which are coarse to pegmatitic in their grain size and contain anorthositic and leucogabbroic parts.

According to Kerkkonen (1979), anorthosite inclusions in the Otanmäki ore zone have a roughly similar orientation to that the ore lenses and have often an amphibolite-rich rim around them. The contacts between the magnetite-ilmenite ore lenses and inclusions are arbitrary and show locally flow structures suggesting that the contacts are magmatic. Folding, banding and plastic deformation are also seen in the ore surrounding the inclusions. The anorthositic lenses in turn portray angular breccia structures in some places (Kerkkonen, 1979).

4.2 Fe-Ti-V oxide ores

The ore zone in the Otanmäki block is E–W-oriented and mostly 100–200 m wide. Additionally, one occurrence of ore ("Välimalmit") is known at a distance of c. 300 m from the main ore occurences, close to the adjacent A-type granitic and syenitic rocks (Fig. 4.3.) Oxide ore lenses tend to be associated with anorthositic bodies. Both primary magmatic contacts and tectonically mobilized boundaries are recognized between the ore lenses and the surrounding rocks (Kerkkonen, 1979). Oxide ore at Otanneva does not crop out and is regarded subeconomic (Soininen and Paarma, 1959).

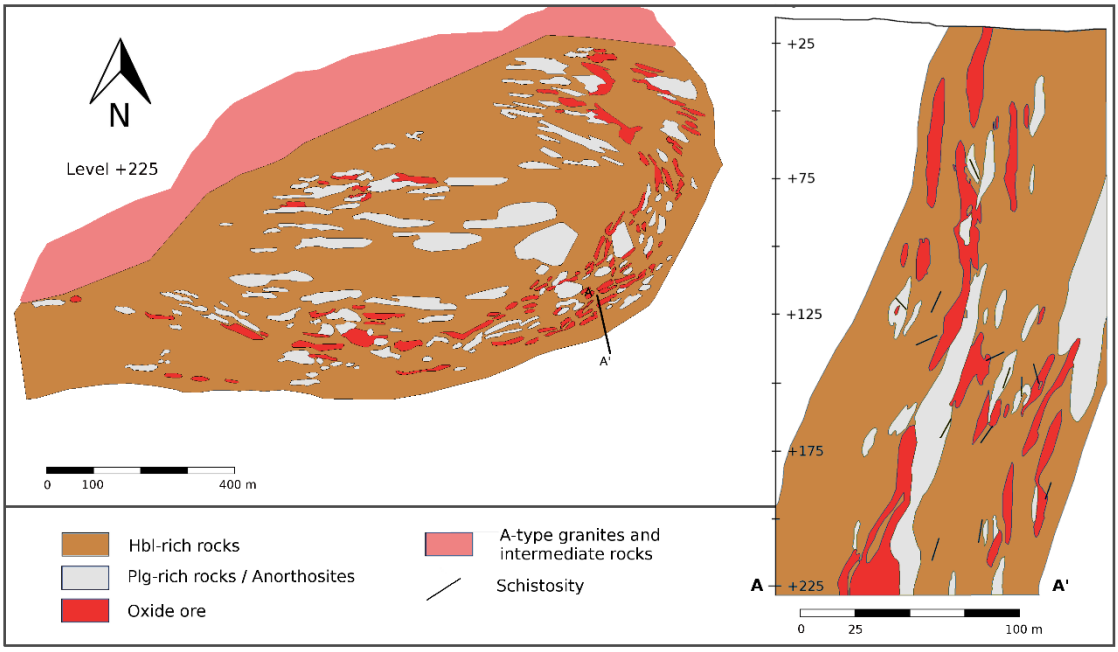

Figure 4.3. Structure of the Otanmäki ore zone. Mine map and cross section A–A' modified after Rautaruukki Oy and Lindholm and Anttonen (1980). Ore lenses and layers occur in a 100–200 m wide zone. An additional occurrence of ore is seen from a 300 m distance from the main ore zone.

The SW-NE-oriented ore zone at Vuorokas is 30–250 meters in width and can be followed through the whole Vuorokas block. Ore lenses and layers at Vuorokas are in a vertical position (Fig. 4.4). The Vuorokas block has two distinct magnetic anomalies similar in magnitude and orientation. The magnetic anomalies in the S part of the block are, however, barren of any mineralization and are likely caused by remnant magnetism (Rautaruukki, 1980).

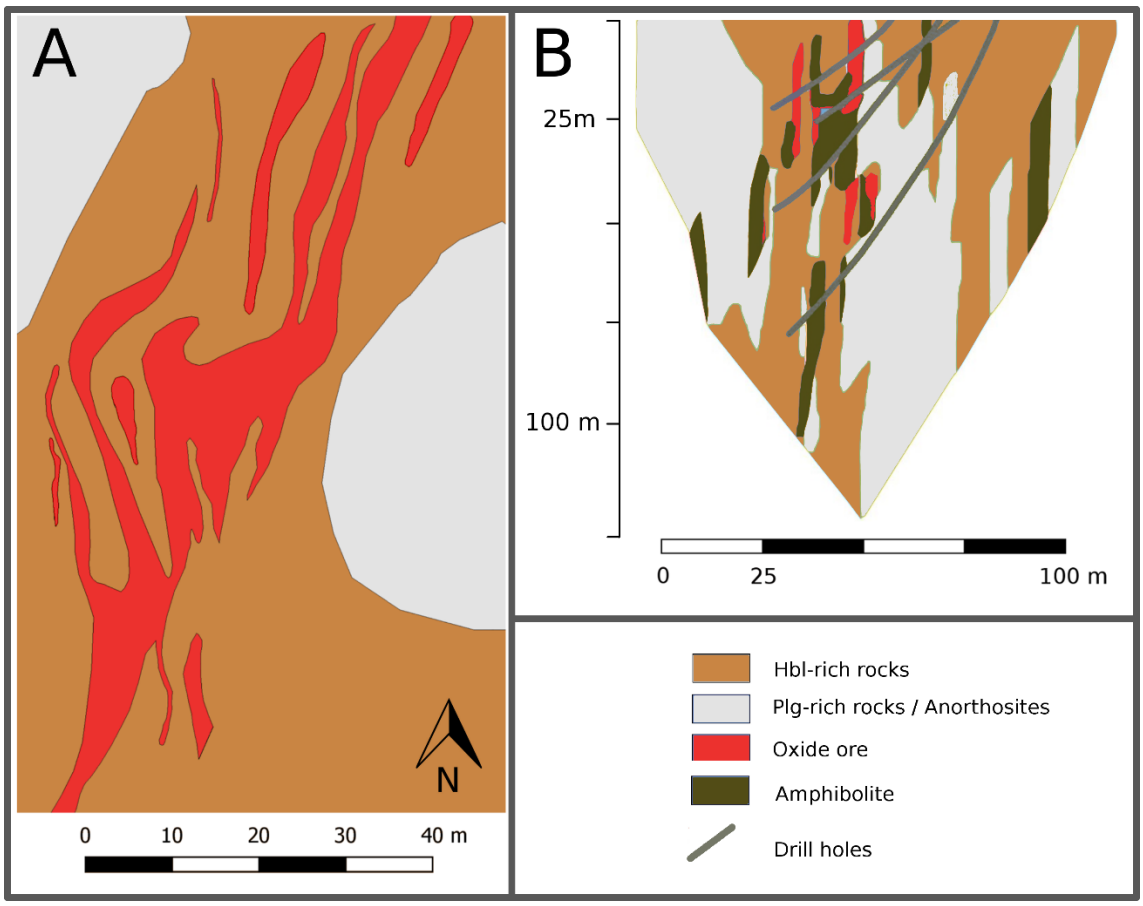

Figure 4.4. Structure of the Vuorokas ore zone. A. Surface map of the Vuorokas open pit area, NE of the underground mine. Modified after Rautaruukki Oy. B. Vertical cross section of the ore zone in the underground mine area. The cross section is a rough lithological model created using one inverse distance weighting (IDW3) interpolation. The amount of anorthositic rocks in this model is estimated disproportionately high. Modified after Parkkinen (2015).

In his licentiate thesis, Kerkkonen (1979) studied the mineralogy of the vanadiferous magnetite-ilmenite ore and observed that ilmenite occurs either as lamellae or inclusions in magnetite or as separate grains. The ilmenite exsolution lamellae in magnetite originates likely from magmatic processes, but the separate occurrence of magnetite and ilmenite is linked to the exsolution of ilmenite from the magnetite-ulvöspinel solid solution during metamorphosis (Kerkkonen, 1979). The occurrence of ilmenite depends on the amount of oxides and the intensity of recrystallization. When magnetite and ilmenite occur separately, their grain size is 0.2–0.8 mm. Nykänen (1995) reported microprobe analyses of magnetite and ilmenite, observing that vanadium in present in both of them with concentration levels of 4400–4500 ppm in magnetite and 1000–2200 ppm in ilmenite.

The mining company divided the ore into three classes (Kerkkonen, 1979), which are shown in Table 4.1. The classification is based on the total amount of magnetite and ilmenite, which is directly proportional to magnetic susceptibility, a quantity which was routinely measured in downhole geophysics in association with underground exploration and grade control (Paarma, 1961).

Table 4.1. Different ore classes in the Otanmäki and Vuorokas mines with corresponding metal grades and mineral concentrations (Kerkkonen, 1979). Chl: chlorite, Hbl: hornblende, Plg: plagioclase.

Ore class	Magnetite	Magnetite + ilmenite	V	Main gangue
I	> 30 %	> 55 %	0.35 - 0.50 %	Chl
II	15 - 30 %	30 - 55 %	0.25 - 0.35 %	Hbl
III	< 15 %	< 30 %	0.15 - 0.25 %	Hbl + Plg

Class I ore is always massive and uniform in oxide ratios. In highly strained zones, magnetite and ilmenite are present as individual grains whereas in less tectonized domains, ilmenite occurs as inclusions and lamellae within magnetite (ilmenomagnetite).

Class II ore is characterized by silicate bands consisting mainly of hornblende. Banded ore of either class I or II was the most common exploited ore type in the Otanmäki mine.

Class III ore includes gabbroic and amphibolitic rocks with disseminated magnetite. Plagioclase is the most common gangue mineral and exhibits varying grain sizes.

As the iron content decreases, the relative amounts of magnetite and ilmenite changes. In class I ore, the magnetite/(magnetite+ilmenite) ratio is usually 0.4–0.6 and in class III ore, it is 0.3–0.5. Rocks completely devoid of magnetite can still contain up to 10 wt% of ilmenite.

5 METHODS

5.1 Geological mapping

5.1.1 Field observations

The Otanmäki intrusion and its surroundings were mapped in scale of 1:50 000 in an area of c. 20 km^2 during the field seasons of 2017 and 2018. Additionally, three areas, approximately 10x20 m in size, were mapped in scale of 1:200. The areas represent different parts in the intrusion and were selected based on the occurrence of different types of leucocratic inclusions that were observed in the large-scale mapping campaign. The detailly mapped areas are: Otanmäki (northern side of the Otanmäki hill), Metsämalmi (NE part of the Otanmäki ore zone) and Vuorokas (north from the Vuorokas ore zone) (Fig. 5.1.).

The coordinates of a total of 385 bedrock observations were collected using a GPS device which uses both GPS and Glonass signals and has an accuracy of a few meters. Dips and directions of schistosity, lineation and fold axis were measured where possible using a geologist's compass. Magnetic susceptibility of each rock type was measured using a Kappameter KT-6 magnetic susceptibility meter. Observations were reported with a code initials-year-running number (e.g., AJMA-2017-1). Photographs were taken during the mapping for later reference. The samples selected for geochemical analyses were photographed in detail with a scale bar.

The geological mapping was focused on the gabbro varieties within the Otanmäki intrusion and, in particular, to the anorthositic inclusions in the ore zone and elsewhere in the intrusions. Observations from surrounding lithologies were made where outcrops near the contacts were available.

Aerial photographs of outcrops were taken with a drone from a height of 15 meters at Metsämalmi and Vuorokas. The photographs were georeferenced and combined with field observations to create geological maps. As the area selected for detailed mapping at Otanmäki did not have a full outcrop coverage, a local equilateral grid was construct-

ed over the outcrops using ropes and 50-m measuring tapes. The accuracy of the grid was verified with GPS points and cross-measurements.

All geographical data were displayed and processed using a QGIS 2.18.9 GIS software. Bedrock observations and their locations on the map are given in Appendices 1 and 2.

5.1.2 Other material

In addition to the data collected for this project, 941 bedrock observations made by Asko Kontinen (GTK), Kimmo Kärenlampi and Juho Tapio (Oulu Mining School) were used in drawing the maps. These observations were collected in the period of 2016–2018 and are mostly from outside of the Otanmäki intrusion. A total of 26 bedrock field observations from Nykänen (1995) were also digitized and used in mapping. Old exploration data by Otanmäki Oy and Rautaruukki Oy were also used. These data include two drill core logs (VUO-92 and VUO-78) and a ground-based magnetic survey map (Pääkkönen, 1943). In addition, geological maps from the Otanmäki, Metsämalmi and Vuorokas areas, prepared by Rautaruukki Oy, were used. The geographical accuracy of the Metsämalmi map was verified with D-GPS measurements with an accuracy of less than 0.50 m.

Two low-altitude, low-resolution aerogeophysical raster maps, a magnetic anomaly map and an electromagnetic anomaly map, from the open data sets of the Finnish Geological Survey (GTK, 2018) were utilized in the interpretation and identification of rock unit boundaries and other structural features. Additionally, four high-resolution aerogeophysical maps from the Otanmäki area were utilized. These maps are modifications from GTK's raw data and were used with permission from GTK.

5.2 Sample collection

During the mapping campaigns, 107 hand samples were collected for reference material and pXRF measurements. The samples weight 1–2 kg depending on their grain size. All sample locations are presented in Appendix 2. The anorthositic inclusions and their adjacent host rocks were sampled based on the information acquired in mapping. Samples were taken throughout the ore and upper zones and from the leucocratic gabbros imme-

diately south of them. A total of 34 samples were taken with a portable core drill or a hammer. Sampling locations and their abbreviations are: Otanmäki (OTA), Otanneva (ON), Metsämalmi (MEM), Vuorokas (VUO), and Rinneaho (RA) (Fig. 5.1). Samples were named with the corresponding abbreviation and a running number (e.g., VUO-5).

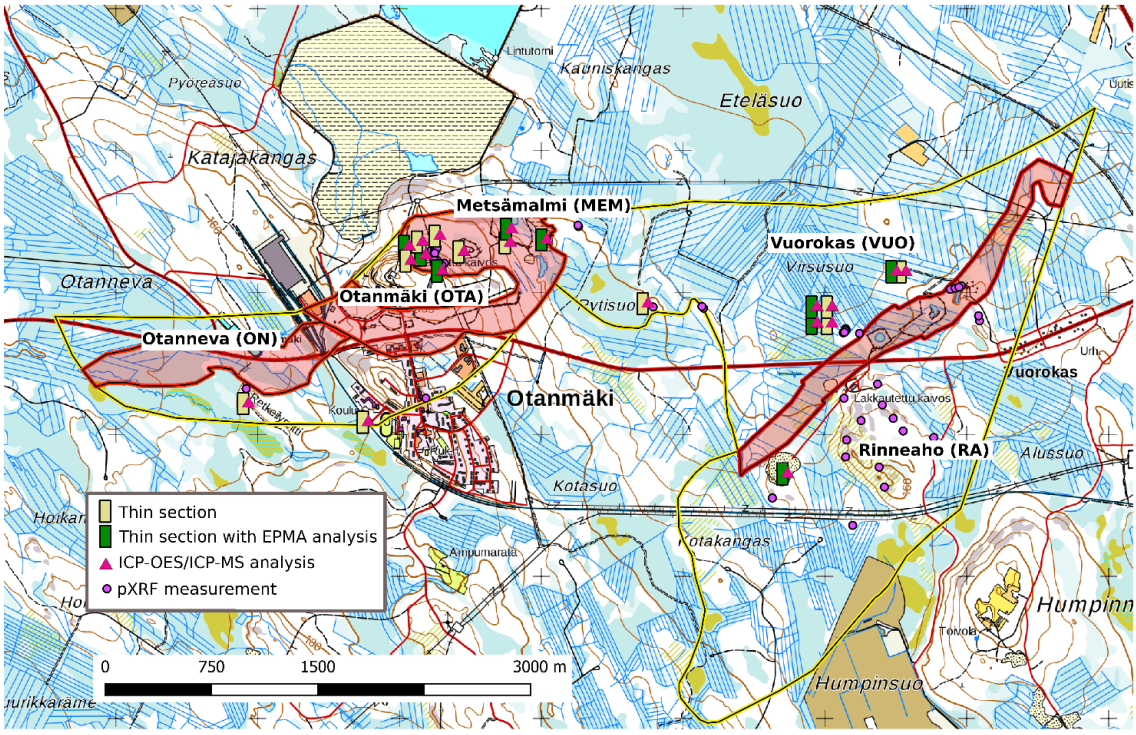

Figure 5.1 Study area with the locations of ICP-OES/ICP-MS analyses, pXRF measurements, thin sections, and thin sections with EPMA analyses. Major outcrop areas and corresponding abbreviations are also presented. Outlines of the Otanmäki intrusion in yellow, ore zones in red. Topographic map: National Land Survey of Finland (2018).

5.3 Sample preparation

All samples were sawed half with a diamond saw in the facilities of Otanmäki Mine Oy at Otanmäki. Crushing and pulverization of the samples for whole-rock analysis were done with jaw and cone crushers and an agate ring mill in the sample preparation facilities of Oulu Mining School, the University of Oulu. The greatly varying grain size of the samples was taken into when selecting an appropriate sample mass for crushing. Polished thin sections were prepared in the thin section laboratory of Oulu Mining School.

5.4 Petrographic microscopy

Polished thin sections were prepared from the 18 samples selected for ICP-OES/ICP-MS analysis and two samples from additional locations. Thin sections were studied with a Leica DM750P transmitted-and reflected-light microscope. Photographs were taken using a Zeiss Axioplan 2 transmitted- and reflected-light microscope mounted with an Axiocam 105 color camera and a Zen 2 core 2.4 computer program.

Thin sections from previous studies from the Otanmäki area were examined for rock type identification and petrographic comparison between different gabbro types. These include 33 thin sections of hand samples from Vuorokas (Nykänen, 1995), 103 thin sections of drill core samples from Vuorokas (Rautaruukki Oy) and 3 thin sections of outcrop samples from the northern part of the Otanmäki hill, provided by GTK (A. Kontinen). The locations of the drill holes are available in Appendix 2 and petrographical observation sheets are available in Appendix 3.

5.5 Electron microprobe analysis

5.5.1 Plagioclase analyses

Nine thin sections were selected for plagioclase analysis using electron microprobe (OTA-1B, OTA-2, OTA-4, MEM-1, MEM-4, VUO-1, VUO-2A, VUO-4, RA-2B) and 64 analyses were done. Analyses were done with a JEOL JXA-8200 microprobe at the Center of Microscopy and Nanotechnology (CMNT), the University of Oulu. The focus of microprobe analyses was mainly on the determination of the plagioclase composition in anorthositic inclusions and their host rocks. Analysis points were selected from plagioclase crystals showing primary magmatic features. Rim and core compositions of each grain were measured separately. Operating conditions were an accelerating voltage of 15 kV, an electron beam current of 15 nA, and a beam diameter of 5 µm. The following components were quantified: SiO_2, TiO_2, Al_2O_3, FeO_{tot}, CaO, Na_2O, K_2O, MnO, SrO, MgO, and BaO. The results of microprobe analyses are presented in Appendix 4.

5.5.2 Previously published data

Electron microprobe data published by Nykänen (1995) were also used in this study. The data set consists of 110 plagioclase analyses from gabbroic rocks occurring south of the Vuorokas ore zone, with 32 of them being from hand samples and 78 from drill cores. These analyses were performed with a JEOL JXCA 733 microanalyzer at the Oulu University Institute of Electron Optics with the following analytical conditions: 15 kV accelerating voltage, 10–33 nA electron beam current, and 10 µm beam diameter. The quantified components were SiO_2, Al_2O_3, FeO_{tot}, CaO, Na_2O, and K_2O.

5.6 Geochemical analyses

The geochemical data used in this study consist of 311 analyses from four different data sets. All analyses contain the following major oxides: SiO_2, Al_2O_3, FeO_{TOT}, CaO, MgO, Na_2O, K_2O, TiO_2, Mn_2O, and P_2O_5. Additionally, each data set includes selected trace elements and lanthanides. Normative mineral compositions were calculated with GCD-Kit 4.1. The chemical datasets are described below and summarized in Table 5.1. All analytical data are available in Appendices 5–9.

5.6.1 ICP-OES and ICP-MS

Selected crushed and pulverized samples were sent for analysis to the Bureau Veritas Minerals laboratory in Vancouver, Canada. A total of 18 samples were analyzed. The samples were digested with lithium borate fusion and ACS grade nitric acid dissolution. Major element concentrations were obtained by Inductively Coupled Plasma Optical Emission Spectroscopy (ICP-OES). Inductively Coupled Plasma Mass Spectrometer (ICP-MS) was used for trace element concentrations of the following 34 elements: V, Cr, Ni, Be, Co, Cs, Ga, Hf, Nb, Rb, Sn, Sr, Ta, Th, U, W, Zr, Y, Ba, Sc, La, Ce, Pr, Nd, Sm, Eu, Gd, Tb, Dy, Ho, Er, Tm, Yb, and Lu.

Two certified rock standards were included in the analysis: vanadium-bearing titaniferous magnetite oxide ore (AMIS 0368, African Mineral Standards, 2013) and NIM-N norite (SA Bureau of Standards, 1984). Student's t-test was used to compare the analytical results with the standard values given by the distributors and found to be accurate.

5.6.2 Portable XRF

Portable XRF (pXRF) instruments were used to measure the composition of 58 sawed hand samples. For each sample, three separate measurements from randomly selected points on the cut rock slab surface were made using factory-delivered calibration and a 60-second measurement time. An average of the three separate measurement points was used. The used pXRF instruments are able to quantify major oxides (SiO_2, Al_2O_3…) and some trace elements (V, Cr, Ni, Cu, Zn, Co, Sr, Ta, U, Zr and Ba).

Sodium is too light to be quantified with pXRF spectrometers (Young et al., 2016). To obtain estimated Na_2O contents in the rocks, Na_2O/Al_2O_3 ratios were calculated from the ICP-OES/ICP-MS data. Na_2O and Al_2O_3 show a strong positive correlation as Na_2O is largely hosted by plagioclase in the rocks. Na_2O/Al_2O_3 ratios were calculated for three groups of rocks: gabbros (0.15), lecogabbroic-anorthositic rocks (0.19), and oxide ore (0.10). These ratios were used to estimate Na_2O based on the measured Al_2O_3 content in the pXRF data.

Six samples representing different rock types were analyzed with both ICP-OES/ICP-MS and pXRF, in order to test the pXRF accuracy and the suitability of Na_2O/Al_2O_3 ratios for the Na_2O estimation in the pXRF data. Comparison of data with Student's t-test showed an excellent correlation in major elements including Na_2O, which was calculated from Al_2O_3. Based on these data, pXRF measurements were used in the rock type classification of gabbroic and anorthositic rocks. Portable XRF measurements are available in Appendix 6.

5.6.3 Previously published data

Nykänen (1995) published 197 analyses of gabbroic rocks from the southern part of the Vuorokas block. These data were added to the geochemical database. The samples of Nykänen (1995) were analyzed for major oxides and S, Cl, Sc, V, Cr, Ni, Cu, Zn, Rb, Sr, Y, Zr, Nb, Mo, Sn, Ba, and Bi by XRF. Additionally, lanthanides La, Ce, Nd, Sm, Eu, Gd, Yb and Lu were quantified by instrumental neutron activation analysis (INAA) for 13 samples. The elements V, Ni, Cu, Zn, Ge, Ag, Cd and Pb were (re)analyzed by V. Nykänen from the same 13 samples with Inductively Coupled Plasma Emission

Spectrometer (ICP-ES) and Directly Coupled Plasma Emission Spectrometer (DCP-ES). Analyses are available in Appendix 8.

In addition, 38 previously unpublished analyses from different oxide ore types from the Vuorokas block were available for this study and received from Vesa Nykänen (pers. comm., 2018). Major oxides were determined with X-ray fluorescence spectroscopy at the University of Oulu and trace elements V, Cr, Ni, Cu, Zn, S, Co, Sr, Zr, Y, Ba and Sc with Inductively Coupled Plasma Mass Spectrometer at the Nordic Volcanological Institute, Island. Analyses are available in Appendix 9.

Table 5.1. Geochemical data sets, quantified elements and used methods.

	ICP-OES/ ICP-MS	***pXRF***	***Nykänen (1995)***	***V. Nykänen (unpubl.)***
Number of analyses/ Quantified element	*20*	*58*	*197*	*38*
SiO_2, Al_2O_3, Fe_{TOT}, MgO, CaO, MnO, K_2O, TiO_2, P_2O_5	*ICP-OES*	*pXRF*	*XRF*	*XRF*
Na_2O	*ICP-OES*	*Na_2O/Al_2O_3 ratio*	*XRF*	*XRF*
V	*ICP-MS*	*pXRF*	*XRF*	*ICP-MS*
Cr		*pXRF*		
Ni		*pXRF*		
Cu	-	*pXRF*		
Zn	-	*pXRF*		
S	-	-		
Be	*ICP-MS*	-	-	-
Co		*pXRF*	-	*ICP-MS*
Cs		-	-	-
Ga		-	-	-
Hf		-	-	-
Nb		-	*XRF*	-
Rb		-		-
Sn		-	-	-
Sr		*pXRF*	*XRF*	*ICP-MS*
Ta		*pXRF*	-	-
Th		-	-	-
U		-	-	-
W		-	-	-
Zr		*pXRF*	*XRF*	*ICP-MS*
Y		-		
Ba		*pXRF*		
Sc		-		
La, Ce, Pr, Nd, Sm, Eu, Gd, Tb, Dy, Ho, Er, Tm, Yb, Lu, Ce, Pr	*ICP-MS*	-	*INAA (12 samples)*	-

6 GEOLOGY OF THE OTANMÄKI INTRUSION

The Otanmäki intrusion consists of differentiated gabbro located between Archean gneisses and Otanmäki suite granites and intermediate igneous rocks of the Otanmäki-Kuluntalahti nappe. It is divided into three major tectonic blocks, Otanneva, Otanmäki and Vuorokas (Fig. 6.1), each of which bears laterally continuous oxide ore zones. The area between Otanmäki and Vuorokas is complexly faulted and may consist of several smaller tectonic units. The contacts of the Otanmäki intrusion to its country rocks are presumably fault bound apart from a small area at Vuorokas.

The Otanmäki and Otanneva blocks cover an area of 1.4 and 1.6 km^2, respectively, while the Vuorokas block extends over an area of 7 km^2. The Otanmäki block is known to extend to a depth of 800 m (Lindholm and Anttonen, 1980). Based on geophysical modelling, all of the intrusion blocks continue at least to a depth of 2 km, although the model has its uncertainties (Lahti et al., 2018). According to Lahti et al. (2018), the whole Otanmäki intrusion occupies an approximate volume of 5 km^3.

Stratigraphically, the Otanmäki intrusion is divided into three major units, the Lower Zone, the Ore Zone, and the Upper Zone. The Lower Zone consists of isotropic gabbros and gabbronorites. Especially at Vuorokas, Lower Zone rocks have locally gradational contacts with pegmatoidal vari-textured gabbros, which are anorthositic to leucogabbroic in composition. The Lower Zone rocks and vari-textured gabbros have a sharp contact with the Ore Zone, which comprises oxide ore lenses and layers, gabbro, magnetite gabbro, and gabbro amphibolite. The Ore Zone rock assemblage changes progressively into the Upper Zone, which has the same assemblage but isotropic gabbro dominates. Both the Ore and Upper Zone portray occasional modal layering. Anorthositic autoliths of 1–30 meters in diameter are met throughout the Ore and Upper Zones. Fine-grained marginal amphibolites are locally met at the intrusion borders.

All rocks in the area are metamorphosed in amphibolite facies. Gabbros are largely recrystallized and variously deformed, and in places, they are cut by diabase dikes, A-type granite veins and coarse-grained late Svecofennian granites. The lithological terminology used in this and previous studies is summarized Table 6.1. Figures 6.1 and 6.2 show a map and a magmatic stratigraphy column of the Otanmäki intrusion, respectively.

Table 6.1. Nomenclature of rock and ore types used in this and previous studies.

This study		*Pääkkönen (1956)*	*Kerkkonen (1979), Rautaruukki Oy*	*Nykänen (1995)*
General classification	***Name***			
Surrounding lithologies	Archean gneisses	striped gneiss	presvecokarelian complex	archean gneiss complex
	Katajakangas metaturbidite	-	supracrustic succession	Katajakangas turbidite
	Otanmäki suite A-type granites and intermediate rocks	gneissose granite	alkali gneiss	alkali granite
	Kajaani granite suite	massive granite	microcline granite	Kajaani granite massif
Otanmäki intrusion	Anorthositic autoliths	anorthosite	anorthosite / leucogabbro	anorthosites
	Upper Zone gabbros	(Gabbro at Pikku Otanmäki)	gabbro/ metagabbro/ ortoamphibolite	gabbroic and anorthosic rocks
	Magnetite gabbro	-	magnetite gabbro/ class III ore	magnetite gabbro
	Gabbro amphibolite	amphibolite / hornblende schist	dark orthoamphibolite/ hornblende rock/ hornblende gabbro	-
	Ore Zone gabbros	(gabbro at Pikku Otanmäki)		gabbroic and anorthosic rocks
	Gabbro pegmatite	-	-	(anorthositic layers)
	Vari-textured gabbro (VTG)	(gabbro at Rinne-aho/uralite gabbro)	-	(anorthositic layers)
	Lower Zone gabbros	(gabbro at Rinne-aho/uralite gabbro)	gabbro	gabbro norite, olivine gabbro norite
	Marginal amphibolites	-	orthoamphibolite/ metagabbro	-
Ore classification	class I ore	extra prime ore class I ore	class I ore	class I ore
	class II ore	class II ore	class II ore	class II ore
	class III ore	-	class III ore/ magnetite gabbro	class III ore

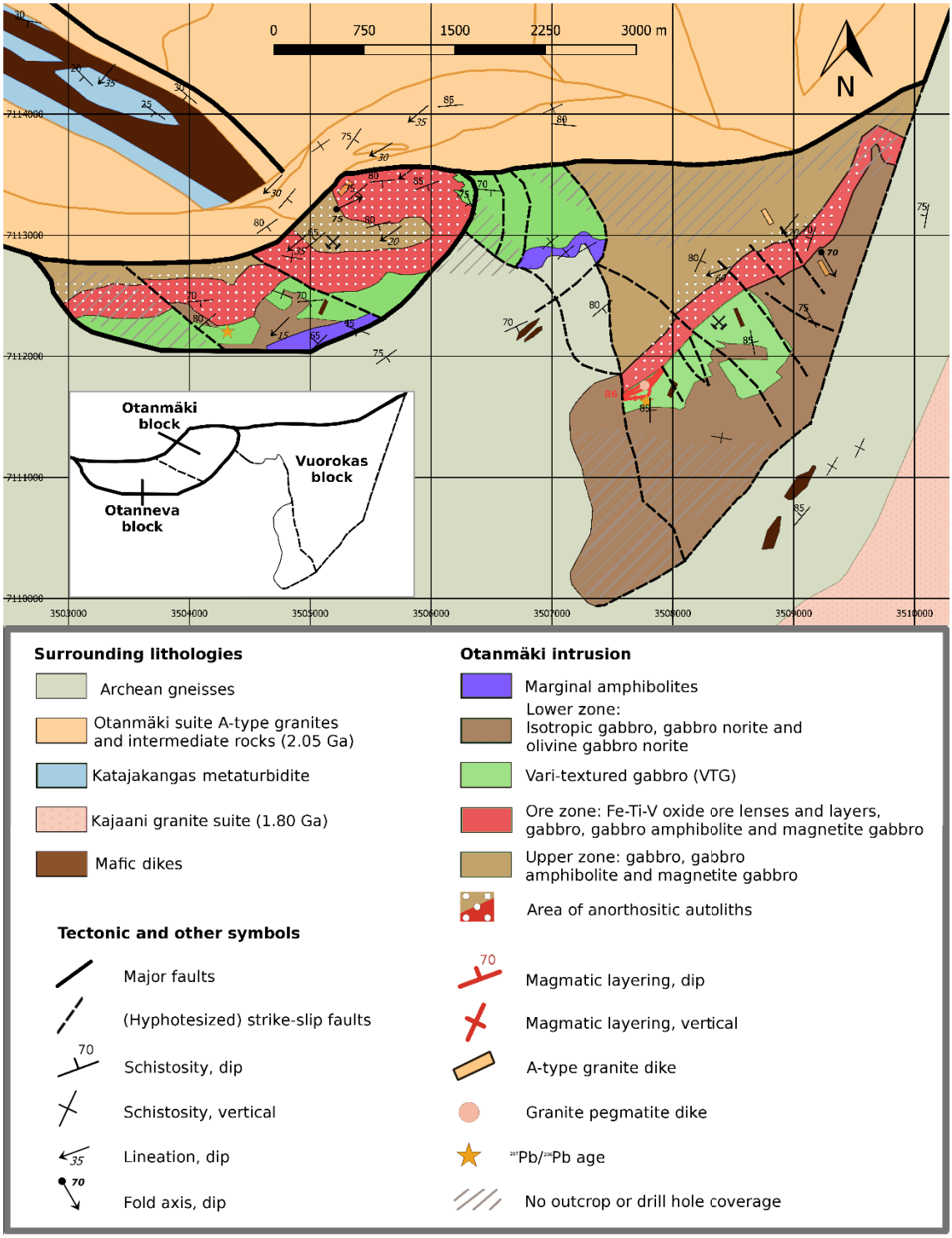

Figure 6.1. Geological map of the Otanmäki intrusion. Coordinates in KKJ3 Finland uniform coordinate system.

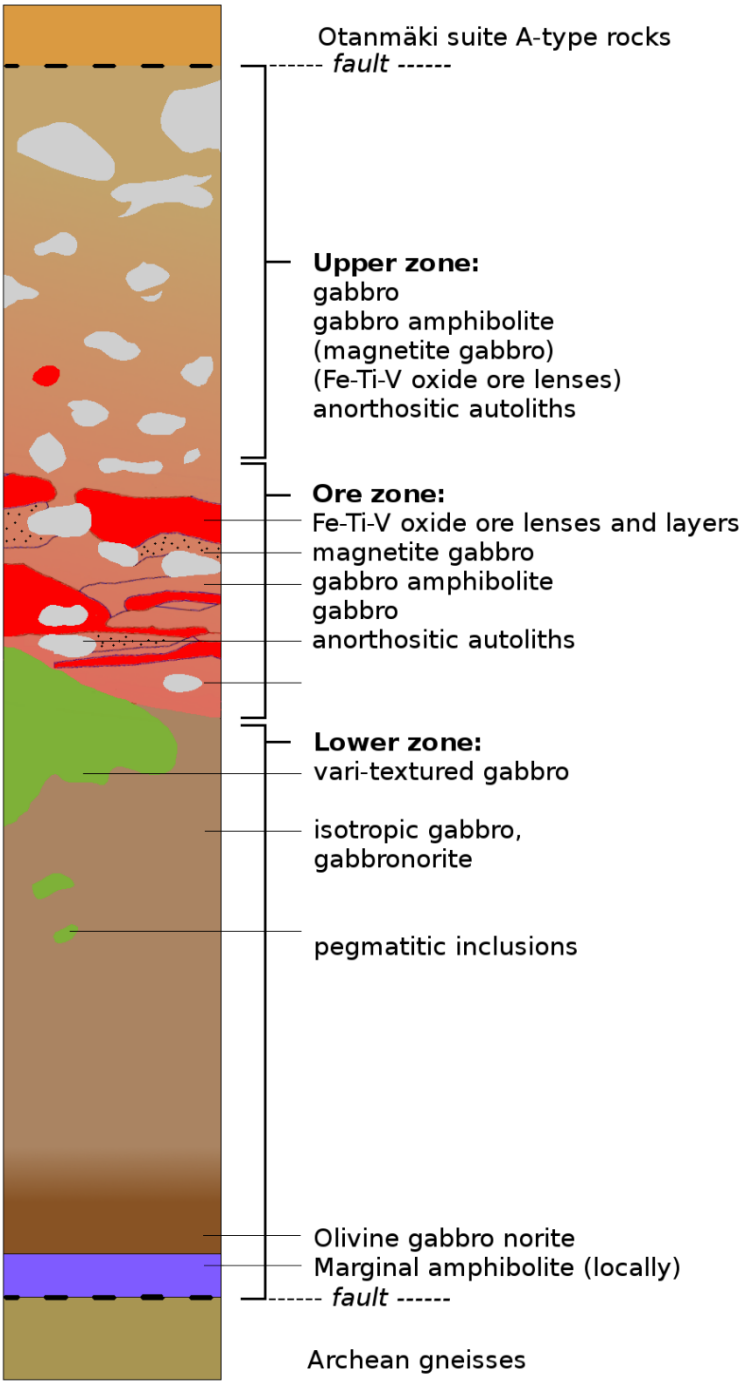

Figure 6.2. Schematic magmatic stratigraphy in the Otanmäki intrusion (not to scale).

6.1 Country rocks

6.1.1 Archean rocks

The Otanmäki intrusion is bordered in the south by Archean migmatitic TTG gneisses with amphibolite mesosomes. Gneisses are dominantly light in color and show a great variation in their texture and structure. Gneisses are in places cut by deformed metadiabase dikes.

6.1.2 Katajakangas metaturbidite

A small formation of Lower Kaleva-type metaturbidites (Finnilä, 2000) occurs as an enclave within A-type granites in the Otanmäki area. The sedimentary unit is known as the Katajakangas formation and is composed mostly of metapelite with minor cm-scale psammitic intercalations and layers of amphibolitized mafic rocks (Puumalainen, 1986).

6.1.3 Otanmäki suite A-type granites and intermediate rocks

The Otanmäki intrusion shares its northern contact with rocks of the Otanmäki-Kuluntalahti nappe, which consists of A-type felsic and intermediate igneous rocks including monzonites, syenites, monzodiorites and peralkaline to peraluminous granites (Kärenlampi et al., 2019). The rocks are rich in alkali feldspar, pinkish, fine to medium grained and pervasively gneissic. The contact to gabbros is seen in some outcrops north of the Otanmäki hill where both the gabbros and the A-type rocks are strongly sheared and show no evidence for intervening. The A-type granites host Nb-Zr-REE mineralization and their age of emplacement is ca. 2050 Ma (Kärenlampi et al., 2019).

6.1.4 Kajaani granite suite

Archean gneisses and the A-type rocks are in places intruded by late Svecofennian microcline granites assigned to the Kajaani granite suite (Väyrynen, 1928; Kontinen and Paavola, 2006). The rocks in this suite are coarse-grained to pegmatitic in grain size and completely undeformed. They were intruded at ca. 1.80 Ga (Vaasjoki et al., 2001; Kontinen and Paavola, 2006), representing the last stages of the Svecofennian magmatism.

6.1.5. Mafic rocks

The satellite intrusions of Pentinpuro, Isoaho, Hautakangas, Koski and Märkö host oxide ore bodies as lenses with gabbroic to anorthositic wall rocks similarly to Otanmäki and Vuorokas (e.g., Lindholm and Anttonen, 1980). They are also structurally in a similar position between Archean TTG gneisses and Otanmäki suite A-type rocks, forming together a discontinuous semi-circle at the margin of the Archean complexes (Fig. 3.1). The satellite intrusions are often grouped together with the Otanmäki intrusion because of their similar geology (Kerkkonen, 1979; Lindholm and Anttonen 1980). The presence of Otanmäki-type oxide mineralization in the otherwise small satellite intrusions implies a strong genetic connection with the main intrusion.

At the northern contact between Otanmäki suite A-type rocks and Archean gneisses lies the Kemiläistenräme mafic unit (Kärenlampi et al., 2019; Fig. 3.1). This lenticular, NW-SE-trending body consists of strongly sheared metagabbroic-leucodioritic gneisses. This mafic unit has been traditionally grouped together with the Otanmäki gabbros owing to its position between the two lithological units (Kerkkonen, 1979), but it is not known to contain magnetite-ilmenite ore mineralization characteristic to the 2.06 Ga Otanmäki mafic intrusion (Lahti et al., 2018).

6.2 Otanmäki intrusion

6.2.1 Marginal amphibolites

Fine-grained, dark amphibolites have been observed at two locations between the Archean gneisses and Lower Zone gabbros and are referred to as marginal amphibolites. They share similarities in appearance with the multiple diabase dikes in the area, but lack a diabasic texture. Based on their similar mineral composition with the Lower Zone gabbros, they are regarded as belonging to the Otanmäki intrusion and possibly represent a lower chilled margin of the magmatic body.

At the SE flank of the Otanneva block, there is an occurrence of fine-grained, dark amphibolite (type sample OTA-10). The rock is pervasively recrystallized, consisting mainly of amphibole group minerals with minor equigranular plagioclase and dissemi-

nated pyrite (Fig. 6.3). The rock is extremely schistose and shows signs of ultramylonitic shearing.

A similar occurrence of amphibolite crops out at Rytisuo between Vuorokas and Metsämalmi (type sample VUO-20). The area is traditionally considered to represent the upper part of the Vuorokas block (e.g. Kerkkonen, 1979; Nykänen, 1995). Similarly to OTA-10, the grain size of the rock is less than 1 mm, it is dark in color and consists of c. 80% amphibole group minerals (Fig. 6.4). Regardless of the vicinity to the contact with the Archean basement, the marginal amphibolites at Vuorokas are only slightly schistose, whereas the foliation in the Otanneva marginal amphibolites is parallel to the hypothesized fault. The Vuorokas amphibolites also show local relics of primary plagioclase crystals with Am-group mineral overgrowths. Magnetite and ilmenite are present as accessory minerals.

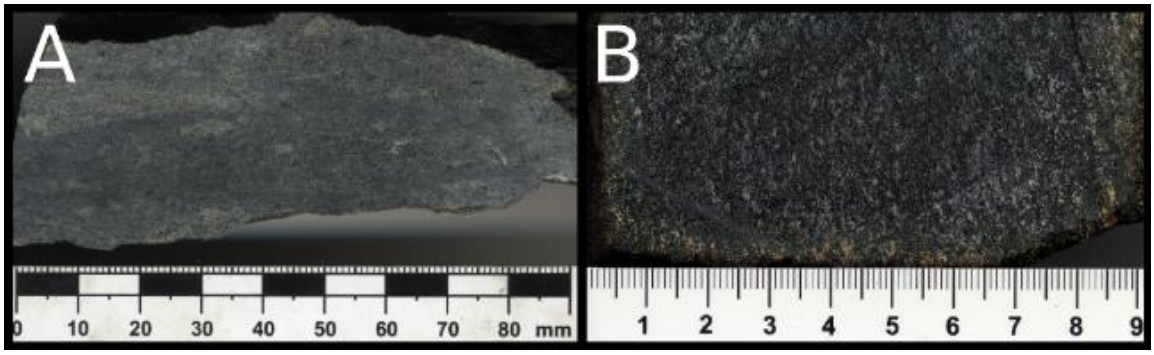

Figure 6.3. Scanned images of sawed hand samples of marginal amphibolite. A. Strongly sheared amphibolite from the SE margin of the Otanneva block (OTA-10) B. Less tectonized amphibolite from Rytisuo (AJMA-18-65).

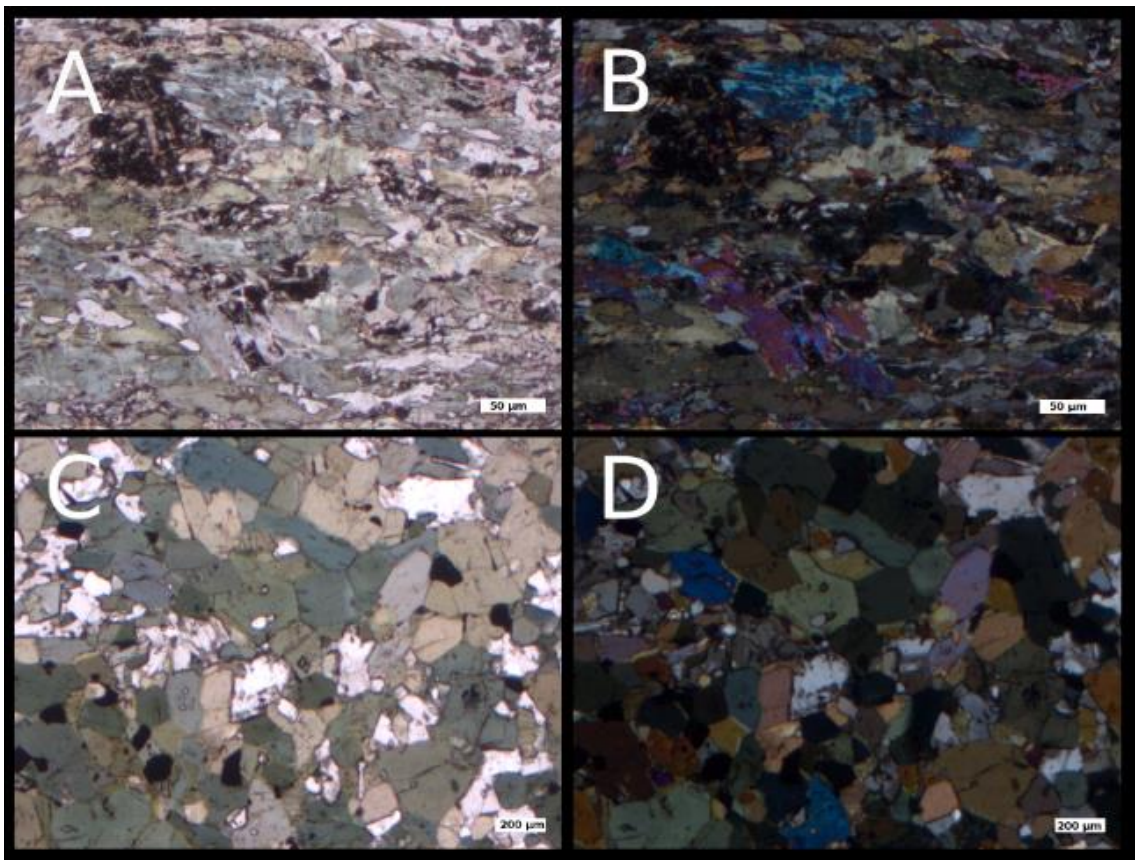

Figure 6.4. Photomicrographs of marginal amphibolites. A. and B., sample OTA-10, C. and D., sample VUO-20. A and C taken in plane-polarized light, B and D in cross-polarized light.

6.2.2 Lower Zone gabbros

The southern part of the Vuorokas block (at Rinneaho) has many well exposed outcrops of isotropic, medium- to coarse-grained melagabbro (Fig. 6.5). Gabbros in the Vuorokas Lower Zone vary from moderately schistose to non-schistose and have the best preserved magmatic features, with primary ortho- and clinopyroxene being observed in some hand samples from the SE flank of the Vuorokas block (Fig. 6.6). A similar gabbronoritic mineral assemblage is seen in thin sections from a depth interval of 60–70 m in drillcore VU 101. The rocks are meso- and adcumulates with occasional disseminated ilmenite.

The Lower Zone gabbros at Rinneaho have locally pegmatitic inclusions few cm to few m in diameter with clearly defined borders and a similar texture to that of the vari-textured gabbros. Drillholes from the upper part of the Vuorokas Lower Zone are reported to intersect anorthositic rocks (Nykänen, 1995). Based on outcrop observations, they do not necessarily represent laterally continuous layers but rather sporadic plagioclase-rich spots, possibly anorthositic vari-textured gabbros. Small-scale magmatic layering is seen in outcrop AJMA-17-192 in an otherwise isotropic gabbro.

The Lower Zone gabbros in the Otanneva block are melanocratic, medium grained and isotropic. Several outcrops portray large, euhedral plagioclase crystals up to 5 mm in size (ON-2, Fig. 6.5B and 6.6A). This porphyritic texture is regarded as primary rather than a result of metamorphic recrystallization. Similar large, euhedral plagioclase crystals are locally seen in gabbros at Rinneaho (AJMA-17-349).

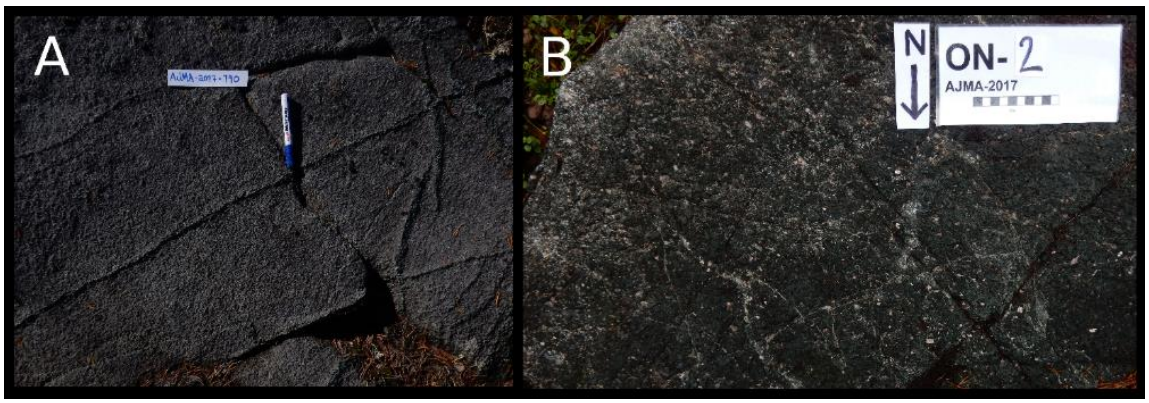

Figure 6.5. Outcrop images of Lower Zone gabbros. A. Isotropic melanogabbro at Rinneaho (AJMA-17-190) with a 14-cm-long pen pointing to the north. B. Isotropic gabbro with phenocrystic plagioclase at Otanneva (ON-2). Scale bar 10 cm.

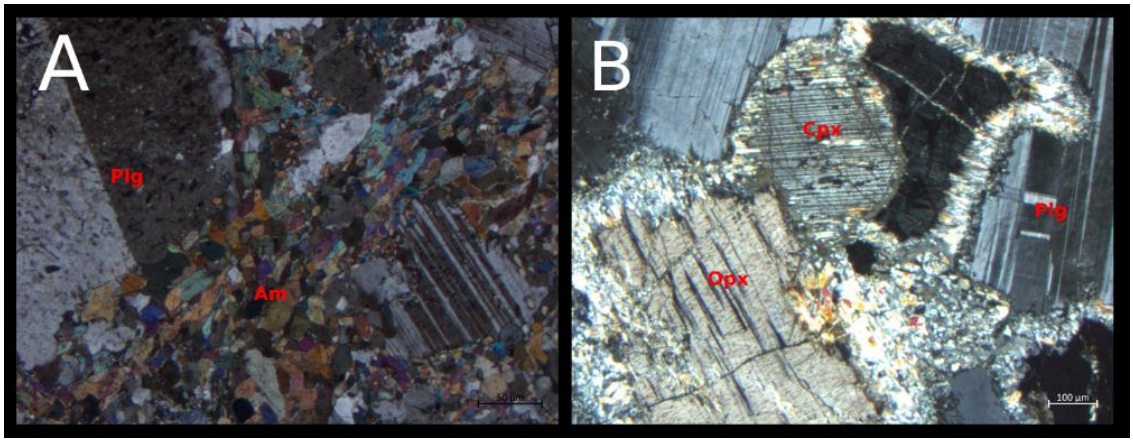

Figure 6.6. Photomicrographs of Lower Zone gabbros. A. Porphyritic gabbro from Otanneva with large, euhedral plagioclase crystals in a fine-grained groundmass (ON-2) B. Gabbronorite from the Vuorokas Lower Zone with primary pyroxenes still partly preserved. Sample from X-KKJ3: 3509070, Y-KKJ3: 7112010.

6.2.3 Lower Zone vari-textured gabbros (VTG)

Vari-textured gabbros are a voluminous rock type in the upper parts of the Lower Zone, especially at Vuorokas. The term vari-textured gabbro (also: *varied-textured gabbro* and *VTG*) is here applied to all leucocratic gabbroic rocks that show a large variation in grain size and color index on an outcrop scale. The term is used in unison with Peltonen and Kontinen (2004) who use it to describe gabbros in the Jormua ophiolite, which are coarse grained to pegmatoidal and show no clear modal layering. Lighfoot (2016) uses the term for gabbros with a great variation in grain size, which also applies to VTGs at Otanmäki and Vuorokas.

After London (2008), an extremely coarse or varying grain size or skeletal crystal habit would qualify a rock as pegmatitic. Here the term “vari-textured gabbro” is nevertheless chosen to cover both pegmatites and coarse-grained cumulate gabbros. Pegmatites are described separately when needed.

Vari-textured gabbros are more leucocratic than other gabbro types in the Otanmäki intrusion apart from the anorthositic autoliths. The variable grain size and mineral proportions in the VTGs appear usually on an outcrop scale of few meters (Fig. 6.7). The degree of textural variation, however, fluctuates from place to place and results in some level of uncertainty when discriminating between Lower Zone gabbros and VTGs: a small outcrop of seemingly isotropic gabbro might just be a local, more homogenous fraction of VTG. Vari-textured gabbros do not form a uniform layer but a convoluted unit with gradational and arbitrary contacts to Lower Zone gabbros.

VTG textures are best observed macroscopically (Fig. 6.8). Microscopic examination of Rinneaho pegmatites reveals large primary plagioclase crystals, which are recrystallized at crystal margins (Fig. 6.9). Rocks display ad-, meso- and orthocumulate textures. Primary mafic minerals are rare; few samples contain primary bronzite. Amphibole group minerals typically constitute an intercumulus groundmass composed of cryptocrystalline to 1.0-mm-sized grains. Pegmatitic rocks at Rinneaho are also characterized by ubiquitous disseminated sulfides.

A type occurrence of vari-textured gabbro is found at Rinneaho near the Vuorokas mine tower and a nearby aggregate quarry. The grain size variation in these outcrops is large, and pegmatitic, up to 50-cm-long individual crystals are observed regularly. At Rinneaho, the outcrop coverage is very good and the VTGs can be distinguished confidently from isotropic Lower Zone gabbros. VTGs are a dominating feature below the western part of the Vuorokas Ore Zone, but in the eastern part, isotropic gabbros dominate.

Dominantly pegmatitic VTGs are also seen at Rytisuo between Otanmäki and Vuorokas. This previously almost unstudied area has contacts to marginal amphibolites in a similar way as in the Otanneva block. The degree of tectonic strain in the Rytisuo VTGs increases when moving northwest towards the Metsämalmi area. Heavily sheared

wedges of leucocratic gabbro with a maximum width of 70 m that are found at Metsämalmi are regarded as a continuation of this unit. The leucogabbroic wedges are larger than any of the anorthositic inclusions, they have less oxide minerals than the surrounding gabbros and are positioned at the lowermost part of the Ore Zone. It is possible that the VTGs at Metsämalmi represent leucogabbroic autoliths in the Ore Zone rather than Lower Zone rocks, but because of their size, position and the fact that they are not seen to be surrounded on all sides by Ore Zone rocks, as the autoliths are, characterize them as Lower Zone varied-textured gabbros.

In the Otanneva block, the Lower Zone VTGs are dominantly coarse grained and, compared to the corresponding rocks at Vuorokas, their grain size varies less and distinction between VTG and isotropic gabbros is less straightforward. The whole Lower Zone at Otanneva could also be described as being composed of isotropic gabbro with sporadic occurrences of VTG (or vice versa).

In the aggregate quarry at Vuorokas, the VTGs show gradational change to rhythmically layered gabbros (Fig. 6.10). This layered unit reaches an approximate width of 50 m and dips to the north at an angle of 85°. The outcrops of the layered unit represent the nearest outcrops to the Vuorokas Ore Zone.

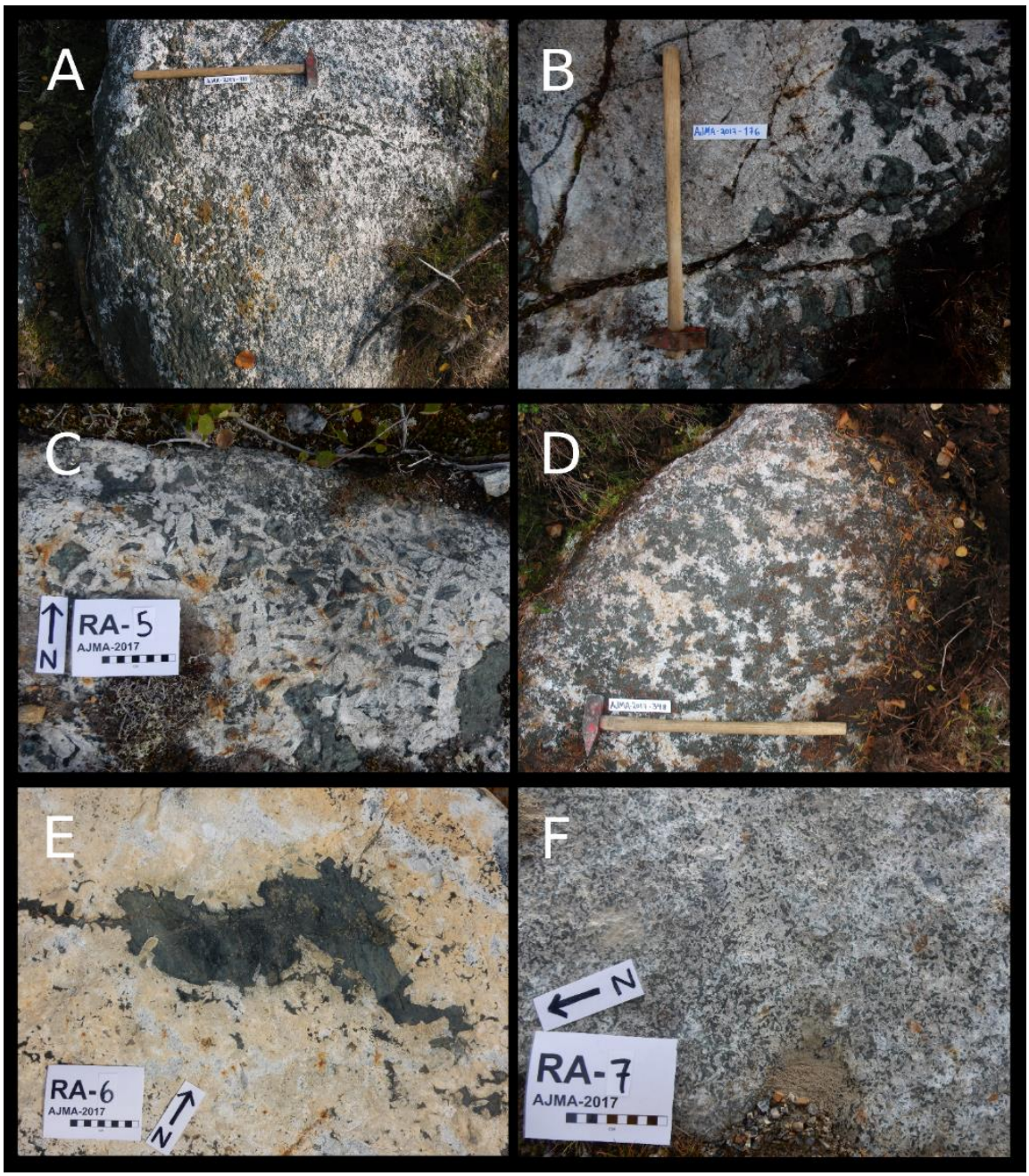

Figure 6.7. Outcrop images of vari-textured gabbro. A. Irregularities in the grain size and modal proportions over a distance of one meter; a typical VTG structure (AJMA-17-310). B. Gabbro pegmatite and anorthositic adcumulate (AJMA-17-176). C. Pegmatoid with large euhedral plagioclase at Rinneaho (RA-5). Scale bar 10 cm. D. Mottled anorthosite (AJMA-17-348) E. Coarse plagioclase cumulate with fine-grained ultramafic intercumulus material (RA-6). F. Medium-grained mesocumulate (RA-7). In A, B and D, 60-cm-long hammer points to the north.

Figure 6.8. Scanned image of a hand sample of vari-textured gabbro (RA-2B). Meso- to adcumulate textures and a great variation in grain size are typical for the VTGs.

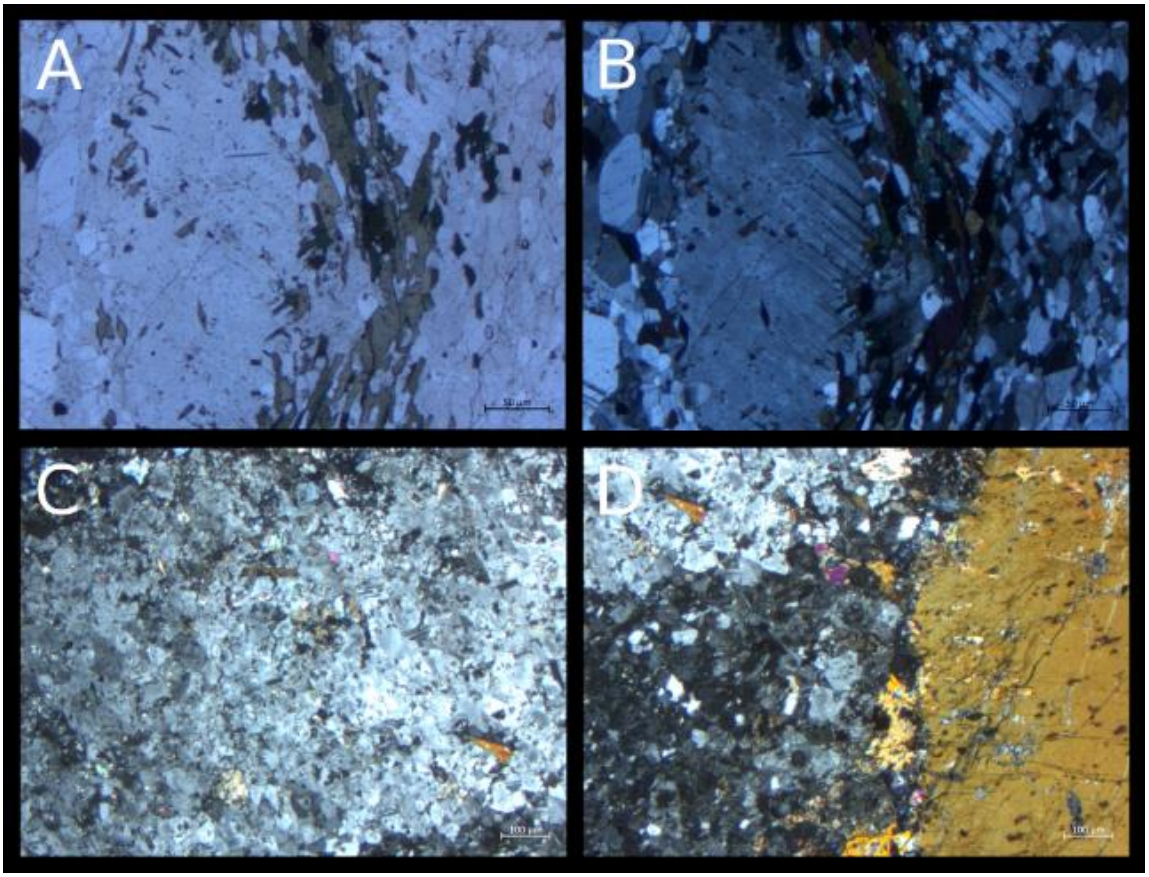

Figure 6.9. Photomicrographs of vari-textured gabbros. A. and B. Large primary plagioclase crystal surrounded by equigranular plagioclase and amphibole grains in a strongly sheared rock. MEM-4, plain- and cross-polarized light. C. Central part of a large plagioclase completely re-crystallized to smaller grains. Cross-polarized light. D. Contact between recrystallized plagio-clase and a large amphibole crystal (continuation of C).

Figure 6.10. Vertical modal layering in the Vuorokas Lower Zone. Layering likely marks the transition from VTG-pegmatoids to Ore Zone rocks. Length of the measuring stick is 1 m.

6.2.4 Ore Zone and Fe-Ti-V oxide ore

Borders of the Ore Zone on the map of Fig. 6.1 are mainly delineated after aeromagnetic anomalies. Based on observations from Metsämalmi and Vuorokas, its lower contact with Lower Zone isotropic gabbros or VTGs is sharp. In contrast, the upper contact is gradational. Both Ore Zone and Upper Zone consist of gabbro, gabbro amphibolite, magnetite gabbro and anorthositic autoliths, but the relative amounts of the rock types differ. The Ore Zone is dominated by magnetite-rich gabbro, gabbro amphibolite and oxide ore lenses and layers, whereas the Upper Zone is mostly gabbroic.

The ore lenses and layers are hosted by gabbro, gabbro amphibolite and magnetite gabbro. The rock types differ in terms of their degree of tectonic strain and oxide mineral content. The Ore Zone gabbro is melanocratic and small to medium grained (Figs. 6.11 and 6.12) and varies texturally from isotropic to moderately foliated. Gabbroic rocks in the Ore Zone often have disseminated ilmenite (+ magnetite). In many places, ilmenite grains are recrystallized to rutile or titanite. In areas of high tectonic strain, the rock is recrystallized into gabbro amphibolite. The term “gabbro amphibolite” is widely used in previous studies, for example, in all surface maps and drill core logs by Rautaruukki

Oy. Here the term is used in unison with Pääkkönen (1956), Kerkkonen (1979) and Paarma (1961), referring to dark, hornblende-rich, fine-grained rock which is often tectonically strained to having an almost schistose appearance. Magnetite gabbro, a gabbro type with abundant disseminated magnetite, is present throughout the Ore Zone and in rocks above it.

The Ore Zone rocks portray occasionally modal magmatic layering, although it is not a dominating feature. The layering is present in cm-scale changes in the mineral mode and is occasionally coupled with differences in the relief of outcrop surfaces as more mafic layers have partly been weathered away. In the least deformed parts of the Metsämalmi outcrop area, for example, modal magmatic layering in magnetite gabbro can be followed along strike for about 10 meters. Areas of moderate to strong degree of tectonic reworking portray also several up to 2-m-wide units with layering, but their magmatic origin is questionable.

At Vuorokas, oxide ore crops out only in the old open pit representing a central part of the Vuorokas block, where it is present as bifurcated layers and lenses 2–10 m in width and more than 90 meters in lateral continuation (Fig. 4.4; Rautaruukki Oy, this study). In its contact towards a large leucogabbroic autolith, the oxide ore displays structures that potentially represent magmatic lamination. Oxide ore in the Vuorokas open pit has a sharp southern contact to a minor occurrence of mottled anorthosite (AJMA-18-30), which is either a minor VTG occurrence or a large autolith.

Thin sections from drillholes intersecting the Vuorokas Ore Zone (VU 78, VU 85, VU 92, VU 93, VU 112 and VU 114) reveal a set of rock types similar to those found in outcrops: gabbro, (magnetite) gabbro amphibolite, varyingly sheared anorthosite and class I–III ore. Alteration minerals such as chlorite are met in drillcore and ground samples alike.

A major surface occurrence of oxide ore at Otanmäki is present in the approximately 3-hectare Metsämalmi outcrop area, where the ore forms branched layers and lenses. Class I ore is often surrounded by class II ore and magnetite gabbro, with a gradational contact between the ore types. Gabbro is mostly recrystallized to amphibolite. Anor-

thositic to leucogabbroic autoliths are found within all rock types: oxide ore, gabbro amphibolite, and magnetite gabbro. The primary lithological features at Metsämalmi are overprinted by strong tectonic reworking and many ore layers and ore lenses are tectonically thickened or stretched.

Solitary ore lenses are also met above the main magnetic anomaly, i.e., above the Ore Zone. In these occurrences, the ore is present as rounded lenses less than 2 m in diameter and share contacts with isotropic Upper Zone gabbros and anorthositic autoliths.

Class I massive-semimassive ore consists of sub- to anhedral magnetite and ilmenite grains and chlorite (Fig. 6.13). Ilmenite is present as euhedral to subhedral grains up to 0.25–5.0 mm in diameter. A minor silicate mineral is chlorite, which is present as interlayers and inclusions and takes up to approximately 10% of the total volume. A small amount of recrystallized plagioclase is also present in class I ore (sample OTA-6).

Compared to class I ore, class II ore contains more chlorite and minor sulfides and is also more strongly foliated. Similar to class I ore, ilmenite is present as euhedral grains of 0.25–3.0 mm in diameter in the magnetite dominated ore. Euhedral to subheral, acicular amphibolite group minerals constitute a minor silicate mineral group in the matrix. Again, contrarily to Rautaruukki Oy's classification, almost no plagioclase is visible in the studied sample (MEM-2).

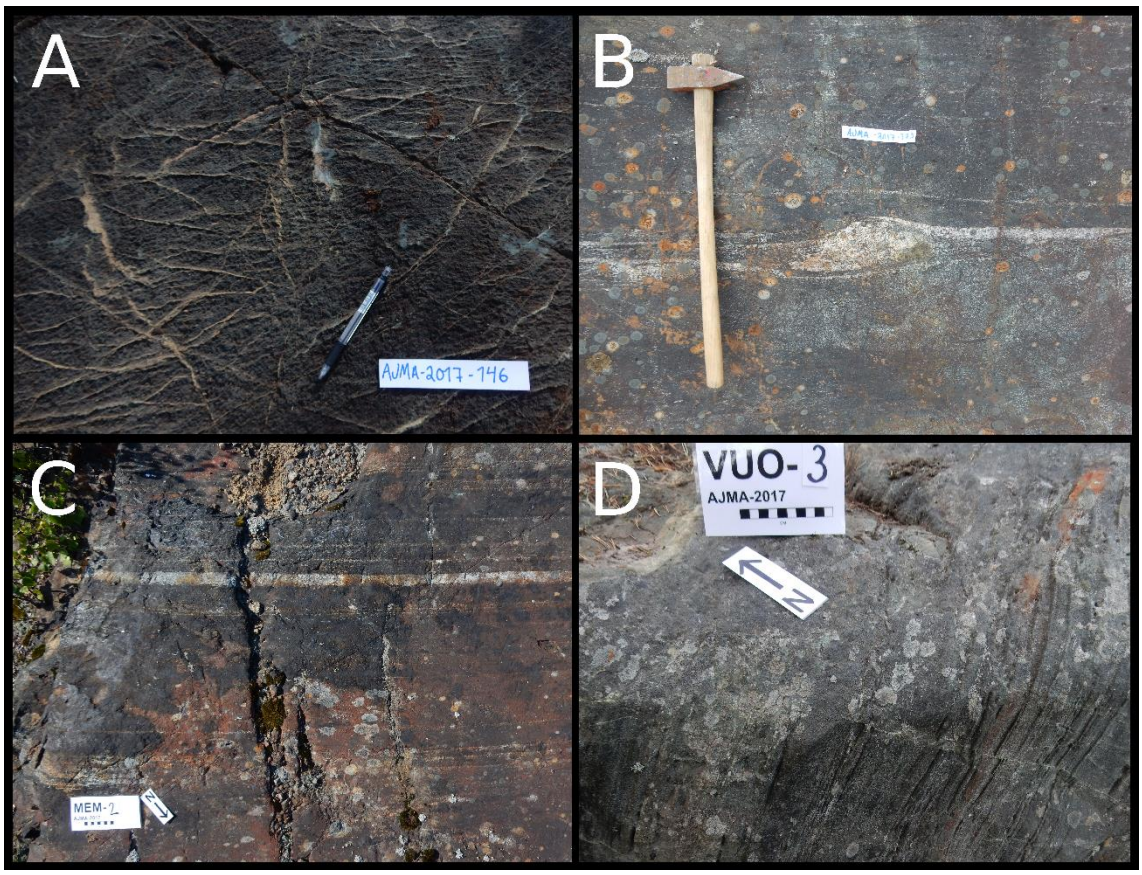

Figure 6.11. Outcrop photographs of Ore Zone rock types. A. Isotropic gabbro from Vuorokas (AJMA-17-146). 14-cm-long pen points to the north. B. Gabbro amphibolite from Metsämalmi (AJMA-17-173). 60-long hammer points to the north. C. Modally layered magnetite gabbro from Metsämalmi. Scale bar 10 cm. D. Oxide ore from the Vuorokas open pit with potential preserved magmatic lamination (VUO-3).

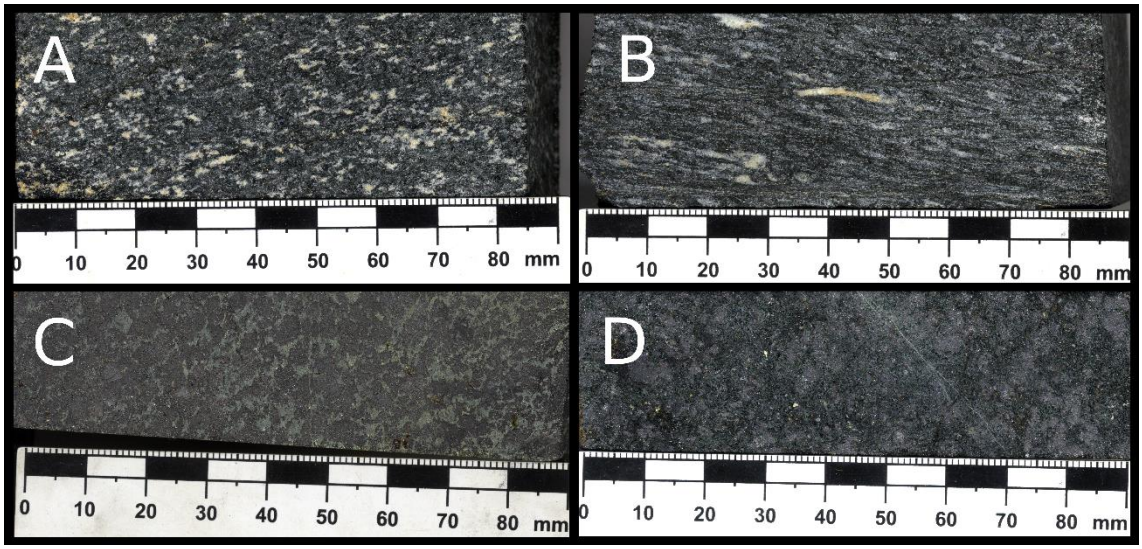

Figure 6.12. Scanned images of Ore Zone rock types. A. Gabbro (OTA-1B) B. Gabbro amphibolite (VUO-15). C. Class I ore (OTA-6). Main silicate mineral, chlorite, fills the space between oxide crystals. Magnetite and ilmenite are separated to large individual grains. D. Class II ore (MEM-2).

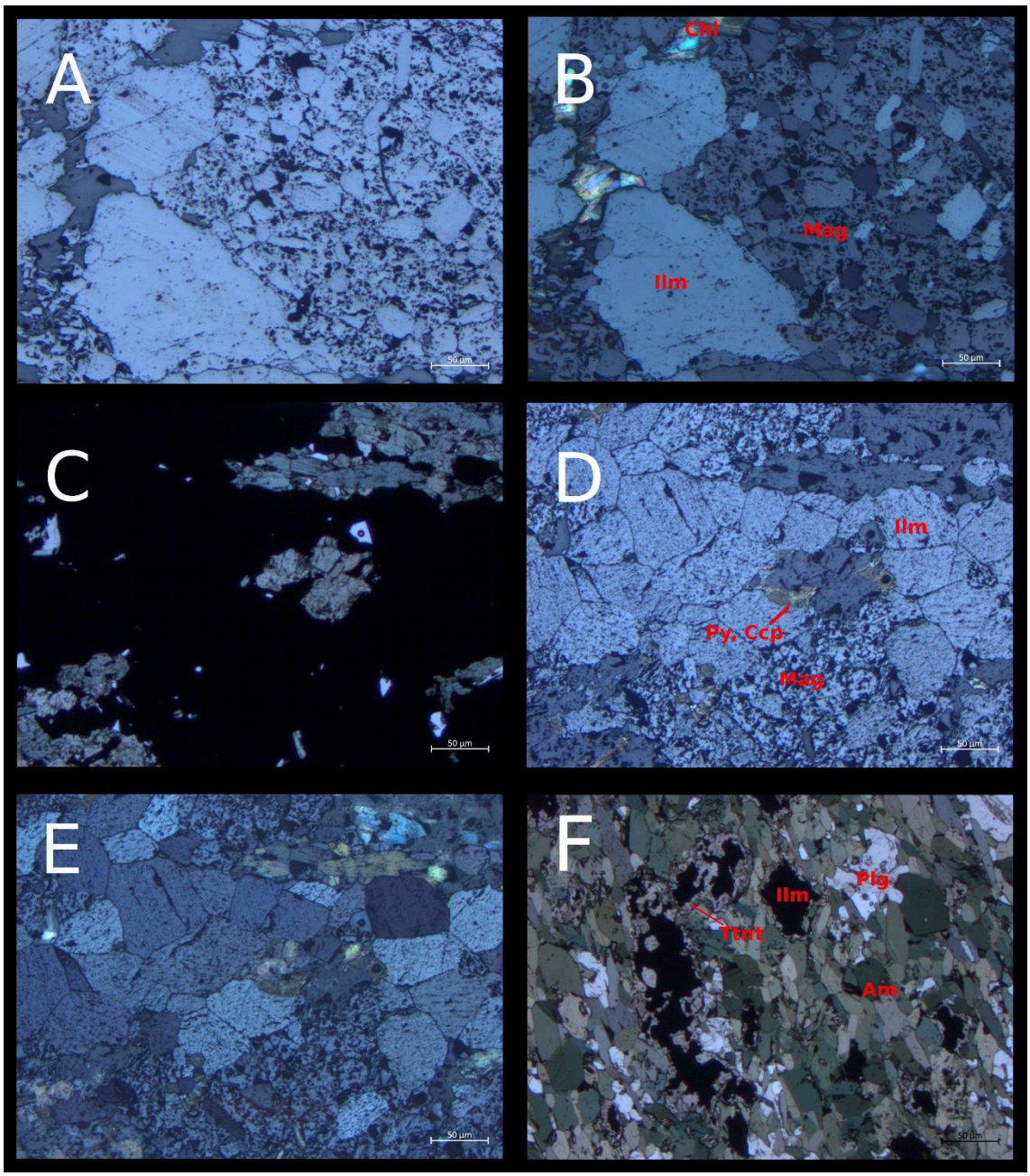

Figure 6.13. Photomicrographs of Ore Zone rocks from Otanmäki. A and B. Class I ore, plain- and cross-polarized reflected light (OTA-6). C., D. and E. Class II ore, cross-polarized transmitted light, plain and cross-polarized reflected light (MEM-2). Minor pyrite (Py) and chalcopyrite (Ccp) occur in the magnetite (Mag) and ilmenite (Ilm) dominated sample. F. Gabbro (OTA-1B). Amphiboles (Am) and plagioclase (Plg) are the most common silicate minerals. Ilmenite is present as an accessory oxide mineral, and it is recrystallized to titanite (Ttnt), and to smaller extent, rutile, on its borders.

6.2.5 Upper Zone

The Ore Zone shifts gradually into the overlying Upper Zone, which is observed in changes in ratios of rock types. The rocks are principally the same, but in Upper Zone, isotropic, untectonized gabbro dominates (Fig. 6.14). Anorthositic autoliths are met in almost all Upper Zone outcrops. At Otanmäki, the outcrop coverage in the upper part is good, whereas at Vuorokas, most of the upper part is under a thick peat cover and the northernmost field observations are just 200 m north of the Ore Zone.

Similarly to the Ore Zone rock types, small-scale layering is infrequently observed in the otherwise isotropic Upper Zone gabbros. At Otanmäki, this layering is present as subtle changes in mineral proportions in otherwise homogenous gabbro. Rarely, in the vicinity of autoliths, vertical layering is seen to be conformable with the autolith borders both at Otanmäki and Vuorokas (Fig. 6.14D and 6.15). Similarly to the Ore Zone rocks, layering is not a prominent feature and cannot be followed along strike for more than a few meters.

The Otanmäki and Vuorokas gabbros are devoid of apatite apart from few minor occurrences in the Vuorokas Lower Zone (Nykänen, 1995). Apatite gabbro is locally present in the generally phosphorus-poor Upper Zone at Otanmäki (X-KKJ3: 3505152; Y-KKJ3: 7113236) (Fig. 6.16; A. Kontinen, pers. comm., 2018). The occurrence of apatite is rare, but locally plentiful apatite implies that apatite saturation was reached at least in a restricted parts of the magma chamber during the crystallization of the Upper Zone gabbros.

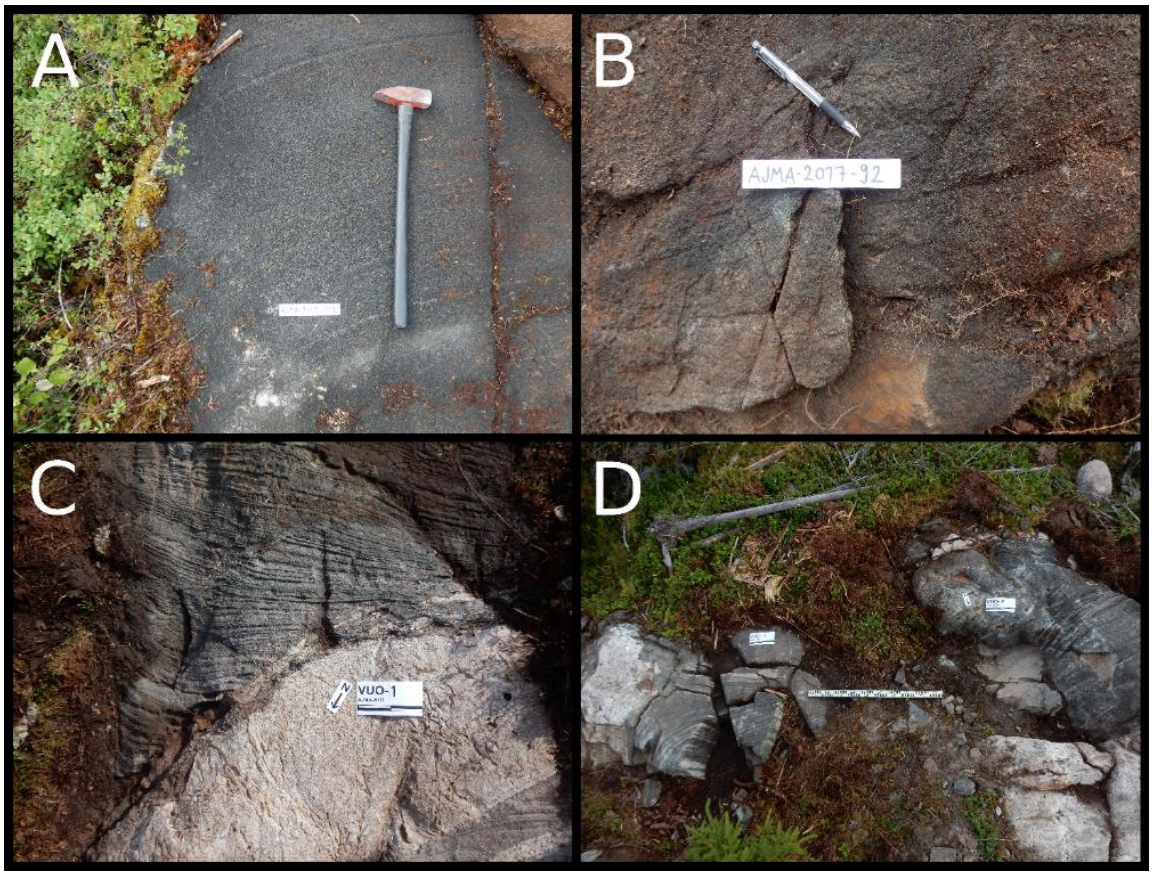

Figure 6.14. Outcrop images of Upper Zone gabbros. A. Layered gabbro from Otanmäki (AJMA-17-107). 60-cm-long hammer points to the north. B. Isotropic gabbro from Vuorokas (AJMA-17-92). 14 cm long pen points north. C. A-type granitic vein cutting magmatic laminae in Vuorokas Upper Zone gabbro (VUO-1). Scalebar 20 cm. D. Curved modal layering at Vuorokas (VUO-7, VUO-8). Length of the measuring stick is 1 m.

Figure 6.15. Scanned image of a hand sample of layered gabbro from the Vuorokas Upper Zone (VUO-7). This rock represents an approximately 10-m-long and 1-m-wide zone seen to follow the borders of anorthositic autoliths (Fig. 6.14D).

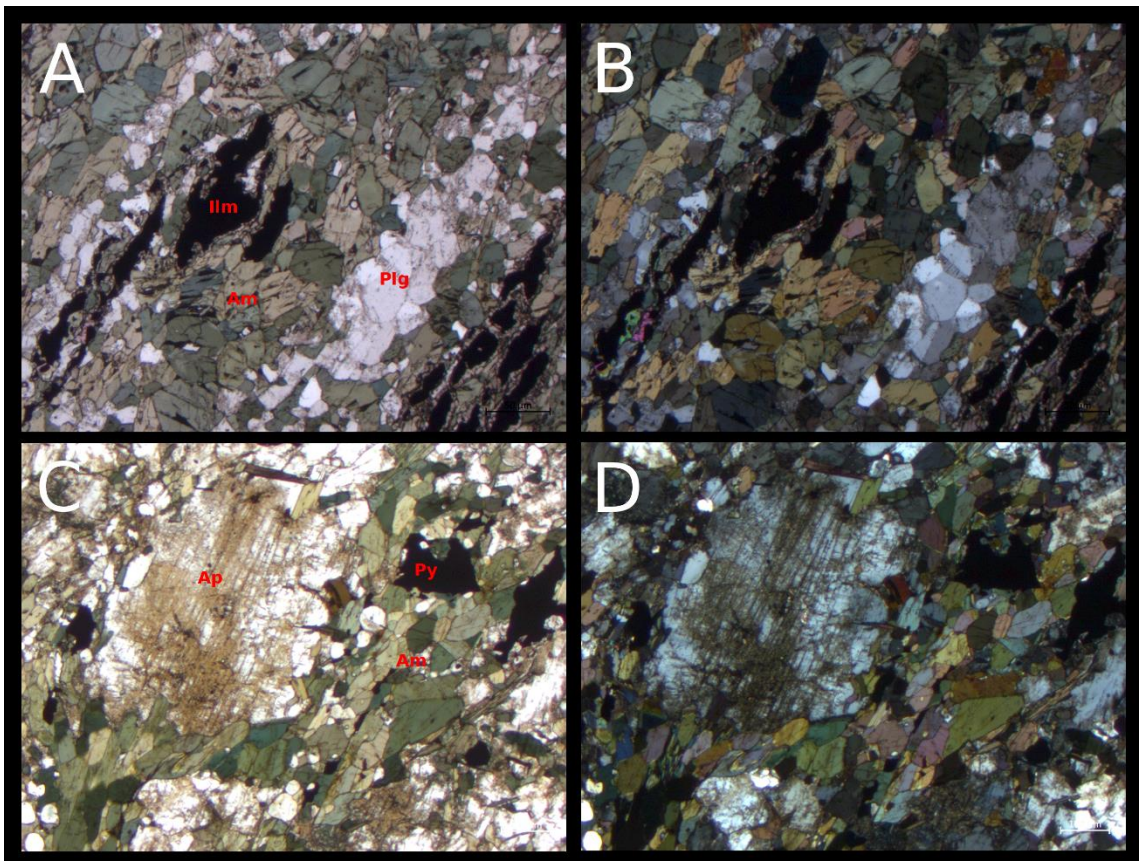

Figure 6.16. Photomicrographs of Upper Zone gabbros. A and B. Gabbro amphibolite from Vuorokas (VUO-15), plain- and cross-polarized light. C. and D. Apatite (Ap) gabbro from Otanmäki, plain- and cross-polarized light.

6.2.6 Mafic and felsic dikes

Several dikes from few centimeters to few meters in width crosscut older rock units in the Otanmäki area, including the Archean basement, Otanmäki suite A-type rocks, Katajakangas metaturbidites, and the Otanmäki intrusion rocks. Diabase dikes up to 20 m in width are met within the A-type granites and intermediate rocks whereas only minor dikes cut the Otanmäki intrusion: two of them have been observed in the Lower Zone at Vuorokas and one in the Lower Zone at Otanneva. The smaller dikes are anything between few centimeters to few meters in width and can be locally followed for tens of meters. They are tectonically relatively undisturbed and usually have a vertical position. Similar minor dikes are reported by Kerkkonen (1979) to occur at the +425 level in the Otanmäki mine. Minor diabase dikes are also present in the surrounding Archean gneisses, often striking parallel to major faults.

Fine-grained A-type granite dikes are observed in two outcrops at Vuorokas. They are approximately 1 m thick and can be followed laterally for 1–4 meters (Fig. 6.14C). Similar dikes also cut Otanmäki Upper Zone gabbros near the contact to the Otanmäki suite A-type rocks. The dikes also have A-type granite chemistry but they have not been dated, rendering it unclear whether they belong to the Otanmäki suite (Kärenlampi et al., 2019).

More coarse-grained and quartz-rich, narrow dikes of pegmatitic granite are seen in a layered Lower Zone gabbro in the Rinneaho quarry. Pöschl (1964), Kerkkonen (1979) and Marmo et al. (1966) have also reported veins of microcline granite and albite-quartz veins from the +125 and +255 levels of the Otanmäki mine. Pegmatite granite also cuts diabase dikes in the Archean basement (A. Kontinen, pers. comm., 2017).

6.3 Deformation and metamorphism

Otanmäki and Vuorokas blocks are separated from each other by a SE-NW- or N-E-trending fault or several faults (e.g. Lindholm and Anttonen, 1980; Havola, 1997; this study). The eastern part of the Otanmäki block is further separated by sinistral faulting from the Otanneva block, which is again split into half with a sinistral fault of a similar orientation. SE-NW-trending faults are also present at Vuorokas where they cut the Ore Zone into four structural domains (Nykänen, 1995; Parkkinen, 2015). Most of the faults within the intrusions are lateral strike-slip faults, with a major documented movement having been occurred along the strike. They run from SE to NW and can be sinistral or dextral.

Based on interpretations of geophysical data, the poorly exposed NE part of the Vuorokas intrusion block (at Rytisuo-Virsusuo, between Otanmäki and Vuorokas) is complexly faulted and may consist of several smaller tectonic blocks of the Otanmäki intrusion gabbros and/or other rock types, as suggested by Havola (1997). The southernmost tip of the Vuorokas block is completely unexposed and has not been subject to drilling campaigns.

The Otanmäki intrusion shares its 8-km-long upper contact with the Otanmäki-Kuluntalahti nappe. The contact is evident in the northern parts of the Otanmäki hill and

the Metsämalmi outcrop area, being manifested by an approximately 165°/85°-oriented extreme schistosity in both the A-type rocks and the gabbros. The northern contact of the Otanmäki block and Otanmäki suite A-type rocks is also confirmed by underground drilling by Rautaruukki Oy.

The southern contact between the Otanmäki block and Archean migmatites is likely a major fault with possibly both horizontal movement and thrusting. Although the contact is not exposed, geophysical measurements and the strong schistosity at the intrusion borders indicate closeness to a dominant fault system. As illustrated in Fig. 6.17, the Otanmäki intrusion block shows a roughly W-E-trending strike and a deep dip towards N or S. In the western limb of the Ore Zone at Otanmäki, the schistosity forms a large semicircle, following the sinistral folding of the Ore Zone. The orientation of the Ore Zone fold is also observed in roughly 275°/75°-dipping minor folds in the Otanmäki Upper Zone gabbros. Similar J-shaped anomalies of low conductance, indicating potential sheared faults, are seen in the aerogeophysical maps.

The eastern and western flanks of the V-shaped Vuorokas block are regarded to be controlled by faults. The nearest outcrops on both sides are at a distance of about 150 m from the margin faults. The rocks at each flank show a tectonic orientation parallel to the faults, but the schistosity is not as definite or intensive as at Otanmäki, suggesting a lesser amount of movement along strike. The central parts of the Vuorokas block are mostly undeformed. A penetrative, approximately 240/65-dipping mineral lineation is characteristic to the Upper Zone gabbros in the eastern part of the Vuorokas block.

A group of marginal amphibolite outcrops at Rytisuo is the only location where contacts of the Vuorokas gabbro and the adjacent TTG gneisses can be pinned down with an accuracy of a few meters. The contact is regarded as untectonized: the Vuorokas marginal amphibolites show non-coherent degrees and orientations of tectonic strain and, similarly to the adjacent VTG, are relatively undeformed. The degree of tectonic strain observed in the Rytisuo VTGs increases steadily when moving from Rytisuo to NW towards Otanmäki, culminating to gneissose foliation in the rocks near the Metsämalmi area.

In the Otanmäki area, middle amphibolite facies dominates in the Paleoproterozoic rocks (Zelt, 1974; Kärenlampi et al., 2019). Fluid flow and metamorphic rehydration are evident from amphibolitization of mafic rocks at Otanmäki and Vuorokas. Amphibolite facies metamorphism has mostly destroyed primary magmatic features: plagioclase is largely recrystallized and equigranular, and mafic silicates are pervasively recrystallized to hornblende or other amphibole group minerals. Recrystallization is a prominent feature in the Ore Zone, which has undergone the most intensive tectonic shearing. Many of the Ore Zone rocks show chloritization. Epidote is also a common accessory mineral (Fig. 6.18). Ilmenite, when occurring as a minor phase in gabbroic rocks, is often altered to rutile (TiO_2) and titanite ($CaTiSiO_5$). In the Vuorokas Lower Zone, VTG pegmatites near to fracture zones have been locally subjected to potassium alteration.

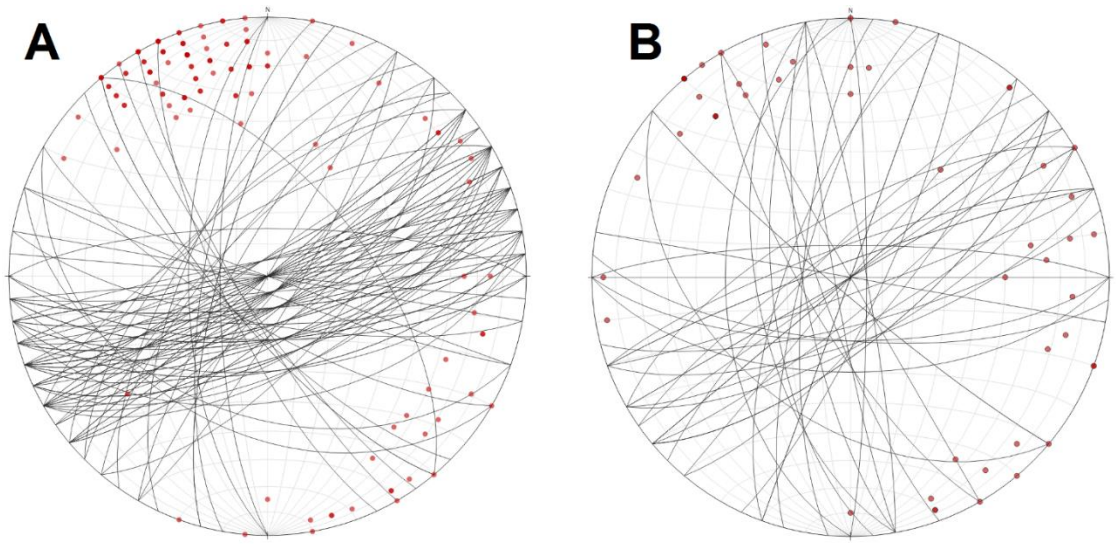

Figure 6.17. Stereonet projection of structural elements from the Otanmäki intrusion. A. Schistosity, Otanmäki block, 125 measurements. The Otanmäki block and especially the Ore Zone are characterized by a steep schistosity dipping with an average orientation of 80°/312°. B. Schistosity, Vuorokas block, 50 measurements. Schistosity in the Vuorokas area is less prominent although a similar trend to that at Otanmäki can be observed from the otherwise scarce data.

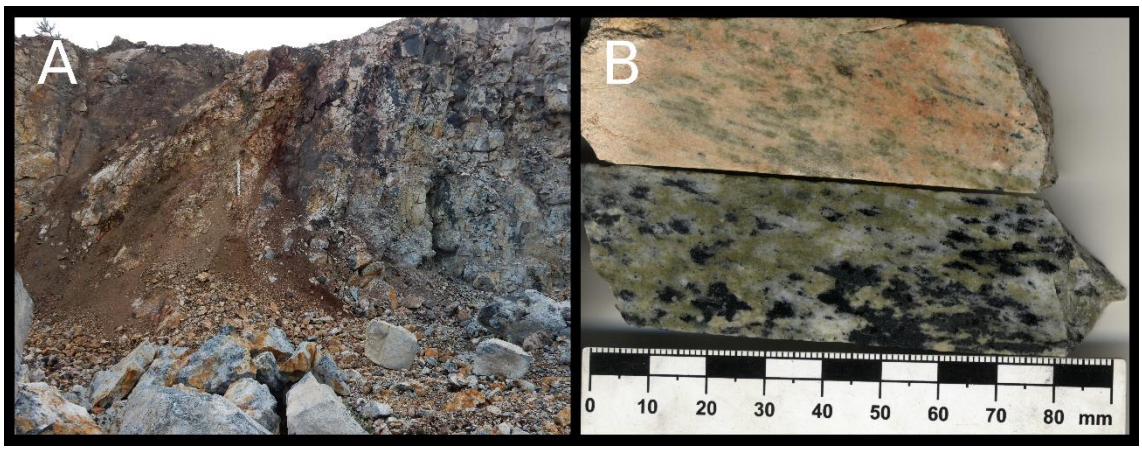

Figure 6.18. Signs of hydrothermal alteration in the Otanmäki intrusion rocks. A. Hydrothermal alteration around a heavily sheared fault in the Lower zone VTGs at Vuorokas. Length of the measuring stick is 1 m. B. Scanned image of rock slabs showing pervasive potassium alteration and epidotization in an anorthositic autolith (VUO-5).

7 ANORTHOSITIC AUTOLITHS

7.1 Position in the stratigraphy

The presence of light-colored, often rounded inclusions of plagioclase rich rocks are seen throughout the Ore Zone and Upper Zone in almost every outcrop both at Otanmäki and Vuorokas. The Ore Zone rocks at Otanneva are in general poorly exposed, but the few outcrops within the area reveal similar features.

Autoliths were mapped and studied in detail in three main outcrop areas, Otanmäki, Metsämalmi and Vuorokas (see Fig. 5.1.). These areas represent both different heights in the magmatic stratigraphy and lateral positions in the intrusion: the Ore Zone (Metsämalmi, MEM), Ore Zone-Upper Zone transition (Otanmäki, OTA), and the Upper Zone (Vuorokas, VUO).

Samples for thin sections and detailed mineralogical-chemical analyses were taken from small (<1 m), medium-sized (1–3 m) and large (>3 m) inclusions. Sample locations were selected in a way that all autolith sizes, textures and shapes could be covered as well as possible. Two autoliths (OTA-5 and OTA-3) were sampled both from the center and border to study mineralogical variations within a single autolith.

The autoliths are dominantly anorthosites in their mineral composition. Some autoliths contain more mafic minerals and could be classified as gabbroic anorthosites (Ashwal, 1993). However, in unison with previous studies (e.g., Talvitie and Paarma, 1980), the autoliths are referred to as “anorthositic autoliths” albeit that a small fraction of them are in fact leucogabbroic in composition.

Figures 7.1 and 7.2 present detailed maps from autolith-bearing areas in the Ore and Upper Zones. In addition to hand samples and microscopic studies, aerial photographs, historical data by Rautaruukki Oy, and field observations from the 2017–2018 mapping campaign were used to construct these maps. Sampling locations are marked on the maps.

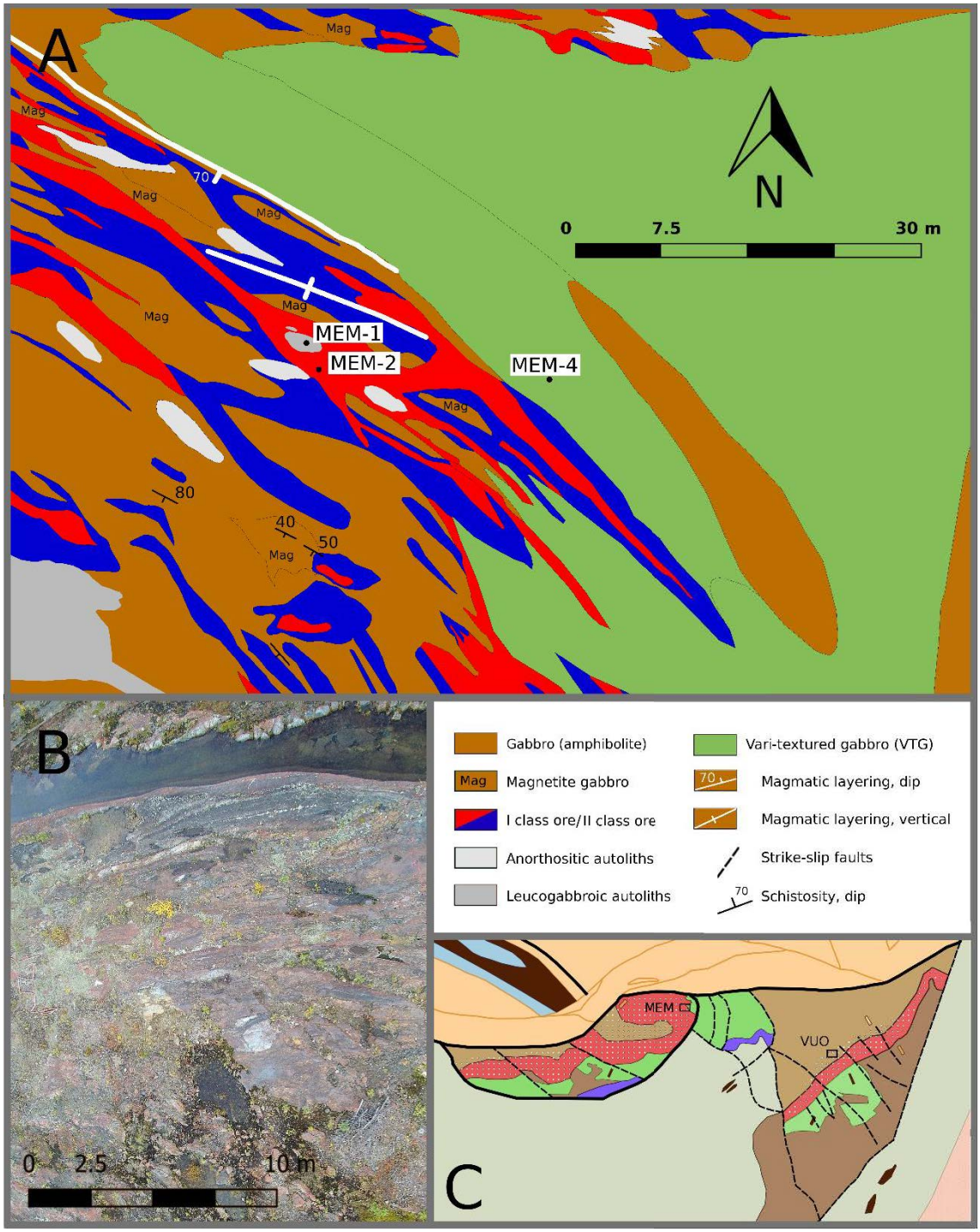

Figure 7.1. Anorthositic autoliths in the Ore Zone at Metsämalmi, Otanmäki. A. Detailed geological map from the SE part of the Metsämalmi outcrop area. Dominantly rounded autoliths of few meters in diameter are found in all Ore Zone rock types. B. Aerial photograph from the same area. Autolith MEM-1 can be seen in the middle. C. Locations of the mapping areas marked with black rectangles on the Otanmäki intrusion map. Legend as in Fig. 6.1.

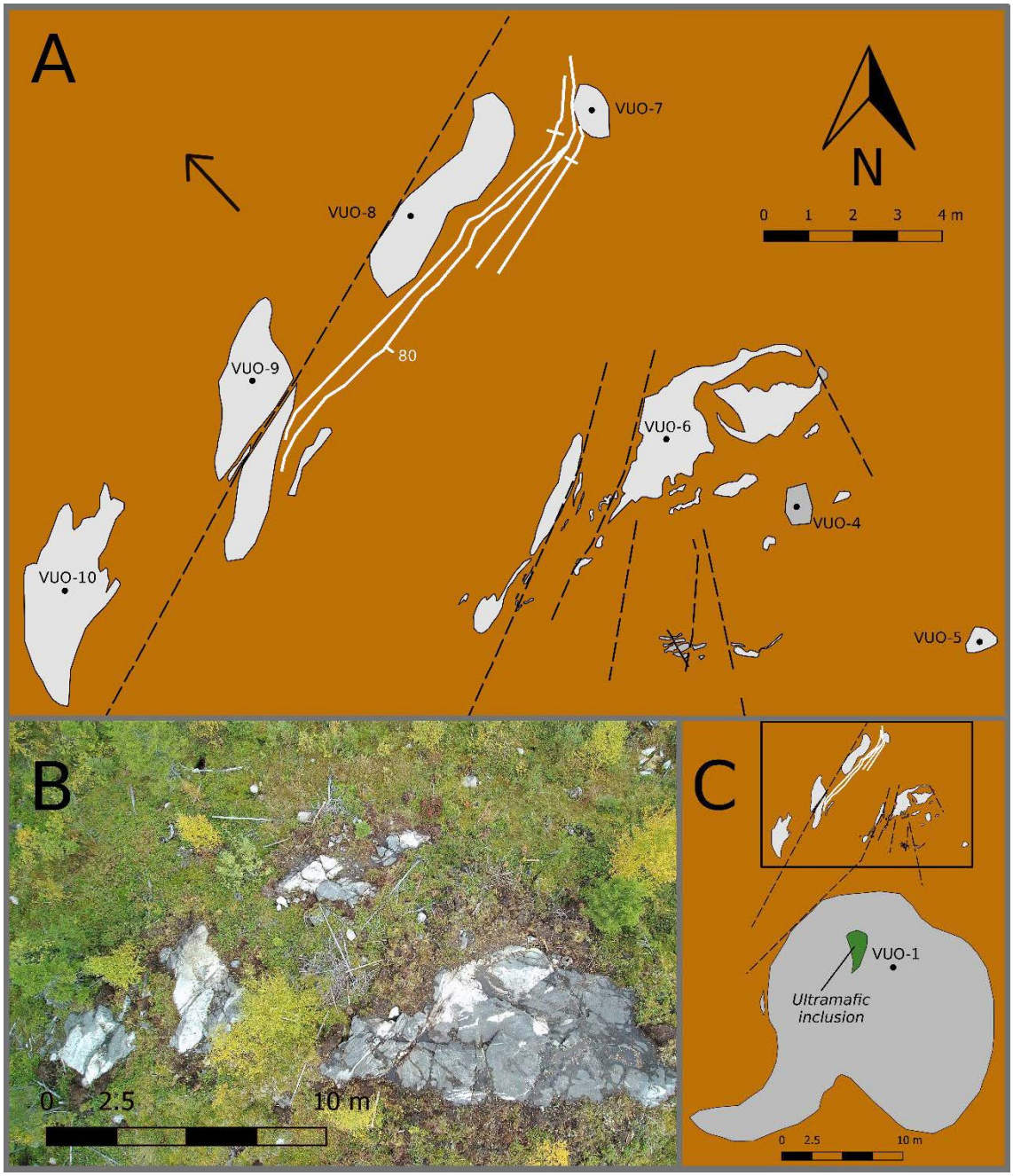

Figure 7.2. Anorthositic autoliths in the Upper Zone at Vuorokas. A. Detailed geological map from the Vuorokas outcrop area. Autoliths with different sizes and shapes are seen: angular (VUO-4), rounded (VUO-5) and irregular with wedges protruding surrounding rocks (VUO-6). Borders with outward broken halo of smaller fragments can be seen at VUO-6 and neighboring autoliths with small fragments separated from them. Arrow points the top of magmatic stratigraphy. Legend as in Fig. 7.1. B. Aerial photograph from the same area. C. Closer view showing the largest leucogabbroic autolith (sample VUO-1), in the Vuorokas area.

7.2 Descriptions of autoliths and their contact relations

Autoliths are most commonly hosted by gabbro amphibolite in the Ore Zone and gabbro in the Upper Zone. In the Ore Zone, inclusions may also either share contacts with the ore or be completely enveloped by it. Most commonly, the size of an autolith is around 1–3 m but the smallest autoliths are just tens of centimeters in diameter, whereas the largest ones are more than 30 m across, covering an area of more than 500 m^2. According to an underground mine map by Rautaruukki Oy (Fig. 4.2), autoliths above the Ore Zone are larger than those within it, reaching a diameter up to 100 meters. The trend of larger autoliths occurring higher in the magmatic stratigraphy is observed on the surface, too. The two largest mapped autoliths (VUO-1 and OTA-5) are both roughly 30 meters in diameter, show variations in their texture and occur either in the Ore Zone-Upper Zone transition or above it.

The autoliths show a great variation in their shape and contact relations with their host rocks (Figs. 7.3 and 7.4). The shape of many autoliths could be best described as amoeboid-shaped fragments or rounded polygons. When autoliths are more lenticular, "cigar-shaped", their longitudinal axis is consistently parallel to the magmatic stratigraphy.

Contacts with host rocks vary from straight to undulative. Some of the autolith margins are straight, and the autoliths are present as angular, brecciated fragments, which could be classified as a magmatic breccia. The angular forms indicate emplacement of a completely solidified mass into a semi-solidified host. Breccia-like contacts between anorthositic rocks and surrounding ore are also reported from the Otanmäki Ore Zone by Paarma (1954, 1961). Contacts are not always perfectly straight and invariable but show locally irregular, sinuous borders in a cm scale. The more dynamic contacts suggest emplacement of semisolidified material, which is more compacted than its host but still soft enough to be slighly malleable. Whereas most autoliths are somewhat spherical, larger autoliths also portray wedges and lobes of a varying angularity, protruding into the host from the main anorthosite mass (Fig. 7.3A and B). The intervening wedges and even finger-like extensions imply settling of ductile material that was still prone to changes in its form. These irregular borders can even show an outward broken halo of smaller pieces. Especially at Vuorokas, a set of jagged fragments, smaller slivers and

pieces is seen to surround a larger group of autoliths (Figs. 7.2 and 7.3A). The different shapes and contacts of autoliths imply varying degrees of solidification upon settling in the lower parts of the magma chamber.

Magmatic layering is seen to follow autolith borders at Otanmäki (OTA-3) and Vuorokas (VUO-7). Centimeter-scale layers are draped over the autoliths from the upper side of the magmatic stratigraphy (Fig. 6.14D, 7.4C) This suggests that crystal settling in the Ore and Upper Zone continued after the emplacement of the autoliths. Similar block impact structures of layering following autolith borders have been reported from the Skaergaard and Sept Iles intrusions (Irvine et al., 1998; Namur et al., 2011).

The autolith-host rock contacts are identical in gabbro (amphibolite) and ore and seem to be not dependent on the type of the host rock. Based on the outcrop observations, a trend of more rounded autoliths occurring in the Ore Zone and more angular in the Upper Zone can be noted, but it should be regarded with caution because the main Ore and Upper Zone outcrop areas are differently deformed.

Upon later movements, the borders between plagioclase-rich autoliths and softer gabbroids have in places behaved as tectonic planes of weakness. Later shearing, brecciation and faulting with subsequent recrystallization, chloritization and mm-scale hydrothermal veining are evident at some lithological boundaries. Faulting is not bound only to lithological contacts, as many faults cut across autoliths and their hosts alike. Partitioning of tectonic strain between host gabbros and autoliths has favored the latter, with most of the strain being directed to the gabbros while the autoliths are less deformed. At Metsämalmi, the autoliths are also tectonically elongated and foliated in some places.

At Otanmäki, pegmatitic inclusions or pockets few cm in diameter are seen dispersed in the Ore and Upper Zone gabbros. They are leucogabbroic, usually coarser grained than the autoliths, and likely formed by in-situ crystallization. Similar segregations are seen in the Vuorokas Lower Zone rocks. Although this is a minor feature in the Ore and Upper Zones, they must not be confused with the autoliths that have a similar leucocratic appearance.

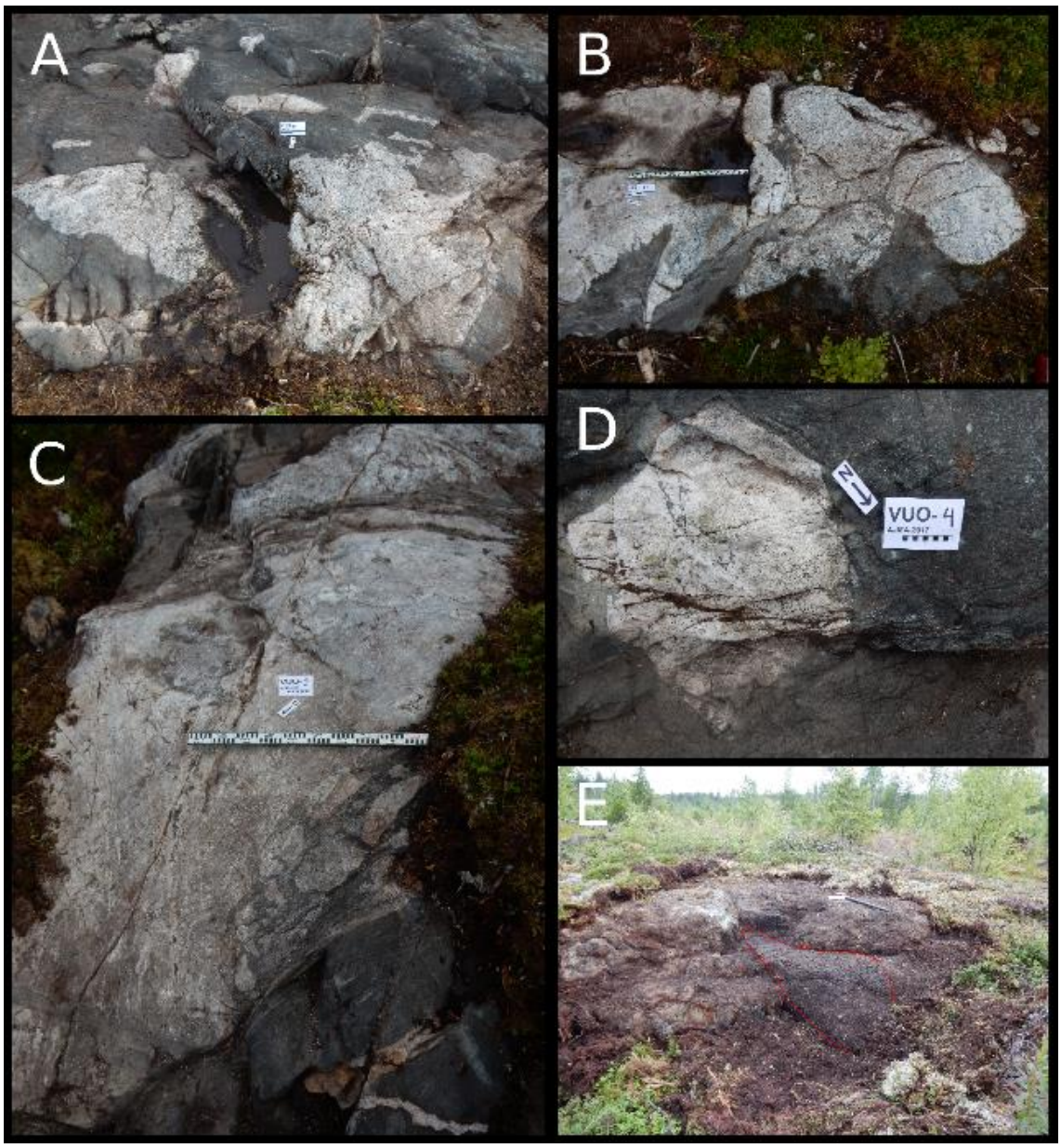

Fig. 7.3. Outcrop images of autoliths from the Upper Zone at Vuorokas. A. Autolith with outward broken borders showing a broken halo of fragments (VUO-6). Scale bar 20 cm B. Autolith with variously rounded wedges and lobes cutting into surrounding gabbro (VUO-13). Length of the measuring stick 1 m. C. A larger autolith (VUO-9) with a border that has worked as a tectonic plane of weakness in later movements. Movement is evident from strain, but breccia structure on the border could also be of magmatic origin. D. Angular, breccia-type autolith (VUO-4). E. Largest outcrop of VUO-1 with a 550-m^2-sized autolith showing a meter-wide ultramafic inclusion (borders reinforced with red outline) in the foreground. 60-cm-long hammer points to the north.

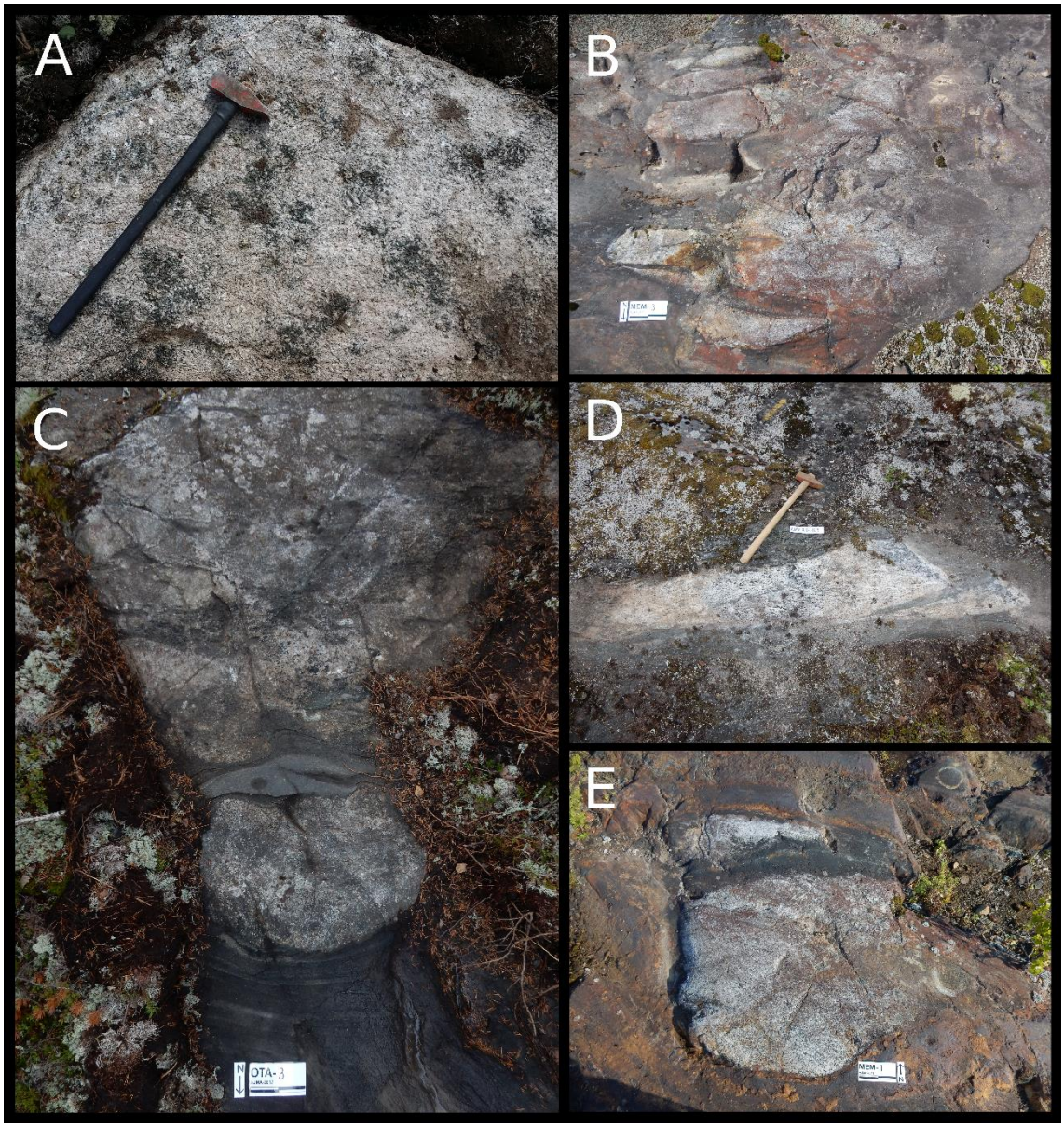

Figure 7.4. Outcrop images of autoliths from the Ore Zone at Otanmäki and Metsämalmi. A. Anorthositic autolith with a mottled texture (OTA-2). 60-cm-long hammer points to the north. B. Border of a 250-m^2 autolith with finger-like extensions protruding the host gabbro amphibolite (MEM-3). Anorthosite–amphibolite border enhanced in red. Scale bar 20 cm. C. 3-m-wide autolith with magmatic layering following the autolith borders (OTA-3) D. Thoroughly schistose autolith in the most sheared parts of the Metsämalmi outcrop area (AJMA-17-169). E. Rounded leucogabbroic autolith enveloped by oxide ore (MEM-1). An ultramafic rim can be seen at the northern border.

7.3. Textures and mineralogy

The autoliths are typically medium grained and anorthositic in their mineral composition (Fig. 7.5.). The majority of the autoliths can be described as homogenous and consistent in character, but some display similar textures to those of Lower Zone varitextured gabbros, including a variable grain size and color index, a mottled texture and the presence of up to 1-m-wide ultramafic inclusions within the main anorthosite mass. These characteristics are seen especially in larger autoliths, such as VUO-1 and OTA-5. Changes in the grain size and mafic material proportions suggest differences in the cooling rate and possibly parental magma composition and could even indicate a different provenance for some autoliths.

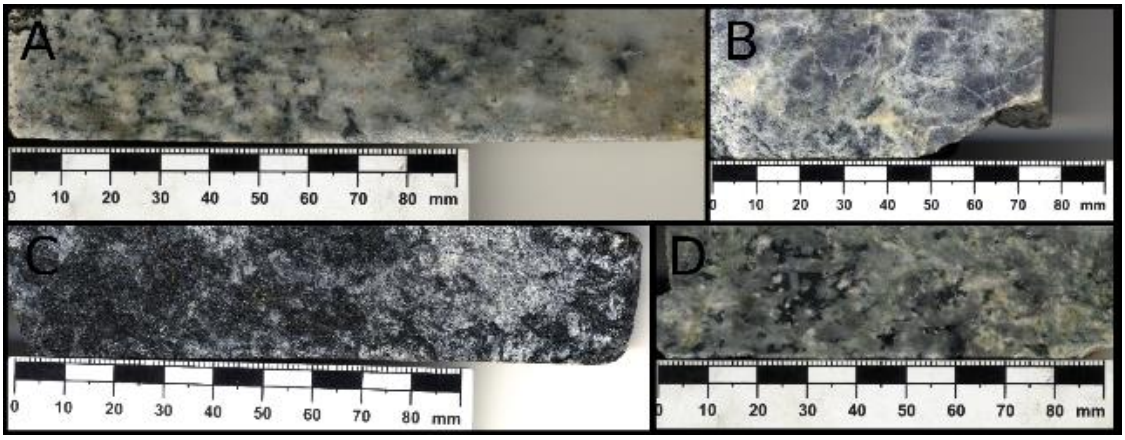

Figure 7.5. Scanned images of sawed hand samples of autoliths. A. Medium- to fine-grained anorthositic autolith from the Upper Zone at Vuorokas (VUO-5). B. Almost monomineralic, medium- to large-grained autolith (OTA-4) with >10-mm-sized primary plagioclase crystals C. Fine-grained leucogabbroic autolith (MEM-1) from Metsämalmi. This is the only studied inclusion completely surrounded by oxide ore. Largely recrystallized plagioclase, ubiquitous disseminated magnetite+ilmenite. D. Anorthositic autolith (VUO-2A). Minor disseminated ilmenite is altered to titanite and rutile (spots with a red tint).

Autoliths in the Otanmäki underground mine have been reported to have an amphibolite-rich rim around them (Kerkkonen, 1979). Similar observations have been made from the Metsämalmi area where ultramafic bands are seen around some autoliths. This feature is limited to observations in the Otanmäki Ore Zone and results possibly from heavy amphibolitization around the inclusions.

The grain size of plagioclase in the autoliths varies from 0.03 to >10 mm. Plagioclase has recrystallized to varying extent, and equigranular triple points are common. Primary

euhedral plagioclase crystals can yet be seen in almost every sample. The primary crystals are larger and more dirty-looking than the completely recrystallized ones, but they may have undergone metamorphic equilibration at their borders (Fig. 7.6).

The varying degree of shear that is seen in the inclusions in the field is also evident in thin sections. Generally, the plagioclase rich autoliths are less strained than their host rocks but locally they can be completely schistose.

Plagioclase is the only primary mineral in every sample but its composition is likely metamorphically altered. Mafic minerals are always altered to amphiboles, chlorite, and epidote. Disseminated oxides are seen in some samples, especially in MEM-1, which is enveloped by class II ore. The larger than normal oxide content could result from metamorphic equilibration between the autolith and its host rock. Similarly to gabbros, disseminated ilmenite in the autoliths is often altered to titanite and rutile. In general, the mineralogy indicates operation of pervasive metamorphic fluid flow and wide-spread recrystallization.

Mineralogical features are seen to vary between autoliths within a small distance. Autolith VUO-2B is hydrated, pervasively recrystallized with the primary textures being totally destroyed whereas the neighboring autolith VUO-2A shows large, up to 5-mm-sized primary plagioclase crystals and disseminated ilmenite. The degree of recrystallization varies also within a single autolith (e.g., OTA-3A-B and OTA-5A-B).

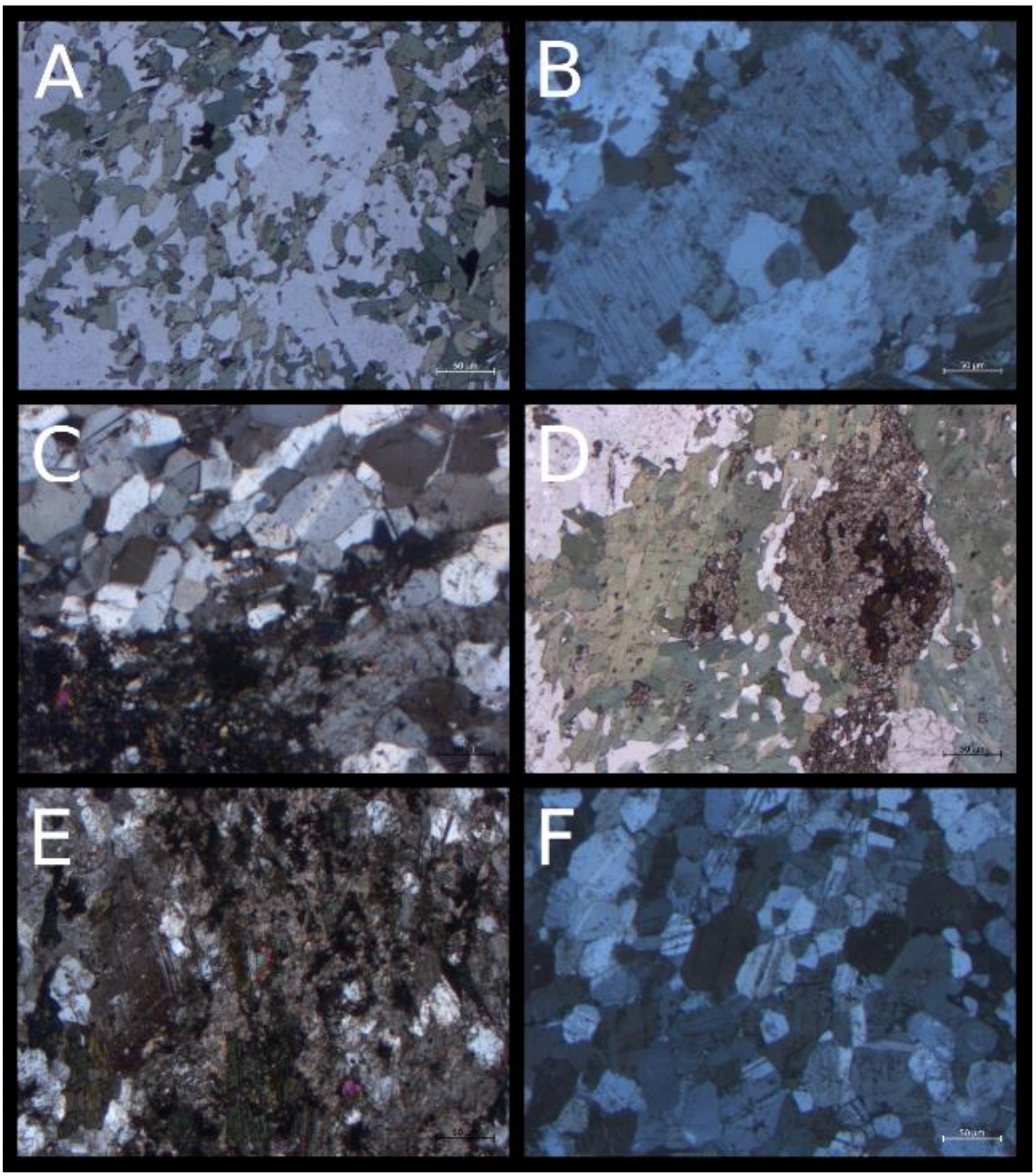

Figure 7.6. Photomicrographs of autoliths. A. Leucogabbroic autolith with largely recrystallized plagioclase (MEM-1). B. Magmatic plagioclase crystal 5 mm in diameter (OTA-2). Recrystallization of both plagioclase and amphiboles is seen at crystal margins. C. Strongly recrystallized autolith (OTA-3A). D. Typical assemblage of altered mafic minerals: green amphiboles surround titanite and rutile. (OTA-3B). E. Completely recrystallized and altered autolith with no primary textures visible (VUO-2B). F. Monomineralic anorthositic autolith (VUO-4).

8 GEOCHEMISTRY

8.1 Major elements

When handling major element data, analyses from all three datasets were taken into consideration: 18 ICP-OES/ICP-MS analyses, 61 pXRF measurements, 197 analyses from Nykänen (1995), and 37 analyses by V. Nykänen (unpubl.). In the case of trace elements, ICP-OES/ICP-MS analyses and data from V. Nykänen (1995; unpubl.) are taken into consideration. Table 8.1 shows selected major element compositions of different rock types in the Otanmäki intrusion.

Gabbroic rocks (10–90 % plagioclase) from Otanmäki and Vuorokas are in general poor in silica. The Ore and Upper Zone gabbros and marginal amphibolites have the lowest SiO_2 content whereas the anorthositic autoliths dominate the other end of the spectrum with SiO_2 contents between 47.5 and 60.2wt% (Figs. 8.1A and B). The SiO_2 contents of most of the Lower Zone samples fall in the range of 47–52 wt%. In general, the SiO_2 content seems to correlate with the plagioclase content. In contrast to SiO_2, the CaO content varies little in the sample set (Fig. 8.1B). Both silica-poor Ore and Upper Zone gabbros and silica-rich anorthositic autoliths have a very constant CaO content of around 10 wt% but the Lower Zone gabbros show slightly higher CaO concentrations. The amount of CaO seems to be not strictly proportional to the normative plagioclase content, which suggests that CaO is hosted both by plagioclase and clinopyroxene (now altered to amphibole).

The Al_2O_3 content in the rocks varies greatly, being lowest in class I ore (2.5–7.3 wt%) and highest in autoliths (20.8–27.7 wt%) (Fig. 8.1A). Analogously to SiO_2, the Al_2O_3 content in the rocks is chiefly controlled by plagioclase, as VTGs and autoliths have the highest Al_2O_3 contents. As seen in Fig. 8.5, the Lower Zone rocks show a great variation in their Al_2O_3 content from 3.4 wt% (melagabbro) to 28.0 wt% (anorthosite), which attests to a great variation in the plagioclase content among the Lower Zone rocks. Nykänen (1995) interprets the large variations in the Al_2O_3 content in the Vuorokas Lower Zone to reflect the presence of different rock types and rhythmic layering. Although rhythmic layering is not seen on outcrops, the Lower Zone has modally different gabbro types and heterogeneities in the form of pegmatitic pockets and meter-scale tex-

tural variations of the vari-textured gabbros, which could easily explain the fluctuation in the Al_2O_3 content. Majority of the Ore and Upper Zone gabbros and marginal amphibolites have a very similar, nonvariable Al_2O_3 content (10–15 wt%) (Figs. 8.1A and 8.5).

As seen if Fig. 8.5, the Otanmäki intrusion rocks show a distinct growth in Mg-number upwards in the magmatic stratigraphy (or towards N-NW in the field). The highest Mg-number values are in the Vuorokas Lower Zone melanogabbros (64–69). Mg-number in the Lower Zone gabbros averages 57 and decreases steadily through vari-textured gabbros (50) to Ore Zone gabbros (27) and Upper Zone gabbros (21). As deduced from mineralogical observations, the Ore Zone autoliths are in general more iron rich (1.7–9.7 wt% FeO_{TOT}) than the Upper Zone autoliths (1.4–4.9 wt% FeO_{TOT}). This is also reflected in their Mg-numbers, which in the Ore Zone autoliths are between 23 and 26 and in the Upper Zone autoliths between 21 and 42. The Mg-number values of the marginal amphibolites vary between 31 and 57.

In the gabbroic and anorthositic rocks, the MgO content is directly proportional to that of FeO_{TOT}, as seen in Fig. 8.1C. Both elements are dominantly hosted by Mg-Fe silicates, such as olivine and pyroxene, which are in most samples recrystallized to amphiboles. The lowest MgO and FeO_{TOT} contents are systematically observed in the anorthositic autoliths followed by VTG and plagioclase-rich Lower Zone rocks. The FeO_{TOT}/MgO ratio in the Ore and Upper Zone gabbros and marginal amphibolites, however,< deviates from the otherwise constant trend, as seen in Fig. 8.1C. This owes to the high amount of FeO_{TOT} in the Ore and Upper Zone gabbros which is highest among the gabbros in the intrusion, up to 10 times higher than that of the Lower Zone rocks (Figs. 8.1D and 8.6). The same applies to TiO_2. It should be noted that the difference in the FeO_{TOT} and TiO_2 contents between the Ore and Upper Zone gabbros is minor. This further underlies that the difference between the Ore Zone and the Upper Zone does not rise from the presence of chemically or mineralogically different rock types but rather from different proportions of rock types, i.e. ore/gangue mineral ratios.

Both isotropic and vari-textured Lower Zone gabbros at Vuorokas were comprehensively sampled, but the analyses of the samples with an exact known stratigraphic position

do not show a rise in the FeO_{TOT} or Ti content towards the Ore Zone (Fig. 8.6). This implies that Fe and Ti enrichment occurred as crystallization of the Lower zone proceeded. Eventually, the conditions switched to favor the crystallization of Fe-Ti-oxides, resulting in the crystallization of the Ore Zone rock types.

The Lower Zone gabbros are extremely low in phosphorus, with only 9% of the analyzed samples showing P_2O_5 above the detection limit (3 ppm) though occasionally, P_2O_5 may reach values up to 0.4 wt%. The Upper Zone gabbros and autoliths have slightly higher P_2O_5 content in average, but the highest readings (0.04 wt%) are chiefly from pXRF measurements and likely result from an insufficient precision of the instrument. An ICP-MS analysis shows 0.2 wt% P_2O_5 in an Upper Zone gabbro sample, while the level of P_2O_5 in an Ore Zone gabbro sample is below the detection limit (0.01 wt%). Combined with the apatite gabbro observations from the Upper Zone at Otanmäki, a minor phosphorus enrichment in the Upper Zone likely happened as crystallization proceeded. Compared to the global average P_2O_5 content of gabbros at 0.24 wt% (Le-Maitre, 1976), the Otanmäki intrusion is poor in phosphorus.

Table 8.1 Major element compositions of different rock types in the Otanmäki intrusion.

Rock type	**Sample ID**	SiO_2	Al_2O_3	FeO_{TOT}	MgO	CaO	Na_2O	K_2O	TiO_2	P_2O_5	MnO	$Total$	***Mg#***
Marg. Afb.	**OTA-10**	47.93	12.33	8.68	9.70	13.88	1.44	0.97	1.02	0.18	0.18	96.31	**53**
Marg. Afb.	**VUO-20**	45.68	13.80	14.21	8.71	10.74	1.82	0.30	1.49	<0.01	0.17	96.92	**38**
Lower zone gabbro	**VUO102 /30.90**	44.53	14.46	11.68	20.71	5.64	1.82	0.50	0.22	0.02	0.20	99.78	**64**
Lower Zone gabbro	**VUO97/ 96.96**	49.64	17.67	6.45	10.07	13.28	1.89	0.25	0.45	0.05	0.12	99.87	**61**
VTG	**RA-2B**	51.1	25.1	2.5	1.8	12.4	4.2	0.2	0.3	0.0	0.0	97.80	**42**
VTG	**MEM-4**	48.7	24.5	6.6	1.2	10.7	4.4	0.3	1.6	0.1	0.1	98.20	**16**
Ore zone gabbro	**OTA-1B**	41.0	13.1	16.6	6.7	11.0	2.2	0.3	6.2	<0.01	0.2	97.17	**29**
Class I ore	**VU112/ 70.00**	1.8	4.7	67.6	3.5	0.0	0.0	0.0	18.3	0.0	0.3	96.21	**-**
Class II ore	**VU78/ 601.50**	23.1	12.1	39.8	4.4	6.5	1.9	0.2	9.8	0.0	0.2	97.90	**-**
Class III ore	**VU114/ 105.40-**	32.4	6.0	25.3	12.4	10.9	0.8	0.1	11.9	0.0	0.3	100.09	**-**
Upper zone gabbro	**VUO-15**	41.4	13.0	15.4	7.4	10.4	2.2	0.5	6.3	0.0	0.2	96.86	**33**
Ore zone autolith	**OTA-4**	53.6	26.4	1.7	0.5	9.6	5.6	0.2	0.4	0.1	0.0	98.16	**23**
Upper zone autolith	**VUO-4**	51.0	23.8	4.9	1.3	10.5	4.6	0.6	0.3	<0.01	0.1	97.05	**21**

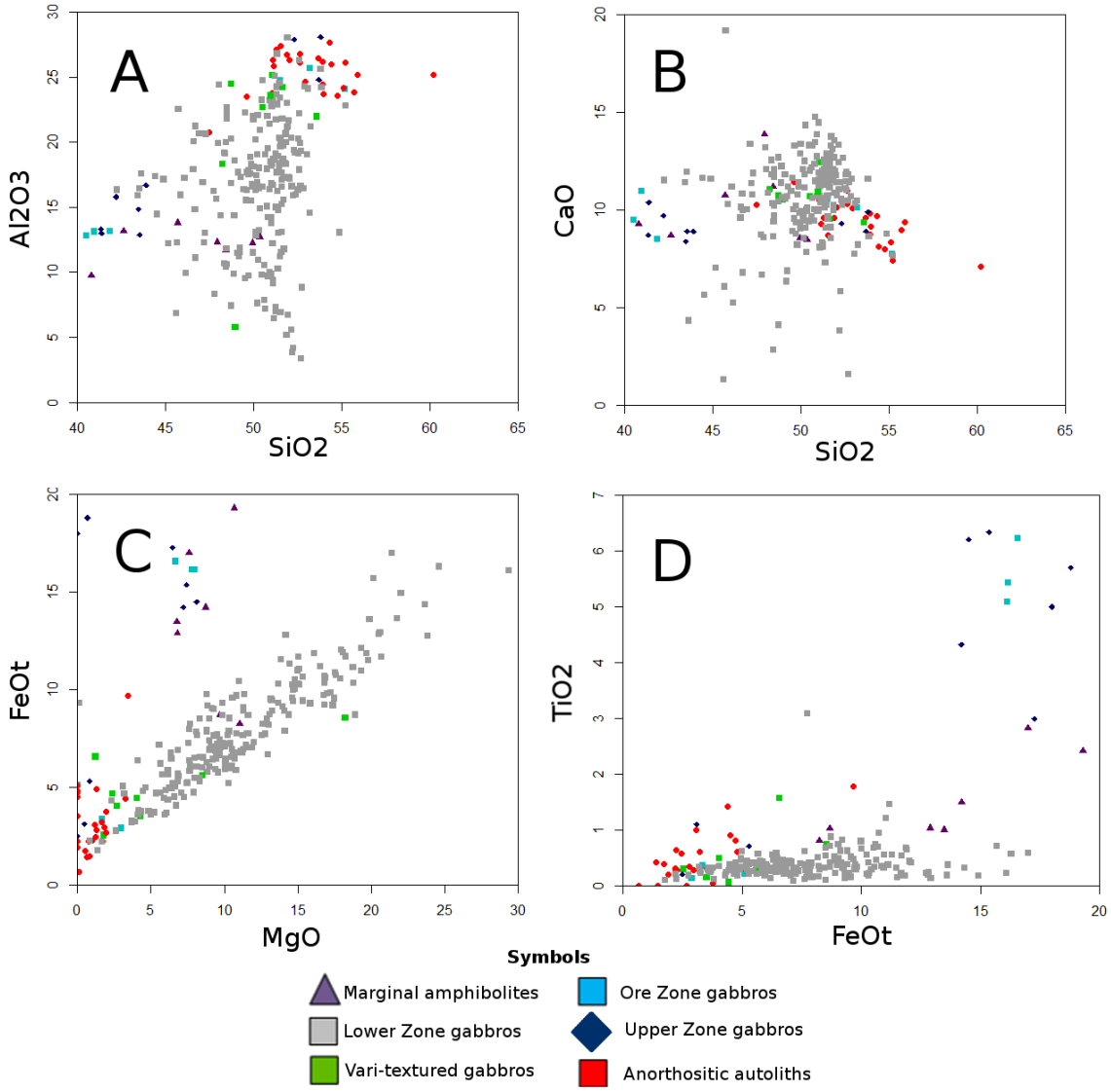

Figure 8.1. Binary plots of major oxides for the Otanmäki intrusion gabbroic and anorthositic rocks. A. Al_2O_3 vs. SiO_2. B. CaO vs. SiO_2. C. FeO_{TOT} vs. MgO. D. TiO_2 vs. FeO_{TOT}. All data in wt%. See text for more information.

CIPW-normative mineral compositions were calculated for all samples and are listed in Appendix 7. Selected normative mineral compositions for gabbroic rocks are presented in Table 8.2 and for anorthositic autoliths in Table 8.3. Figures 8.2, 8.3 and 8.4. present the CIPW-normative mineral compositions of each data set plotted to the IUGS classification diagram for gabbroic rocks. Most of the gabbroic rocks from marginal amphibolites to Upper Zone gabbros plot dominantly in the olivine gabbro/olivine norite/olivine gabbro norite field. As stated by Nykänen (1995), the amount of different rock types in the Lower Zone is quite excessive if all samples were named based on their normative compositions.

Table 8.2. CIPW-normative mineral compositions of different rock types. Qtz = quartz, Or = orthoclase, Al = albite, An = anorthite, Mag = magnetite, Ilm = ilmenite, Ap = apatite, Cpx = clinopyroxene (diopside), Opx = orthopyroxene (hypersthene), Ol = olivine.

Rock type	**Sample ID**	*Qtz*	*Or*	*Al*	*An*	*Mag*	*Ilm*	*Ap*	*Ne*	*Cpx*	*Opx*	*Ol*	Total
Marg. Afb.	**OTA-10**	0.00	5.7	12.2	24.3	1.4	1.9	0.4	0.00	35.1	4.67	10.6	96.4
Marg. Afb.	**VUO-20**	0.0	1.8	15.4	28.6	2.3	2.8	0.0	0.0	20.3	9.7	16.2	97.1
Lower zone gabbro	**VUO102/ 30.90**	0.0	1.5	16.0	39.0	1.0	0.9	0.1	0.0	21.4	9.2	10.9	100.0
Lower zone gabbro	**VUO97/ 96.96**	0.0	1.5	20.3	40.0	1.2	0.6	0.1	0.9	14.9	0.0	20.4	100.0
VTG	**RA-2B**	0.0	1.3	32.0	48.9	0.4	0.6	0.1	2.1	10.3	0.0	2.2	97.8
VTG	**MEM-4**	0.0	1.5	31.7	46.1	1.1	3.0	0.3	3.1	5.3	0.0	6.1	98.3
Ore zone gabbro	**OTA-1B**	0.0	1.6	14.7	25.0	2.7	11.8	0.0	2.3	24.2	0.0	15.1	97.4
Upper zone gabbro	**VUO-15**	0.0	3.0	15.7	24.0	2.5	12.1	0.1	1.7	22.4	0.0	15.7	97.0

Table 8.3. CIPW-normative mineral compositions of anorthositic autoliths. Mineral abbreviations as in Table 8.2.

Sample_ID	*Qtz*	*Or*	*Al*	*An*	*Mag*	*Ilm*	*Ap*	*Ne*	*Cpx*	*Opx*	*Ol*	Total
MEM-1	0.0	1.0	28.6	38.1	1.6	3.4	0.1	3.0	10.6	0.0	11.6	97.8
OTA-2	0.0	1.2	43.1	42.6	0.5	1.9	0.4	1.1	5.2	0.0	2.6	98.6
OTA-4	0.0	1.2	45.5	46.4	0.3	0.7	0.1	1.1	0.7	0.0	2.2	98.2
OTA-5A	0.0	4.7	37.1	46.9	0.4	1.2	0.2	2.9	2.2	0.0	2.5	98.1
VUO-1	0.0	3.0	29.6	45.6	0.7	2.7	0.1	1.5	8.9	0.0	6.1	98.1
VUO-2A	0.0	6.0	37.1	47.2	0.4	0.5	0.1	1.7	0.0	0.0	4.2	97.6
VUO-4	0.0	3.3	34.9	42.6	0.8	0.7	0.0	2.2	8.0	0.0	4.8	97.1
VUO-5	0.0	1.1	45.2	45.5	0.2	0.8	0.1	1.5	2.5	0.0	1.4	98.3

The olivine gabbronoritic composition of the Lower Zone rocks is seen both in the analyses from Nykänen (1995) and in the calculations based on the less accurate pXRF measurements (Figs. 8.3 and 8.4). Some of the analyses by Nykänen (1995) are from an area of vari-textured gabbros, but due to the uncertain contact between the rock types and the limited sample descriptions, all analyses are considered to represent "Lower Zone rocks". In this work, all the analytical results from the Lower Zone are treated as a whole, and differentiation between olivine normative rocks and other cumulates, for example, is not done.

As seen in Figs. 8.2 and 8.3, the Lower Zone VTGs have a higher plagioclase content than the Lower Zone gabbros and plot dominantly in the leucogabbro field. The most plagioclase-rich Lower Zone rocks in Fig. 8.4 likely represent vari-textured gabbros or leucocratic layers or blebs in the isotropic Lower Zone gabbros. All VTG analyses have minor normative magnetite and ilmenite, especially MEM-4, which is spatially close to the Ore Zone rocks. The normative mineralogy is consistent with microscopic observations. Two VTG samples (AJMA-17-385.1 and AJMA-18-1) show minor normative quartz. Sample AJMA-17-332.1 has an abnormally high olivine content of 13.3 wt% compared to normative olivine in other VTGs, which is at the level of 0.0–7.6 wt%. This might result from the imprecise pXRF method when analyzing samples with a pegmatoidal grain size or other large-scale compositional variations. In the case of vari-textured gabbros, RA-2B is regarded as a type sample because it was analyzed with ICP-OES/-MS using a substantial sample size.

The Upper Zone and Ore Zone rocks are very similar in terms of their normative mineral composition and, similarly to the Lower Zone gabbros, plot dominantly in the olivine gabbronorite field. However, the large amount of disseminated oxides in the Ore Zone rocks may cause some uncertainties in the normative mineralogy.

As seen in Fig. 8.3, pXRF data show a large variation in the Upper Zone gabbros, with two samples (AJMA-17-135.1 and AJMA-17-137.2) being normative anorthosites. These two samples are from modally layered gabbros, and their compositions may also be affected by the inaccuracy and imprecision of the pXRF measurements. Based on pXRF data, the Upper Zone gabbros seem to be slightly richer in normative plagioclase than the Ore Zone gabbros. The result is expected from the higher SiO_2 and Al_2O_3 contents in the Upper Zone rocks. However, the differences are not large and the data are scarce and hence any conclusions should be regarded as directional.

Both the normative and modal plagioclase contents in the majority of autoliths are higher than 90%. The three samples that plot in the leucogabbroic field in Fig. 8.2 are VUO-1 (a large inclusion portraying VTG structures), MEM-1 (a small inclusion enclosed in class II ore), and VUO-4. Apart from VUO-4, the results are consistent with field, hand sample and microscopic observations. The leucogabbroic anorthosites could be classified as gabbroic anorthosites (Ashwal, 1993). Compared to other samples, the autoliths are also enriched in potassium (Fig. 8.9) which is reflected in their higher content of normative orthoclase. The K_2O content varies between 0.2 and 1.8 wt% and is similar to that in the Lower Zone rocks (0.0–1.8 wt%). In the Lower Zone VTGs, pervasive potassium alteration is occasionally seen near faults. The enrichment in K_2O is likely a later feature, possible linked to the fluids related to Svecofennian metamorphism.

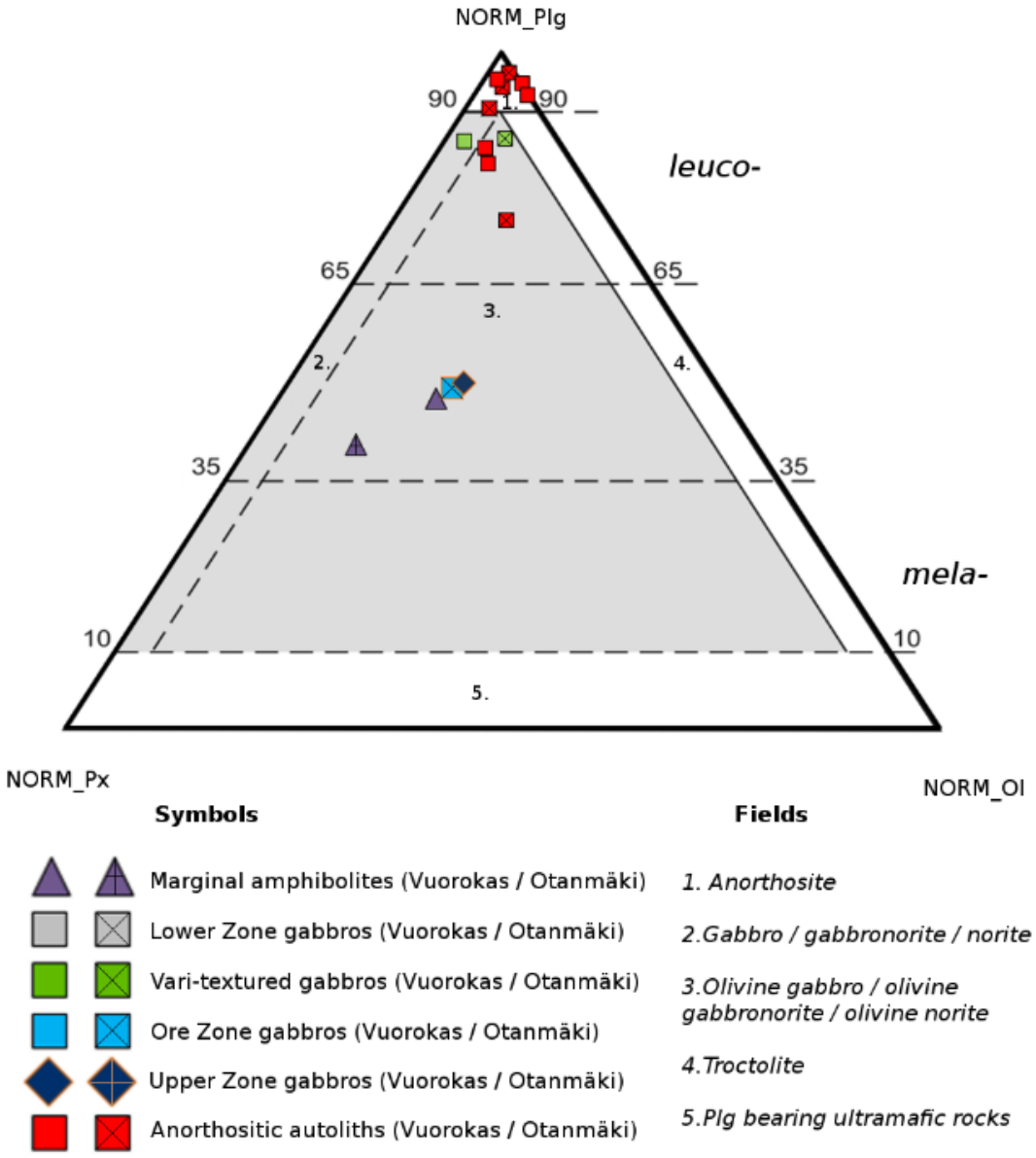

Figure 8.2. CIPW-normative compositions calculated based on ICP-OES analyses and plotted on the IUGS classification diagram for gabbroic rocks (Streckeisen, 1976).

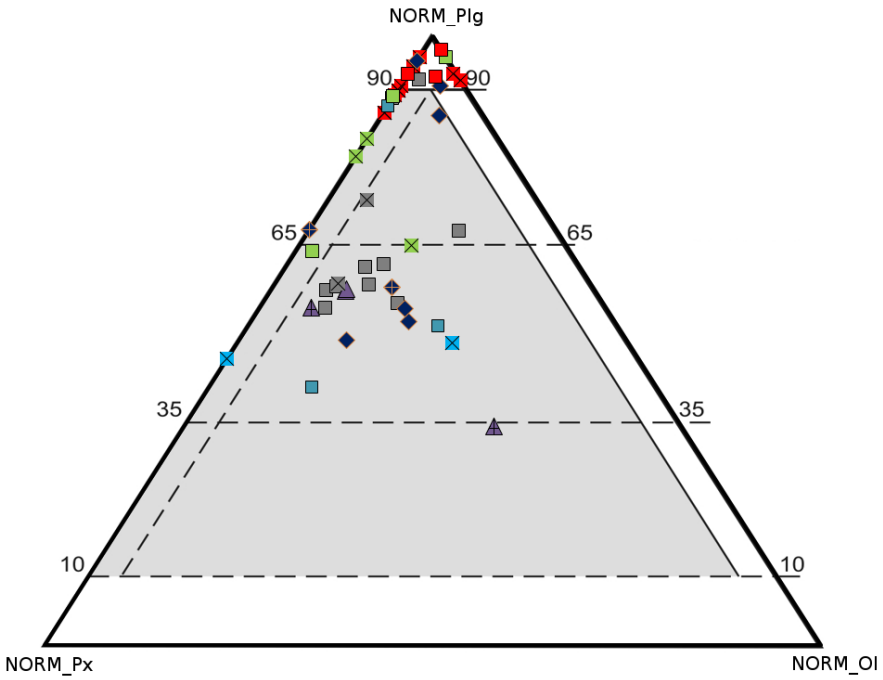

Figure 8.3. CIPW-normative compositions calculated based on pXRF measurements and plotted on the IUGS classification diagram for gabbroic rocks. Symbols and fields as in Fig 7.1.

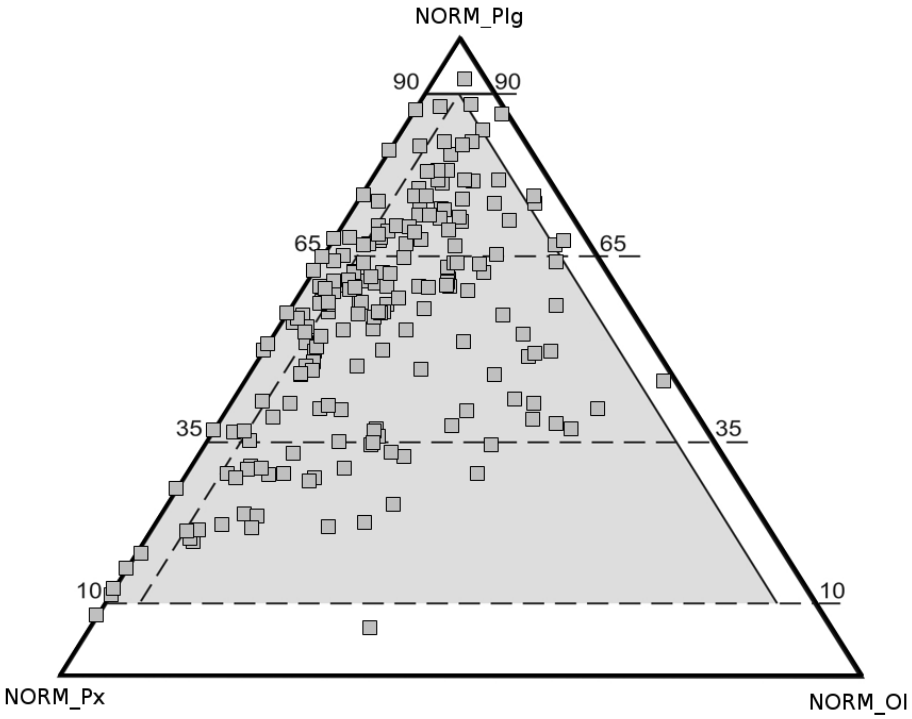

Figure 8.4. CIPW-normative compositions calculated based on the analytical data from Nykänen (1995) and plotted on the IUGS classification diagram for gabbroic rocks. Symbols and fields as in Fig 8.2.

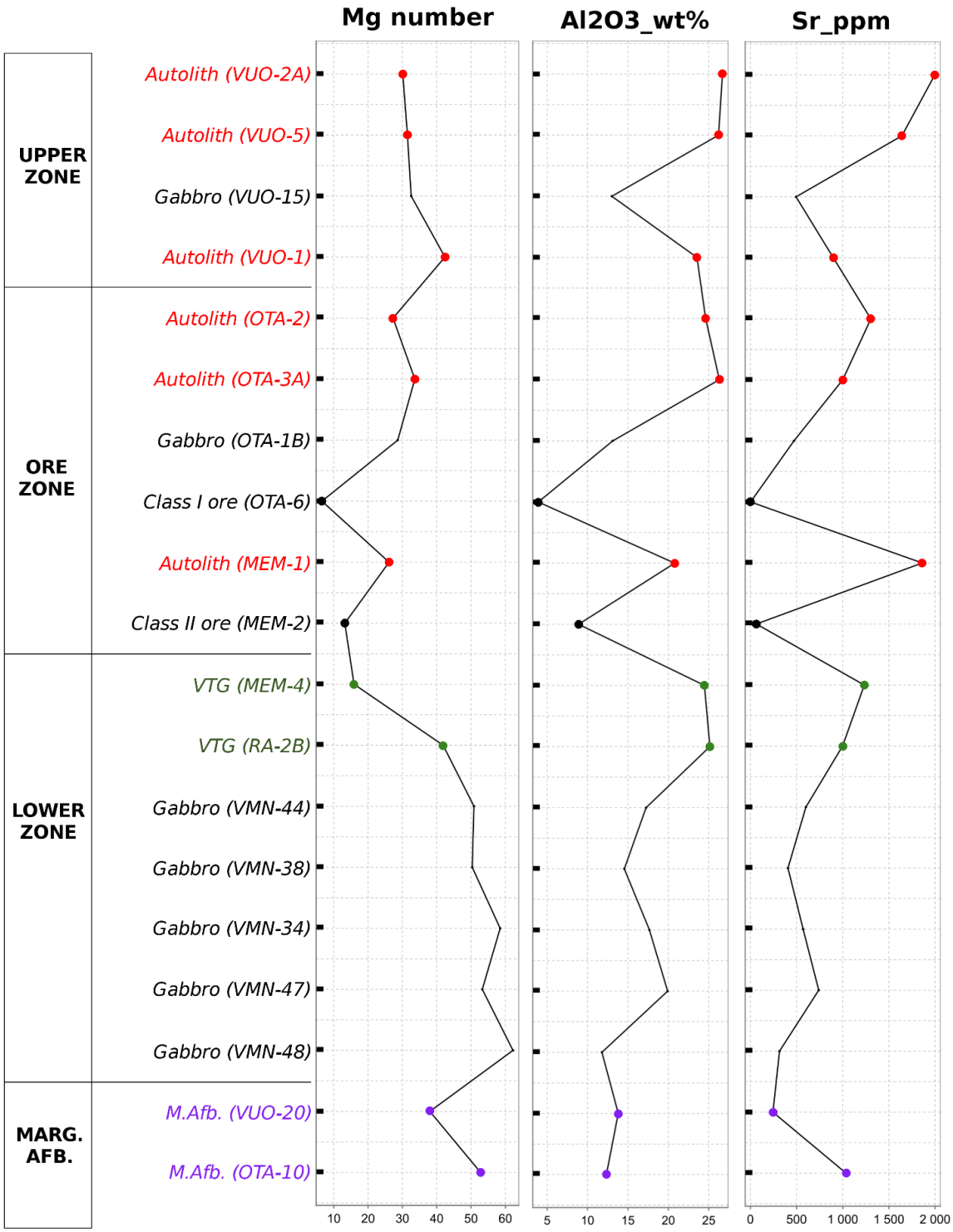

Figure 8.5. Mg number and Al_2O_3 and Sr concentrations of selected samples plotted in stratigraphic order.

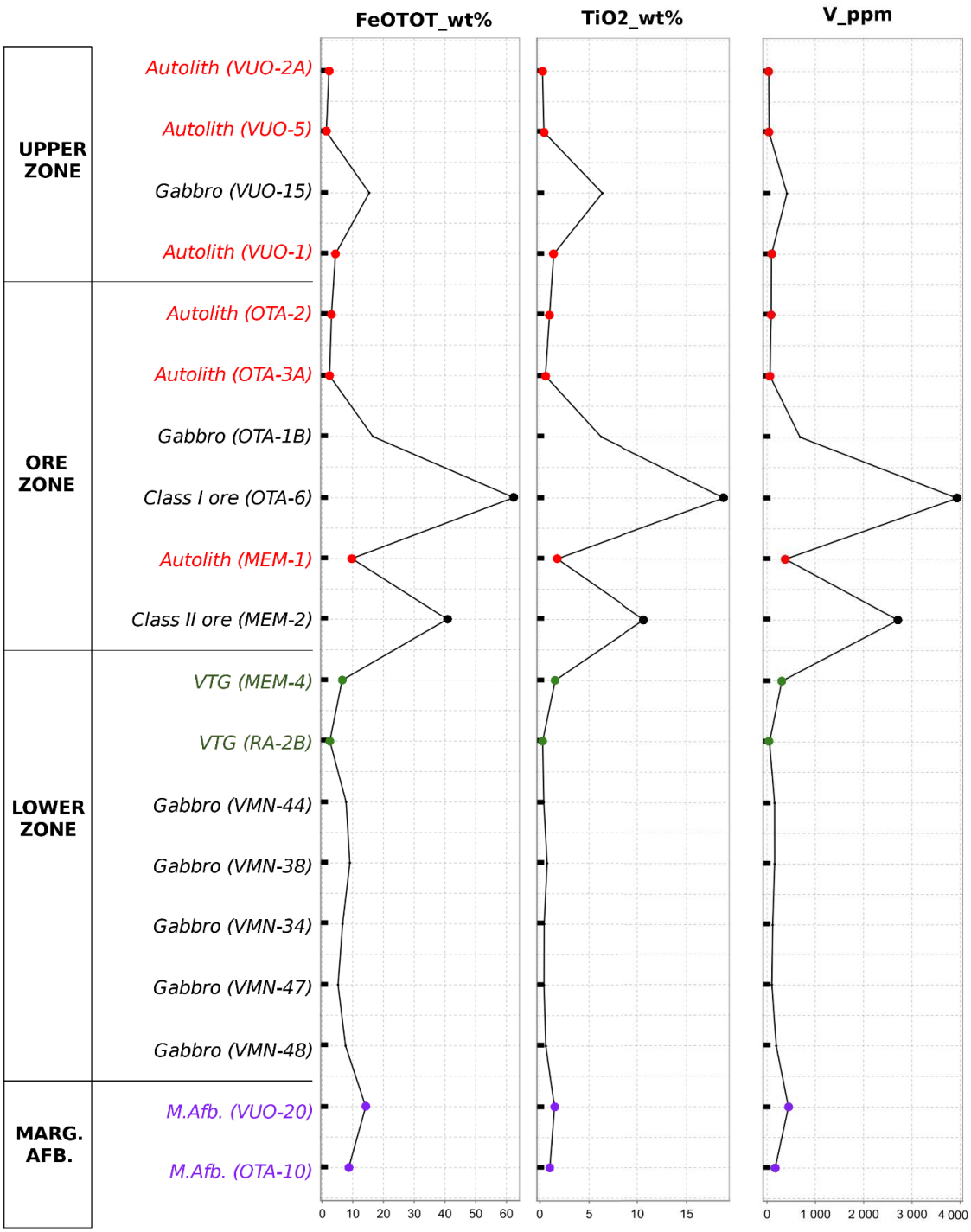

Figure 8.6. FeO_{TOT}, TiO_2 and V concentrations of selected samples plotted in stratigraphic order.

8.2 Trace elements

The observation of progressive magmatic differentiation as a function of stratigraphic height, as seen in major elements, is reinforced by the behavior of trace elements in the intrusion rocks. Compatible elements, such as chromium, are predicted to be more abundant in the lowermost part of a magma chamber. As illustrated by Fig. 8.7A, Cr correlates positively with Mg-number and is highest in the melagabbros (normative olivine-gabbronorites) in the SE part of the Vuorokas Lower Zone. Nickel substitutes for iron and magnesium in olivine and is consequently predicted to be enriched in the more primitive parts of magma series. Gabbroic rocks at Otanmäki and Vuorokas have varying contents of Ni (0–2350 ppm) but the element seems to correlate dominantly with sulfur (Fig. 8.7B). Also Cu is (9–2420 ppm) evidently incorporated by sulfides (Nykänen, 1995). The correlation is not so obvious in the oxide ore where Ni and Cu are up to 10 times less abundant (1–640 ppm Ni, 0–303 ppm Cu). The Sc contents are highest in the Lower Zone olivine-gabbronorites at Vuorokas (around 60 ppm) and lowest in the autoliths (<10 ppm; Fig 8.5C). The Rb data do not reveal discernible trends, with 97% of the rock compositions being below 40 ppm with a standard deviation of 6.4.

Among the gabbroic rocks, vanadium is most abundant in the samples from the Ore Zone and Upper Zone which show a major V enrichment in comparison to the Lower Zone rocks (Figs. 8.6 and 8.7D). The lowest V content is in the autoliths within the Ore Zone and Upper Zone. An abnormally high V content of 377 ppm is seen in Ore Zone autolith MEM-1. The small autolith is surrounded by oxide ore and has also anomalously high Fe and Ti values. In general, V behaves similarly to FeO_{TOT} and TiO_2 as seen in Fig. 8.6. The elements seem to have been enriched in the residual magma upon crystallization, being subsequently incorporated in Fe-Ti oxides during the crystallization of the Ore Zone.

Regarding incompatible elements, an opposite trend to that observed with Sc and Cr is seen. Strontium has been incompatible to the oxide ore (2–730 ppm) and compatible to the autoliths (890–2080 ppm), with gabbros plotting between them (Figs. 8.5, 8.7C and E). The niobium contents are rather constant, 1.0–4.5 ppm in the autoliths and Lower Zone rocks but show a minor increase towards the higher parts in the stratigraphy with

concentrations of 7.8 ppm and 16.6 ppm in the Ore and Upper Zone gabbros, respectively. The Zr content in all the samples varies between 0–100 ppm but does not correlate with rock type or stratigraphic height (Fig. 8.5E).

The Cr (157–513 ppm), Ni (108–252 ppm) and Sc (20–49 ppm) contents in the marginal amphibolites are similar to other gabbroic rocks (Figs. 8.5A–C). This is in harmony with the normative mineral compositions and intermediate Mg-numbers of the marginal rocks. The trace element characteristics (e.g., V, Sr Nb, Zr, LREE) differ greatly between the marginal amphibolites from Otanmäki and Vuorokas. However, the occurrence of compositionally different chilled margins within one intrusion is not uncommon (Latypov et al., 2007). This may result from differences in magmatic processes but could also be a consequence of a different degree of metamorphic hydration and mobilization of elements.

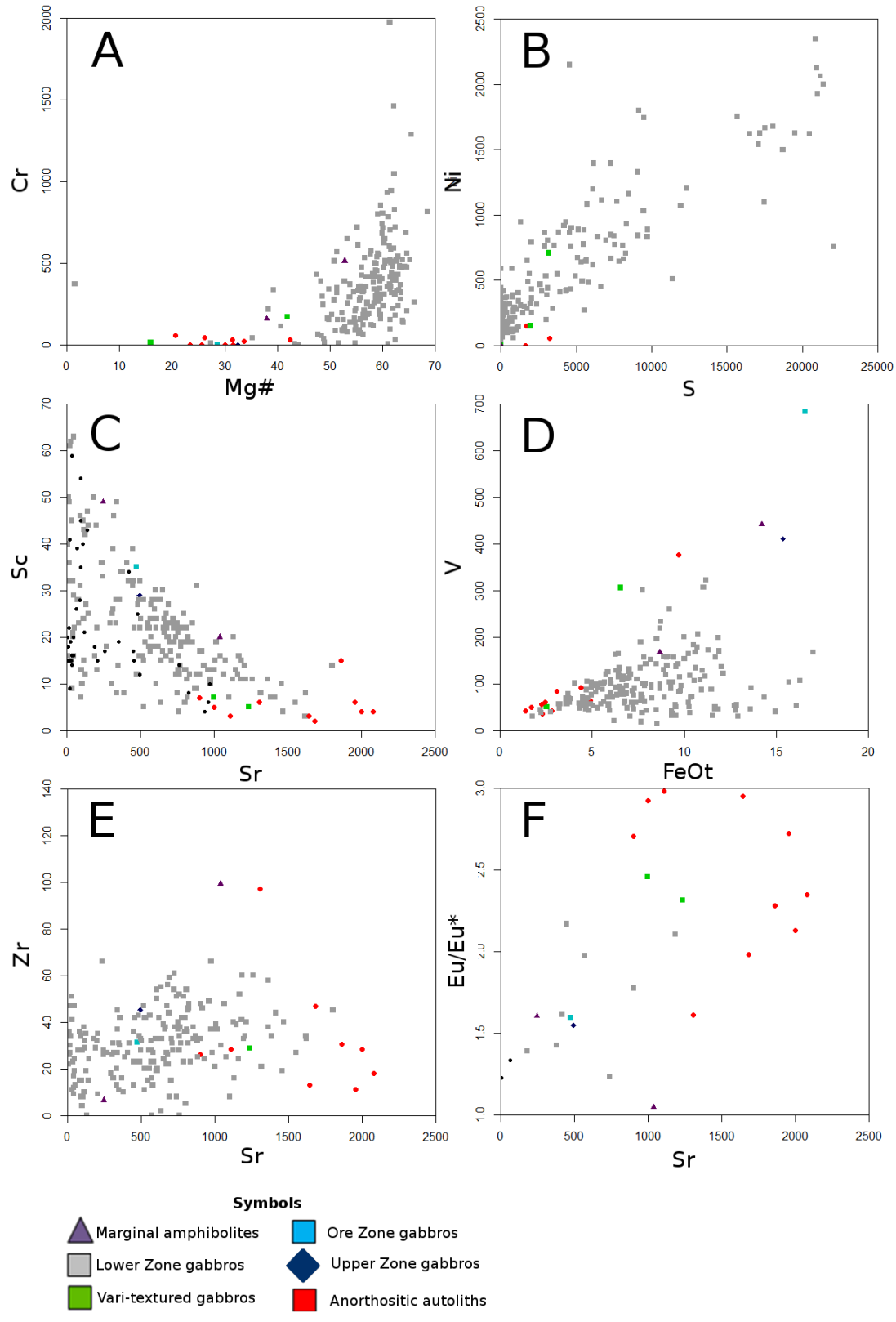

Figure 8.7. Binary plots of major and trace element compositions from the Otanmäki intrusion gabbroic and anorthositic rocks. A. Cr (ppm) vs. Mg-number. B. Ni vs. S (ppm). C. Sc vs Sr (ppm). Also ore analyses are included. D. V (ppm) vs. FeO_{TOT} (wt%). E. Zr vs. Sr (ppm). F. Eu/Eu* vs. Sr (ppm).

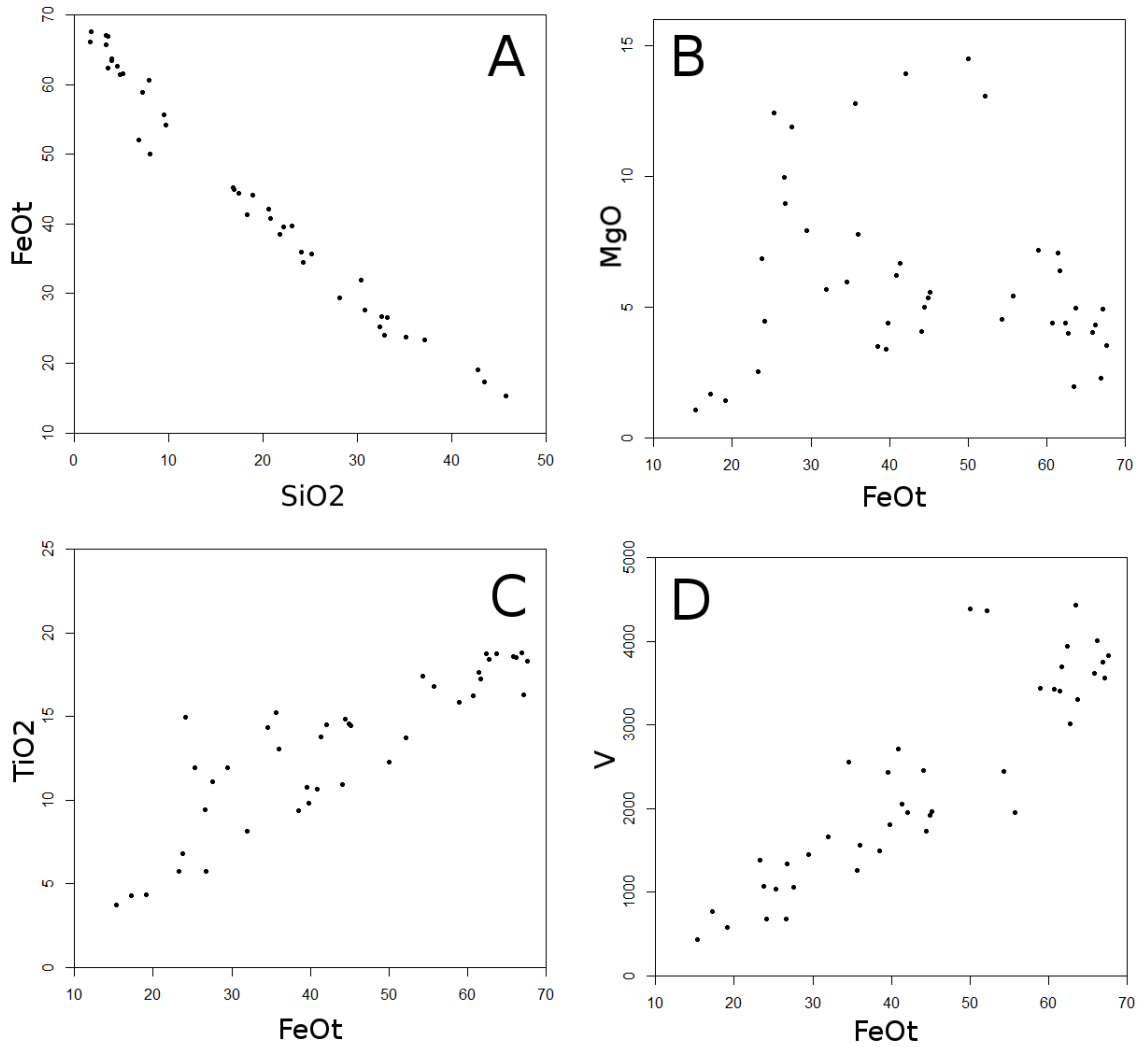

Figure 8.8. Binary plots of major and trace elements from the Fe-Ti-V oxide ore. A.FeO_{TOT} vas. SiO_2 (wt%). B. MgO vs. FeO_{TOT} (wt%). C. TiO_2 vs. FeO_{TOT} (wt%). D. V (ppm) vs FeO_{TOT} (wt%).

In the oxide ore, FeO_{TOT}, TiO_2 and V contents show positive correlations with each other as illustrated by Figs. 8.6 and 8.8. Class I ore has the highest abundances of TiO_2 (12.3–22.2 wt%) and V (3000–4400 ppm) followed by class II ore (9.3–17.4 wt% TiO_2; 1200–4400 ppm V), class III ore (5.7–14.9 wt% TiO_2, 700–1700 ppm V) and magnetite gabbros (3.7–5.7 wt% TiO_2, 400–1400 ppm V). FeO_{TOT} is inversely proportional to SiO_2 (Fig. 8.8A). Unlike in the gabbroic rocks, there seems to be no correlation between FeO_{TOT} and MgO within the ore classes (Fig. 8.8B). The oxide ore is about 10 times more in enriched in Ti than its host rocks as seen in Fig. 8.9.

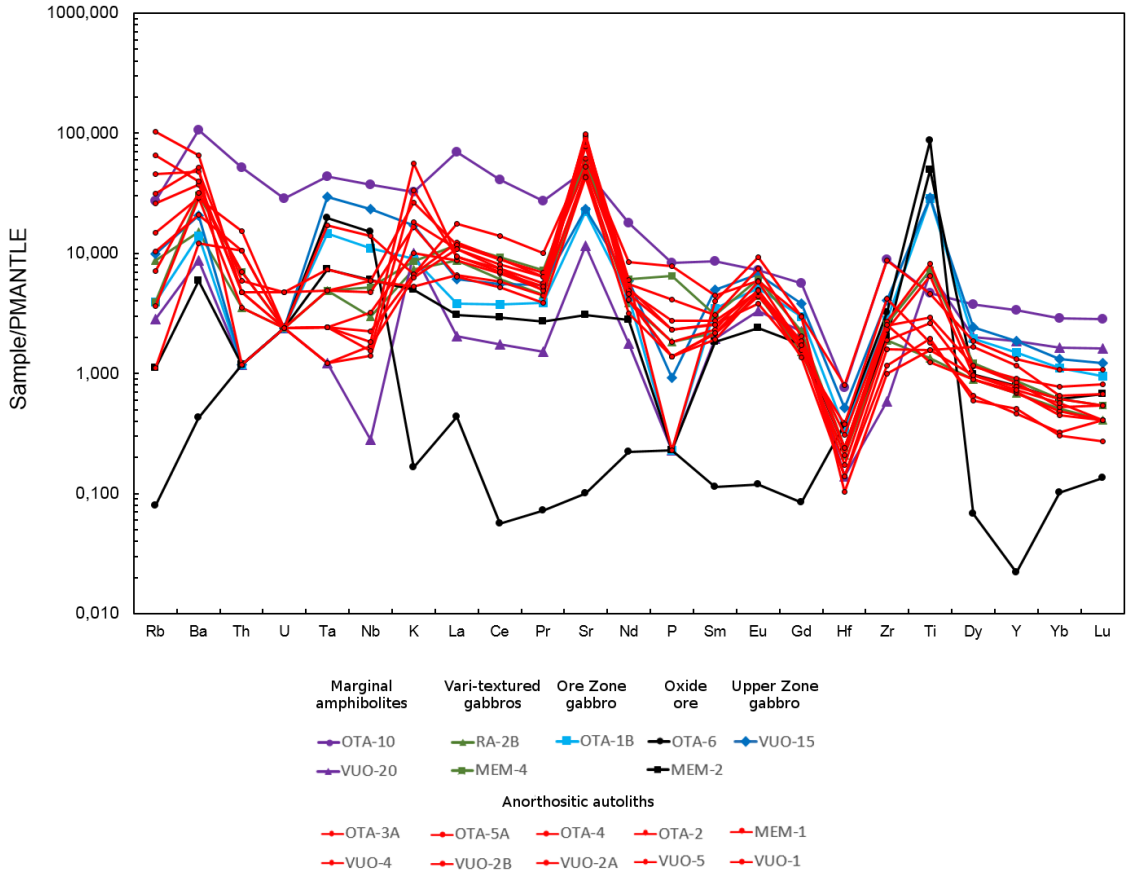

Figure 8.9. Trace element compositions of gabbroic rocks, anorthositic autoliths and oxide ore on primitive mantle-normalized spidergram. Normalizing values after Sun and McDonough (1989).

On a primitive mantle-normalized spidergram the anorthositic autoliths stand out from the other mafic rocks with up to 100-fold enrichment in Rb, K and Sr (Fig. 8.9). The trends originate dominantly from the plagioclase dominated mineralogy of the autoliths. Titanium content in the autoliths, as well as in the Lower Zone VTGs, is close to primitive mantle composition and significantly lower than that of Ore and Upper zone gabbros. In many respects, however, the trace element signature of the autoliths is similar with the intrusion gabbros suggesting derivation from the same magma.

Chondrite-normalized REE patterns of 25 samples are presented in Figs. 8.10 and 8.11. In these plots, values for Pr, Gd, Dy, Ho and Er for Lower Zone gabbros were approximated using geometric means of neighboring elements. The levels of Eu anomalies were calculated for all samples with geometric means ($Eu/Eu^*=Eu_N/\sqrt{[Sm_N*Gd_N]}$), as suggested by Taylor and McLennan (1985).

All the gabbro and anorthosite samples show analogous REE patterns with an approximately 5–100-fold enrichment in LREE (La–Gd) and a moderate enrichment in HREE (Tb-Lu) compared to chondritic values.

In an environment of low fO_2, Eu is present dominantly as an Eu^{2+} ions. Divalent Eu behaves similarly to Sr and substitutes Ca in feldspars resulting in a positive Eu-anomaly in plagioclase-rich rocks. Such positive anomalies are seen systematically in all gabbro samples. This may result solely from the high amount of cumulus plagioclase, especially in the Vuorokas Lower Zone but it also could indicate reducing conditions during the crystallization of the Lower Zone. The smallest Eu anomaly is in a sample from the SE part of the Vuorokas block (X-KKJ3: 3431020, Y-KKJ3: 7112010) and the highest one in an autolith (VUO-4).

Although the REE patterns are similar, the degree of REE fractionation between gabbro types varies. The Lower Zone gabbros from Vuorokas plot in the lowest position in the REE diagram and have Eu/Eu* values between 1.2 and 2.2. The Ore Zone and Upper Zone gabbros show almost identical REE patterns but the Upper Zone sample is slightly more enriched in total REE, implying a higher degree of magmatic differentiation. The vari-textured gabbros also plot close to each other and have similar, LREE-enriched REE patterns to those of the Lower Zone gabbros.

The exceptionally low REE values in OTA-6, a class I ore sample, result most likely from the low abundance of silicate minerals in the magnetite- and ilmenite-dominated sample. MEM-2, a class II ore sample, has more silicates to accommodate REE minerals and compared with the gabbros, has a similarly shaped REE pattern.

The REE patterns of the marginal amphibolites stand out among the other gabbro types (Fig. 8.11B). Both OTA-10 and VUO-20 are enriched in HREE in comparison to the other gabbroic rocks. VUO-20 shows a relatively flat REE pattern with an approximately 8-fold enrichment compared to chondritic values. VUO-20 also shows the lowest LREE values among the samples (excluding class I ore). Contrarily to VUO-20, marginal amphibolite OTA-10 is the most LREE-enriched sample. This indicates contamination with crustal material, likely Archean gneiss. The LREE depletion in VUO-20

could also result from metamorphism, but the marginal amphibolite occurrences at Vuorokas are relatively little strained and recrystallized in comparison with marginal amphibolite OTA-10, which was sampled adjacent to a major fault and would be expected to have been more prone to metamorphic-hydrothermal alteration.

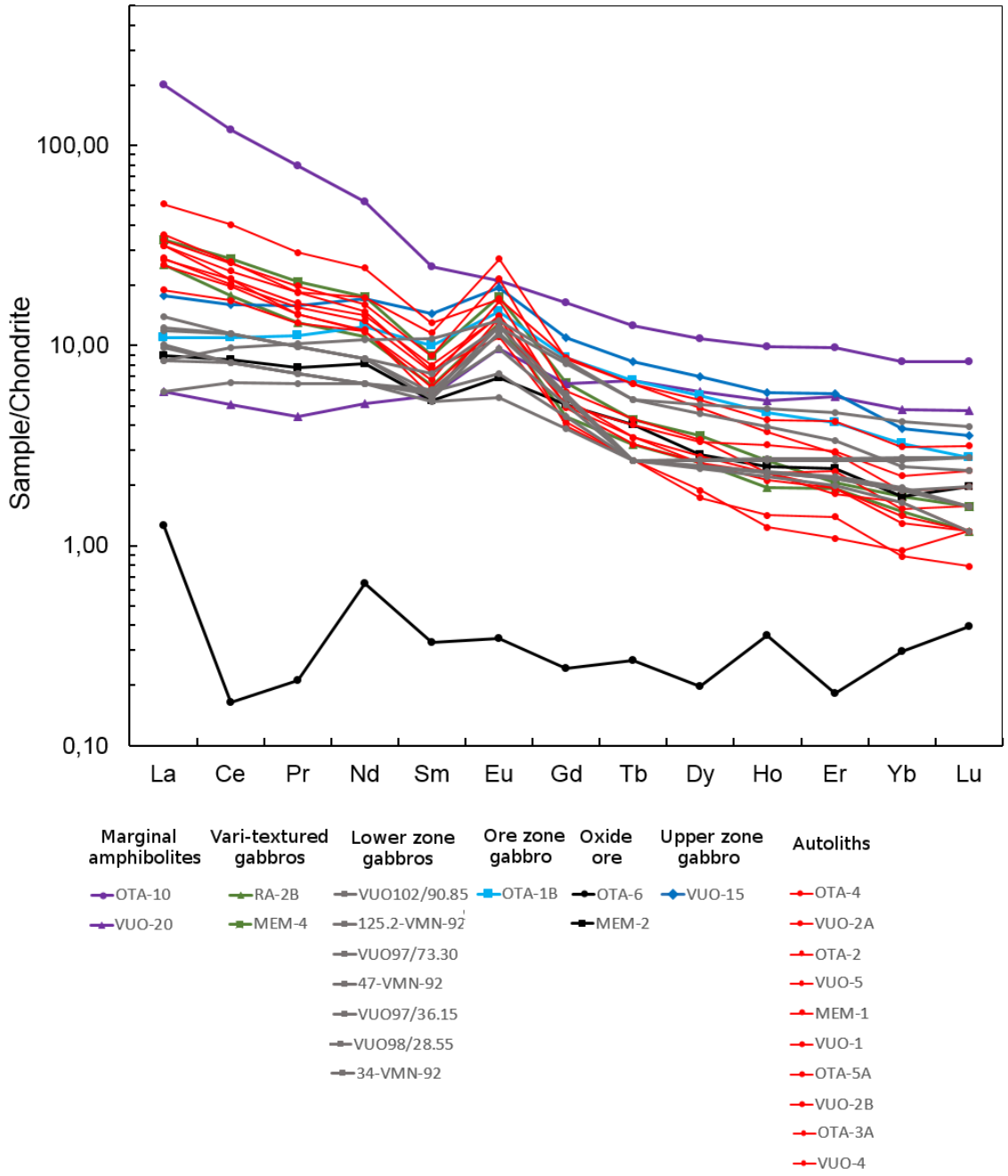

Figure 8.10. Chondrite-normalized REE patterns for gabbroic rocks, oxide ore and autoliths. Normalizing values Sun and McDonough (1989). Lower Zone compositions from Nykänen (1995).

Autoliths are consistently more enriched in LREE and depleted in HREE than the other rock types in the Otanmäki intrusion. Autoliths and VTGs have the highest Eu/Eu* values (1.6–3.0) among the gabbro types. The europium anomaly (Eu/Eu*) correlates with Sr (Fig. 8.7F) which results from the high amount of plagioclase in the rocks.

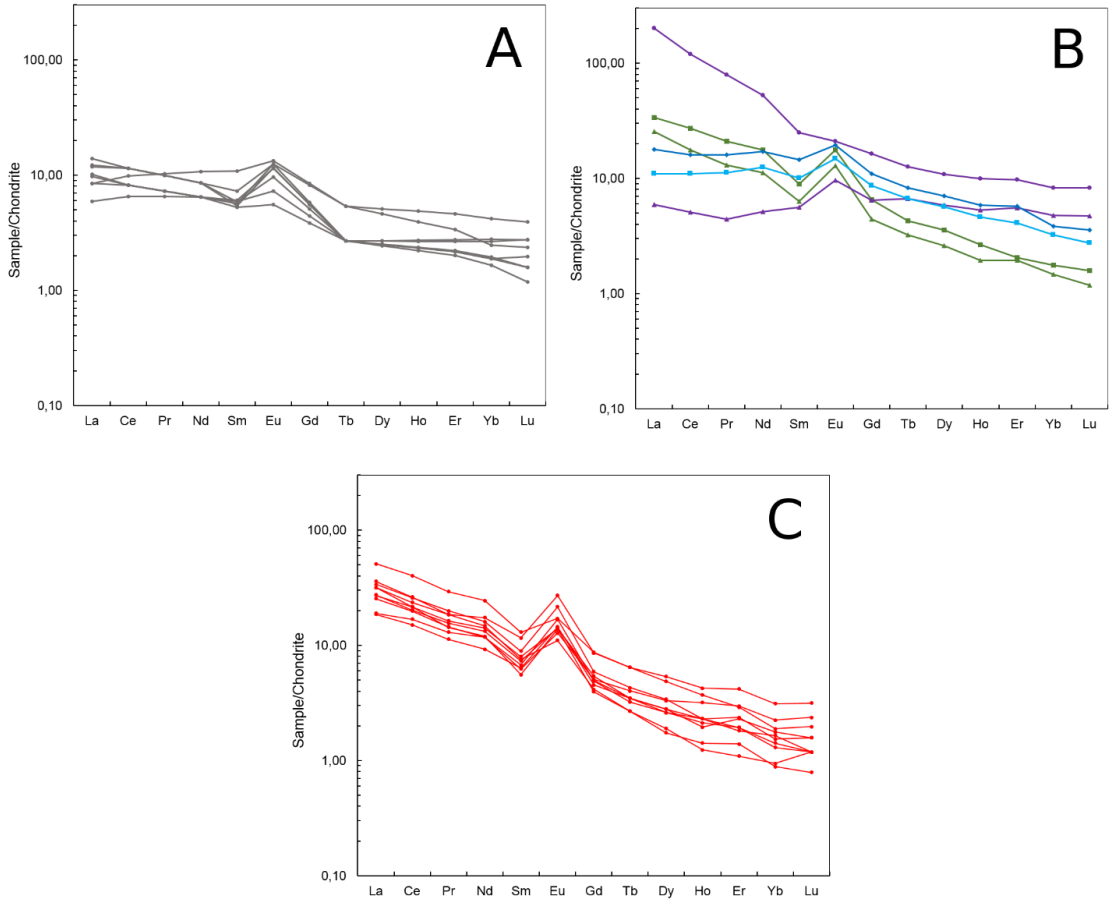

Figure 8.11. Chondrite-normalized REE patterns for different rock groups. Normalizing values Sun and McDonough (1989). A. Lower Zone gabbros (Nykänen, 1995) B. Marginal amphibolites, varied-texture gabbros, Ore Zone and Upper Zone gabbros. C. Anorthositic autoliths. Legend as in Fig. 8.10.

In summary, two major trends can observed in the distribution of major and trace elements in the intrusion rocks. Firstly, the Otanmäki intrusion is a differentiated intrusion showing a trend of progressive magmatic crystallization from the Lower Zone to the Upper Zone. This is seen in the higher contents of SiO_2, Al_2O_3, Sr and total REE, in addition to lower Mg-numbers, in the upper parts of the intrusive bodies. The trend is corroborated by an opposite behavior of compatible trace elements, such as Cr and Sc. The most primitive parts are the olivine-normative melagabbros on the SE flank of the

Vuorokas intrusion block. The Ore Zone and Upper Zone gabbros share many characteristics but the latter are more evolved.

Secondly, the Lower Zone is depleted in Fe, Ti and V in comparison to the Ore and Upper Zone. The Lower Zone-Ore Zone transition is imminent in the geochemical data as a sudden shift in the concentrations of Fe, Ti and V. The anorthositic autoliths share many trace element characteristics with the gabbroic rocks but differ in the concentrations of elements such as Sr, K and lower Ti concentrations, which attest dominantly to their plagioclase dominated mineral composition.

9 PLAGIOCLASE COMPOSITIONS

A total of 64 electron microprobe analyses were made on 9 polished thin sections from different rock samples. The primary aim was to compare plagioclase compositions in the anorthositic autoliths and other gabbroic rocks, also using data from previous studies. Plagioclase is the only primary cumulus mineral phase seen in the samples throughout the intrusion, enabling a systematic study of changes in the plagioclase major and trace element composition and, consequently, in the magma composition as a function of stratigraphic height. The focus was on the plagioclase-rich autoliths and similar leucocratic rocks in the intrusion, i.e., the vari-textured gabbros at Rinneaho and Metsämalmi. Samples were selected to represent different parts of the intrusion and different heights in the magmatic stratigraphy. One host gabbro, (OTA-1B), was included in the analyzed samples. Other samples are VTG pegmatite (RA-2B), sheared VTG near the Ore Zone (MEM-4), Ore Zone gabbro (OTA-1B), and autoliths (MEM-1, OTA-2, OTA-4, VUO-2A, VUO-1 and VUO-4.)

Most of the plagioclase in the studied samples is largely recrystallized, but primary euhedral to subhedral plagioclase crystals could be found in every sample. Analysis points were selected from those plagioclase crystals that most likely represent primary magmatic crystals, which are typically larger, do not portray triple junctions in the crystal corners and generally look more “dirty” than their recrystallized counterparts. Typically, 3 to 5 spots were analyzed from plagioclase crystals from each thin section. The plagioclase compositions were measured from the center and border of the grains to assess the presence of potential compositional zoning.

The compositional data obtained in this study were combined with 110 electron microprobe analyses of plagioclase from the Vuorokas Lower zone by Nykänen (1995). Calculated anorthite contents of plagioclase are presented in Fig. 9.1 and selected plagioclase compositions of different rock types are listed in Table 9.1. All analytical data are available in Appendix 4.

Table 9.1 Chemical compositions of selected plagioclase analyses.

Sample_ID	**MEM-1**	**VUO-1**	**RA-2B**	**OTA-1B**
Rock type	**autolith**	**autolith**	**VTG**	**gabbro**
SiO_2	57.23	52.03	52.69	57.26
TiO_2	0.00	0.02	0.00	0.00
Al_2O_3	26.62	30.62	29.25	25.98
FeO	0.05	0.02	0.07	0.11
CaO	8.35	12.92	11.85	7.56
Na_2O	6.12	3.70	4.16	6.02
K_2O	0.06	0.04	0.10	0.21
MnO	0.00	0.00	0.00	0.00
MgO	0.02	0.01	0.00	0.00
Sr (ppm)	2700	0	1860	0
Ba (ppm)	180	0	360	0
Total (wt%)	98.80	99.35	98.20	97.40

As seen in Fig. 9.1, the analytical data from the Lower Zone at Vuorokas are very consistent: 94% of the gabbroic rocks have a uniform labradoritic plagioclase composition. The data become slightly more dispersed upwards in the magmatic stratigraphy, but it must be taken into consideration that the stratigraphic height of the drill hole samples from the Lower Zone is but an estimation. The Lower Zone VTG at Rinneaho (RA-2B) has a similar plagioclase composition with the Lower Zone isotropic gabbros. The other vari-textured gabbro sample (MEM-4) has a slightly less calcic plagioclase composition with more variation in its anorthite content. MEM-4 is sampled from a large leucogabbroic mass, which is higher in the stratigraphy and in contact with the Ore Zone rocks at Metsämalmi. Its transitional composition between Lower Zone and Ore Zone is expected and likely reflects an evolving magma composition and/or later metamorphic equilibration.

In general, the plagioclase composition in a magma chamber is expected to show a descending An-content as a function of stratigraphic height as crystallization proceeds and calcium is incorporated in plagioclase and pyroxenes. As a result, the residual magma becomes enriched in sodium, a process recorded by decreasing An in plagioclase (Frost and Frost, 2013). This trend is observed in the studied sample set where the Lower

Zone-Ore Zone transition is seen as an abrupt change in the plagioclase composition from labradorite to andesine, reflecting progressive crystallization.

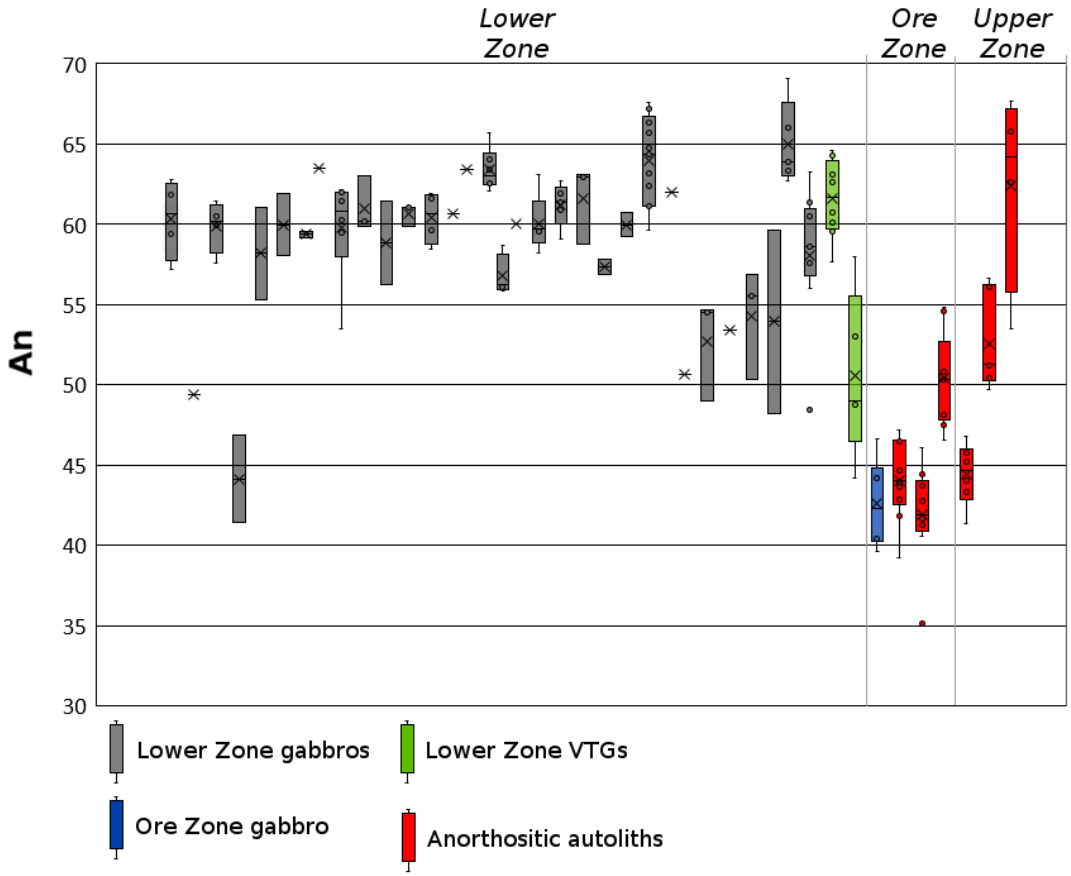

Figure 9.1. Anorthite content of plagioclase as a function of stratigraphic height.

As Fig. 9.1 illustrates, the Ore and Upper Zone autoliths have a somewhat similar andesitic plagioclase composition. Sample VUO-1 deviates from this compositional trend. It has a similar labradoritic plagioclase composition ($An_{62.37}$) to that of the Lower Zone vari-textured gabbros ($An_{44–65}$). Autolith VUO-1 was sampled from a large Upper Zone autolith (Fig. 7.2.), which also shares textural characteristics with the VTGs. The largely different plagioclase composition of VUO-1, together woth the textural observations, suggests that the larger autolith represents a different type of anorthositic autoliths, possibly linked to the vari-textured gabbros.

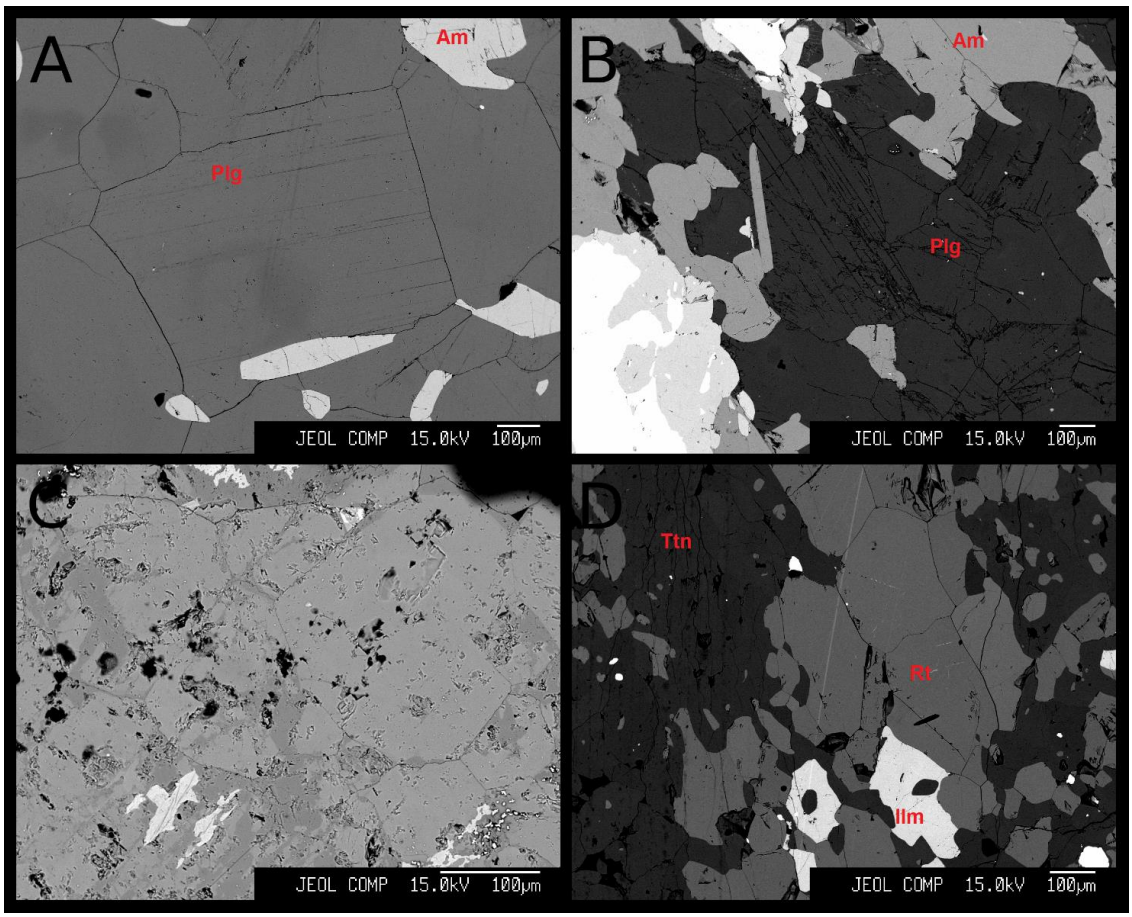

Figure 9.2. Back-scattered electron images of anorthositic autoliths. A. Largely recrystallized plagioclase crystals (Plg) and amphibole (Am) with a larger, subhedral crystal in the middle possibly representing primary plagioclase. (MEM-1) B. Larger subhedral plagioclase crystal (in the middle) with amphibole intergrowth and recrystallization on the borders (OTA-1B). C. Completely recrystallized and altered monomineralic anorthosite (OTA-4) with no primary textures. D. Typical mineral assemblage of ilmenite (Ilm) and its alteration products titanite (Ttn) and rutile (Rt) (VUO-1).

The plagioclase grains studied from the anorthositic autoliths show minor reverse compositional zoning. In 14 crystals out of 19, the An content rises from the center to the border and decreases in five. Zoning is not seen in back-scattered electron images (Fig. 9.2).

Besides the major elements in plagioclase, strontium and barium were also included in the analysis. Both are incompatible lithophile elements and potential indicators of magmatic differentiation. The Ba concentration in plagioclase varies between 0 and 800 ppm and were not used since most of the compositions falling below the detection limit. Strontium concentrations were quantified for almost all samples. Strontium in plagioclase varies between 0–4200 ppm with an average concentration of 1761 ppm and a

high standard deviation of 1000 ppm and the results should only be regarded as indicative. Sr concentration was plotted together with average plagioclase composition as a function of stratigraphic height (Fig. 9.3). To compare mineral chemistry data with ICP-OES/ICP-MS analyses, whole rock Sr and CIPW-normative plagioclase composition were plotted together with the EPMA data.

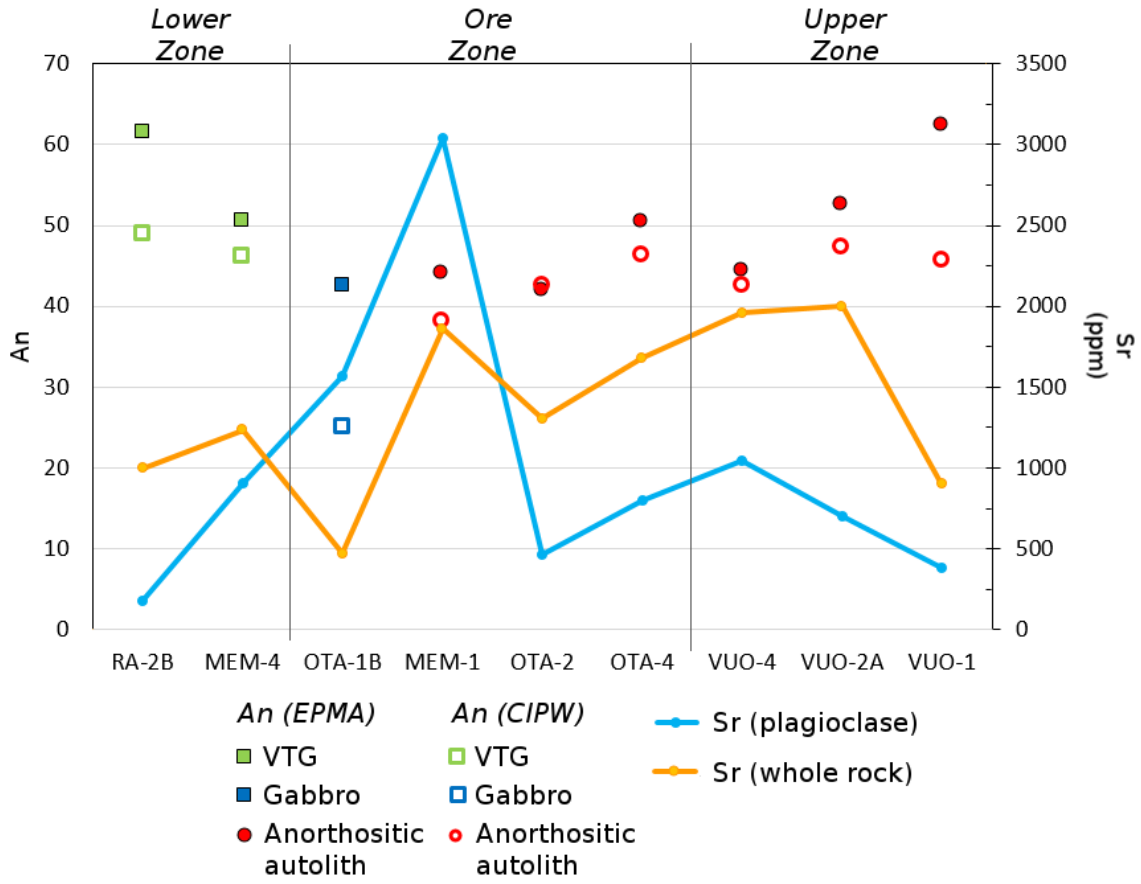

Figure 9.3. Average An and Sr contents from EPMA and ICP-OES/ICP-MS analyses as a function of stratigraphic height.

In whole rock geochemistry the highest Sr concentrations are observed in the anorthositic autoliths (899–2077 ppm) and the lowest concentrations in class I ore (2–31 ppm). As seen in Fig. 9.3, the whole rock Sr content and plagioclase Strontium content follow the same trend. Sr is dominantly hosted by plagioclase as more leucocratic rocks show a higher Sr content in both sample sets. However, the whole rock analyses show Sr concentrations above those in the plagioclase. This is slightly enigmatic and possibly attest to strontium mobilization during metamorphosis. The plagioclase Sr content does not seem to correlate with stratigraphic height or rock type as much as with vicinity to the oxide ore: the highest Sr contents are seen in an autolith (MEM-1) and an Ore Zone

gabbro (OTA-1B) which both ore in contact with oxide ore. Then again, the limited data set does not allow far-reaching conclusions. As seen in Fig. 9.3, the CIPW-normative anorthite content generally coincides with the plagioclase composition obtained from the EPMA analyses though sporadic mismatches are seen.

10 DISCUSSION

10.1 Magmatic emplacement

Gabbros of the Otanmäki intrusion intruded the Archean craton margin at 2058 ± 13 Ma (Huhma et al., 2018). Like many other mafic intrusions, including the the Bushveld complex (Silver et al. 2004), the Otanmäki intrusive complex is located near a craton margin, where ascending magmas can utilize pre-existing translithospheric structures (Maier, 2015). The magmatic event was connected to the last rifting events of the Archean Karelia craton upon its break up at 2.1–2.05 Ga (Nironen, 2017).

The Otanmäki and Vuorokas intrusive bodies have a similar structure with isotropic gabbro and vari-textured gabbro in the lower part overlain by a heterogeneous gabbro-oxide ore assemblage, which is characterized by the presence of similar anorthositic autoliths in both blocks. Gabbros at Otanmäki and Vuorokas resemble each other geochemically and mineralogically and they have the same age (Huhma et al., 2018). When geochemical similarities are coupled with structural observations, it can be concluded that the Otanmäki and Vuorokas intrusive bodies represent the same magmatic event, having been developed in a single magma chamber, which was separated into separate blocks by later tectonic events. Together they are therefore referred to as the Otanmäki intrusion.

The Otanmäki intrusion is spatially closely associated with Otanmäki suite A-type granites and intermediate rocks, having a vertical fault contact to the latter rocks. The genesis of A-type granitoids and syenites can potentially be linked to mafic intrusions through extensive fractionation of basaltic parental magma, as is envisaged to have happened in the Sept Iles intrusion (Higgins and Doig, 1986). However, according to Kärenlampi et al. (2019), the Otanmäki suite A-type rocks and the Otanmäki intrusion gabbros originate from different sources based on their Y/Nb ratios and are therefore not cogenetic. The Otanmäki suite is possibly parautochthonous and its genesis is equally linked to the lithospheric break-up of the Archean Karelia craton (Kontinen et al., 2013a; Kärenlampi et al., 2019). Narrow A-type dikes are found cutting gabbros of the Otanmäki intrusion. If the dikes can be proven to belong to the Otanmäki A-type suite, it would give a minimum age of crystallization for the Upper Zone rocks.

10.2 Structure of the intrusion

10.2.1 Marginal amphibolites

Two occurrences of fine-grained and variably sheared marginal amphibolites are known from the intrusion. Due to their appearance and position between the Lower Zone rocks and the Archean gneisses, they could represent a chilled margin. Chilled margins have traditionally been thought to represent parental magma that cooled rapidly without fractionating, and they have been used to determine the primary unfractionated parental magma composition (McBirney, 1993; Blatt et al., 2006). Fine-grained chilled margins are not very common: marginal rocks in many layered intrusions of the Fennoscandian Shield, for example, do not shows signs of chilling (Latypov et al., 2007). The marginal amphibolite in the Otanneva block is marked on previous maps, but that at Rytisuo is not reported in previous studies. Neither of them have been sampled previously.

The relation between the composition of a chilled margin and the parental magma is proven to be more complicated than traditionally assumed (Latypov et al., 2007). Latypov et al. (2007) suggest that primary chilled margins are often destroyed by the heat flow from the magma chamber and replaced by subsequently formed "secondary chilled margins". Secondary chilled margins are cumulates that crystallized in high temperatures from liquids by Soret fractionation, i.e., a temperature gradient driven mass transport. Latypov et al. (2007) argue that secondary chilled margins are more common than primary chilled margins and cannot therefore be used as indicators of parental magma composition.

The marginal amphibolites of the Otanmäki intrusion have a somewhat similar normative composition to those of the intrusion gabbros but their trace element contents differ. Based on REE data, the marginal amphibolite at Rytisuo (VUO-20) could theoretically represent the most primary member among the gabbro types. Its trace element composition (V, Sr, Zr, LREE; Figs. 8.7 and 8.11B) differs significantly from that of the marginal amphibolite in the Otanneva block. The two marginal amphibolites either originate from different magmatic processes or their composition is unevenly altered by metamorphic events. Magmatic causes for anomalous features in chilled margins include a variety of processes, such as contamination, changes in the composition of intruding

magma, supercooling and loss of magma from the magma chamber (Latypov et al., 2007) and it is not uncommon for an intrusion to have compositionally different chilled margins.

The subject of chilled margins is only touched upon in this study. The marginal amphibolites, probable chilled margins, could be studied in more detail, but as described above, but it is questionable whether they can provide information of the parental magma composition.

10.2.2 Lower Zone

The Lower Zone is distinguished by the presence of isotropic, medium- to coarse-grained meso- and adcumulates. Occasionally, gabbros in the Vuorokas Lower Zone still contain unaltered primary magmatic mineral facies. Isotropic Lower Zone gabbros at Vuorokas and Otanneva have occasionally larger, euhedral plagioclase crystals which could theoretically represent an earlier crystallized mineral fraction from lower, unknown parts of the magma chamber or a feeder dike. More thorough mineral chemistry analyses are required to confirm their origin.

The stratigraphy column constructed by Nykänen (1995) contains an olivine gabbro layer in the S part of the Vuorokas block. In the map by Havola (1997), there are two occurrences of olivine gabbro in the SE part of the block. Neither of these units were observed in the mapping campaign of this work. However, the rocks at the SE flank of the Vuorokas block have a more primitive, olivine gabbronoritic composition. Owing to that, their high Mg numbers, enrichment in Cr and low Sr contents in comparison to other rocks in the intrusion, the SE parts of the Vuorokas block are, in unison with Nykänen (1995), regarded as representatives of the lowest parts of the magma chamber.

Sporadic occurrences of gabbroic pegmatites in the isotropic gabbro are present throughout the Vuorokas Lower Zone. The pegmatite occurrences become more frequent near the Ore Zone and become the dominating rock type in the upper parts where they form the most striking feature of the Lower Zone: the vari-textured gabbros. Their contacts to the isotropic gabbro are often obscure, and the upper parts of the Lower Zone are relatively heterogenous in terms of grain size, mineral composition and cumu-

lus terminology. The 2.44 Ga Koillismaa intrusion in northeastern Finland contain similar, coarse-grained anorthositic-leucogabbroic rocks beneath the Fe-Ti-V oxide ore-bearing magnetite gabbros (Karinen et al., 2015). Also their contact to the above lying ore-bearing rocks is sharp.

Vari-textured gabbros are likely in-situ pegmatites (in contrast to intrusive pegmatites) (London, 2008). As Lower Zone cumulates crystallized, the residual magma became richer in volatiles (Nykänen, 1995). This trend is recorded by the VTGs, which based on their grain size and sulfide content, crystallized in an environment where partial pressure of fluids was high.

The Skaergaard intrusion has also gabbro pegmatites whose crystallization was likely affected by an external fluid source from marine sediments (Irvine et al., 1998). Although the intrusion of the Otanmäki gabbros partially postdates the formation of Kalevian deep-sea sediments, the intrusion is exclusively hosted by Archean rocks and the degree of crustal contamination of the gabbros is minimal (Patchett et al., 1981; Huhma et al., 2018).

10.2.3 Ore Zone

In this study, the intrusion is divided into three major zones. Ore and Upper Zones are examined separately because of their different rock type assemblages. The Ore Zone hosts close to 100% of the known oxide ore lenses, and all the mining operations took place within it.

The Ore and Upper Zone gabbros have a similar appearance and normative mineral composition to those of the Lower Zone isotropic gabbros. However, the Ore and Upper Zone gabbros are distinguished by their high oxide mineral content and higher concentrations elements such as TiO_2, V, Nb and total REE (Figs. 8.6 and 8.11). Also the An content of plagioclase drops drastically when moving from the Lower Zone to the Ore Zone (Fig. 9.1). Notwithstanding their similar appearance, the Lower and Ore Zone gabbros differ from each other greatly and attest to a major change in the magma chamber upon the onset of the crystallization of the Ore Zone rocks. The structure and ore mineralogy of the Ore Zone shares similarities with the Mustavaara Fe-Ti-V oxide de-

posit in northern Finland, which also has a sharp lower contact to leucocratic, coarse-grained gabbros and a gradational upper contact to less ferrous gabbros (Karinen et al., 2015). The magnetite gabbros at Mustavaara are also similar to those at Otanmäki and Vuorokas: they are small- to medium-grained plagioclase-augite-ilmenomagnetite adcumulates with ferromagnesian minerals recrystallized to amphibole.

Oxide ore is present as lenses, or, more rarely, layers. The layer-like form of the oxide ore is best seen in the geological map from the Vuorokas open pit where oxide ore forms one heavily bifurcated layer (Fig. 4.4A). The location represents the easternmost ground occurrence of the Ore Zone. The Ore Zone at Otanmäki, in contrast, has layers and lenses atop each other (Fig. 4.3); Kerkkonen (1979) separates up to five layers from the eastern part of the Ore Zone at Otanmäki (Figs. 4.2A). At the Vuorokas underground mine, between these two occurrences, the ore is reportedly present as long, separate lenses but only in 1–3 "layers" or levels (Fig. 4.4B, Parkkinen, 2015). Oxide ore at Otanneva, west from Otanmäki, does not crop out, and ore occurrences at Otanneva are not substantial enough to be economic, at least not in near the surface (Soininen and Paarma, 1959; Paarma, 1961). Ore occurrences east from the Vuorokas open pit towards the intrusion margin are similarly narrow and subeconomic.

The presence of a complexly accumulated congregation of ore lenses in the assumed central parts of an intrusion surrounded on both sides by narrower layers that thin towards the intrusion borders is interpreted to have originated from gravitational movements in the magma chamber, as described by Maier et al. (2013) and Maier (2015) (Fig. 10.1). Subsidence of the magma chamber center may result in accumulation of the oxide cumulate mushes in its central parts and hydrodynamic sorting of dense phases (Maier, 2015). Smaller intrusions, such as the Otanmäki intrusion, cool faster than larger ones and subsidence is less prominent, resulting possibly in less continuous, wider reefs (Maier, 2015). This model could explain the less continuous nature and lensoidal occurrence of the Fe-Ti-V ore throughout the Ore Zone of the Otanmäki intrusion. Sorting of a magnetite slurry or gravitational concentration of oxide crystals is also proposed to have affected the ore formation in the Mustavaara Fe-Ti-V oxide deposit and Kemi Cr deposit, which are similarly hosted by relatively small mafic intrusions (Karinen et al., 2015; Maier and Hanski, 2017). In the Mustavaara deposit, a sharp basal con-

tact, similar to that observed in the Otanmäki intrusion, is regarded as supporting evidence for the view of gravitative concentration (Karinen et al., 2015).

Tectonic thickening and stretching have clearly affected the occurrence of the ore, especially in the western part of the Otanmäki block. However, the lensoidal nature of the oxide ore throughout the intrusion, also in its lesser tectonized parts, and its concentration in the assumed intrusion center and narrow occurrences towards the borders argue for magmatic processes in the emplacement of the ore as opposed to the view that the Ore Zone represents a tectonically shattered layer (Nykänen, 1995).

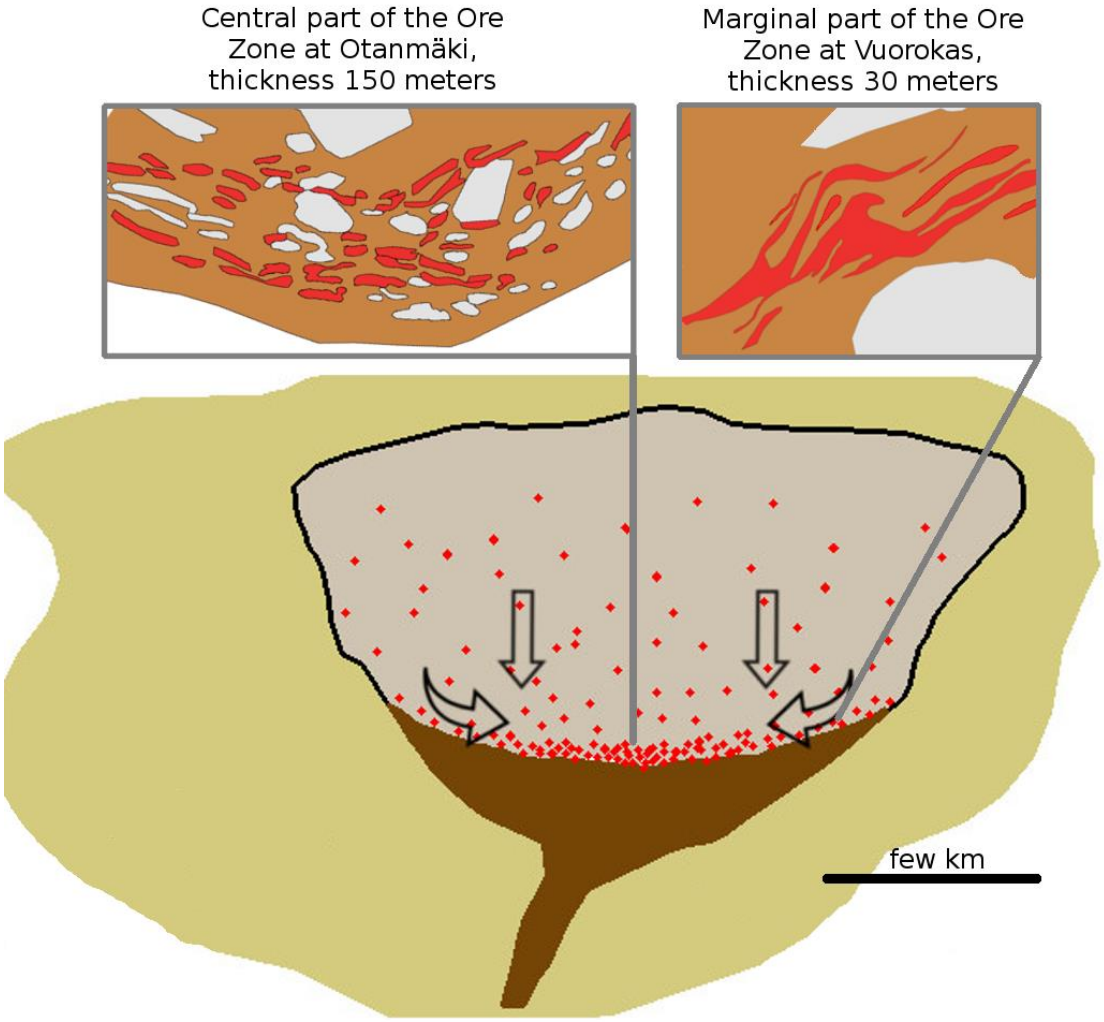

Figure 10.1. A model proposed for the Fe-Ti-V oxide ore genesis by gravitation-driven slumping of semi-consolidated oxide slurry in the Otanmäki magma chamber. See text for more information.

10.2.4 Upper Zone

The Upper Zone is regarded as a continuum of the Ore Zone. The majority of the Upper Zone consists of isotropic, locally layered gabbros whose major and trace element compositions (e.g. Mg#, P_2O_5, REE; Figs. 8.5 and 8.11) suggest more advanced magmatic differentiation in comparison to the Ore Zone. In the Upper Zone, one occurrence of apatite-rich gabbro has been found but the P_2O_5 content in general is low in all rock types. The Otanmäki Fe-Ti-V deposit is by no means comparable to the so-called iron oxide-apatite deposits, such as the Kiruna in northern Sweden or Kauhajoki Ti-P-Fe deposit in western Finland (Jonsson et al., 2013; Sarapää et al., 2015).

10.2.5 A layered intrusion?

Both the Otanmäki and Vuorokas intrusive bodies have been referred to as layered intrusions (e.g. Nykänen, 1995; Vuollo and Huhma, 2005). They have a differentiated, even layer-like structure, with the most prominent feature being the continuous, 30- to 200-m-wide Ore Zone that extends through the whole intrusion. The enrichment of Fe and Ti in the upper part of a magma chamber is typical to layered intrusions, as well as the occurrence of anorthosites in the upper parts (Ashwal, 1993; Maier, 2015).

The Lower Zone is largely formed by gravitational crystal settling, which is characteristic to layered intrusions (e.g., Blatt et. al., 2006), but in the Otanmäki intrusion, the process did not lead to the formation of extensive magmatic layering. Magmatic layering is occasionally seen in Ore and Upper Zone outcrops as well as in ore lenses in the Otanmäki mine (Kerkkonen, 1979). In addition to the position of ore and anorthosite lenses, the vertical layering provides evidence that the intrusive bodies are turned to their side at an approximately 90° angle from their primary position. However, the Otanmäki intrusion lacks a well-developed layering and a continuous stratigraphic horizon often associated with layered intrusions – if the heterogenous Ore Zone is not regarded as such. To avoid misinterpretation, the term “differentiated mafic intrusion” is preferred in this study.

10.3 Satellite intrusions

A total of five satellite intrusions are known within a 15-km radius from the Otanmäki intrusion. They have a similar structure with the Otanmäki intrusion: a gabbroic lower part and a leucogabbroic upper part, which hosts oxide ore lenses (Lindholm and Anttonen, 1980). The satellite intrusions likely represent the same magmatic with the main intrusion, and together they are referred to as the Otanmäki intrusive complex.

The genesis of an oxide ore necessitates progressive crystallization and enrichment in Fe, and the magma that formed the satellite intrusions had presumably fractionated previously in a larger magma chamber. The satellite intrusions are relatively thin (150–700 m) and the presence of a typical Ore Zone rock assemblage could imply that they are not only tectonically removed slivers, but originated at least partly through the magmatic processes that occurred at the time of the Ore Zone crystallization in the larger magma chamber.

The satellite intrusions may have intruded the Archean gneisses during the crystallization of the Ore Zone. Semi-solidified crystal slurries may locally inject areas of lower pressure, such as fractures in the surrounding rocks, to form sills (Robb, 2005; Maier, 2015). The satellite intrusions have a limited outcrop coverage and are not well studied. Research on their geology should also yield information on the evolution of the main magma chamber. The presence (or absence) of anorthositic autoliths in the satellite intrusions, for example, could shed light on the temporal relations between oxide ore crystallization, autolith emplacement and the possible injection of the satellite intrusions.

10.4 Anorthositic autoliths

Leucocratic, fine- to medium-grained plagioclase-rich inclusions are seen throughout the Ore and Upper Zone both at Otanmäki and Vuorokas. The inclusions are dominantly anorthositic in composition and show dynamic contacts, which implies their settling from an upper part of the magma chamber into their Ore and Upper Zone host rocks. Based on mineralogical observations and geochemical data, the rocks are regarded plagioclase adcumulates whose trace element characteristics indicate that they represent the most differentiated member among the Otanmäki intrusion mafic rocks. They are simi-

lar to the gabbroic rocks of the intrusions in terms of their chondrite-normalized, LREE-enriched REE patterns and other trace element characteristics (Figs. 8.9 and 8.10), which suggests derivation from the same magma. Based on these indicators, the anorthositic inclusions are regarded as being of cognate origin, i.e., they are derived from the same magma as their host rocks and are therefore referred to as autoliths.

10.4.1 Contacts to country rocks

Some autoliths are angular, breccia fragment-type bodies, others show smaller pieces broken from a larger autoliths towards the magma chamber floor. The irregular, wedge shapes of the anorthositic autoliths together with their sinuous contacts to host gabbros and ore indicate that the autoliths were solidified to different degrees upon their emplacement in the Ore and Upper Zones. A comparable association of anorthositic autoliths from the Skaergaard intrusion is described by Irvine et al. (1998). Similarly to the Otanmäki intrusion, the anorthositic autoliths in the Skaergaard are present in various sizes from below 0.5 m to over 200 m in diameter. Some are angular whereas others are vaguely rounded or irregular in shape (Irvine et al., 1998). Similarly, Namur et al. (2011) report anorthositic autoliths in the Sept Iles intrusion that are also angular to slightly rounded in shape. Irvine et al. (1998) regard the varying shapes of the autoliths as a consequence of different degrees of solidification upon their emplacement: angular blocks were already well solidified when they broke loose from their site of crystallization whereas the more irregular autoliths were still “mushy”.

Some of the autolith-host rock contacts at Otanmäki and Vuorokas have provided planes for tectonic movement but undisturbed magmatic contacts can be seen especially in Upper Zone rocks. Similarly to autoliths in the Skaergaard and Sept Iles intrusions, magmatic layering is seen to drape over the autoliths on the top side of magmatic stratigraphy (Irvine et al., 1998; Namur et al., 2011). Also the habit of lenticular autoliths to occur parallel to the stratigraphy is reported from the Skaergaard intrusion by Irvine et al. (1998).

Unlike the spatially limited ore lenses, anorthositic autoliths occur throughout the Ore and Upper Zone (Fig. 6.1A and B) and are met in areas of both strong and nonexistent tectonic strain. The ubiquitous occurrence of the diversely shaped autoliths throughout

the upper half of the intrusion, and their sinuous contacts to their host gabbros and ore suggest strongly that their distribution in the intrusions is primarily controlled by magmatic processes rather than resulting from boudinage or brittle deformation of one or several anorthosite layers.

10.4.2 Composition of the autoliths

The majority of the anorthositic autoliths are fine to medium grained and almost monomineralic. The plagioclase composition in the autoliths is different to that of the Lower Zone gabbros but similar to their hosts, the Ore and Upper Zone gabbros. The identical plagioclase composition with the host rocks could imply that they crystallized at the same time in the magmatic evolution from a compositionally similar magma. In a dense magma, isolated plagioclase crystals may discharge from the cotectic assemblage and float to higher parts in the magma chamber. Their ascent might be facilitated or enhanced by convection currents (Irvine et al., 1998; Higgins and Chandrasekharam, 2007). Metamorphic reactions may contribute to the current plagioclase composition, and the comparison of plagioclase from the partly primary Vuorokas Lower Zone to, say, the thoroughly recrystallized Metsämalmi area is not without complications. Nonetheless, the plagioclase composition of the Ore and Upper Zone gabbros and autoliths is determined to be andesinic throughout the intrusion and likely reflects a change in the evolving magma chamber more than a later metamorphic overprint.

Some, typically larger autoliths have a larger grain size, contain more ferromagnesian minerals and portray mottled or pegmatitic textures associated with the Lower Zone vari-textured gabbros. These VTG-type autoliths are seen both in the Ore and Upper Zone. Kerkkonen (1979) also reported the presence of coarse-grained, partly pegmatoidal gabbro inclusions in the Otanmäki underground mine. These inclusions have often a mottled texture and may have anorthositic and leucogabbroic parts within themselves and they likely represent the VTG-type autoliths described on this study. Contacts of the VTG-type autoliths to country rocks (e.g. OTA-5, VUO-1) seem to not differ from those of other autoliths.

A large VTG-type autolith turned out to have a similar plagioclase composition to that in the Lower Zone vari-textured gabbros. This suggests that it originates from the Lower

Zone and was incorporated in the magma by positive buoyancy and/or subsequent magma pulse(s) after its crystallization. The autolith also shares textural and compositional characteristics with those of the vari-textured gabbros. With the available data, especially the scarce mineral chemistry data, it cannot be reliably established whether the VTG-type autoliths represent a fundamentally different component in comparison to the smaller, more monomineralic autoliths. In contrast, it could also imply that the crystallization of the Ore and Upper Zone anorthositic autoliths was a dynamic process, with the amount of interstitial mafic component varying over distance and/or time. Irvine et al. (1998) separate four different classes of leucocratic autoliths in the Skaergaard intrusion based on differences in the abundance and assemblages of mafic minerals. A similar approach could be applied to the autoliths in the Otanmäki intrusion, especially if more abundant mineral chemistry data were available. A separation of the autoliths into several classes is not done in this study, apart from the autoliths with vari-textured characteristics being referred to as VTG-type autoliths.

10.4.3 Formation of roof anorthosite and sinking of autoliths in the magma chamber

Anorthositic autoliths in the Sept Iles and Skaergaard intrusions are regarded as having crystallized in the upper part of the magma chamber, from where they sank to the lower parts as changes in the magma chamber, such as density fluctuations or faulting, destabilized the upper zone anorthosites (Irvine et al., 1998; Namur et al., 2011). The formation of an anorthositic rocks at the top of a magma chamber necessitates positive plagioclase buoyancy in the melt. When a melt becomes enriched in FeO, as it is evidenced to have happened during the crystallization of the Vuorokas Lower Zone, the magma density might be high enough to allow crystallizing plagioclase to be positively buoyant and concentrate in the upper part of the magma chamber. Consequently, upon Fe(-Ti)-oxide crystallization, the residual magma becomes poorer in iron and less dense, preventing plagioclase flotation and allowing fragments of the anorthositic upper part to sink (Irvine, 1987; Namur et al., 2011).

Namur et al. (2011) suggest that during the crystallization of the Sept Iles intrusions, sequences of plagioclase flotation alternated with periods of negative plagioclase buoyancy. This formed massif anorthosites at the top of the magma chamber and sinking blocks at the base of the intrusion. The decrease in the plagioclase buoyancy was a re-

sult of oxide mineralization in the melt and subsequent decrease in melt density. Correspondingly, Irvine et al. (1998) suggest that in the Skaergaard intrusion plagioclase was buoyant through most of the crystallization history of the magma. Plagioclase crystals floated through convective flow to the Upper Border Series and formed anorthositic rocks that later broke into autoliths which descended back to lower parts in magma chamber. The detachment of autoliths from the upper border series massif anorthosite is thought to have occurred through upper border stoping and magma convection (Irvine et al., 1998). The distribution of the autoliths may also be affected by lateral currents in the chamber (Irvine et al., 1998).

Many layered intrusion contain anorthositic autoliths, but the Sept Iles intrusion is the only known occurrence where significant volumes of roof anorthosites, the provenance of the autoliths, is known (Namur et al., 2011). In the Skaergaard intrusion, the anorthositic upper part of the magma chamber is not known (Irvine et al., 1998). Also in the Otanmäki intrusion, none of the intrusion blocks have a known anorthositic upper part. The leucocratic vari-textured gabbros at Rytisuo can theoretically represent a "roof anorthosite", but they are considered to belong to the Lower Zone rocks, as discussed in Chapter 6. Most of the Upper Zone at Vuorokas is not exposed, and hence, theoretically there could be hidden occurrences of more massif anorthosite. It is also possible that the hypothesized upper part anorthosites were completely deposited back to the magma chamber in the latter parts of magmatic evolution or removed by later tectonic movements.

10.4.4 Factors affecting plagioclase buoyancy

Plagioclase can be buoyant in mafic melts (e.g., Bottinga and Weill, 1970; Campbell et al., 1978). Magma chambers cool dominantly from their roof (Irvine, 1970), and the accumulation of plagioclase at the top of a basaltic intrusion may allow anorthosite formation at the magma chamber roof (Scoates, 2000). As crystallization proceeds, density changes in magma can allow, or prohibit, plagioclase buoyancy (Robb, 2005; Namur et al., 2011).

Namur et al. (2011) calculated that in the early stages of magmatic differentiation in the Sept Iles intrusion, an FeO-rich tholeiitic melt underwent density increase from 2.70 to

2.75 gcm^{-3} through fractionation of troctolites. This resulted in plagioclase being positively buoyant and forming anorthosites at the top of the magma chamber. Upon crystallization of Fe-Ti oxide-bearing gabbros, the melt density decreased to 2.16 gcm^{-3}, the formation of roof anorthosites seized and plagioclase started sinking in the chamber. Plagioclase flotation was, however, not very efficient, and positively buoyant plagioclase is also reported from lower parts of the chamber.

To verify the theory of sinking of autoliths through descended magma density, proper density calculations should be made. Density calculations of liquids require knowledge of the water content of the melt, melt liquidus temperatures, the pressure of the crystallization and how oxygen fugacity evolved with magmatic differentiation (Bottinga and Weill, 1970) and are not within the scope of this study.

10.4.5 Genesis of the anorthositic autoliths in the Otanmäki magma chamber

The occurrence of anorthositic autoliths virtually everywhere above the Lower Zone indicates, together with the contacts to country rocks, that their genesis is linked to magmatic processes affecting the whole magma chamber during the crystallization of the Ore and Upper Zones. The autoliths share many similarities with leucocratic autoliths in other mafic intrusions: a varying size and shape, fluctuations in the quantity of mafic minerals, parallel orientation to the stratigraphy and contacts to host rocks, which include draping of magmatic layers.

Based on obvious similarities in the field relations with the leucocratic autoliths in other intrusions described in the literature, the model of plagioclase flotation and sinking of diversely solidified anorthosite blocks from the upper parts of the magma chamber is regarded as the most viable mechanism for the generation of autoliths in the Otanmäki intrusion (Fig. 10.2). During the crystallization of the Ore and Upper Zone, part of the crystallizing plagioclase has likely risen to the top of magma chamber and solidified there. Blocks of this massif “roof anorthosite” later descended into lower parts of the magma chamber during the crystallization of Ore and Upper Zones. Sinking of the autoliths could have resulted from several processes, such as convective magma flow in the chamber or faulting of the magma chamber roof. The suggested gravitational movements in the chamber could also destabilize partly solidified cumulates. With the limits

of the data taken into consideration, the cause of sinking can only be speculated upon, but the crystallization of the Fe-Ti-oxides with a subsequent decrease in the residual melt density has likely at least contributed to the process. The Otanmäki intrusion does not have a known "roof anorthosite", the extrapolated place of origin of the autoliths. That is however not uncommon for an autolith-bearing intrusion.

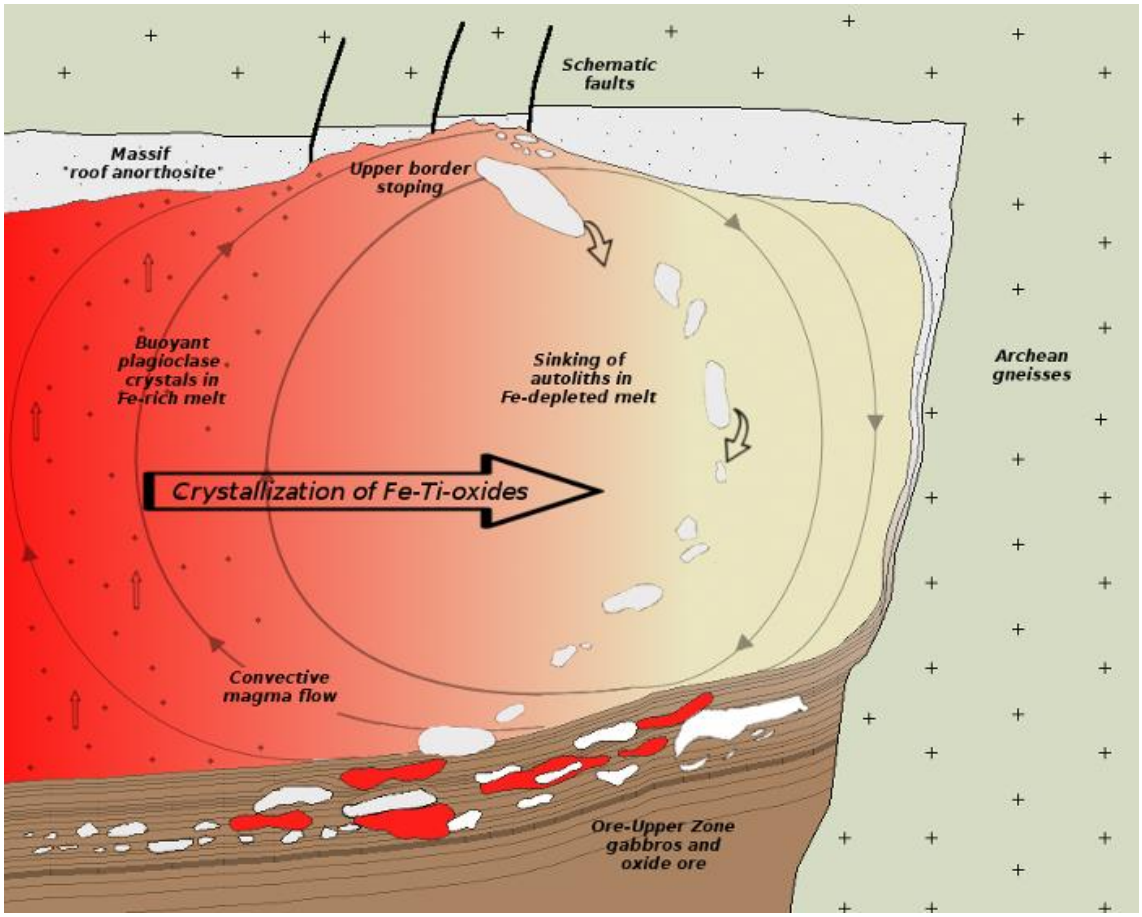

Figure 10.2. A model proposed for the formation of anorthositic autoliths in the Otanmäki magma chamber. Plagioclase crystals are buoyant in an Fe-Ti-enriched melt and crystallize at the top of the cooling magma chamber. Oxide ore crystallization and subsequent decrease in the melt density leads to destabilization of the roof anorthosite and sinking of varyingly solidified blocks. The processes may be enhanced by convective magma flow and faulting of the magma chamber roof.

10.5 Magmatic evolution

The parental magma of the Otanmäki intrusion is an Fe-Ti-V-enriched tholeiitic melt (Nykänen, 1995). An ultramafic lower part traditionally associated with layered intrusions, as well as a feeder dike, are not known to occur in the intrusion. The more mafic

parts are either under Quaternary deposits, in a non-recognized feeder dike or a deep-seated chamber, or removed by later tectonic movements.

Nykänen (1995) proposed that slow cooling and crystallization in the Vuorokas Lower Zone enabled cumulus growth of plagioclase, gravitational settling and compression of the solidified crystalline mush. Crystallization occurred under reducing conditions and at relatively high pressure of 7 kbar (Nykänen, 1995) The low amount of intercumulus fraction in the Vuorokas lower part plagioclase-rich rocks implies separation of crystalline fraction and the residual melt through compaction of the crystalline mush and/or convective currents in the melt. Residual melt rose into upper parts in the magma chamber and enrichment of residual melt in volatiles.

The crystallization of the Ore Zone and the genesis of the Fe-Ti-V oxide ore occurred in the later stages of magmatic differentiation. The deposition of the ore may have been controlled by several factors but is likely set off by an increase in the oxygen fugacity and a decrease in temperature as the intrusions cooled and became more rich in Fe, Ti and V (Nykänen, 1995). Ore zone rocks are not seen as dikes in the Lower Zone, suggesting that it was relatively solidified when the Ore Zone started to crystallize.

The Ore Zone is extremely heterogenous: layers of different grades of oxide ore alternate with (magnetite) gabbro and anorthositic autoliths. Also the host gabbro is compositionally discordant: it is locally rich in magnetite, has locally ultramafic rims in the contacts with the anorthositic autoliths and occasionally portrays layering with more leucocratic sequences. The structure of the Ore Zone implies that partly crystallized Ore Zone cumulate mushes were subject to gravity-induced movements. This view is in unison with Talvitie and Paarma (1980) who suggest that the magmatic differentiation at Otanmäki was controlled by dynamic mechanical processes rather than purely gravitational processes.

The crystallization of the Ore Zone has likely associated with one or more periods of plagioclase flotation, which may have alternated with stages of negative plagioclase buoyancy forming anorthositic parts at the roof of the magma chamber and diversely solidified, descended blocks of anorthosite in the semi-solidified Ore Zone. The anor-

thositic autoliths are regarded as cumulates from the same magma that generated the other intrusion rocks, and their genesis does not necessitate a second pulse of Al- and Si-rich melt produced by fractional crystallization in another magma chamber, as suggested by Nykänen (1995).

The temporal relations between the two suggested models, gravity induced movements and deposition of autoliths from higher parts in the magma chamber, requires further study. The flow structures in the oxide ore around anorthositic autoliths, as reported by Kerkkonen (1979), suggest that at least part of the gravitation-driven movements postdate the deposition of the autoliths in the Ore and Upper Zones.

10.6 Deformation and metamorphism

Based on field observations and geophysical data, the Otanmäki intrusion and the surrounding lithologies have undergone several deformation events. A detailed structural analysis is beyond the scope of this study, but some statements can be made.

The larger Vuorokas block is in parts totally untectonized and portrays locally conserved primary magmatic mineralogy, whereas the boomerang-shaped Otanmäki block is characterized by strong shearing and recrystallization. The Otanmäki and Otanneva blocks have been transferred approximately two kilometers to the north from the Vuorokas block by dextral movements. The movement has been roughly N-S oriented consisting of several conjugate strike-slip faults. Smaller N-S-oriented faults with dextral or sinistral movement are common in the research area.

The area between Otanmäki and Vuorokas is poorly exposed and based on geophysics, is assumed to be complexly faulted. The A-shaped area between the Otanmäki and Vuorokas blocks is here considered to represent Archean rocks (Fig. 6.1). This is based on geophysics and the views of previous researches. However, there are no outcrops or drill hole data from the area, and the it could also contain Otanmäki intrusion rocks, likely those belonging to the Lower Zone of the Otanmäki block.

In a second deformation phase, the Otanmäki block has been pushed back by left-hand movement(s) leading to the separation of the Otanneva block by a sinistral fault and the

boomerang-shaped folding of the whole Otanmäki block. It is possible that the Otanmäki block has overturned in this movement completely, as oxide ore occurrences are known to exist in the northernmost part of the intrusion block ("Välimalmi", see Fig. 4.2) in an otherwise unusually high part of the stratigraphy. The upper contact of the Otanmäki block is faulted, with the uppermost part of the magma chamber being displaced by tectonic movements.

Tectonic strain is distributed unevenly in the Otanmäki block and the Ore Zone has endured most of the tectonic stress. This is due the heterogeneous composition of the Ore Zone and partitioning of tectonic strain between rock types. Ore lenses and layers are the most ductile whereas the hard, plagioclase-rich autoliths endure the strain better. Amphibolitization and recrystallization is most prominent in the Otanmäki Ore Zone, having contributed to the quality and beneficiation properties of the ore by exsolution of ilmenite from magnetite-ulvöspinel solid solution (Kerkkonen, 1979). Recrystallization and hydration has further increased the textural heterogeneity of different gabbro types.

The Vuorokas block is regarded as more autochtonous than the Otanmäki block, but most of its contacts to the Archean gneisses are nevertheless considered faulted. Additionally, a fold is seen in geophysics in the NE corner of the Vuorokas Ore Zone. This suggests that some roughly N–S-oriented sinistral movement has occurred also at the eastern flank of the Vuorokas block.

10.7 Suggestions for follow-up research

The mapping campaign covered almost all outcrops within the Otanmäki intrusion. Anorthositic autoliths were nonetheless only mapped in detail in limited areas, and small-scale mapping could be expanded to the NE part of the Otanmäki block where autoliths are seen regularly and the outcrop coverage is good. The vari-textured gabbros are the closest compositional counterpart to the autoliths in the intrusion, and occurrences of VTG should be sampled more thoroughly, especially at Rytisuo, to allow their comparison with the autoliths and ascertain whether they truly represent Lower Zone rocks displaced by faulting or possibly the missing roof anorthosite. Furthermore, this study is largely based on mapping of surface structures. There are available drill cores from the

exploration campaigns of Rautaruukki Oy, and the project could be expanded to cover underground structures as well.

Larger autoliths from the Skaergaard intrusion are reported to be internally layered, a feature which is thought to originate from the crystallization at the magma chamber roof (Irvine et al., 1998). If more extensive outcrops were created over the larger autoliths, it could be studied if similar features are found in the autoliths of the Otanmäki intrusion. Additionally, in one Lower Zone outcrop (AJMA-2017-176), a fine grained anorthositic rock is seen to have an uncommonly straight contact with a pegmatite. This could indicate settling of a solidified anorthosite block. It could be further studied whether similar processes of anorthosite sinking have been active at least partly during the crystallization of the Lower Zone.

This is the first study focusing on the anorthositic rocks in the Otanmäki intrusion. Based on the results, the anorthositic rocks represent a crucial component in the magmatic evolution of the Ore and Upper Zones. The new data on the composition of the autoliths could be used to preliminary modelling of parental magma composition and magmatic differentiation, but the narrow data set should be expanded by further sampling of both anorthositic autoliths and their host rocks for more rigorous modelling. New calculations on the parental magma composition could also be done. The view of the magmatic evolution of the Lower Zone is largely based on the work by Nykänen (1995). The conception of the evolution of the Ore and Upper Zones is grounded on a relatively limited sample set, and a more comprehensive geochemical study would further clarify our understanding of the crystallization of the Ore and Upper Zone.

To get more information on the composition of the autoliths and their relation to the gabbroic rocks in the Otanmäki intrusion, a more thorough mineral chemistry investigation would be required. If plagioclase compositions were analyzed from more autoliths, the differences between the monomineralic and vari-textured autoliths could be studied specifically. Mineral chemistry research could clarify if some autoliths, such as the VTG-type autoliths, comprise plagioclase fraction crystallized at a different time during the magmatic evolution, and possibly result in a grouping of the autoliths based on their mineral composition rather than their size or texture. The abundance and assemblage of

mafic minerals in the autoliths may be more variable than currently assumed, which should be clarified in the future. Also the knowledge on the mineral chemistry of the oxide ore is not up to modern standards and a comprehensive mineral chemistry study might be imperative if the mining operations are to be restarted.

11 CONCLUSIONS

1. The Otanmäki intrusion comprises tectonically dismembered blocks of a differentiated mafic intrusion emplaced into Archean TTG gneisses. All the major tectonic blocks, Otanneva, Otanmäki and Vuorokas, host stratabound Fe-Ti-V oxide ore mineralization. The parental magma was a Ti- and V-enriched Fe-tholeiitic melt.

2. Stratigraphically, the intrusion is divided to three major units: the Lower Zone, the Ore Zone, and the Upper Zone. The voluminous part of the Lower Zone at Vuorokas is 1100 m in thickness whereas the Ore Zone thickness varies between 30 and 300 m. The Lower zone consists dominantly of medium-grained isotropic gabbro and, in its upper parts, leucocratic vari-textured gabbro. The rocks are dominantly plagioclase-rich ad- and mesocumulates. The Ore Zone is very heterogenous and comprises oxide ore lenses, magnetite gabbro, gabbro and gabbro amphibolite. In the Upper Zone, isotropic gabbro dominates. Anorthositic autoliths are present both in the Ore and Upper Zones. Fine-grained marginal amphibolites have been found in two locations between the Lower Zone rocks and the Archean gneisses.

3. The Fe-Ti-V oxide ore occurs in the Ore Zone as 3–50-m-wide, up to 200-m-long lenses and layers. Crystallization of the Ore and Upper Zones was a dynamic event affected by gravitational movements of partially solidified oxide slurry towards the magma chamber center, which is suggested to be located now in the Otanmäki block. Tectonic thickening and metamorphic recrystallization have later contributed to upgrading of the magnetite-ilmenite ore.

4. The Ore and Upper Zones are characterized by the presence of ubiquitous plagioclase-rich autoliths. They are from less than one meter to tens of meters in diameter. Lenticular autoliths lie typically parallel to the magmatic stratigraphy. Autoliths are mostly fine- to medium-grained and relatively monomineralic and anorthositic in composition but some are texturally and mineralogically similar to the Lower Zone vari-textured gabbros. The autoliths are angular to rounded in shape and have contacts that imply gravitational settling of variably solidified blocks on a semi-solidified substratum.

5. The autoliths bears many similarities to leucocratic autoliths reported from other mafic intrusions, such as the Skaergaard intrusion in Greenland and the Sept Iles intrusion in Canada, showing a variation in size and shape, fluctuations in the quantity of mafic minerals, parallel orientation to the stratigraphy and contacts to host rocks that include draping of magmatic layers. The autoliths have a similar plagioclase composition to that of their host gabbros (An_{35-68}). Based on mineralogical studies and major and trace element contents, the autoliths represent strongly differentiated plagioclase adcumulates.

6. Crystallization of the Ore and Upper Zone likely involved one or more sequence(s) of positive plagioclase buoyancy when parts of the crystallizing plagioclase ascended to higher levels in the magma chamber and solidified there. None of the major intrusion blocks have a known “roof anorthosite”, the potential place of origin of the autoliths. It is possible that massive anorthosites occurred at the top of the magma chamber, but were either deposited completely back to the magma chamber or removed by later faulting.

7. The deposition of the autoliths back into lower parts of the magma chamber was most likely affected by the crystallization of Fe-Ti oxides and a subsequent decrease in the density of the residual melt. The anorthositic upper parts in the magma chamber were destabilized and varyingly solidified parts of it started to sink as autoliths. Other processes, such as magmatic convection or faulting of the magma chamber roof, could have enhanced the process. Some autoliths were completely solidified upon their emplacement on the rocks of the Ore and Upper Zones whereas others were still slightly malleable.

8. The intrusion was fragmented by later deformation events. Firstly, a N–S-oriented dextral faulting separated the Otanmäki and Otanneva blocks from the Vuorokas block. Later, NW-oriented sinistral movements separated the Otanmäki and Otanneva blocks from each other and resulted in the curved shape of the Otanmäki block.

12 ACKNOWLEDGEMENTS

I wish to thank the following people for their help during my Master's project:

- My supervisors Kimmo Kärenlampi and Eero Hanski for their tireless guidance through this process and for pushing me to leave no stone unturned.
- Asko Kontinen for the idea to characterize the anorthositic rocks at Otanmäki and constructive criticism along the way.
- Vesa Nykänen for kindly providing me with previously unpublished analytical data. Heikki Salmirinne for geophysical maps.
- Shenghong Yang and Marko Moilanen for tutoring in magmatic petrology.
- Jouko Jylänki and Otanmäki Mine Oy for material and logistical support.
- Jari Kurkela for aerial drone photography and Leena Palmu for assistance with the EPMA.
- Ellie Capuano, Anne Brandt Johannesen, David Garcia-Balbuena, Juho Tapio, Henriikka Ikäheimo and Lassi Mäkisalo for stimulating discussions on the geology of Otanmäki and other things.

Financial support from the Academy of Finland (grant #281859) is acknowledged.

13 LITERATURE

African Mineral Standards. 2013. Certificate of analysis – AMIS0368 Vanadium bearing titaniferous magnetite, certified reference material. South Africa, 2013.

Alapieti, T.T., Kujanpää, J., Lahtinen, J.J. and Papunen, H. 1989. The Kemi stratiform chromitite deposit, northern Finland. Economic Geology 84, 1057–1077.

Arai, T. and Maruyama, S. 2017. Formation of anorthosite on the Moon through magma ocean fractional crystallization. Geoscience Frontiers 8 (2), 299–308.

Arndt, N. 2013. The formation of massif anorthosite: Petrology in reverse. Geoscience Frontiers 4(2), 195–8.

Ashwal, L.D. 1993. Anorthosites. Berlin: Springer-Verlag, Berlin.

Ashwal, L. D. 2010. The temporality of anorthosites. The Canadian Mineralogist 48 (4), 711–728.

Blatt, H., Owens, B.E. and Tracy, R.J. 2006. Petrology: Igneous, Sedimentary and Metamorphic. 3rd Edition. W.H. Freeman and Company, New York, 530 pp.

Bottinga Y. and Weill, D.F. 1970. Densities of liquid silicate systems calculated from partial molar volumes of oxide components. American Journal of Science 269, 169–182.

Boudreau, A.E. and McBirney, A.R. 1997. The Skaergaard Layered Series. Part III. Non-dynamic Layering. Journal of Petrology 38 (8), 1003–1020.

Buddington, A.F. 1939. Adirondack Igneous Rocks and their Metamorphism. Geological Society of America Memoir 7, 343 pp.

Campbell, I.H., Roeder, P.L. and Dixon, J.M. 1978. Plagioclase buoyancy in basaltic liquids as determined with a centrifuge furnace. Contributions to Mineralogy and Petrology 67, 369–377.

Charlier, B., Namur, O., Toplis, M.J., Schiano, P., Cluzel, N., Higgins, M.D. and Auwera, J.V. 2011. Large-scale silicate liquid immiscibility during differentiation of tholeiitic basalt to granite and the origin of the Daly gap. Geology 39, 907–910.

Crowson, P. 2001. Minerals Handbook 2000–2001. Mining Journal Books, Kent, U.K.

Farmer, G.L. 2003. Continental basaltic rocks. In: Rudnick, R.L. (Ed.) The Crust – Treatise on Geochemistry, Volume 3. Elsevier-Pergamon, Oxford, 85−121.

Finnilä, J., 2000. Provenance and paleoweathering of the early Proterozoic metasediments in the western parts of Kainuu and Kuusamo schist belts. M.Sc. Thesis, University of Oulu, 90 p. (in Finnish)

Frost, B.R. and Frost, C.D. 2013. Essentials of Igneous and Metamorphic Petrology, 1st Edition. Cambridge University Press, New York, 314 pp.

Geological Survey of Finland, 2018. Aerogeophysical low-altitude maps 1:20 000 https://hakku.gtk.fi/en/locations/search (1.5.2018)

Gross, G.A. 1996. Mafic intrusion-hosted titanium-iron. In: Eckstrand, O.R., Sinclair, W.D. and Thorpe, R.I. (Eds.) Geology of Canadian mineral deposit types. Geological Survey of Canada, 573–582.

Gross, G.A., Gower, C.F. and Lefebure, D.V. 1997. Magmatic Ti-Fe-V Oxide Deposits. In: Geological Fieldwork 1997, British Columbia Ministry of Employment and Investment, Paper 1998-1, 24J-1–3.

Grove, T.L. 2000. Origin of magmas. In: Sigurdsson, H. (Ed): Encyclopedia of Volcanoes. Academic press, San Diego, 133–147.

Hamilton, P.J. 1977. Sr isotope and trace element studies of the great dyke and Bushveld mafic phase and their relationship to early Proterozoic magma genesis in southern Africa. Journal of Petrology 18: 24–52.

Hamilton, M.A, Scoates, J.C. and Rämö, O.T. 2010. The petrology of anorthosites, related granitic rocks, and UHT assemblages: a tribute to Ronald F. Emslie. Canadian Mineralogist 48, 705–1039.

Hanski, E. and Melezhik, V. A. 2013. Litho- and chronostratigraphy of the Paleoproterozoic Karelian formations. In: Melezhik, V., Prave, A.R., Fallick, A.E., Kump, L.R., Strauss, H., Lepland, A. and Hanski, E.J. (Eds.) Reading the archive of Earth's oxygenation, Vol. 1: The Palaeoproterozoic of Fennoscandia as context for the Fennoscandian arctic Russia – drilling early earth project. Springer-Verlag, Berlin, 39–110.

Havola, M. 1997. Kajaani: Kallioperäkartta 1 : 100 000 – Maps of pre-quaternary rocks, map sheet 3431. Geological Survey of Finland.

Higgins, M. D. and Doig, R. 1986. Geochemical constraints on the processes that were active in the Sept Iles complex. Canadian Journal of Earth Sciences 23, 670–681.

Higgins, M. and Chandrasekharam, D. 2007. Nature of sub-volcanic magma chambers, Deccan province, India: evidence from quantitative textural analysis of plagioclase megacrysts in the giant plagioclase basalts. Journal of Petrology 48, 885–900.

Hokka, J. and Torppa, A. 2016. Otanmäki Fe-Ti-V. In: Boyd, R., Bjerkgård, T., Nordahl, B. and Schiellerup, H. (Eds.) Mineral resources in the Arctic. NGU – Geological Survey of Norway, 354–357.

Huhma, H., Hanski, E., Kontinen, A., Vuollo, J., Mänttäri, I. and Lahaye, Y. 2018. Sm–Nd and U–Pb isotope geochemistry of the Palaeoproterozoic mafic magmatism in eastern and northern Finland. Geological Survey of Finland, Bulletin 405, 150 pp.

Huhtelin T. 2015. The Kemi Chromite Deposit. In: Maier, W.D., Lahtinen, R. and O'Brien, H. (Eds.) Mineral deposits of Finland. Elsevier, Amsterdam, 165–78.

Hölttä, P. and Heilimo, E. 2017. Metamorphic map of Finland. Geological Survey of Finland, Special Paper 60, 77–128.

Hölttä, P., Heilimo, E., Huhma, H., Juopperi, H., Kontinen, A., Konnunaho, H., Lauri, L., Mikkola, P., Paavola, J. and Sorjonen-Ward, P. 2012. Archaean complexes of the Karelia Province in Finland. Geological Survey of Finland, Special Paper 54, 9−20.

Irvine T. N. 1970. Heat transfer during solidification of layered intrusions I: sheets and sills. Canadian Journal of Earth Sciences 7, 1031–106.

Irvine, T.N. 1982. Terminology for layered intrusions. Journal of Petrology 23, 127–612.

Irvine, T.N. 1987. Layering and related structures in the Duke Island and Skaergaard intrusions: similarities, differences, and origins. In: Parsin, I. (Ed.) Origins of igneous layering. Reidel, Dordrecht, 185–245.

Irvine, T.N., Andersen, J.C.O. and Brooks, C.K. 1998. Included blocks (and blocks within blocks) in the Skaergaard intrusion – geologic relations and the origins of rhythmic modally graded layers. Bulletin of the Geological Society of America 110, 1398–1447.

Jaanus-Järkkälä, M. 1989. En bassängstruktur av tidigt proterozoiska sedimentära och intrusiva bergarter i Otanmäki. MSc thesis, Åbo Akademi. 58 pp.

Jakobsen, J.K., Veksler, I.V., Tegner, C. and Brooks, C.K. 2005. Immiscible iron- and silica-rich melts in basalt petrogenesis documented in the Skaergaard intrusion. Geology 33, 885–888.

Johnson, C.M. 1991. Large-scale crust formation and litosphere modification beneath middle to late cenozoic calderas and volcanic fieds, western north America. Journal of Geophysical Research 96, 13485–13507.

Jonsson, E., Troll, V., Högdahl, K., Harris, C., Weis, F., Persson Nilsson, K.S. and Skelton, A. 2013. Magmatic origin of giant 'Kiruna-type' apatite-iron-oxide ores in central Sweden. Scientific Reports 3, 1644.

Karinen, T., Hanski, E. and Taipale, A. 2015. The Mustavaara Fe-Ti-V deposit. In: Maier, W.D., Lahtinen, R. and O'Brien, H. (Eds.) Mineral deposits of Finland. Elsevier, Amsterdam, 179–194.

Kerkkonen, O., 1979. Genesis and evolution of the Otanmäki titanium-iron ore in the light of the magnetite-ilmenite pair. Licentiate Thesis, University of Oulu, Finland. (in Finnish)

Kontinen, A. 1986. Early Proterozoic stratigraphy and sedimentation in the Hyrynsalmi area, eastern Finland. In: Sokolov, V. A. and Heiskanen, K.I. (Eds.) Early Proterozoic of the Baltic Shield. Proceedings of the Finnish - Soviet symposium held in Petrozavodsk 19–27th August, 1985. Committee for Scientific and Technical co-operation between Finland and Soviet Union, Petrozavodsk, 75–103.

Kontinen, A. 1987. An early proterozoic ophiolite – the Jormua mafic-ultramafic complex, Northeastern Finland. Precambrian Research 35, 313–341.

Kontinen, A. and Hanski, E. 2015. The Talvivaara black shale-hosted Ni-Zn-Cu-Co deposit in eastern Finland. In: Maier, W.D., Lahtinen, R. ja O'Brien, H. (Eds.) Mineral deposits of Finland. Elsevier, Amsterdam, 557–612.

Kontinen, A. and Paavola, J. 2006. A preliminary model of the crustal structure of the eastern Finland Archaean complexes between Vartius and Vieremä, based on constraints from surface geology and FIRE 1 seismic survey. Geological Survey of Finland, Special Paper 43, 223–240.

Kontinen, A., Paavola, J. and Lukkarinen, H. 1992. K-Ar ages of hornblende and biotite from late Archaean rocks of eastern Finland – interpretation and discussion of tectonic implications. Bulletin of the Geological Survey of Finland, 31 pp.

Kontinen, A., Huhma, H., Lahaye Y. and O'Brien, H. 2013 (a). New U-Pb zircon age, Sm-Nd isotope and geochemical data for Otanmäki suite granites in the Kainuu area, central Finland. In: Hölttä, P. (Ed) Geological Survey of Finland, Report of Investigation 198, 65–69.

Kontinen, A., Huhma, H., Lahaye Y. and O'Brien, H. 2013 (b). New U-Pb zircon age, Sm-Nd isotope and geochemical data on Proterozoic granitic rocks in the area west of the Oulunjärvi lake, central Finland. In: Hölttä, P. (Ed) Geological Survey of Finland, Report of Investigation 198, 70–74.

Korneliussen, A., McEnroe, S.A., Nilsson, L.P., Schiellerup, H., Gautneb, H., Meyer, G.B. and Sterseth, L.R. 2000. An overview of titanium deposits in Norway. NGU Bulletin 436, 27–38.

Krause, H., Gierth, E. and Schott, W. 1985. Ti–Fe deposits in the south Rogaland igneous complex with special reference to the Ana-Sira anorthosite massif. NGU Bulletin 402, 25–37.

Kushiro, I. 2001. Partial melting experiments on peridotite and origin of mid-ocean ridge basalts. Annual Review of Earth and Planetary Sciences 29, 71–107.

Kärenlampi, K., Kontinen, A., Huhma, H. and Hanski, E. 2019. Geology, geochronology and geochemistry of the 2.05 Ga gneissic A1-type granites and related intermediate rocks in central Finland: implication for the tectonic evolution of the Karelia craton margin (in press).

Laajoki, K. 1998. Karjalaiset liuskealueet. In: Lehtinen M., Nurmi, P. and Rämö T. (Eds.) Suomen kallioperä: 3000 vuosimiljoonaa. Geological Society of Finland, Helsinki, 165–197.

Laajoki, K. 2005. Karelian supracrustal rocks. In: Lehtinen, M., Nurmi, P.A. and Rämö, O.T. (Eds.) Precambrian geology of Finland – key to the evolution of the Fennoscandian shield. Elsevier, Amsterdam, 279–342.

Lahti, I., Salmirinne, H., Kärenlampi, K. and Jylänki, J. 2018. Geophysical surveys and modelling of Nb-Zr-REE deposits and Fe–Ti–V ore-bearing gabbros in the Otanmäki area, central Finland. Geological Survey of Finland, Open File Work Report 75/2018.

Lahtinen, R., Huhma, H., Kontinen, A., Kohonen, J., Sorjonen-Ward, P., 2010. New constraints for the source characteristics, deposition and age of the 2.1–1.9 Ga metasedimentary cover at the western margin of the Karelian Province. Precambrian Research 176, 77–93.

Lahtinen, R., Huhma, H., Lahaye, Y., Kousa, J. and Luukas, J. 2015. Archean–Proterozoic collision boundary in central Fennoscandia: Revisited. Precambrian Research 261, 127−165.

Latypov, R., Chistyakova, S. and Alapieti, T. 2007. Revisiting problems of chilled margins associated with marginal reversals in mafic-ultramafic intrusive bodies. Lithos 99,178–206.

Laznicka, P. 2006. Giant metal deposits – future sources of industrial metals. Springer, Berlin. 732 pp.

LeMaitre, R.W., 1976. Some problems on the projection of chemical data into mineralogical classifications. Contributions to Mineralogy and Petrology 56, 181–189.

Lightfoot, P.C. 2016. Nickel sulfide ores and impact melts: origin of the Sudbury igneous complex. Elsevier, Amsterdam, 680 pp.

Lindholm, O., Anttonen, R., 1980. Geology of the Otanmäki Mine, in: Häkli, T.A., (Ed.), Precambrian Ores of Finland: Guide to Excursions 078 A + C, Part 2 (Finland). Proceedings of the 26th International Geological Congress. Geological Survey of Finland, Espoo, Paris, pp. 25–33.

London, D., 2008. Pegmatites. Mineralogical Association of Canada. 347 pp.

Luukas, J., Kousa, J., Nironen, M. and Vuollo, J. 2017. Major stratigraphic units in the bedrock of Finland, and an approach to tectonostratigraphic division. Geological Survey of Finland, Special Paper 60, 9-40.

Maier, W.D. 2015. Geology and Petrogenesis of Magmatic Ni-Cu-PGE-Cr-V Deposits: An Introduction and Overview. In: Maier, W.D., Lahtinen, R. ja O'Brien, H. (Eds.) Mineral Deposits of Finland. Elsevier, Amsterdam, 73–92.

Maier, W.D and Hanski, E. 2017. Layered mafic–ultramafic intrusions of Fennoscandia: Europe's Treasure Chest of Magmatic Metal Deposits. Elements 13, 415–420.

Maier, W.D., Barnes, S.J. and Groves, D.I. 2013. The Bushveld complex, South Africa: formation of platinum–palladium, chrome- and vanadium-rich layers via hydrodynamic sorting of a mobilized cumulate slurry in a large, relatively slowly cooling, subsiding magma chamber. Mineralium Deposita 48: 1–56.

Maier W.D., Karykowski, B.T. and Yang, S. 2016. Formation of transgressive anorthosite seams in the Bushveld complex via tectonically induced mobilisation of plagioclase-rich crystal mushes. Geoscience Frontiers 7(6), 875–889 .

Marmo, V., Hoffren, V., Hytönen, K., Kallio, P., Lindholm, O. and Siivola, J. 1966. On the granites of Honkamäki and Otanmäki, Finland, with special reference to the mineralogy of accessories. Bulletin de la Commission Géologique de Finland 221. 34 pp.

McBirney, A.R. 1993. Igneous Petrology. 2nd edition. Jones and Barlett publishers, Boston. 508 pp.

McBirney A.R. 1996. The Skaergaard intrusion. In: Cawthorn R. D. (Ed.) Layered intrusions. Elsevier Science B.V., Amsterdam, 147–180 .

McBirney, A.R. and Noyes, R.M. 1979. Crystallization and layering of the Skaergaard intusion. Journal of Petrology 20, 487–554.

Mutanen, T. and Huhma, H. 2001. U-Pb geochronology of the Koitelainen, Akanvaara and Kevitsa layered intrusions and related rocks. In: Vaasjoki, M. (Ed.) Geological Survey of Finland, Special Paper 33, 229-246.

Mänttäri, I. and Hölttä, P. 2002. U-Pb dating of zircons and monazites from Archean granulites in Varpaisjärvi, central Finland: evidence for multiple metamorphism and Neoarchean terrane accretion. Precambrian Research 118, 101−131.

Namur, O., Charlier, B., Pirard, C., Hermann, J., Liégeois, J.-P. and Auwera, J. 2011. Anorthosite formation by plagioclase flotation in ferrobasalt and implications for the lunar crust. Geochimica et Cosmochimica Acta 75, 4998–5018.

Namur, O., Abily, B., Boudreay, A.E., Blanchette, F., Bush, J.W.M., Ceuleneer G, Charlier, B., Donaldson, C.H., Duchesne, J.-C., Higgins, M.D., Morata, D., Nielsen, T.F.D., O'Driscoll, B. and Pang, K.N. 2015. Igneous layering in basaltic magma chambers. In: Charlier, B., Namur, O., Latypov, R. and Tegner, C. (Eds.) Layered intrusions. Springer, London, 75–152.

Naslund, H.R. 1986. Disequilibrium partial melting and rheomorphic layer formation in the contact aureole of the Basistoppen sill, East Greenland. Contributions to Mineralogy and Petrology 93 (3), 359–367.

Naslund, H.R. and McBirney, A.R. 1996. Mechanisms of formation of igneous layering. In: Cawthorn, R.G. (Ed.) Layered Intrusions. Elsevier, Amsterdam, 1–43.

National Land Survey of Finland, 2018. Topographic database 1:50 000. https://tiedostopalvelu.maanmittauslaitos.fi/tp/kartta (1.5.2018)

Nironen, M. (ed.) 2017. Bedrock of Finland at the scale 1:1 000 000 - Major stratigraphic units, metamorphism and tectonic evolution. Geological Survey of Finland, Special Paper 60.

Nironen, M., Kousa, J., Luukas, J. and Lehtinen, R. (Eds.) 2016. Geological Map of Finland – Bedrock. 1: 1000 000. Geological Survey of Finland.

Nykänen, V., 1995. Crystallization and chemical evolution of the lower- and central part of the Vuorokas block in the Otanmäki intrusion complex. Licentiate Thesis, University of Oulu, 135 p. (in Finnish)

Otanmäki Mine Oy. 2017. Otanmäki Mine. Brochure. http://www.otanmaki.fi/Otanmaki_Mine_brochure_2017.pdf (12.4.2018)

Paarma, H., 1954. The ilmenite-magnetite ore deposit of Otanmäki. In: Aurola, E. (Ed.) The mines and quarries of Finland. Geologinen tutkimuslaitos – geoteknillisiä julkaisuja N:o 55: 36–42. Geological Survey of Finland.

Paarma, H., 1961. Otanmäen geologia. Report. Otanmäki Oy, 1961.

Paavola, J. 1999. Pre-Quaternary Rocks of the Rautavaara Map-Sheet area. Geological Map of Finland 1:100 000, Explanation to the Maps of Pre-Quaternary Rocks, Sheet 3343. Geological Survey of Finland. 53 p (in Finnish).

Parkkinen, J. 2015. Geological modelling and resource estimates – a personal view. https://www.academia.edu/19941735/PowerPoint_Presentation_Geological_Modelling_and_Resource_Estimates_a_personal_view (23.10.2018)

Patchett, P. J., Kouvo, O., Hedge, C. E. and Tatsumoto, M. 1981. Evolution of continental crust and mantle heterogeneity: evidence from Hf isotopes. Contributions to Mineralogy and Petrology 78, 279—297.

Peltonen, P. and Kontinen A. 2004. The Jormua ophiolite: a mafic-ultramafic complex from an ancient ocean-continent transition zone. 2004. In: Kusky, T.M. (Ed.) Precambrian ophiolites and related rocks. Developments in Precambrian Geology vol. 13., 35–71.

Peltonen, P., Kontinen, A. and Huhma, H. 1996. Petrology and geochemistry of metabasalts from the 1.95 Ga Jormua Ophiolite, northeastern Finland. Journal of Petrology 37, 1359−1383.

Peltonen, P., Kontinen, A., Huhma, H., 1998. Petrogenesis of the mantle sequence of the Jormua ophiolite (Finland): melt migration in the upper mantle during Palaeoproterozoic continental break-up. Journal of Petrology 39, 297–329.

Puumalainen, V.-M. 1986. Rock types and structures in the Otanmäki schist formation. MSc thesis, University of Oulu (in Finnish).

Pääkkönen, V. 1943. Vuolijoen Otanmäen malmikenttä. Magneettiset häiriöt 1:2 000. Geologinen toimikunta, 1943.

Pääkkönen V. 1956. Otanmäki - the ilmenite and magnetite ore field in Finland. Bulletin de la Commission géologique de Finlande, Helsinki, 71 pp.

Pöschl, A. 1964. Die Titanomagnetit-lagerstätte Otanmäki in Finnland. Stoffbestand, Bau und Entstehungsgeschichte. Ludwig-Maximilians-Universität, München.

Rask, M. and Vartiainen, R.1989. Rakennuskivitutkimukset Angelissa, Inarin kunnassa tammi-huhtikuussa 1988. Report. Geologial Survey of Finland.

Rautaruukki Oy, 1980. Vuorokkaan gabron malminetsintätutkimukset vuosina 1978–1979. Report of Investigation.

Reynolds I.M., 1985. The nature and origin of titaniferous magnetite-rich layers in the upper zone of the Bushveld complex: a review and synthesis. Economic Geology 80, 1089–1108.

Robb, L. 2005. Introduction to Ore Forming Processes. Blackwell Publishing, Malden MA, 373 pp.

Rudnick, R.L. 1992. Xenoliths – samples of the lower continental crust. In: Fountain, D., Arculus, R. and Kay, R.W. (Eds.) Continental Lower Crust. Elsevier, Amsterdam, 269–316.

SA Bureau of Standards. 1984. Certificate of analysis – NIM-N Norite SARM 4, certified reference material. Republic of South Africa, 1984.

Sarapää, O., Kärkkäinen, N., Ahtola, T., Al-Ani, T. 2015. High-tech metals in Finland. In: Maier, W., O'Brien, H., Lahtinen, R. (Eds.) Mineral deposits of Finland. Elsevier, Amsterdam, p. 613–632.

Scoates, J.S. 2000. The plagioclase-magma density paradox re-examined and the crystallization of Proterozoic anorthosites. Journal of Petrology 41, 627–649.

Silver, P., Fouch, M.J., Gao, S.S. and Schmitz, M. 2004. Seismic anisotropy, mantle fabric, and the magmatic evolution of Precambrian southern Africa. South African Journal of Geology 107, 45–58

Soininen, J. and Paarma, H., 1959. Otannevan geologiset tutkimukset. Report. Otanmäki Oy.

Spera, F.J. 2000. Physical properties of magmas. In: Sigurdsson, H. (Ed.) Encyclopedia of Volcanoes. Academic press, San Diego, 171–190.

Strand, K. 1988. Alluvial sedimentation and tectonic setting of the early Proterozoic Kurkikylä and Kainuu groups in northern Finland. In: Laajoki, K. and Paakkola, J. (Eds) Sedimentology of the Precambrian formations in eastern and northern Finland. Geological Survey of Finland, Special Paper 5, 49–75.

Streckeisen, A., 1976. To each plutonic rocks its proper name. Earth Science Reviews 12, 1–33.

Sun, S.S. and McDonough, W.F. 1989. Chemical and isotopic systematics of oceanic basalts: implications for mantle composition and processes. In: Saunders, A.D. and Norry, M.J. (Eds.) Magmatism in the ocean basins, Vol. 42, Geological Society, Special Publications, London, 313-345.

Talvitie, J. and Paarma, H. 1980. Precambrian basic magmatism and the Ti-Fe ore formation in central and northern Finland. In: Siivola, J. (Ed.) Metallogeny of the Baltic shield – proceedings of the symposium held in Helsinki, Finland, June 12–21, 1978. Geological Survey of Finland, Bulletin 307.

Taylor, S.R. and McLennnan, S.M. 1985. The continental crust: its composition and evolution. Blackwell Scientific Publications, Oxford, 312 pp.

Vaasjoki. M., Kärki, A. and Laajoki, K. 2001. Timing of Palaeoproterozoic crustal shearing in the central Fennoscandian Shield according to U-Pb data from associated granitoids, Finland. Bulletin of Geological Society of Finland 73, 87–101.

Vartiainen, R., 1989. Rakennuskivitutkimukset Angelissa, Inarin kunnassa huhti-syyskuussa 1988. Geological Survey of Finland, Report.

Veksler, I. and Charlier, B. 2015. Silicate liquid immiscibility in layered intrusions. In: . In: Charlier, B., Namur, O., Latypov, R. and Tegner, C. (Eds.) Layered intrusions. Springer, London, 229-258.

Vuollo, J. and Huhma, H. 2005. Paleoproterozoic mafic dikes in NE Finland. In: Lehtinen, M., Nurmi, P.A. and Rämö, O.T. (Eds.) Precambrian geology of Finland – key to the evolution of the Fennoscandian Shield. Elsevier, Amsterdam, 195–236.

Väyrynen, H. 1928. Geologische und petrographische Untersuchungen im Kainuugebiete. Geological Survey of Finland, Bulletin 78.

Wager, L.R., Brown, G.M. and Wadsworth, WJ. 1960. Types of igneous cumulates. Journal of Petrology 1, 73–85.

Wager, L.R. and Brown, G.M. 1968. Layered igneous rocks. Oliver and Boyd, Edinburgh, 588 pp.

Warren, P.H. 1990. Lunar anorthosites and magma-ocean plagioclase-flotation hypothesis: importance of FeO enrichment in the parent magma. American Mineralogist, 75(1), 46–58.

Wood, J.A., Dickey, J.S., Marvin, U.B. and Powell, B.N. 1970. Lunar anorthosites. Science 167, 602–604.

Wilkman, W.W., 1929. Kajaani = Kajana. Maps of prequaternary rocks 1:400 000.

Wilkman, W.W. 1931. Geologisk översiktskarta över Finland – sektionen C4 Kajaani. Beskrivning till bergartskartan. Geologisk Översiktskarta över Finland.

Winter, J.D. 2001 An introduction to igneous and metamorphic petrology. Prentice hall, Upper Saddle River, NJ, 697 pp.

Young, K.E., Evans, A.C., Hodges, K.V., Bleacher, J.E. and Graff, T.G. 2016. A review of the handheld x-ray fluorescence spectrometer as a tool for field geologic investigations on Earth and in planetary surface exploration. Applied Geochemistry 72, 77–87.

Zelt, G. 1974. A petrological investigation of amphibolite rock in the Otanmäki mining region, Finland. MSc Thesis, University of Helsinki.

APPENDICES

1. **Bedrock observation points on map**
2. **Location and geological information of bedrock observation points, analysis samples and drill holes**
3. **Petrographical observation sheets**
4. **Electron microprobe results**
5. **ICP-OES/ICP-MS analysis results**
6. **pXRF measurements**
7. **CIPW normative mineral compositions**
8. **XRF/INAA/ICP-ES/DCP-ES analyses from Nykänen (1995)**
9. **XRF/ICP-MS oxide ore analyses by V. Nykänen**

APPENDIX 1. Bedrock observation points on map. Legend as in Fig. 6.1.

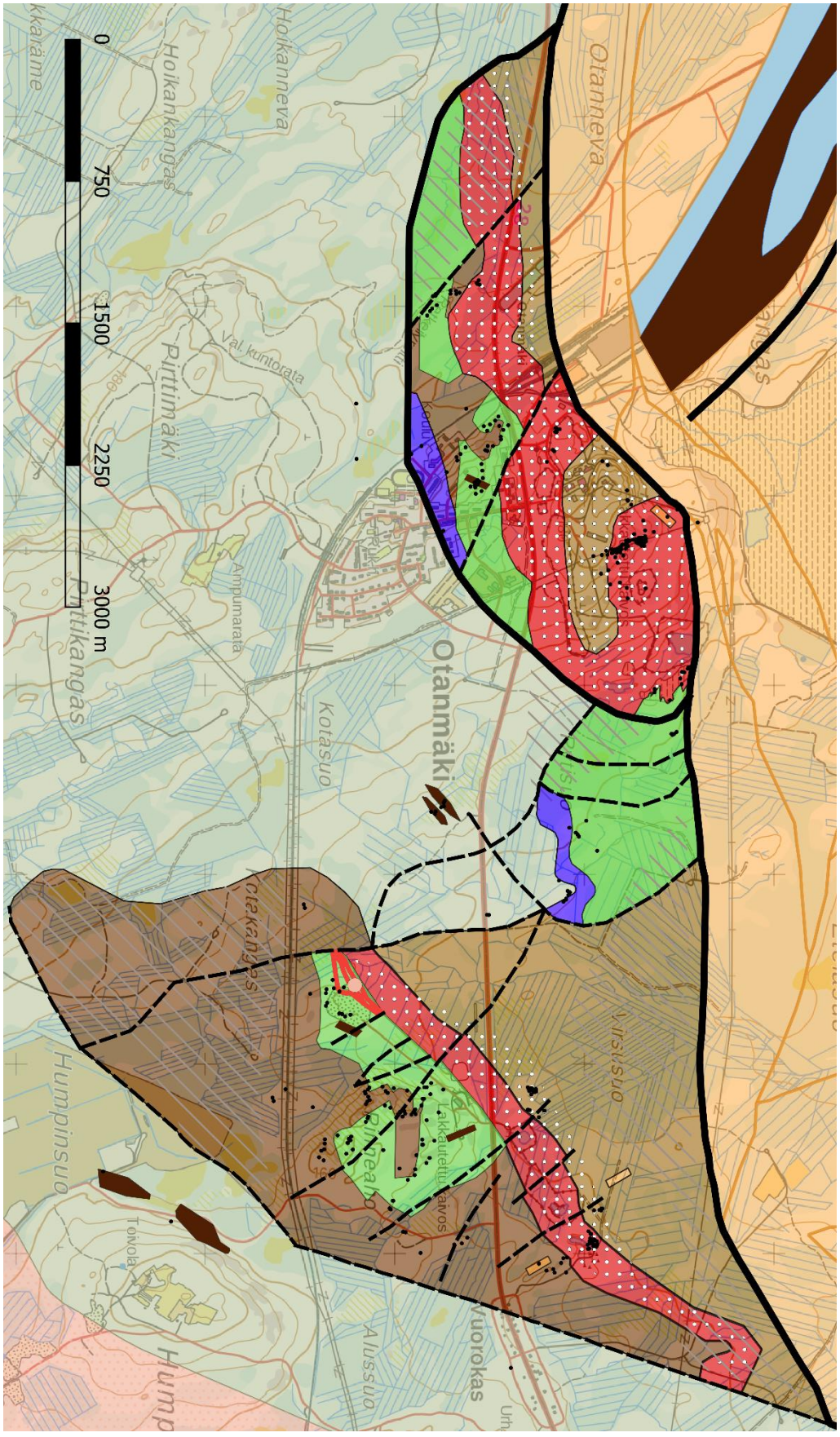

APPENDIX 2. Location and geological information of bedrock observation points, analysis samples and drill holes. Magsus.=magnetic susceptibility (SI unit), S=schistosity, L=lineation, FA=fold axis, dd=dip direction. Coordinates in KKJ3 Finland uniform coordinate system.

No.	Station_code	X-KKJ3	Y-KKJ3	Field_name	Sample	Magsus.	S	S	L	L	FA
						10^5	dd.	dip	dd.	dip	dd./dip
BEDROCK OBSERVATIONS											
1	AJMA-2017-91	3508416	7112680	LG		50					
2	AJMA-2017-92	3508419	7112690	gabbro	92.1	100					
3	AJMA-2017-93	3508307	7112722	LG/MG		200	140	70	240	70	
4	AJMA-2017-94	3508939	7113073	gabbro		200	160	70	220	70	
5	AJMA-2017-95	3509150	7113004	LG		100	290	70	290	70	
6	AJMA-2017-96	3509100	7113012	LG							
7	AJMA-2017-105	3505492	7113026	gabbro	105.1	100					
8	AJMA-2017-106	3505487	7113071	gabbro							
9	AJMA-2017-107	3505486	7113100	gabbro	107.1						
10	AJMA-2017-108	3505486	7113108	gabbro							
11	AJMA-2017-109	3505464	7113094	LG	109.1	20					30/55
12	AJMA-2017-110	3505476	7113123	gabbro		250					
13	AJMA-2017-111	3505475	7113129	LG		50					
14	AJMA-2017-112	3505498	7113142	LG	112.1	30					
15	AJMA-2017-113	3505462	7113134	gabbro	113.1						
16	AJMA-2017-114	3505458	7113138	gabbro							
17	AJMA-2017-115	3505475	7113149	LG		20					
18	AJMA-2017-116	3505456	7113124	gabbro		140					
19	AJMA-2017-117	3505457	7113123	gabbro							
20	AJMA-2017-118	3505454	7113150	gabbro							
21	AJMA-2017-119	3505461	7113153	LG	119.1	25					
22	AJMA-2017-120	3505447	7113163	gabbro		130					
23	AJMA-2017-121	3505438	7113174	gabbro							
24	AJMA-2017-122	3505455	7113169	LG	122.1	30					
25	AJMA-2017-123	3505456	7113174	gabbro	123.1	110					
26	AJMA-2017-124	3505450	7113168	gabbro							
27	AJMA-2017-125	3505468	7113160	gabbro							
28	AJMA-2017-126	3505473	7113168	LG	126.1	20					
29	AJMA-2017-127	3505490	7113184	LG	127.1	130	170	60			
30	AJMA-2017-128	3505432	7113191	gabbro							
31	AJMA-2017-130	3505431	7113180	gabbro							
32	AJMA-2017-131	3508456	7112738	LG	131.1	11	220	85			
33	AJMA-2017-132	3508298	7112679	LG		90			195	50	
34	AJMA-2017-133	3508304	7112694	LG	133.1				220	70	
35	AJMA-2017-134	3508336	7112698	gabbro		60	150	70	250	60	
36	AJMA-2017-135	3508321	7112723	gabbro	135.1						
37	AJMA-2017-136	3508323	7112711	gabbro							
38	AJMA-2017-137	3508323	7112717	gabbro	137.1-2						
39	AJMA-2017-138	3508317	7112705	LG		10					
40	AJMA-2017-139	3508313	7112697	LG		20					

No.	Station_code	X-KKJ3	Y-KKJ3	Field_name	Sample	Magsus.	S	S	L	L	FA
						10^5	dd.	dip	dd.	dip	dd./dip
41	AJMA-2017-140	3508310	7112715	gabbro		70					
42	AJMA-2017-141	3508309	7112690	LG							
43	AJMA-2017-142	3508312	7112685	gabbro							
44	AJMA-2017-143	3508318	7112687	LG							
45	AJMA-2017-144	3508303	7112700	gabbro							
46	AJMA-2017-145	3508422	7112767	gabbro		150					
47	AJMA-2017-146	3509140	7113042	gabbro		180	350	45			
48	AJMA-2017-147	3509128	7113047	gabbro		140					
49	AJMA-2017-148	3509133	7113036	An.		500 (9)					
50	AJMA-2017-149	3509123	7113023	An.		15			250	40	
51	AJMA-2017-150	3509095	7113009	gabbro	150.1	600					
52	AJMA-2017-151	3509059	7113000	gabbro	151.1	600					
53	AJMA-2017-152	3509109	7113024	An.		20			250	40	
54	AJMA-2017-153	3509101	7113024	LG/An.		30			250	30	
55	AJMA-2017-154	3509107	7113031	LG/An.							
56	AJMA-2017-155	3509102	7113031	gabbro		60			240	25	
57	AJMA-2017-156	3509071	7113010	gabbro		200					
58	AJMA-2017-157	3509073	7113014	gabbro							
59	AJMA-2017-158	3508948	7113030	gabbro		120					
60	AJMA-2017-159	3508946	7113058	gabbro		250					
61	AJMA-2017-160	3508948	7113066	gabbro		250					
62	AJMA-2017-161	3508942	7113070	gabbro							
63	AJMA-2017-162	3508938	7113069	gabbro/An.		150					
64	AJMA-2017-163	3509138	7113026	Mag-gb	163.1	1200					
65	AJMA-2017-164	3509121	7113016	LG	164.1	19					
66	AJMA-2017-165	3509123	7113006	Mag-gb		100					
67	AJMA-2017-166	3509108	7113006	LG							
68	AJMA-2017-167	3509130	7112995	Mag-gb							
69	AJMA-2017-168	3506169	7113492	An.		1000					
70	AJMA-2017-169	3506087	7113524	An.		1000					
71	AJMA-2017-170	3506080	7113527	LG/An.		100					
72	AJMA-2017-171	3506119	7113493	LG							
73	AJMA-2017-172	3506106	7113506	LG							
74	AJMA-2017-173	3506139	7113485	Mag-gb		20000					
75	AJMA-2017-174	3508310	7112233	VTG							
76	AJMA-2017-175	3508334	7112165	VTG							
77	AJMA-2017-176	3508359	7112124	VTG							
78	AJMA-2017-177	3506254	7113430	M-gb		60					
79	AJMA-2017-178	3505427	7113196	LG	178.1	100					
80	AJMA-2017-179	3508316	7112720	An.		250	130	75			
81	AJMA-2017-180	3508313	7112722	An.		50	140	70			
82	AJMA-2017-181	3508668	7111577	LG		25					
83	AJMA-2017-182	3508633	7111589	M-gb		40					
84	AJMA-2017-183	3508626	7111604	M-gb		250					
85	AJMA-2017-184	3508595	7111607	gabbro	184.1	40					
86	AJMA-2017-185	3508573	7111608	gabbro							
87	AJMA-2017-186	3508552	7111675	VTG		40					
88	AJMA-2017-187	3508403	7111544	gabbro		25					
89	AJMA-2017-188	3508387	7111825	M-gb		300					
90	AJMA-2017-189	3508373	7111832	M-gb		370					

No.	Station_code	X-KKJ3	Y-KKJ3	Field_name	Sample	Magsus.	S	S	L	L	FA
						10^5	dd.	dip	dd.	dip	dd./dip
91	AJMA-2017-190	3508348	7111837	M-gb							
92	AJMA-2017-191	3508331	7111822	M-gb		100					
93	AJMA-2017-192	3508321	7111819	M-gb	192.1	40					
94	AJMA-2017-193	3508570	7111733	VTG		20					
95	AJMA-2017-194	3508309	7111836	gabbro		25	360	80			
96	AJMA-2017-195	3508300	7111843	VTG							
97	AJMA-2017-196	3508295	7111912	gabbro		320					
98	AJMA-2017-197	3508328	7111939	gabbro	197.1	20					
99	AJMA-2017-198	3508303	7111972	VTG		20					
100	AJMA-2017-199	3508315	7112043	gabbro							
101	AJMA-2017-200	3508431	7112209	VTG							
102	AJMA-2017-201	3508580	7112186	VTG	201.1	15					
103	AJMA-2017-202	3508601	7112126	VTG		15					
104	AJMA-2017-203	3508657	7112091	gabbro	203	25	80	85			
105	AJMA-2017-204	3508727	7112002	gabbro	204.1	100					
106	AJMA-2017-205	3508898	7111969	VTG		200					
107	AJMA-2017-206	3509276	7112882	Kfed gran.	206.1	20	260	60			
108	AJMA-2017-207	3505416	7113208	An.	207.1	30					
109	AJMA-2017-208	3505410	7113198	gabbro		300					
110	AJMA-2017-209	3505408	7113209	gabbro		300	50	60			
111	AJMA-2017-210	3505409	7113209	gabbro		250					
112	AJMA-2017-211	3505411	7113219	gabbro							
113	AJMA-2017-212	3505376	7113241	gabbro/An.		300					
114	AJMA-2017-213	3505404	7113249	gabbro		270	160	80			
115	AJMA-2017-214	3505406	7113235	LG	214.1	70					
116	AJMA-2017-215	3505417	7113256	LG	215.1	100	160	80			
117	AJMA-2017-216	3505419	7113252	gabbro							
118	AJMA-2017-217	3505422	7113255	LG	217.1	50	175	70			
119	AJMA-2017-218	3505426	7113263	Gb-afb	218.1	100	165	75			
120	AJMA-2017-219	3505424	7113265	gabbro		300					
121	AJMA-2017-220	3505430	7113275	gabbro/An.			160	70			
122	AJMA-2017-221	3505428	7113272	An.							
123	AJMA-2017-222	3505423	7113279	An.	222.1						
124	AJMA-2017-223	3505417	7113270	An.	223.1		155	65			
125	AJMA-2017-224	3505412	7113266	gabbro		500	160	65			
126	AJMA-2017-225	3505402	7113270	An.							
127	AJMA-2017-226	3505409	7113275	An.							
128	AJMA-2017-227	3505396	7113265	gabbro							
129	AJMA-2017-228	3505409	7113281	gabbro							
130	AJMA-2017-229	3505395	7113270	gabbro							
131	AJMA-2017-230	3505395	7113283	gabbro							
132	AJMA-2017-231	3505398	7113277	An.							
133	AJMA-2017-232	3505408	7113294	gabbro		2500					
134	AJMA-2017-233	3505418	7113298	An.	233						
135	AJMA-2017-234	3505425	7113293	An.							

No.	Station_code	X-KKJ3	Y-KKJ3	Field_name	Sample	Magsus.	S	S	L	L	FA
						10^5	dd.	dip	dd.	dip	dd./dip
136	AJMA-2017-235	3505421	7113285	gabbro							
137	AJMA-2017-236	3505416	7113285	gabbro							
138	AJMA-2017-237	3505414	7113304	gabbro							
139	AJMA-2017-238	3505439	7113294	An.	238.1						
140	AJMA-2017-239	3505438	7113280	An.	239.1						
141	AJMA-2017-240	3505399	7113303	An.			160	70			
142	AJMA-2017-241	3505387	7113299	An.							
143	AJMA-2017-242	3505357	7113299	An.							
144	AJMA-2017-243	3505365	7113345	gabbro			140	75			275/70
145	AJMA-2017-245	3505453	7113197	VTG		60					
146	AJMA-2017-246	3504991	7113073	LG			155	90			
147	AJMA-2017-247	3509064	7112034	gabbro							
148	AJMA-2017-248	3504714	7112354	gabbro		15					
149	AJMA-2017-249	3504979	7111775	Leucogneiss			320	70			
150	AJMA-2017-250	3504687	7111773	Leucogneiss			340	70			
151	AJMA-2017-251	3504222	7112148	VTG		16					
152	AJMA-2017-252	3504198	7112163	gabbro		35					
153	AJMA-2017-253	3504185	7112174	gabbro							
154	AJMA-2017-254	3504167	7112199	VTG		20					
155	AJMA-2017-255	3504120	7112178	VTG							
156	AJMA-2017-256	3504117	7112192	VTG		20					
157	AJMA-2017-257	3504109	7112192	An.		6					
158	AJMA-2017-258	3504107	7112271	gabbro		40	140	80			
159	AJMA-2017-259	3504090	7112271	VTG			150	80			
160	AJMA-2017-260	3504091	7112300	gabbro	260.1	20					
161	AJMA-2017-261	3504108	7112302	gabbro							
162	AJMA-2017-262	3504101	7112319	gabbro							
163	AJMA-2017-263	3504035	7112420	An./LG		20					
164	AJMA-2017-264	3504059	7112425	An.		15					
165	AJMA-2017-265	3504055	7112413	An.	265.1	20	170	50			
166	AJMA-2017-266	3504050	7112410	An./LG			170	60	230	50	
167	AJMA-2017-267	3505441	7113202	Ore	267.1	80000					
168	AJMA-2017-268	3505440	7113209	An. / LG		80000					
169	AJMA-2017-269	3505437	7113206	Ore		50000					
170	AJMA-2017-270	3507924	7111715	Gb-pegm							
171	AJMA-2017-271	3507908	7111684	VTG							
172	AJMA-2017-272	3507775	7111655	LG							
173	AJMA-2017-273	3507770	7111708	gabbro							
174	AJMA-2017-274	3507908	7111684	gabbro	274.1						
175	AJMA-2017-275	3506195	7113349	Ore							
176	AJMA-2017-276	3506194	7113350	An.							
177	AJMA-2017-277	3506212	7113349	LG							
178	AJMA-2017-278	3508320	7112712	An.							
179	AJMA-2017-279	3509111	7113044	gabbro							
180	AJMA-2017-280	3507912	7111699	Gb-pegm							

No.	Station_code	X-KKJ3	Y-KKJ3	Field_name	Sample	Magsus.	S	S	L	L	FA
						10^5	dd.	dip	dd.	dip	dd./dip
181	AJMA-2017-281	3508321	7112713	gabbro							
182	AJMA-2017-282	3507306	7112882	Gb-afb							
183	AJMA-2017-283	3507318	7112868	Gb-afb	283.1		140	70			
184	AJMA-2017-284	3507284	7112893	tonalite							
185	AJMA-2017-285	3507278	7112898	tonalite			145	90			
186	AJMA-2017-286	3507268	7112902	tonalite			150	75			
187	AJMA-2017-287	3507261	7112890	tonalite			160	85			
188	AJMA-2017-288	3507049	7113046	gabbro			220	45			
189	AJMA-2017-289	3506963	7112943	VTG							
190	AJMA-2017-290	3506927	7112899	Afb	290.1						
191	AJMA-2017-291	3506974	7112949	VTG							
192	AJMA-2017-293	3506953	7112933	VTG							
193	AJMA-2017-294	3506890	7112988	VTG							
194	AJMA-2017-295	3507387	7112464	tonalite			180	90			
195	AJMA-2017-296	3507388	7112474	tonalite							
196	AJMA-2017-297	3507302	7112882	Gb-afb			140	90			
197	AJMA-2017-298	3508371	7111337	M-gb	298.1		190	90			
198	AJMA-2017-299	3508353	7111331	gabbro							
199	AJMA-2017-300	3508308	7111400	M-gb							
200	AJMA-2017-301	3507852	7111620	VTG							
201	AJMA-2017-302	3507868	7111613	VTG							
202	AJMA-2017-303	3507801	7111613	VTG?							
203	AJMA-2017-304	3507780	7111616	VTG							
204	AJMA-2017-305	3507731	7111649	VTG							
205	AJMA-2017-306	3507804	7111530	M-gb	306.1		90	85			
206	AJMA-2017-307	3508276	7112169	Gb-pegm							
207	AJMA-2017-308	3508298	7112145	VTG							
208	AJMA-2017-309	3508359	7112131	gabbro							
209	AJMA-2017-310	3508298	7112133	VTG							
210	AJMA-2017-311	3508415	7112085	VTG							
211	AJMA-2017-312	3508430	7112075	gabbro	312.1						
212	AJMA-2017-313	3508442	7112065	gabbro							
213	AJMA-2017-314	3508440	7112087	gabbro							
214	AJMA-2017-315	3508419	7112081	VTG							
215	AJMA-2017-316	3508437	7112032	gabbro							
216	AJMA-2017-317	3508441	7111994	gabbro							
217	AJMA-2017-318	3508427	7112004	VTG							
218	AJMA-2017-319	3508424	7112012	gabbro							
219	AJMA-2017-320	3508423	7112027	gabbro							
220	AJMA-2017-321	3508453	7112018	gabbro							
221	AJMA-2017-322	3508406	7111954	gabbro							
222	AJMA-2017-323	3508394	7111925	gabbro							
223	AJMA-2017-324	3508318	7111929	gabbro							
224	AJMA-2017-325	3508366	7111844	gabbro							
225	AJMA-2017-326	3508453	7111837	gabbro							

No.	Station_code	X-KKJ3	Y-KKJ3	Field_name	Sample	Magsus.	S	S	L	L	FA
						10^5	dd.	dip	dd.	dip	dd./dip
226	AJMA-2017-327	3508461	7111834	gabbro							
227	AJMA-2017-328	3508481	7111824	gabbro							
228	AJMA-2017-329	3508593	7111729	VTG							
229	AJMA-2017-330	3508591	7111727	VTG							
230	AJMA-2017-331	3508578	7111743	VTG							
231	AJMA-2017-332	3508558	7111747	gabbro	332.1						
232	AJMA-2017-333	3508627	7111755	gabbro							
233	AJMA-2017-334	3508649	7111721	gabbro							
234	AJMA-2017-335	3508684	7111601	gabbro							
235	AJMA-2017-336	3509197	7112887	gabbro					295	45	
236	AJMA-2017-337	3509201	7112867	gabbro					260	60	
237	AJMA-2017-338	3509226	7112855	LG							150/70
238	AJMA-2017-339	3509259	7112814	gabbro	339.1		265	65			
239	AJMA-2017-340	3509266	7112778	M-gb	340.1		285	75			
240	AJMA-2017-341	3509230	7112738	gabbro							
241	AJMA-2017-342	3508394	7112118	gabbro					260	60	
242	AJMA-2017-344	3509061	7112021	gabbro							
243	AJMA-2017-345	3508943	7111956	gabbro	345.1						
244	AJMA-2017-346	3508897	7111966	Gb/VTG??							
245	AJMA-2017-347	3508787	7112046	VTG							
246	AJMA-2017-348	3508762	7112082	VTG							
247	AJMA-2017-349	3508731	7112085	Gb/VTG							
248	AJMA-2017-350	3508671	7112161	VTG							
249	AJMA-2017-351	3508698	7112144	gabbro							
250	AJMA-2017-352	3508601	7112122	VTG							
251	AJMA-2017-353	3508574	7112122	VTG							
252	AJMA-2017-354	3508630	7111916	gabbro							
253	AJMA-2017-355	3508472	7112145	VTG							
254	AJMA-2017-356	3507792	7111685	Contact							
255	AJMA-2017-357	3505359	7112233	Gb-afb	357.1		200	45			
256	AJMA-2017-358	3504953	7112064	Afb	358.1		140	85			
257	AJMA-2017-359	3504911	7112118	Afb	359.1		150	70			
258	AJMA-2017-360	3504995	7112780	gabbro							
259	AJMA-2017-361	3504931	7112812	gabbro							
260	AJMA-2017-362	3504939	7112819	gabbro							
261	AJMA-2017-363	3504836	7112824	gabbro							
262	AJMA-2017-364	3504837	7112831	LG			180	70			
263	AJMA-2017-365	3504826	7112832	gabbro							
264	AJMA-2017-366	3504815	7112827	gabbro			190	90			
265	AJMA-2017-367	3504820	7112834	LG							
266	AJMA-2017-368	3504822	7112848	Gb-afb			150	90			
267	AJMA-2017-369	3505145	7113204	Afb			340	85			
268	AJMA-2017-370	3505196	7113205	LG							
269	AJMA-2017-371	3505200	7113208	Gb-afb	371.1		180	70			
270	AJMA-2017-372	3505221	7113225	gabbro							65/75

No.	Station_code	X-KKJ3	Y-KKJ3	Field_name	Sample	Magsus.	S	S	L	L	FA
						10^5	dd.	dip	dd.	dip	dd./dip
271	AJMA-2017-373	3505305	7113289	gabbro			140	80			
272	AJMA-2017-374	3506963	7112876	Gb-afb							
273	AJMA-2017-375	3505528	7113154	gabbro	375.1		160	80			
274	AJMA-2017-376	3505528	7113154	LG							
275	AJMA-2017-377	3505567	7113105	gabbro							
276	AJMA-2017-378	3505585	7113066	gabbro	378.1						
277	AJMA-2017-379	3505642	7113115	gabbro	379.1		270	65			
278	AJMA-2017-380	3505632	7113166	LG							
279	AJMA-2017-381	3505660	7113202	gabbro	381.1		200	85			
280	AJMA-2017-382	3505716	7113207	An.	382.1		190	75			
281	AJMA-2017-383	3505663	7113302	Ore	383.1						
282	AJMA-2017-384	3506421	7113465	LG			180	70			
283	AJMA-2017-385	3506437	7113443	LG	385.1						
284	AJMA-2017-386	3507915	7111743	VTG							
285	AJMA-2017-387	3505012	7113102	Afb			175	90			
286	AJMA-2018-1	3506432	7113452	VTG	1.1						
287	AJMA-2018-2	3507307	7112880	Afb	2.1			165	70		
288	AJMA-2018-3	3506348	7113518	Monz.	3.1						
289	AJMA-2018-4	3507351	7111502	M-gb		40		150	70		
290	AJMA-2018-5	3507332	7111496	Gb							
291	AJMA-2018-6	3505163	7112405	VTG		20		140	90		
292	AJMA-2018-7	3505125	7112377	VTG		15		165	47		
293	AJMA-2018-8	3505102	7112419	Db		50		120	85		
294	AJMA-2018-9	3505098	7112423	VTG							
295	AJMA-2018-10	3505006	7112435	VTG		15		330	90		
296	AJMA-2018-11	3504937	7112466	Gb		40					
297	AJMA-2018-12	3504933	7112455	LG		15		345	90	220	
298	AJMA-2018-13	3504911	7112468	Gb		50					
299	AJMA-2018-14	3504876	7112538	LG		20					
300	AJMA-2018-15	3504862	7112537	VTG		30					
301	AJMA-2018-16	3504755	7112524	VTG		25					
302	AJMA-2018-17	3504797	7112480	LG		30					
303	AJMA-2018-18	3504806	7112447	VTG		10					
304	AJMA-2018-19	3504918	7112351	VTG		20					
305	AJMA-2018-20	3504953	7112324	VTG							
306	AJMA-2018-21	3504970	7112303	gb							
307	AJMA-2018-22	3504987	7112307	gb		50			160		
308	AJMA-2018-23	3505049	7112251	Sch. gb		35			160		
309	AJMA-2018-24	3509173	7112113	Lsk gb		35			270		
310	AJMA-2018-25	3509129	7112291	gb		25					
311	AJMA-2018-26	3509122	7112331	Karkear. LG		20					
312	AJMA-2018-27	3509092	7112360	gb		20			260		
313	AJMA-2018-28	3508937	7111950	gb		130					
314	AJMA-2018-29	3509780	7112590	Bt-tonalite		300			285		
315	AJMA-2018-30	3509152	7112997	VTG							

No.	Station_code	X-KKJ3	Y-KKJ3	Field_name	Sample	Magsus.	S	S	L	L	FA
						10^5	dd.	dip	dd.	dip	dd./dip
316	AJMA-2018-31	3509277	7112821	A-type vein					280		
317	AJMA-2018-32	3509277	7112821	A-type vein							
318	AJMA-2018-33	3505285	7113417	A-type vein							
319	AJMA-2018-34	3505247	7113469	An.incl.							
320	AJMA-2018-35	3508743	7110436	Maf. Gn.							
321	AJMA-2018-36	3509007	7110795	Kfed gran.							
322	AJMA-2018-37	3506431	7113438	Kfed gran.							
323	AJMA-2018-38	3507206	7112844	Arch.							
324	AJMA-2018-39	3506855	7112367	Arch.							
325	AJMA-2018-40	3506784	7112241	Diabase							
326	AJMA-2018-41	3506795	7112235	Diabase							
327	AJMA-2018-42	3506814	7112236	Diabase							
328	AJMA-2018-43	3506819	7112222	Diabase							
329	AJMA-2018-44	3506841	7112193	Diabase							
330	AJMA-2018-45	3506843	7112169	Diabase/Arch							
331	AJMA-2018-46	3506855	7112189	Diabase							
332	AJMA-2018-47	3505041	7112439	VTG							
333	AJMA-2018-48	3505149	7112435	VTG							
334	AJMA-2018-49	3505103	7112399	Diabase							
335	AJMA-2018-50	3505118	7112399	VTG							
336	AJMA-2018-51	3505130	7112402	VTG							
337	AJMA-2018-52	3505125	7112377	VTG							
338	AJMA-2018-53	3505108	7112413	Diabase							
339	AJMA-2018-54	3505114	7112414	VTG							
340	AJMA-2018-55	3505090	7112414	VTG							
341	AJMA-2018-56	3505107	7112401	Diabase							
342	AJMA-2018-57	3505080	7112442	VTG							
343	AJMA-2018-58	3504911	7112496	LG							
344	AJMA-2018-59	3504826	7112550	VTG							
345	AJMA-2018-60	3504801	7112576	LG							
346	AJMA-2018-61	3504805	7112529	Gabbro							
347	AJMA-2018-62	3504776	7112507	VTG							
348	AJMA-2018-63	3504830	7112465	VTG							
349	AJMA-2018-64	3508546	7112333	Diabase	64.1						
350	AJMA-2018-65	3506963	7112876	Gb-afb	65.1						

No.	Station_code	X-KKJ3	Y-KKJ3	Field_name	Sample	Magsus.	S	S	L	L	FA
		SAMPLES									
351	OTA-1A	3505440	7113209	Gabbro	x						
352	OTA-1B	3505447	7113163	Gabbro	x						
353	OTA-1C	3505476	7113123	Gabbro	x						
354	OTA-2	3505475	7113129	VTG	x						
355	OTA-3A	3505490	7113184	An.incl.	x						
356	OTA-3B	3505490	7113184	An.incl.	x						
357	OTA-4	3505440	7113209	An.incl.	x						
358	OTA-5A	3505397	7113274	An.incl.	x						
359	OTA-5B	3505440	7113274	An.incl.	x						
360	OTA-6	3505440	7113209	Ore	x						
361	OTA-10	3505447	7112064	gb afb	x						
362	MEM-1	3506194	7113350	An.incl.	x						
363	MEM-2	3506195	7113349	Class II ore	x						
364	MEM-3	3506104	7113494	An.incl.	x						
365	MEM-4	3506212	7113349	LG	x						
366	VUO-1	3508317	7112703	An.incl.	x						
367	VUO-22A	3508322	7112712	An.incl.	x						
368	VUO-22B	3508322	7112712	An.incl.	x						
369	VUO-5	3508323	7112711	An.incl.	x						
370	VUO-4	3508320	7112712	An.incl.	x						
371	VUO-15	3508321	7112713	Homog.gb	x						
372	VUO-20	3506927	7112899	gb afb	x						
373	VUO-6A	3509117	7113030	An.incl.	x						
374	VUO-6B	3509099	7113014	An.incl.	x						
375	VUO-7	3509111	7113044	Homog.gb	x						
376	VUO-2A	3508938	7113069	An.incl.	x						
377	VUO-2B	3508938	7113069	An.incl.	x						
378	VUO-9	3508310	7112715	layered gb	x						
379	VUO-11	3508313	7112697	UM incl.	x						
380	VUO-12	3508318	7112711	An.dike	x						
381	ON-1	3504059	7112425	An.incl.	x						
382	ON-2	3504091	7112300	Homog.gb	x						
383	RA-1A	3508310	7112233	UM incl.	x						
384	RA-1B	3508310	7112233	VTG	x						
385	RA-2	3507912	7111699	Gb pegm	x						

No.	Station_code	X-KKJ3	Y-KKJ3	Field_name	Sample	Magsus.	S	S	L	L	FA
DRILL HOLES											
386	VUO-78	3508119	7112799								
387	VUO-85	3507604	7112002								
388	VUO-92	3508882	7113138								
389	VUO-93	3509105	7113058								
390	VUO-97	3508316	7112321								
391	VUO-98	3508586	7112000								
392	VUO-99	3508751	7111798								
393	VUO-100	3508804	7111740								
394	VUO-101	3508510	7111616								
395	VUO-102	3508470	7111676								
396	VUO-112	3508226	7112468								
397	VUO-114	3508171	7112457								
HAND SAMPLES (Nykänen, 1995)											
398	34-VMN-92	7111950	3508950								
399	35-VMN-92	7111980	3508870								
400	37-VMN-92	7111900	3508830								
401	38-VMN-92	7111970	3508790								
402	39-VMN-92	7112010	3508730								
403	40-VMN-92	7112080	3508730								
404	41-VMN-92	7112100	3508620								
405	42-VMN-92	7112160	3508570								
406	44-VMN-92	7112200	3508360								
407	45-VMN-92	7112270	3508270								
408	47-VMN-92	7112010	3509070								
409	48-VMN-92	7112020	3509160								
410	49-VMN-92	7112060	3509160								
411	50-VMN-92	7112090	3509160								
412	64-VMN-92	7112790	3509260								
413	124-VMN-92	7112010	3509140								
414	125-VMN-92	7112000	3509120								
415	143-VMN-92	7111770	3507860								

APPENDIX 3. Petrographical observation sheets.

Thin section type	Polished thin section
Thin section type	Polished thin section
Thin section_ID	**MEM-1**
Sample type	Hand sample
Hole_ID / Depth	-
Location	Metsämalmi
Rock name	ANORTHOSITIC AUTOLITH
Main minerals	Plg, Am
Accessory minerals	
Ore/ opaque minerals	Mag, Ilm
Texture	Equigranular
Mineral alteration	Amphibolitization
Rock/hydrothermal alteration	
EPMA analyses	5 Plg crystals
Description	Ubiquitous disseminated Mag+Ilm. Plg largely metamorphically stabilized and equigranular, not schistose. Locally acicular Am. Abnormally high Ti, Fe and Sr in geochemical analysis. Only autolith with abundant oxides seen on microscope.

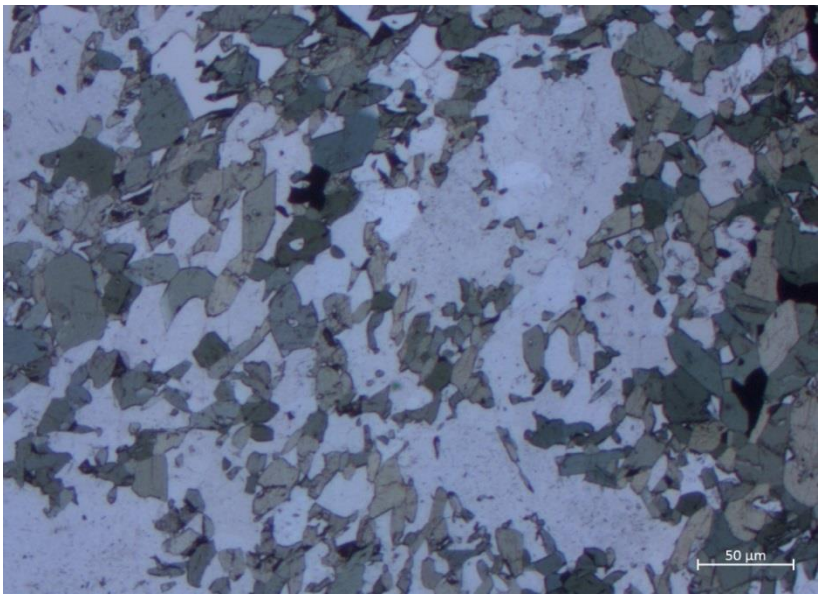

Fig. MEM-1.5. Equigranular inclusion with abundant disseminated Mag+Ilm.

Thin section_ID	**MEM-2**
Sample type	Hand sample
Hole_ID / Depth	-
Location	Metsämalmi
Rock name	CLASS II ORE
Main minerals	Am, Mag, Ilm
Accessory minerals	Plg, Ep
Ore/ opaque minerals	Mag, Ilm
Texture	(Foliated)
Mineral alteration	(Ilmenomagnetite -> Mag + Ilm)
Rock/hydrothermal alteration	Amphibolitization
EPMA analyses	-
Description	Foliated. Ilm separated into Ø 0.25-3.0mm mm euhedral grains. Eu to subheral and acicular Am group minerals. Surprisingly almost no Plg visible.

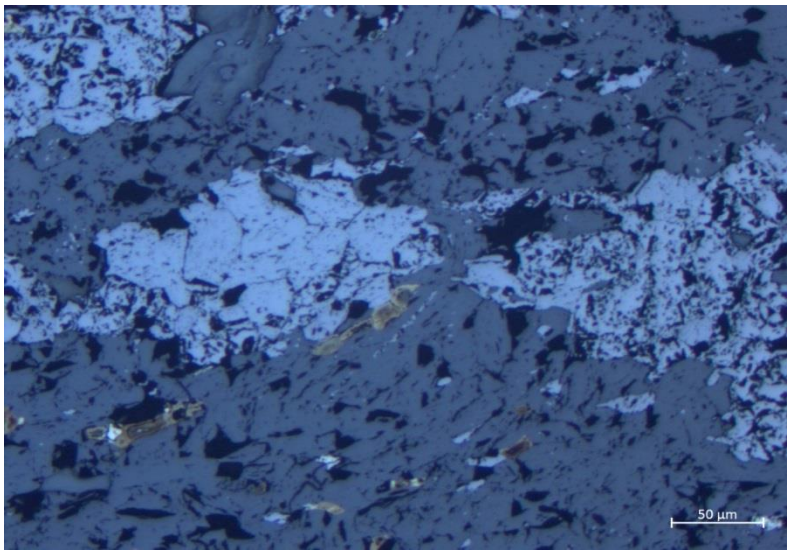

Fig. MEM-2.11

Thin section type	Polished thin section
Thin section_ID	**MEM-4**
Sample type	Hand sample
Hole_ID / Depth	-
Location	Metsämalmi
Rock name	VARI-TEXTURED GABBRO
Main minerals	Plg, Am
Accessory minerals	Ttn, Ilm, Py
Ore/ opaque minerals	Py, Ilm, Mag, Ccp
Texture	Equigranular, foliated
Mineral alteration	Ilm - > Ttn
Rock/hydrothermal alteration	Amphibolitization
EPMA analyses	3 Plg crystals
Description	Strongly recrystallized; Plg rounded, equigranular. Light and dark minerals separated in bands. Relicts of larger, primary Plg seen. Eu-subhedral Py most common opaque. Sulphides found also in Vuorokas lower zone VTG.

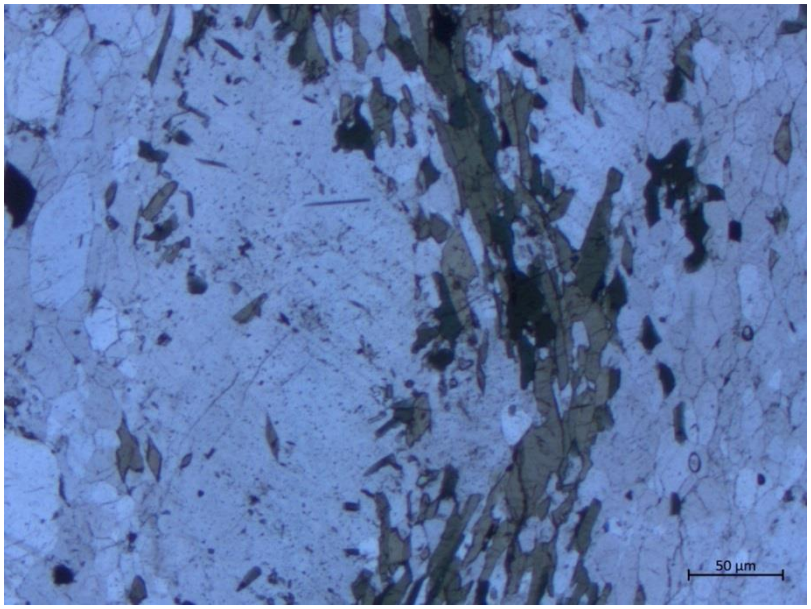

Fig. MEM-4.8

Thin section type	Polished thin section
Thin section_ID	**ON-2**
Sample type	Hand sample
Hole_ID / Depth	-
Location	Otaneva
Rock name	PORPHYRITIC GABBRO
Main minerals	Am, Plg
Accessory minerals	-
Ore/ opaque minerals	-
Texture	Porphyritic
Mineral alteration	
Rock/hydrothermal alteration	Amphibolitization
EPMA analyses	-
Description	Weakly oriented, rich in Am group minerals. Has large (≤ 6 mm) euhedral Plg crystals in fine grained groundmass. Plg also present in fine grained equigranular form. No opaques. Later cryptocrystalline veining.

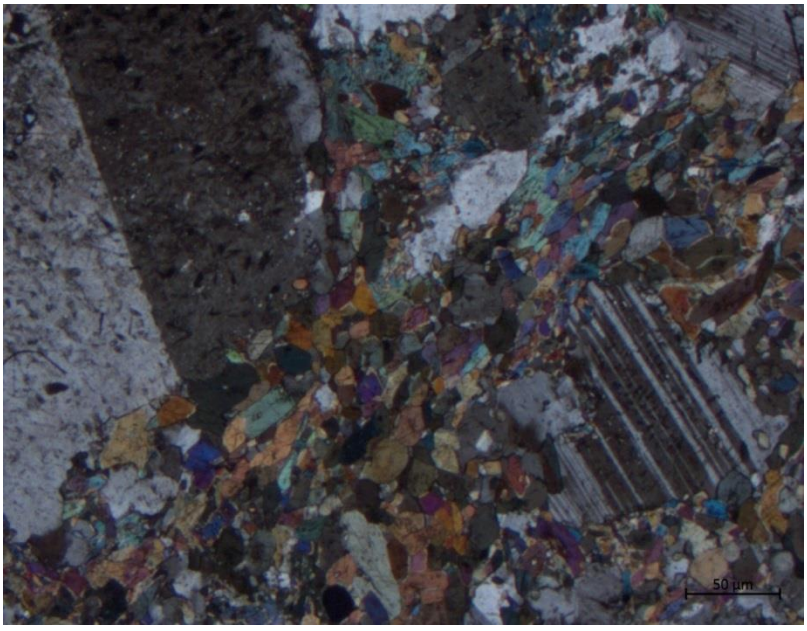

Fig. ON-2.6.

Thin section type	Polished thin section
Thin section_ID	**OTA-1B**
Sample type	Hand sample
Hole_ID / Depth	-
Location	Otanmäki
Rock name	MAGNETITE GABBRO
Main minerals	Am, Plg
Accessory minerals	Ilm, Mg, Ep
Ore/ opaque minerals	Ilm, Mg
Texture	Foliated
Mineral alteration	Ilm -> Ttn
Rock/hydrothermal alteration	Amphibolitization
EPMA analyses	5 Plg crystals
Description	Foliated, dark gabbroamphibolite. Mg+Ilm dissemination. Alteration rims around ilmenite.

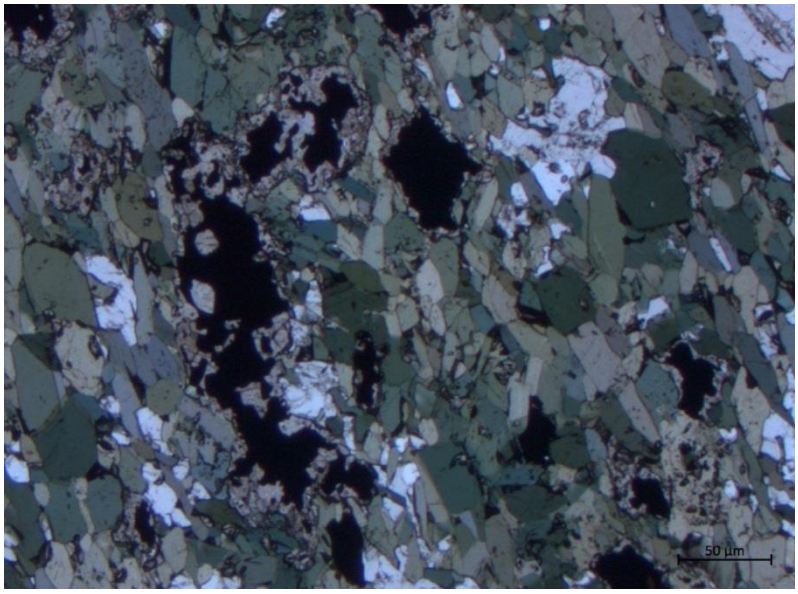

Fig. OTA-1B.1

Thin section type	Polished thin section
Thin section_ID	**OTA-2**
Sample type	Hand sample
Hole_ID / Depth	-
Location	Otanmäki
Rock name	ANORTHOSITIC AUTOLITH
Main minerals	Plg, Am
Accessory minerals	Ep, Ttn, Rt
Ore/ opaque minerals	Mag, Ilm
Texture	Equigranular, moderately foliated
Mineral alteration	Ilm -> Ttn, Rut
Rock/hydrothermal alteration	Amphibolitization, epidotization
EPMA analyses	5 Plg crystals
Description	More mafic, a bit gabbro-like appearance, no pervasive foliation. Primary, coarse grained Plg shapes locally visible.

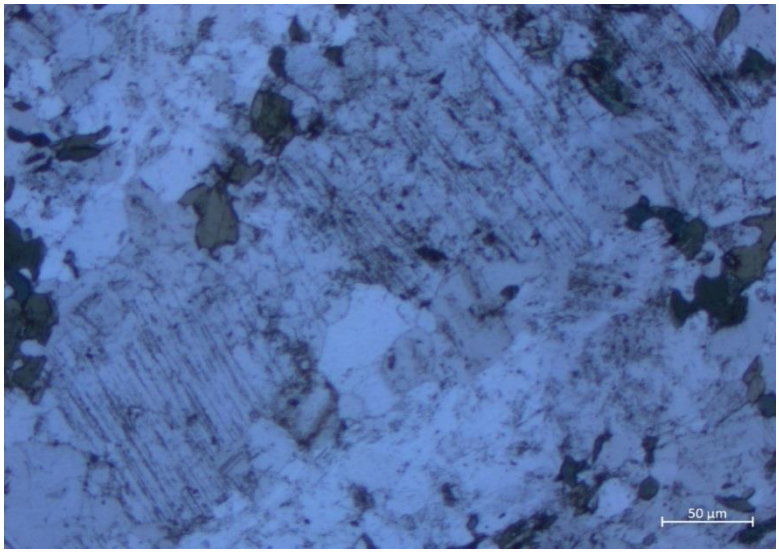

Fig. OTA-2.1

Thin section type	Polished thin section
Thin section_ID	**OTA-3A**
Sample type	Hand sample
Hole_ID / Depth	-
Location	Otanmäki
Rock name	ANORTHOSITIC AUTOLITH
Main minerals	Plg
Accessory minerals	Am, Ttn, Rt
Ore/ opaque minerals	Mag
Texture	(Equigranular)
Mineral alteration	Ilm -> Ttn, Rut
Rock/hydrothermal alteration	Amphibolitization
EPMA analyses	-
Description	Grain size from cryptocrystalline to 5 mm Ø subhedral Plg. Magmatic features better preserved than in OTA-3B, different part of the same inclusion.

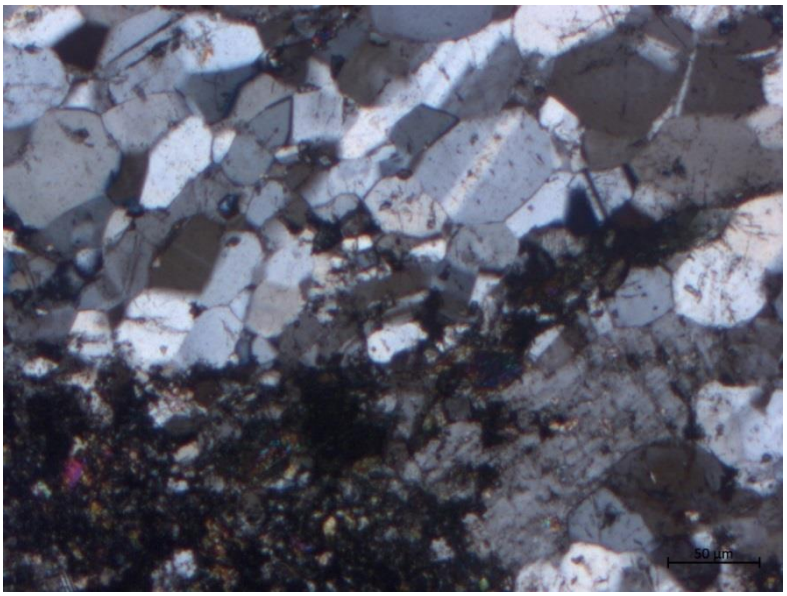

Fig. OTA-3A.2

Thin section type	Polished thin section
Thin section_ID	**OTA-3B**
Sample type	Hand sample
Hole_ID / Depth	-
Location	Otanmäki
Rock name	ANORTHOSITIC AUTOLITH
Main minerals	Plg, Am
Accessory minerals	Ttn, Rt, Bt, Chl
Ore/ opaque minerals	-
Texture	(Equigranular)
Mineral alteration	Ilm -> Ttn, Rut
Rock/hydrothermal alteration	Amphibolitization
EPMA analyses	-
Description	Leucogabbroic, pervasively recrystallized. Varying grain size, relicts of primary, coarse grained Plg still visible. Type locality and sample for Ttn/Rt alteration, no primary Ilm left. Same inclusions as OTA-3A, but richer in Am group minerals.

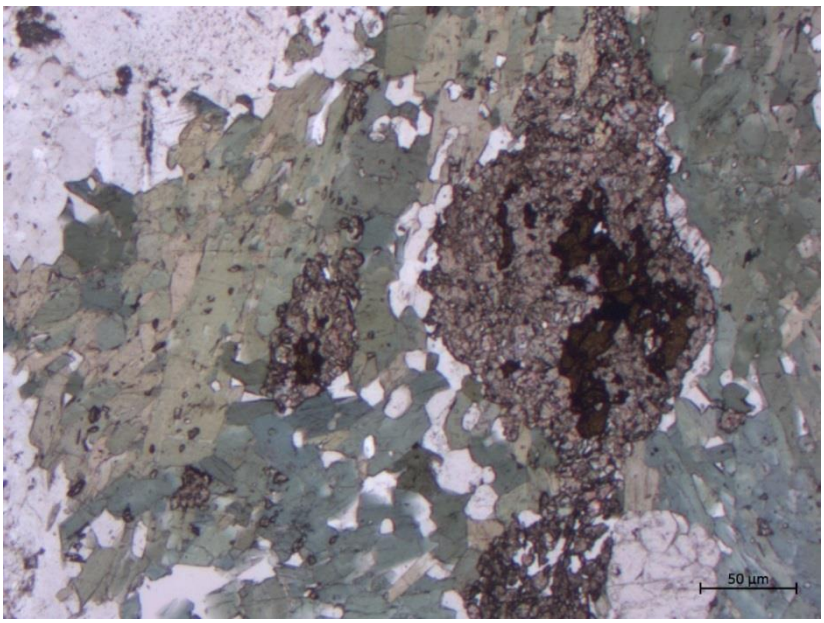

Fig. OTA-3B.1 Type locality: Ilm completely altered to Ttn and Rt.

Thin section type	Polished thin section
Thin section_ID	**OTA-4**
Sample type	Hand sample
Hole_ID / Depth	-
Location	Otanmäki
Rock name	ANORTHOSITIC AUTOLITH
Main minerals	Plg, Am
Accessory minerals	Qtz, Bt
Ore/ opaque minerals	Ilm
Texture	(Equigranular)
Mineral alteration	
Rock/hydrothermal alteration	Amphibolitization
EPMA analyses	5 Plg crystals
Description	Large Ø > 10 mm Plg grains with occasional Hbl inter-growths.

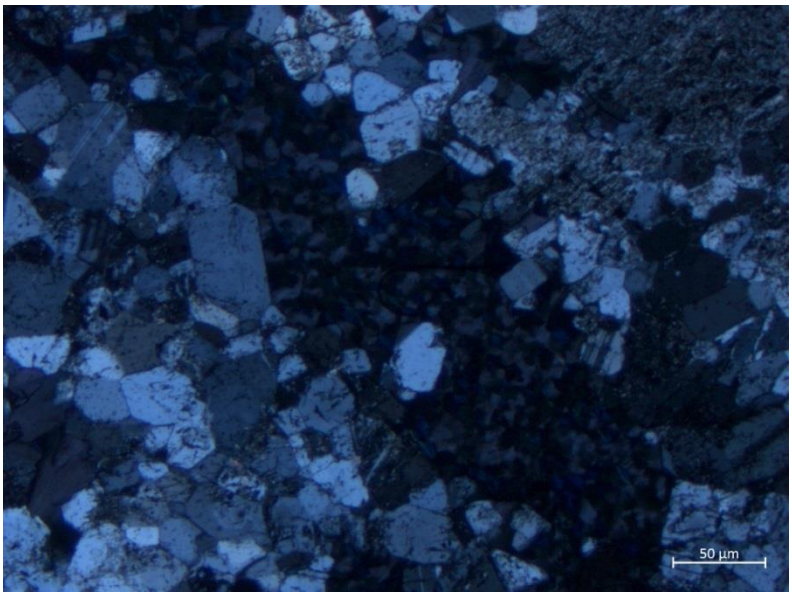

Fig. OTA-4.1

Thin section type	Polished thin section
Thin section_ID	**OTA-5A**
Sample type	Hand sample
Hole_ID / Depth	-
Location	Otanmäki
Rock name	ANORTHOSITIC AUTOLITH
Main minerals	Plg, Am
Accessory minerals	Rt, Bt, Chl
Ore/ opaque minerals	Ilm
Texture	(Equigranular)
Mineral alteration	Bt, Chl, Ep
Rock/hydrothermal alteration	Amphibolitization
EPMA analyses	-
Description	Largest mapped autolith at Otanmäki. Primary magmatic textures visible, but largely recrystallized. Grain size varies 0.03 - 0.5 mm.

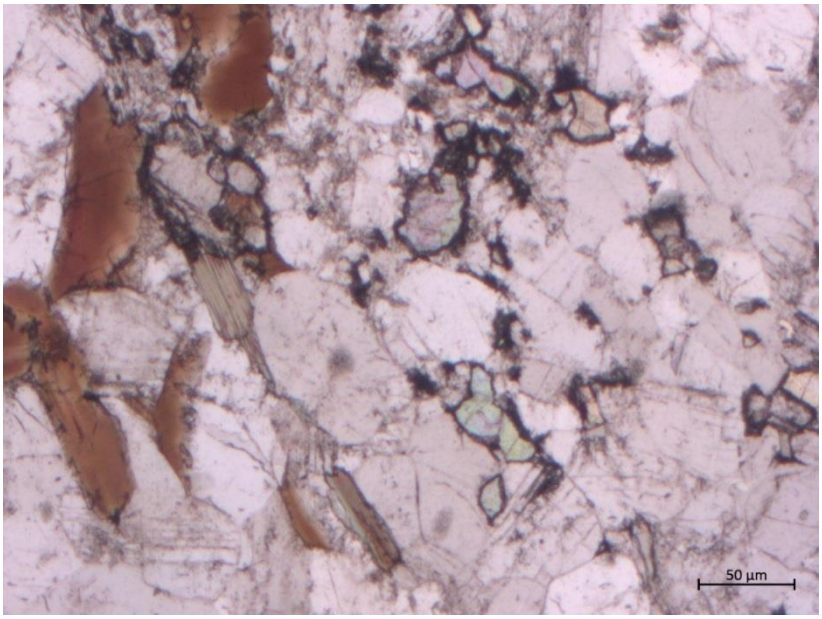

Fig. OTA-5A.1

Thin section type	Polished thin section

Thin section type	Polished thin section

Thin section_ID	**OTA-6**
Sample type	Hand sample
Hole_ID / Depth	-
Location	Otanmäki
Rock name	CLASS I ORE
Main minerals	Mag, Ilm, Chl
Accessory minerals	Plg
Ore/ opaque minerals	Mag, Ilm
Texture	Massive
Mineral alteration	(Ilmenomagnetite -> Mag + Ilm)
Rock/hydrothermal alteration	Chl
EPMA analyses	-
Description	Massive-semimassive iron ore. Anhedral Mag groundmass with Chl interlayers/inclusions. Ilm separated in Ø 0.25-5.0 mm eu-subhedral grains. c. 10 % Chl with minor recrystallized Plg. Devoid of visible tectonic overprint.

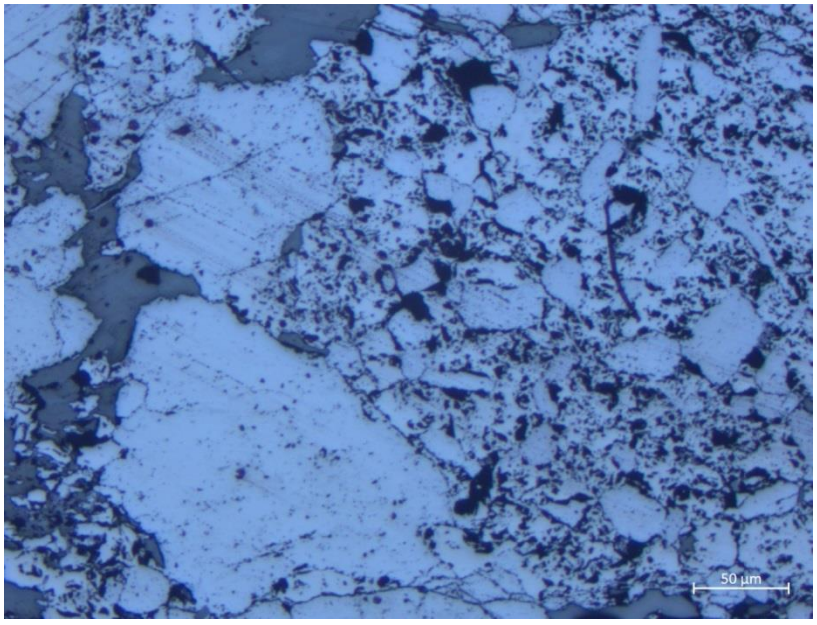

Fig. OTA-6.1

Thin section_ID	**OTA-10**
Sample type	Hand sample
Hole_ID / Depth	-
Location	Otanmäki village
Rock name	MARGIN AMPHIBOLITE
Main minerals	Am, Plg
Accessory minerals	
Ore/ opaque minerals	Subhedral Py, Mag
Texture	Foliated
Mineral alteration	
Rock/hydrothermal alteration	Amphibolitization
EPMA analyses	-
Description	c. 80 % Am group minerals. Strongly foliated. Portrays an ultramylonitic shear zone with oxide mineralization and Chl alteration. Plg rare, equigranular and below 1 mm Ø.

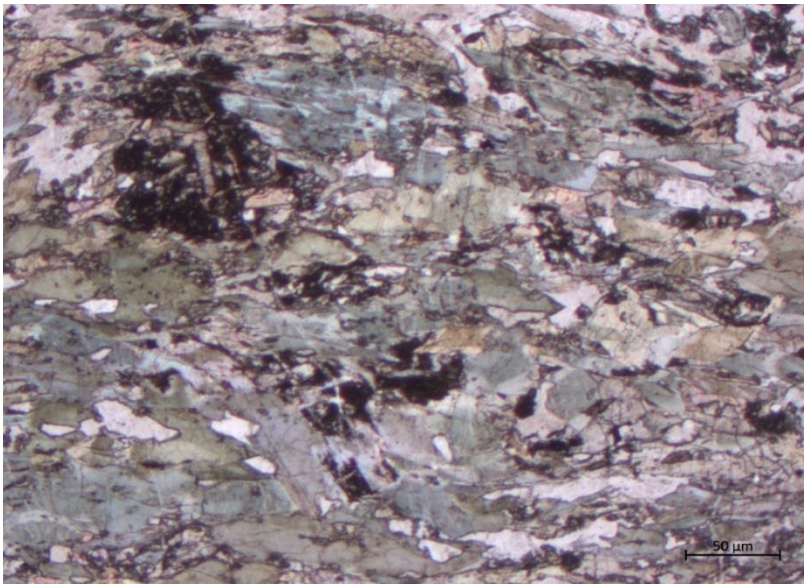

Fig. OTA-10.1 Strongly foliated amphibolite.

Thin section type	Polished thin section
Thin section_ID	**RA-2B**
Sample type	Hand sample
Hole_ID / Depth	-
Location	Rinneaho
Rock name	VARI-TEXTURED GABBRO
Main minerals	Plg
Accessory minerals	Am
Ore/ opaque minerals	
Texture	Coarse grained, Plg > 30 mm Ø
Mineral alteration	Secondary Qtz veining
Rock/hydrothermal alteration	Amphibolitization
EPMA analyses	4 Plg crystals, 1 Am
Description	Recrystallized on crystal bounders. Several primary Plg crystals. Ground mass grain size from cryptocrystalline to 1.0 mm. (In hand sample some crystals tens of cm's.)

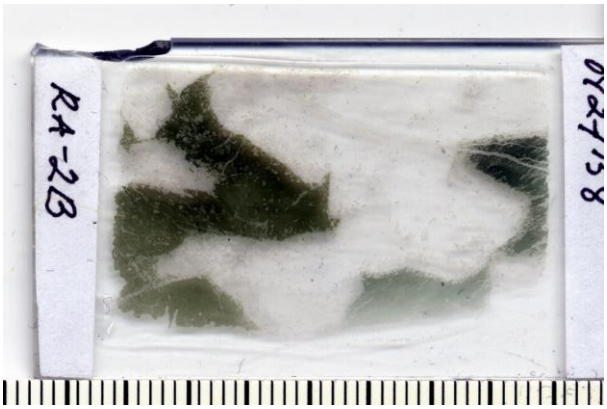

Fig. RA-2B.1. Thin section.

Thin section type	Polished thin section
Thin section_ID	**VUO-1**
Sample type	Hand sample
Hole_ID / Depth	-
Location	Vuorokas
Rock name	ANORTHOSITIC AUTOLITH
Main minerals	Plg, Am
Accessory minerals	Bt, Chl, Ttn, Rt
Ore/ opaque minerals	
Texture	equigranular/schistose
Mineral alteration	
Rock/hydrothermal alteration	Amphibolitization, Bt + Chl
EPMA analyses	3 Plg crystals, 1 Ttn, 1 Rt
Description	Largest mapped inclusion in Vuorokas. Minerals oriented, triple points commonplace. Plg grain size varies . Larger, primary grains visible at places. Schistose.

Fig. VUO-1

Thin section type	Polished thin section
Thin section_ID	**VUO-2A**
Sample type	Hand sample
Hole_ID / Depth	-
Location	Vuorokas
Rock name	ANORTHOSITIC AUTOLITH
Main minerals	Plg, Am
Accessory minerals	
Ore/ opaque minerals	Euhedral Mag, Py
Texture	(Primary magmatic)
Mineral alteration	Ilm -> Ttn, Rut
Rock/hydrothermal alteration	Amphibolitization
EPMA analyses	4 Plg crystals
Description	Locally large Ø 5 mm primary Plg crystals. Plg shows Afb intergrowths at places. Grain size noticeaby different from the neighbouring VUO-2B.

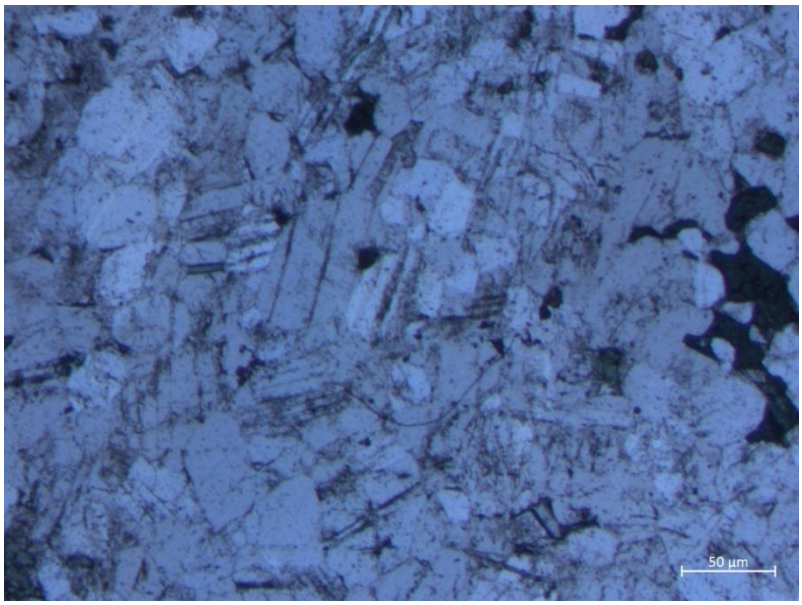

Fig. VUO-2A

Thin section type	Polished thin section
Thin section_ID	**VUO-2B**
Sample type	Hand sample
Hole_ID / Depth	-
Location	Vuorokas
Rock name	ANORTHOSITIC AUTOLITH
Main minerals	Plg
Accessory minerals	Chl
Ore/ opaque minerals	Ilm
Texture	-
Mineral alteration	
Rock/hydrothermal alteration	Amphibolitization
EPMA analyses	-
Description	Am minerals locally euhedral. Plg < 1 mm Ø. Hydrated, cryptocrystalline, pervasively altered. Primary textures virtually nonexistent. Noticeably different from the neighboring VUO-2A.

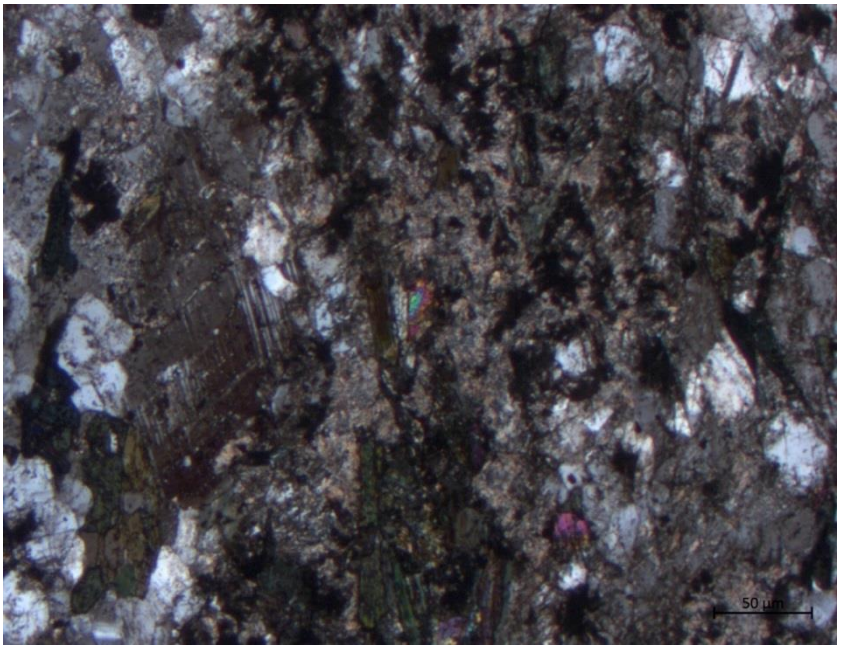

Fig. VUO-2B.2

Thin section type	Polished thin section
Thin section_ID	**VUO-4**
Sample type	Hand sample
Hole_ID / Depth	-
Location	Vuorokas
Rock name	ANORTHOSITIC AUTOLITH
Main minerals	Plg
Accessory minerals	Am, Mag, Py
Ore/ opaque minerals	Euhedral Mag, Py
Texture	Equigranular
Mineral alteration	Ilm -> Ttn, Rut
Rock/hydrothermal alteration	Amphibolitization
EPMA analyses	4 Plg crystals, 1 Am
Description	Very leucocratic. Locally large Ø 5 mm primary Plg crystals, otherwise equigranular.

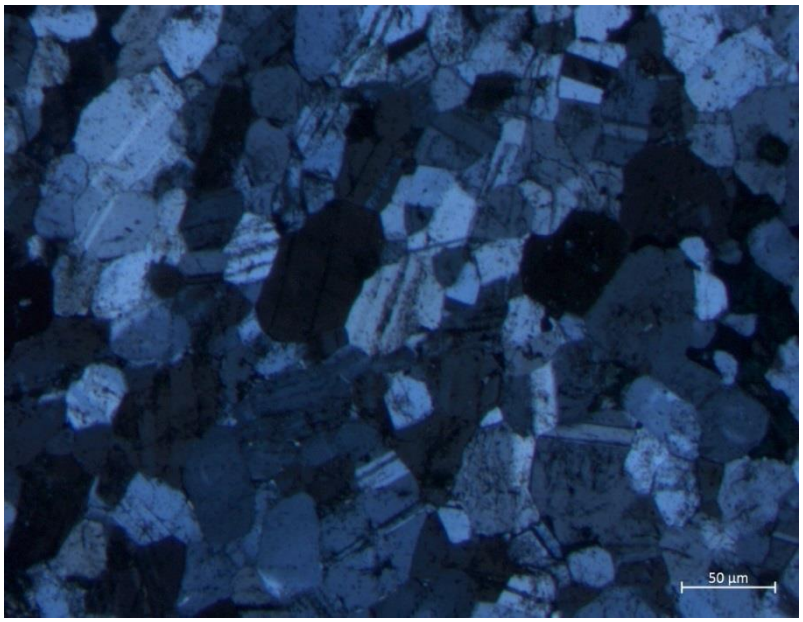

Fig. VUO-4.1

Thin section type	Polished thin section
Thin section_ID	**VUO-5**
Sample type	Hand sample
Hole_ID / Depth	-
Location	Vuorokas
Rock name	ANORTHOSITIC AUTOLITH
Main minerals	Plg
Accessory minerals	Am, Ep
Ore/ opaque minerals	-
Texture	Foliated, equigranular
Mineral alteration	
Rock/hydrothermal alteration	Amphibolitization
EPMA analyses	-
Description	Light, equigranular, foliated, altered Plg rich rock. Relicts of up to 2 mm Ø Plg grains visible. Recrystallized from the rims inward.

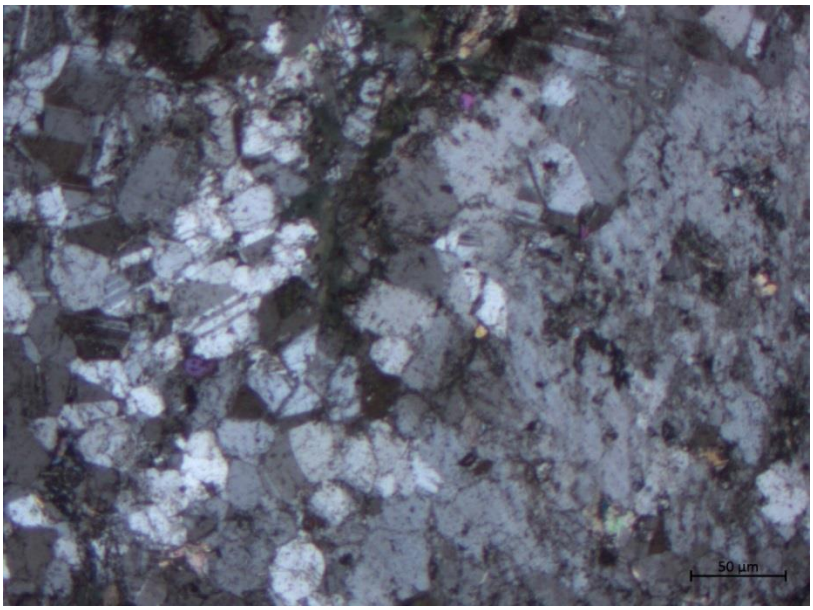

Fig. VUO-5.1

Thin section type	Polished thin section
Thin section_ID	**VUO-15**
Sample type	Hand sample
Hole_ID / Depth	-
Location	Vuorokas
Rock name	MAGNETITE GABBRO
Main minerals	Am, Plg
Accessory minerals	Bt, Zr
Ore/ opaque minerals	Mag, Ilm
Texture	Foliated
Mineral alteration	Ilm -> Ttn, Rut
Rock/hydrothermal alteration	Amphibolitization
EPMA analyses	-
Description	Strongly foliated and recrystallized dark gabbroamphibolite. Ubiquitous disseminated Mag+Ilm. Ilm altered from the rims.

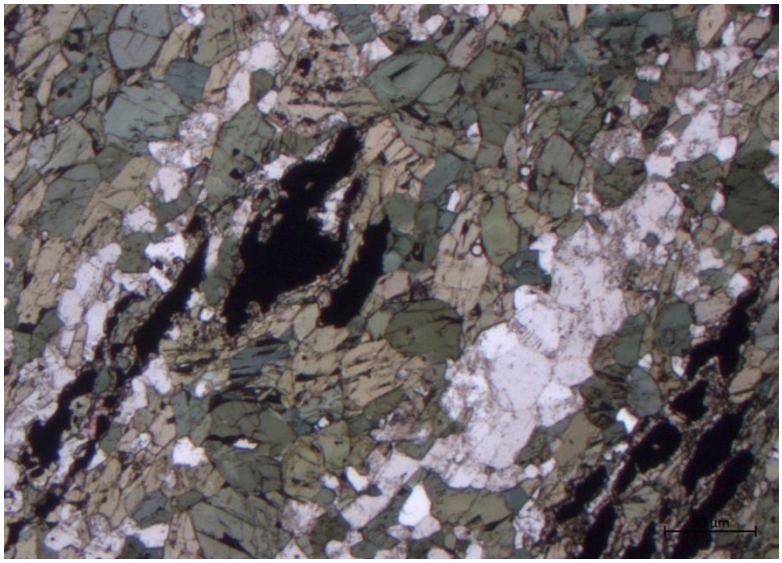

Fig. VUO-15.1

Thin section type	Polished thin section
Thin section_ID	**VUO-20**
Sample type	Hand sample
Hole_ID / Depth	-
Location	Vuorokas
Rock name	MARGIN AMPHIBOLITE
Main minerals	Am, Plg
Accessory minerals	-
Ore/ opaque minerals	Ilm, Mag
Texture	Equigranular
Mineral alteration	-
Rock/hydrothermal alteration	Amphibolitization
EPMA analyses	-
Description	80 % Afb. Less strained than OTA-10, mild tectonic orientation. Am grain size < 1 mm. Primary Plg rare; few hydrated crystals visible. Plg shows undulatory extinction and Am group minerals overgrowth.

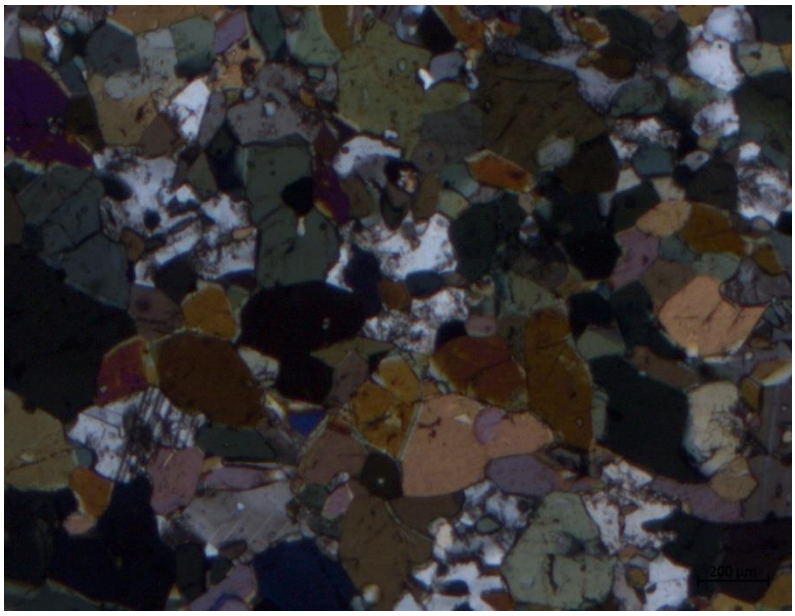

Fig. VUO-20.2

APPENDIX 4. Electron microprobe results.

	No.	1	2	3	4	5	6	7	8
		MEM-1	MEM-1	MEM-1	MEM-1	MEM-1	MEM-1	MEM-1	MEM-1
SiO2	wt%	56.59	56.78	57.23	56.30	58.11	55.41	57.80	57.48
TiO2	wt%	0.00	0.00	0.00	0.01	0.01	0.00	0.01	0.02
Al2O3	wt%	26.76	26.95	26.62	27.90	25.88	27.02	26.38	26.55
FeO	wt%	0.08	0.07	0.05	0.04	0.03	0.07	0.03	0.02
CaO	wt%	8.82	8.84	8.35	9.53	7.64	8.98	8.38	8.48
Na2O	wt%	6.17	6.00	6.12	5.97	6.51	5.52	6.43	5.89
K2O	wt%	0.06	0.08	0.06	0.07	0.05	0.06	0.03	0.05
MnO	wt%	0.00	0.00	0.00	0.01	0.00	0.00	0.02	0.00
BaO	wt%	0.02	0.02	0.02	0.00	0.00	0.00	0.01	0.00
Sr	ppm	2367.66	2553.70	2739.73	2908.84	2959.58	3001.86	3120.24	3187.89
Ba	ppm	161.22	161.22	170.17	0.00	0.00	0.00	107.48	0.00
Total	wt%	98.78	99.07	98.80	100.16	98.57	97.42	99.47	98.87
An	wt%	43.95	44.65	42.81	46.69	39.24	47.17	41.79	44.17
Ab	wt%	55.67	54.85	56.82	52.92	60.45	52.49	58.02	55.50
Or	wt%	0.38	0.50	0.37	0.39	0.31	0.34	0.20	0.34

	No.	9	10	11	12	13	14	15	16
		MEM-1	MEM-1	MEM-4	MEM-4	MEM-4	MEM-4	MEM-4	OTA-1B
SiO2	wt%	55.78	56.85	57.00	53.07	56.49	54.26	55.33	57.71
TiO2	wt%	0.03	0.00	0.00	0.00	0.00	0.00	0.00	0.02
Al2O3	wt%	27.18	26.97	26.43	29.29	26.98	28.37	27.42	26.46
FeO	wt%	0.08	0.09	0.09	0.07	0.00	0.05	0.06	0.08
CaO	wt%	9.03	8.82	8.33	11.81	9.10	10.56	9.86	8.30
Na2O	wt%	6.44	5.60	5.73	4.66	5.25	5.10	5.61	5.75
K2O	wt%	0.02	0.04	0.14	0.09	0.07	0.12	0.10	0.07
MnO	wt%	0.04	0.00	0.00	0.00	0.00	0.00	0.00	0.05
BaO	wt%	0.00	0.06	0.00	0.01	0.00	0.00	0.04	0.09
Sr	ppm	3357.01	4177.24	481.99	769.49	921.70	1023.17	1344.50	1082.36
Ba	ppm	35.83	528.44	0.00	44.78	0.00	0.00	394.09	761.31
Total	wt%	98.99	98.94	97.78	99.11	98.00	98.57	98.57	98.65
An	wt%	43.60	46.45	44.15	58.00	48.73	52.99	48.97	44.16
Ab	wt%	56.29	53.31	54.98	41.47	50.81	46.29	50.44	55.37
Or	wt%	0.12	0.24	0.86	0.54	0.46	0.72	0.59	0.47

	No.	17	18	19	20	21	22	23	24
		OTA-1B	OTA-1B	OTA-1B	OTA-1B	OTA-1B	OTA-2	OTA-2	OTA-2
SiO2	wt%	57.49	51.49	57.26	57.16	56.78	58.11	59.29	57.65
TiO2	wt%	0.00	0.01	0.00	0.00	0.00	0.01	0.00	0.00
Al2O3	wt%	26.69	24.82	25.98	26.66	27.04	25.94	25.37	25.91
FeO	wt%	0.05	0.01	0.11	0.08	0.16	0.05	0.04	0.05
CaO	wt%	8.19	7.27	7.56	8.85	8.93	8.14	7.06	8.00
Na2O	wt%	6.56	6.08	6.02	6.13	5.58	6.19	7.14	6.20
K2O	wt%	0.16	0.07	0.21	0.08	0.11	0.18	0.09	0.15
MnO	wt%	0.00	0.03	0.00	0.02	0.00	0.00	0.00	0.01
BaO	wt%	0.09	0.04	0.04	0.04	0.05	0.02	0.03	0.06
Sr	ppm	1116.18	1183.83	1843.40	1877.22	2300.02	0.00	0.00	0.00
Ba	ppm	824.00	340.35	367.22	331.39	420.96	134.35	277.65	564.26
Total	wt%	99.35	89.94	97.40	99.25	98.92	98.62	99.02	98.04
An	wt%	40.46	39.60	40.41	44.17	46.64	41.65	35.15	41.24
Ab	wt%	58.63	59.98	58.23	55.33	52.69	57.28	64.32	57.83
Or	wt%	0.92	0.42	1.36	0.50	0.67	1.07	0.53	0.93

	No.	25	26	27	28	29	30	31	32
		OTA-2	OTA-2	OTA-2	OTA-2	OTA-2	OTA-2	OTA-4	OTA-4
SiO2	wt%	57.05	56.48	56.85	57.12	57.39	57.80	56.17	54.80
TiO2	wt%	0.00	0.00	0.00	0.02	0.00	0.02	0.01	0.02
Al2O3	wt%	26.71	27.14	27.04	26.07	26.08	26.07	27.21	27.57
FeO	wt%	0.06	0.10	0.11	0.09	0.12	0.11	0.02	0.05
CaO	wt%	9.05	9.12	8.83	8.11	8.27	8.32	9.48	9.99
Na2O	wt%	6.21	5.85	6.19	6.12	6.03	6.61	5.73	5.29
K2O	wt%	0.08	0.07	0.14	0.15	0.14	0.19	0.10	0.09
MnO	wt%	0.00	0.00	0.01	0.00	0.02	0.00	0.00	0.00
BaO	wt%	0.03	0.02	0.00	0.01	0.04	0.00	0.00	0.00
Sr	ppm	219.85	355.15	414.34	1023.17	1048.54	1082.36	219.85	287.50
Ba	ppm	286.61	152.26	0.00	53.74	313.48	0.00	0.00	0.00
Total	wt%	99.22	98.82	99.21	97.82	98.20	99.24	98.74	97.84
An	wt%	44.38	46.09	43.71	41.86	42.76	40.57	47.46	50.82
Ab	wt%	55.16	53.46	55.49	57.20	56.40	58.33	51.93	48.66
Or	wt%	0.46	0.45	0.81	0.93	0.84	1.10	0.61	0.52

	No.	33	34	35	36	37	38	39	40
		OTA-4	OTA-4	OTA-4	OTA-4	OTA-4	OTA-4	OTA-4	RA-2B
SiO2	wt%	55.85	55.44	55.78	53.98	53.87	55.60	54.97	51.70
TiO2	wt%	0.00	0.00	0.00	0.05	0.05	0.00	0.00	0.01
Al2O3	wt%	27.45	27.86	27.95	28.11	29.24	27.42	27.77	30.00
FeO	wt%	0.01	0.04	0.04	0.13	0.07	0.02	0.03	0.02
CaO	wt%	9.71	10.10	9.85	10.72	11.28	9.57	10.01	12.87
Na2O	wt%	5.72	5.46	5.32	4.84	5.15	6.02	5.36	3.86
K2O	wt%	0.09	0.07	0.09	0.07	0.06	0.09	0.14	0.08
MnO	wt%	0.02	0.03	0.03	0.00	0.01	0.01	0.01	0.00
BaO	wt%	0.00	0.01	0.02	0.00	0.02	0.02	0.04	0.00
Sr	ppm	355.15	541.18	735.67	1056.99	1056.99	1217.66	1699.64	0.00
Ba	ppm	0.00	80.61	188.09	0.00	197.04	152.26	313.48	0.00
Total	wt%	98.90	99.07	99.17	98.02	99.88	98.90	98.55	98.52
An	wt%	48.14	50.36	50.32	54.82	54.58	46.51	50.39	64.55
Ab	wt%	51.32	49.22	49.13	44.74	45.06	52.95	48.79	34.99
Or	wt%	0.54	0.42	0.55	0.44	0.36	0.54	0.82	0.46

	No.	41	42	43	44	45	46	47	48
		RA-2B	RA-2B	RA-2B	RA-2B	RA-2B	RA-2B	RA-2B	VUO-1
SiO2	wt%	52.74	51.90	53.08	51.88	52.17	52.69	53.46	52.03
TiO2	wt%	0.02	0.00	0.00	0.02	0.02	0.00	0.01	0.02
Al2O3	wt%	29.19	29.02	29.60	29.93	29.75	29.25	29.20	30.62
FeO	wt%	0.03	0.06	0.07	0.05	0.04	0.07	0.07	0.02
CaO	wt%	12.18	11.85	11.82	12.52	12.34	11.85	11.74	12.92
Na2O	wt%	3.88	4.40	4.74	3.82	4.01	4.16	4.26	3.70
K2O	wt%	0.10	0.07	0.08	0.05	0.11	0.10	0.07	0.04
MnO	wt%	0.00	0.02	0.00	0.04	0.01	0.00	0.00	0.00
BaO	wt%	0.00	0.01	0.01	0.00	0.00	0.04	0.06	0.00
Sr	ppm	0.00	0.00	0.00	253.68	355.15	355.15	448.17	33.82
Ba	ppm	0.00	62.70	107.48	0.00	8.96	331.39	492.61	0.00
Total	wt%	98.15	97.32	99.42	98.33	98.48	98.20	98.92	99.35
An	wt%	63.07	59.57	57.67	64.24	62.58	60.76	60.11	65.75
Ab	wt%	36.33	40.04	41.84	35.47	36.76	38.62	39.46	34.04
Or	wt%	0.60	0.40	0.49	0.29	0.66	0.63	0.43	0.22

	No.	49	50	51	52	53	54	55	56
		VUO-1	VUO-1	VUO-1	VUO-2A	VUO-2A	VUO-2A	VUO-2A	VUO-2A
SiO2	wt%	52.20	51.24	55.09	53.62	55.13	55.00	54.64	53.41
TiO2	wt%	0.00	0.00	0.03	0.00	0.00	0.01	0.00	0.01
Al2O3	wt%	29.58	30.87	28.14	29.10	28.03	27.92	28.25	29.23
FeO	wt%	0.01	0.04	0.03	0.01	0.05	0.03	0.14	0.01
CaO	wt%	12.51	13.68	10.47	11.05	10.11	10.01	10.30	11.05
Na2O	wt%	4.07	3.55	4.93	4.76	5.25	5.56	5.28	4.50
K2O	wt%	0.08	0.10	0.16	0.04	0.06	0.05	0.23	0.27
MnO	wt%	0.05	0.00	0.00	0.00	0.03	0.01	0.00	0.00
BaO	wt%	0.03	0.03	0.04	0.00	0.00	0.00	0.01	0.02
Sr	ppm	126.84	481.99	896.33	0.00	481.99	676.48	896.33	930.15
Ba	ppm	223.91	286.61	394.09	0.00	0.00	26.87	80.61	134.35
Total	wt%	98.55	99.57	99.01	98.60	98.71	98.67	98.96	98.62
An	wt%	62.63	67.64	53.46	56.06	51.36	49.71	51.19	56.64
Ab	wt%	36.91	31.76	45.56	43.70	48.27	49.99	47.47	41.71
Or	wt%	0.46	0.60	0.98	0.24	0.36	0.30	1.34	1.65

	No.	57	58	59	60	61	62	63	64
		VUO-2A	VUO-4	VUO-4	VUO-4	VUO-4	VUO-4	VUO-4	VUO-4
SiO2	wt%	55.57	43.24	57.07	56.77	56.51	56.79	56.21	56.46
TiO2	wt%	0.00	0.73	0.00	0.00	0.01	0.01	0.00	0.02
Al2O3	wt%	27.72	11.91	26.64	26.83	26.88	26.87	27.05	26.66
FeO	wt%	0.00	17.65	0.02	0.05	0.03	0.07	0.04	0.07
CaO	wt%	9.91	11.84	8.84	9.08	8.82	8.88	9.15	8.80
Na2O	wt%	5.36	1.28	6.87	5.99	5.72	6.35	5.69	6.12
K2O	wt%	0.04	0.71	0.11	0.14	0.10	0.11	0.10	0.08
MnO	wt%	0.02	0.24	0.00	0.04	0.00	0.01	0.02	0.00
BaO	wt%	0.00	0.04	0.00	0.00	0.05	0.00	0.02	0.02
Sr	ppm	1243.02	0.00	414.34	608.83	1048.54	1310.67	1344.50	1530.53
Ba	ppm	0.00	340.35	0.00	0.00	474.70	0.00	179.13	179.13
Total	wt%	98.79	98.00	99.61	98.97	98.23	99.27	98.45	98.44
An	wt%	50.38	78.98	41.32	45.22	45.73	43.32	46.78	44.06
Ab	wt%	49.35	15.40	58.06	53.96	53.67	56.04	52.64	55.46
Or	wt%	0.27	5.62	0.62	0.82	0.60	0.64	0.58	0.48

APPENDIX 5. ICP-OES/ICP-MS analysis results.

			1	2	3	4	5	6
		MDL	RA-2B	OTA-10	VUO-20	OTA-1B	VUO-15	MEM-2
SiO2	wt%	0.01	51.06	47.93	45.68	40.96	41.38	20.77
Al2O3	wt%	0.01	25.14	12.33	13.8	13.12	13	8.89
Fe2O3	wt%	0.04	2.81	9.65	15.8	18.42	17.09	45.39
MgO	wt%	0.01	1.82	9.7	8.71	6.65	7.42	6.22
CaO	wt%	0.01	12.43	13.88	10.74	10.95	10.38	5.85
Na2O	wt%	0.01	4.24	1.44	1.82	2.23	2.22	1.07
K2O	wt%	0.01	0.22	0.97	0.3	0.27	0.51	0.15
TiO2	wt%	0.01	0.29	1.02	1.49	6.23	6.34	10.64
P2O5	wt%	0.01	0.04	0.18	<0.01	<0.01	0.02	<0.01
MnO	wt%	0.01	0.03	0.18	0.17	0.19	0.22	0.25
Cr2O3	wt%	0.002	0.025	0.075	0.023	<0.002	<0.002	0.004
Ba	ppm	1	106	741	61	97	144	41
Ni	ppm	20	269	252	108	<20	<20	383
Sc	ppm	1	7	20	49	35	29	26
LOI	wt%	-5.1	1.7	2.1	1.2	0.6	1.1	0
Sum	wt%	0.01	99.8	99.61	99.72	99.68	99.71	99.27
Be	ppm	1	1	1	<1	<1	<1	1
Co	ppm	0.2	21.2	36.7	68.9	52	49.2	199.4
Cs	ppm	0.1	0.2	0.1	<0.1	<0.1	0.2	<0.1
Ga	ppm	0.5	20.2	15.5	18.9	20.4	18.6	33.6
Hf	ppm	0.1	0.6	2.2	0.4	1	1.5	0.7
Nb	ppm	0.1	2.1	26.7	0.2	7.8	16.6	4.3
Rb	ppm	0.1	5.5	17.4	1.8	2.5	6.3	0.7
Sn	ppm	1	<1	1	<1	<1	<1	1
Sr	ppm	0.5	998.4	1036.7	244.4	471.2	494.2	64.4
Ta	ppm	0.1	0.2	1.8	<0.1	0.6	1.2	0.3
Th	ppm	0.2	0.3	4.4	<0.2	<0.2	<0.2	0.2
U	ppm	0.1	<0.1	0.6	<0.1	<0.1	<0.1	<0.1
V	ppm	8	50	168	442	684	411	2711
W	ppm	0.5	<0.5	<0.5	<0.5	<0.5	<0.5	<0.5
Zr	ppm	0.1	21.1	99.4	6.5	31.2	45.3	22.4
Y	ppm	0.1	3.1	15.2	8.5	6.8	8.4	3.6
La	ppm	0.1	6	47.5	1.4	2.6	4.2	2.1
Ce	ppm	0.1	10.8	73.1	3.1	6.7	9.8	5.2
Pr	ppm	0.02	1.24	7.49	0.42	1.06	1.51	0.74
Nd	ppm	0.3	5.2	24.4	2.4	5.8	8	3.8
Sm	ppm	0.05	0.96	3.81	0.86	1.53	2.21	0.81
Eu	ppm	0.02	0.75	1.22	0.56	0.86	1.13	0.4
Gd	ppm	0.05	0.91	3.35	1.33	1.78	2.26	1.04
Tb	ppm	0.01	0.12	0.47	0.25	0.25	0.31	0.15
Dy	ppm	0.05	0.66	2.75	1.49	1.43	1.78	0.72
Ho	ppm	0.02	0.11	0.56	0.3	0.26	0.33	0.14
Er	ppm	0.03	0.32	1.61	0.92	0.68	0.95	0.4
Tm	ppm	0.01	0.04	0.21	0.14	0.09	0.1	0.04
Yb	ppm	0.05	0.25	1.41	0.81	0.55	0.65	0.3
Lu	ppm	0.01	0.03	0.21	0.12	0.07	0.09	0.05
TOT/C	wt%	0.02	0.07	0.06	<0.02	<0.02	<0.02	<0.02
TOT/S	wt%	0.02	0.32	0.19	0.11	0.13	0.24	1.05

			7	8	9	10	11	12
		MDL	OTA-6	MEM-4	MEM-1	OTA-2	OTA-3A	OTA-4
SiO2	wt%	0.01	3.57	48.74	47.47	52.91	51.08	53.64
Al2O3	wt%	0.01	3.9	24.47	20.78	24.62	26.31	26.44
Fe2O3	wt%	0.04	69.36	7.29	10.76	3.41	2.7	1.9
MgO	wt%	0.01	4.37	1.24	3.42	1.15	1.23	0.52
CaO	wt%	0.01	<0.01	10.74	10.27	10.08	11.45	9.58
Na2O	wt%	0.01	<0.01	4.43	4.03	5.34	4.59	5.61
K2O	wt%	0.01	<0.01	0.26	0.16	0.2	0.3	0.2
TiO2	wt%	0.01	18.77	1.56	1.77	0.99	0.57	0.39
P2O5	wt%	0.01	<0.01	0.14	0.03	0.17	0.04	0.05
MnO	wt%	0.01	0.38	0.06	0.11	0.04	0.03	0.02
Cr2O3	wt%	0.002	0.028	0.002	0.006	<0.002	0.003	<0.002
Ba	ppm	1	3	214	84	201	202	146
Ni	ppm	20	68	45	66	<20	37	<20
Sc	ppm	1	20	5	15	6	5	2
LOI	wt%	-5.1	-1.2	0.8	0.8	0.9	1.5	1.4
Sum	wt%	0.01	99.17	99.76	99.63	99.79	99.85	99.79
Be	ppm	1	<1	<1	1	1	<1	1
Co	ppm	0.2	98.5	26.8	46.5	6.9	11.5	3.7
Cs	ppm	0.1	<0.1	<0.1	<0.1	<0.1	0.2	0.3
Ga	ppm	0.5	40.7	24.3	22.6	20.8	21.3	22.7
Hf	ppm	0.1	1.1	0.7	0.9	2.3	0.5	1.1
Nb	ppm	0.1	10.8	3.7	4.2	9.9	2.3	1.6
Rb	ppm	0.1	<0.1	2.5	0.7	2.3	9.4	6.6
Sn	ppm	1	1	<1	<1	<1	<1	<1
Sr	ppm	0.5	2.1	1233.4	1861	1304.4	999.3	1682.5
Ta	ppm	0.1	0.8	0.2	0.2	0.7	0.1	0.1
Th	ppm	0.2	<0.2	0.6	0.9	1.3	0.3	0.9
U	ppm	0.1	<0.1	0.1	<0.1	0.1	<0.1	<0.1
V	ppm	8	3937	306	377	84	61	50
W	ppm	0.5	<0.5	<0.5	<0.5	<0.5	<0.5	<0.5
Zr	ppm	0.1	35.9	28.7	30.4	97.1	21	46.7
Y	ppm	0.1	0.1	3.9	4.1	6	3.1	2.1
La	ppm	0.1	0.3	8	4.5	12.1	6	8.5
Ce	ppm	0.1	<0.1	16.6	10.3	24.6	12.1	16
Pr	ppm	0.02	<0.02	1.99	1.23	2.77	1.37	1.76
Nd	ppm	0.3	<0.3	8.2	5.5	11.4	5.5	6.9
Sm	ppm	0.05	<0.05	1.36	0.95	1.98	1.03	1.15
Eu	ppm	0.02	<0.02	1.02	0.74	0.99	0.97	0.64
Gd	ppm	0.05	<0.05	1.34	1.04	1.79	1	0.85
Tb	ppm	0.01	<0.01	0.16	0.15	0.24	0.12	0.1
Dy	ppm	0.05	<0.05	0.9	0.84	1.36	0.66	0.48
Ho	ppm	0.02	<0.02	0.15	0.18	0.24	0.12	0.07
Er	ppm	0.03	<0.03	0.34	0.49	0.69	0.32	0.18
Tm	ppm	0.01	<0.01	0.05	0.06	0.09	0.04	0.03
Yb	ppm	0.05	<0.05	0.3	0.38	0.53	0.24	0.16
Lu	ppm	0.01	<0.01	0.04	0.06	0.08	0.03	0.03
TOT/C	wt%	0.02	<0.02	<0.02	<0.02	<0.02	0.07	0.04
TOT/S	wt%	0.02	<0.02	0.21	0.19	<0.02	0.12	<0.02

			13	14	15	16	17	18
		MDL	OTA-5A	VUO-1	VUO-5	VUO-4	VUO-2A	VUO-2B
SiO2	wt%	0.01	52.03	49.59	53.9	51.04	51.89	51.13
Al2O3	wt%	0.01	26.31	23.54	26.21	23.77	26.7	25.84
Fe2O3	wt%	0.04	2.48	4.88	1.55	5.47	2.53	3.1
MgO	wt%	0.01	0.77	3.23	0.64	1.28	0.98	1.29
CaO	wt%	0.01	10.11	11.43	9.81	10.5	9.6	9.29
Na2O	wt%	0.01	5.02	3.82	5.68	4.59	4.74	4.47
K2O	wt%	0.01	0.79	0.5	0.19	0.55	1.01	1.68
TiO2	wt%	0.01	0.63	1.41	0.42	0.34	0.27	0.34
P2O5	wt%	0.01	0.09	0.03	0.03	<0.01	0.06	0.05
MnO	wt%	0.01	0.03	0.05	0.02	0.06	0.03	0.03
Cr2O3	wt%	0.002	<0.002	0.004	0.004	0.008	<0.002	<0.002
Ba	ppm	1	333	262	224	362	278	459
Ni	ppm	20	<20	43	<20	<20	<20	<20
Sc	ppm	1	3	7	3	6	4	4
LOI	wt%	-5.1	1.6	1.3	1.3	2.1	1.9	2.5
Sum	wt%	0.01	99.84	99.82	99.79	99.73	99.73	99.73
Be	ppm	1	2	3	<1	<1	1	<1
Co	ppm	0.2	3	14	3.1	42.5	4.4	9.7
Cs	ppm	0.1	0.5	0.3	0.1	0.5	1.7	0.9
Ga	ppm	0.5	22.7	19.6	19.1	19.2	20.6	19.8
Hf	ppm	0.1	0.7	0.6	0.4	0.3	0.7	0.4
Nb	ppm	0.1	4.2	3.4	1.2	1	1.1	1.3
Rb	ppm	0.1	28.9	16.5	4.5	19.8	41.5	65.6
Sn	ppm	1	<1	<1	<1	<1	<1	<1
Sr	ppm	0.5	1106.9	898.8	1640.7	1956.8	1997.6	2076.8
Ta	ppm	0.1	0.3	0.2	<0.1	<0.1	0.1	0.1
Th	ppm	0.2	0.5	0.4	0.6	<0.2	0.4	0.4
U	ppm	0.1	0.1	0.1	<0.1	<0.1	<0.1	<0.1
V	ppm	8	55	91	41	64	36	41
W	ppm	0.5	<0.5	<0.5	<0.5	<0.5	<0.5	<0.5
Zr	ppm	0.1	28.2	26	13.1	11.1	28.4	17.9
Y	ppm	0.1	3.8	3.5	2.3	5.3	3.2	3.3
La	ppm	0.1	8	4.4	7.5	7.5	6.4	6.5
Ce	ppm	0.1	15.8	9.2	13.2	14.4	13.2	12.4
Pr	ppm	0.02	1.89	1.07	1.36	1.75	1.55	1.47
Nd	ppm	0.3	7.5	4.3	5.6	8.1	6.6	6.2
Sm	ppm	0.05	1.36	0.97	0.85	1.77	1.22	1.12
Eu	ppm	0.02	1.25	0.84	0.8	1.57	0.81	0.82
Gd	ppm	0.05	1.21	0.93	0.81	1.76	1.11	1.02
Tb	ppm	0.01	0.16	0.13	0.1	0.24	0.13	0.13
Dy	ppm	0.05	0.86	0.71	0.44	1.23	0.66	0.71
Ho	ppm	0.02	0.13	0.11	0.08	0.21	0.13	0.13
Er	ppm	0.03	0.39	0.38	0.23	0.48	0.32	0.3
Tm	ppm	0.01	0.05	0.04	0.03	0.06	0.03	0.04
Yb	ppm	0.05	0.26	0.3	0.15	0.32	0.22	0.28
Lu	ppm	0.01	0.04	0.04	0.02	0.05	0.03	0.03
TOT/C	wt%	0.02	0.02	0.03	0.06	0.03	0.03	0.04
TOT/S	wt%	0.02	0.02	<0.02	<0.02	0.69	0.06	0.09

APPENDIX 6. pXRF measurements.

No.		1	2	3	4	5	6	7
sample_ID		AJMA-2017-92.1	AJMA-2017-113.1	AJMA-2017-122.1	AJMA-2017-126.1	AJMA-2017-127.1	AJMA-2017-133.1	AJMA-2017-135.1
SiO2	wt%	43.9	42.2	53.2	52.6	52.6	53.7	43.5
Al2O3	wt%	16.7	15.8	25.7	26.8	26.1	24.8	14.8
FeOTOT	wt%	18.0	18.8	5.1	3.5	4.7	5.3	14.2
MgO	wt%	0.0	0.7	0.0	0.0	0.0	0.8	7.2
CaO	wt%	8.9	9.7	10.1	11.0	10.3	8.9	8.4
Na2O	wt%	2.6	2.4	4.9	5.1	5.0	4.7	2.3
K2O	wt%	0.6	0.3	0.5	0.4	0.3	0.4	0.5
TiO2	wt%	5.0	5.7	0.2	0.3	0.8	0.7	4.3
P2O5	wt%	0.0	0.0	0.0	0.0	0.0	0.0	0.1
MnO	wt%	0.2	0.2	0.1	0.0	0.1	0.1	0.2
Sum_Oxides	wt%	95.9	95.8	99.8	99.7	99.9	99.5	95.6
V	ppm	0.0	0.0	0.0	0.0	0.0	0.0	0.0
Cr	ppm	49.0	29.0	0.0	0.0	0.0	6.0	0.0
Ni	ppm	0.0	53.0	59.7	149.0	11.0	0.0	0.0
Cu	ppm	0.0	0.0	27.0	32.0	7.0	0.0	0.0
Zn	ppm	132.0	99.0	42.0	38.0	19.0	14.0	121.0
Co	ppm	0.0	0.0	0.0	70.0	38.0	0.0	0.0
Sr	ppm	1600.5	1493.0	1542.0	2185.0	1744.0	2644.0	935.0
Ta	ppm	0.0	0.0	73.0	28.0	31.0	18.0	37.0
U	ppm	0.0	0.0	0.0	0.0	0.0	7.0	3.0
Zr	ppm	61.0	46.5	25.5	20.0	42.0	41.0	43.0
Ba	ppm	0.0	0.0	0.0	0.0	0.0	0.0	151.0

No.		8	9	10	11	12	13	14
sample_ID		AJMA-2017-137.2	AJMA-2017-150.1	AJMA-2017-151.1	AJMA-2017-163.1	AJMA-2017-164.1	AJMA-2017-184.1	AJMA-2017-192.1
SiO2	wt%	53.8	41.8	55.2	6.8	51.5	48.4	49.7
Al2O3	wt%	28.1	13.2	24.1	6.2	24.8	20.0	17.5
FeOTOT	wt%	2.5	16.1	3.3	52.1	2.9	7.2	6.0
MgO	wt%	0.0	7.8	1.7	13.1	3.0	5.6	10.3
CaO	wt%	9.9	8.5	7.7	0.0	10.6	8.6	9.3
Na2O	wt%	4.3	2.0	3.7	1.2	4.7	3.1	2.7
K2O	wt%	0.7	0.5	0.8	0.0	0.4	0.2	0.2
TiO2	wt%	0.2	5.1	0.4	13.7	0.1	0.1	0.2
P2O5	wt%	0.0	0.1	0.2	0.1	0.1	0.1	0.1
MnO	wt%	0.0	0.2	0.0	0.2	0.0	0.1	0.1
Sum_Oxides	wt%	99.5	95.4	97.0	93.4	98.1	93.3	96.2
V	ppm	0.0	0.0	0.0	4369.0	0.0	0.0	0.0
Cr	ppm	12.0	0.0	0.0	1269.0	144.0	131.0	239.0
Ni	ppm	0.0	0.0	0.0	123.0	22.0	756.0	118.0
Cu	ppm	0.0	0.0	0.0	0.0	0.0	1602.0	86.0
Zn	ppm	10.0	120.0	0.0	254.0	11.0	17.0	27.0
Co	ppm	20.0	17.0	18.0	0.0	17.0	68.0	33.0
Sr	ppm	2633.0	488.0	1587.0	0.0	1214.0	965.0	749.0
Ta	ppm	15.0	31.0	28.0	24.0	31.0	32.0	25.0
U	ppm	8.0	0.0	11.0	17.0	13.0	0.0	0.0
Zr	ppm	35.0	70.0	41.0	53.0	19.0	21.0	8.0
Ba	ppm	0.0	201.0	419.0	150.0	296.0	259.0	0.0

No.		15	16	17	18	19	20	21
sample_ID		AJMA-2017-197.1	AJMA-2017-201.1	AJMA-2017-203.1	AJMA-2017-204.1	AJMA-2017-206.1	AJMA-2017-207.1	AJMA-2017-215.1
SiO2	wt%	50.0	50.5	49.6	47.7	66.0	55.2	55.1
Al2O3	wt%	16.5	22.7	16.3	16.2	15.1	26.1	24.2
FeOTOT	wt%	6.5	4.4	7.1	9.2	6.4	4.8	2.7
MgO	wt%	10.7	4.1	9.9	8.9	0.0	0.0	1.9
CaO	wt%	9.1	10.7	9.5	8.7	0.9	7.4	8.4
Na2O	wt%	2.6	3.5	2.5	2.5	2.9	5.0	4.6
K2O	wt%	0.3	0.3	0.4	0.4	5.4	0.5	0.9
TiO2	wt%	0.3	0.1	0.3	0.4	0.7	0.3	0.0
P2O5	wt%	0.1	0.1	0.1	0.0	0.0	0.1	0.1
MnO	wt%	0.1	0.0	0.1	0.1	0.2	0.0	0.1
Sum_Oxides	wt%	96.1	96.3	96.0	94.1	97.6	99.4	97.9
V	ppm	0.0	0.0	0.0	0.0	0.0	0.0	0.0
Cr	ppm	104.0	0.0	208.0	115.0	105.0	25.5	0.0
Ni	ppm	88.0	148.0	76.0	394.0	37.0	53.0	0.0
Cu	ppm	0.0	436.0	0.0	915.0	19.0	206.0	0.0
Zn	ppm	38.0	0.0	57.0	77.0	111.0	33.0	32.0
Co	ppm	13.0	38.0	37.0	78.0	32.0	0.0	28.0
Sr	ppm	718.0	995.0	709.0	649.0	194.0	1796.8	1363.0
Ta	ppm	26.0	36.0	24.0	8.0	78.0	80.0	28.0
U	ppm	0.0	4.0	0.0	0.0	0.0	31.5	11.0
Zr	ppm	15.0	14.0	8.0	9.0	432.0	42.6	16.0
Ba	ppm	73.0	160.0	265.0	272.0	0.0	0.0	585.0

No.		22	23	24	25	26	27	28
sample_ID		AJMA-2017-217.1	AJMA-2017-220.1	AJMA-2017-222.1	AJMA-2017-231.1	AJMA-2017-231.2	AJMA-2017-233.1	AJMA-2017-238.1
SiO2	wt%	53.9	52.3	54.4	51.3	60.2	51.5	54.3
Al2O3	wt%	24.5	27.9	26.0	27.1	25.2	27.4	27.7
FeOTOT	wt%	3.0	3.1	4.5	4.8	1.9	5.1	2.2
MgO	wt%	1.8	0.5	0.0	0.0	0.0	0.0	0.0
CaO	wt%	8.7	9.3	8.1	9.6	7.1	8.7	9.7
Na2O	wt%	4.7	5.3	4.9	5.2	4.8	5.2	5.3
K2O	wt%	0.7	0.9	0.9	1.2	0.4	1.8	0.8
TiO2	wt%	0.3	1.1	0.9	0.6	0.2	0.3	0.3
P2O5	wt%	0.4	0.0	0.0	0.0	0.0	0.1	0.0
MnO	wt%	0.0	0.0	0.0	0.0	0.0	0.0	0.0
Sum_Oxides	wt%	98.0	100.4	99.7	99.8	99.8	100.1	100.3
V	ppm	0.0	0.0	0.0	0.0	0.0	0.0	0.0
Cr	ppm	0.0	15.0	22.0	0.0	28.5	30.0	11.0
Ni	ppm	0.0	30.0	0.0	0.0	29.0	25.0	0.0
Cu	ppm	28.0	9.0	0.0	0.0	0.0	0.0	0.0
Zn	ppm	0.0	12.0	22.0	33.3	17.0	56.0	0.0
Co	ppm	22.0	0.0	0.0	0.0	0.0	37.0	0.0
Sr	ppm	1266.0	1918.0	1769.0	2011.4	3099.5	1250.0	1489.0
Ta	ppm	48.0	34.0	15.0	0.0	60.0	27.0	0.0
U	ppm	4.0	8.0	0.0	0.0	33.5	0.0	0.0
Zr	ppm	31.0	48.0	73.0	37.5	43.8	40.0	28.0
Ba	ppm	377.0	0.0	0.0	0.0	0.0	0.0	0.0

No.		29	30	31	32	33	34	35
sample_ID		AJMA-2017-260.1	AJMA-2017-281.1	AJMA-2017-283.1	AJMA-2017-298.1	AJMA-2017-306.1	AJMA-2017-312.1	AJMA-2017-332.1
SiO2	wt%	50.3	43.5	77.3	47.9	49.6	49.8	48.2
Al2O3	wt%	16.4	12.9	12.7	15.6	15.5	15.5	18.3
FeOTOT	wt%	5.8	17.3	0.6	8.7	6.9	7.7	5.6
MgO	wt%	10.8	6.5	0.1	11.6	10.5	10.2	8.5
CaO	wt%	9.4	8.9	2.1	8.6	10.0	9.3	11.0
Na2O	wt%	2.5	2.0	2.4	2.4	2.4	2.4	2.8
K2O	wt%	0.3	0.5	0.4	0.2	0.2	0.3	0.2
TiO2	wt%	0.3	3.0	0.0	0.4	0.2	0.3	0.3
P2O5	wt%	0.1	0.4	0.1	0.1	0.1	0.1	0.1
MnO	wt%	0.1	0.2	0.0	0.2	0.2	0.2	0.1
Sum_Oxides	wt%	96.1	95.1	95.8	95.7	95.7	95.8	95.1
V	ppm	0.0	0.0	1393.0	0.0	0.0	0.0	0.0
Cr	ppm	108.0	0.0	0.0	818.0	441.0	0.0	727.0
Ni	ppm	91.0	0.0	0.0	177.0	106.0	66.0	707.0
Cu	ppm	0.0	0.0	0.0	90.0	40.0	28.0	626.0
Zn	ppm	40.0	149.0	0.0	49.0	44.0	48.0	0.0
Co	ppm	13.0	0.0	12.0	62.0	40.0	40.0	38.0
Sr	ppm	636.0	489.0	884.0	647.0	628.0	683.0	780.0
Ta	ppm	19.0	32.0	46.0	27.0	0.0	25.0	23.0
U	ppm	0.0	0.0	8.0	0.0	0.0	0.0	0.0
Zr	ppm	17.0	90.0	46.0	12.0	0.0	9.0	18.0
Ba	ppm	89.0	215.0	270.0	154.0	0.0	278.0	105.0

No.		36	37	38	39	40	41	42
sample_ID		AJMA-2017-339.1	AJMA-2017-340.1	AJMA-2017-345.1	AJMA-2017-357.1	AJMA-2017-358.1	AJMA-2017-359.1	AJMA-2017-385.1
SiO2	wt%	49.4	48.4	49.1	50.3	48.4	49.9	53.6
Al2O3	wt%	16.4	19.1	17.7	12.7	11.7	12.3	22.0
FeOTOT	wt%	6.4	5.8	5.2	12.9	8.2	13.5	3.5
MgO	wt%	9.2	8.8	10.3	6.8	11.1	6.7	4.3
CaO	wt%	11.0	10.3	10.6	8.5	11.2	8.5	9.4
Na2O	wt%	2.5	2.9	2.7	2.0	1.8	1.9	4.2
K2O	wt%	0.4	0.5	0.0	0.6	1.1	0.7	0.4
TiO2	wt%	0.4	0.3	0.3	1.0	0.8	1.0	0.1
P2O5	wt%	0.1	0.1	0.1	0.2	0.3	0.3	0.1
MnO	wt%	0.1	0.1	0.1	0.2	0.2	0.2	0.1
Sum_Oxides	wt%	95.9	96.4	96.0	95.2	94.8	95.1	97.6
V	ppm	0.0	0.0	0.0	0.0	0.0	0.0	0.0
Cr	ppm	605.0	505.0	712.0	0.0	589.0	0.0	0.0
Ni	ppm	130.0	121.0	90.0	63.0	203.0	70.0	0.0
Cu	ppm	34.0	0.0	0.0	144.0	38.0	101.0	0.0
Zn	ppm	43.0	45.0	38.0	89.0	130.0	105.0	10.0
Co	ppm	26.0	29.0	22.0	38.0	20.0	37.0	38.0
Sr	ppm	874.0	745.0	645.0	232.0	1020.0	211.0	1291.0
Ta	ppm	27.0	0.0	16.0	16.0	26.0	27.0	27.0
U	ppm	0.0	0.0	0.0	0.0	0.0	0.0	11.0
Zr	ppm	21.0	20.0	16.0	104.0	115.0	126.0	43.0
Ba	ppm	219.0	0.0	0.0	0.0	1229.0	280.0	158.0

No.		43	44	45	46	47	48	49
sample_ID		AJMA-2018-1	AJMA-2018-2	AJMA-2018-3	AJMA-2018-64	AJMA-2018-65	MEM-4	ON-2
SiO2	wt%	50.9	40.8	48.8	50.5	42.6	51.6	49.9
Al2O3	wt%	23.6	9.7	17.3	12.6	13.2	24.2	16.7
FeOTOT	wt%	4.0	19.3	10.7	13.2	17.0	4.7	6.2
MgO	wt%	2.7	10.7	4.1	6.6	7.6	2.4	10.1
CaO	wt%	10.9	9.3	6.6	8.4	8.7	9.5	9.8
Na2O	wt%	3.5	1.5	2.6	1.9	2.0	4.6	2.6
K2O	wt%	0.4	0.5	2.2	0.4	0.5	0.3	0.2
TiO2	wt%	0.5	2.4	2.1	1.3	2.8	0.3	0.3
P2O5	wt%	0.1	0.4	1.0	0.2	0.4	0.1	0.1
MnO	wt%	0.4	1.9	1.6	1.0	2.2	0.0	0.1
Sum_Oxides	wt%	97.1	96.3	97.1	96.1	96.9	97.8	96.0
V	ppm	0.0	0.0	0.0	0.0	0.0	0.0	0.0
Cr	ppm	0.0	0.0	0.0	0.0	0.0	0.0	235.0
Ni	ppm	0.0	0.0	0.0	0.0	0.0	0.0	86.0
Cu	ppm	0.0	0.0	0.0	0.0	0.0	0.0	20.0
Zn	ppm	0.0	0.0	0.0	0.0	0.0	30.0	43.0
Co	ppm	0.0	0.0	0.0	0.0	0.0	13.0	26.0
Sr	ppm	0.1	0.0	0.2	0.0	0.0	1503.0	656.0
Ta	ppm	0.0	0.0	0.0	0.0	0.0	31.0	17.0
U	ppm	0.0	0.0	0.0	0.0	0.0	11.0	0.0
Zr	ppm	0.0	0.0	0.0	0.0	0.0	24.0	18.0
Ba	ppm	0.0	0.0	0.1	0.0	0.0	163.0	0.0

No.		50	51	52	53	54	55	56
sample_ID		OTA-1B	OTA-2	OTA-6	RA-1B	VUO-11	VUO-12	VUO-15
SiO2	wt%	40.5	55.7	8.0	48.9	37.3	54.7	41.3
Al2O3	wt%	12.8	23.8	7.3	5.7	10.9	23.6	13.3
FeOTOT	wt%	16.2	2.2	50.0	8.5	19.7	3.2	14.5
MgO	wt%	8.0	1.7	14.5	18.2	8.7	1.7	8.1
CaO	wt%	9.5	9.0	0.1	10.5	9.9	8.0	8.7
Na2O	wt%	2.0	3.7	0.7	0.9	1.7	4.5	2.1
K2O	wt%	0.3	0.3	0.0	0.0	0.6	1.3	0.6
TiO2	wt%	5.4	0.3	12.3	0.7	5.8	0.6	6.2
P2O5	wt%	0.1	0.3	0.1	0.1	0.1	0.2	0.1
MnO	wt%	0.2	0.0	0.2	0.1	0.3	0.0	0.2
Sum_Oxides	wt%	95.0	96.9	93.2	93.8	94.9	97.7	95.2
V	ppm	1417.0	0.0	4390.0	0.0	720.0	0.0	0.0
Cr	ppm	0.0	0.0	906.0	2934.0	0.0	0.0	0.0
Ni	ppm	0.0	0.0	42.0	274.0	0.0	0.0	0.0
Cu	ppm	0.0	0.0	0.0	57.0	52.0	24.0	0.0
Zn	ppm	99.0	0.0	125.0	64.0	92.0	0.0	101.0
Co	ppm	94.0	38.0	39.0	0.0	17.0	13.0	47.0
Sr	ppm	763.0	1803.0	0.0	73.0	147.0	2160.0	864.0
Ta	ppm	29.0	28.0	33.0	0.0	37.0	35.0	31.0
U	ppm	0.0	15.0	18.0	0.0	0.0	16.0	0.0
Zr	ppm	35.0	84.0	57.0	22.0	72.0	36.0	46.0
Ba	ppm	252.0	299.0	157.0	0.0	288.0	506.0	335.0

No.		57	58
sample_ID		VUO-4	VUO-5
SiO2	wt%	53.9	55.9
Al2O3	wt%	23.7	25.2
FeOTOT	wt%	3.8	1.5
MgO	wt%	1.9	0.8
CaO	wt%	9.2	9.4
Na2O	wt%	4.5	4.8
K2O	wt%	0.5	0.3
TiO2	wt%	0.0	0.0
P2O5	wt%	0.1	0.1
MnO	wt%	0.1	0.0
Sum_Oxides	wt%	97.7	98.0
V	ppm	0.0	0.0
Cr	ppm	0.0	0.0
Ni	ppm	0.0	0.0
Cu	ppm	0.0	0.0
Zn	ppm	11.0	0.0
Co	ppm	16.0	26.0
Sr	ppm	2553.0	2058.0
Ta	ppm	27.0	35.0
U	ppm	18.0	18.0
Zr	ppm	26.0	27.0
Ba	ppm	429.0	326.0

APPENDIX 7. CIPW-normative mineral compositions.

No.		1	2	3	4	5	6	7	8
sample_ID		AJMA-2017-92.1	AJMA-2017-113.1	AJMA-2017-122.1	AJMA-2017-126.1	AJMA-2017-127.1	AJMA-2017-133.1	AJMA-2017-135.1	AJMA-2017-137.2
Quartz	wt%	0.91	0	0	0	0	1.08	0	3.05
Corundum	wt%	0	0	0	0	0	0.42	0	2.2
Orthoclase	wt%	3.55	1.77	2.95	2.36	1.77	2.36	3.16	4.14
Albite	wt%	21.82	20.64	40.93	37.27	40.75	39.93	19.4	36.72
Anorthite	wt%	32.22	31.27	46.7	49.06	48.04	44.15	28.64	49.12
Nepheline	wt%	0	0	0.24	3.18	0.69	0	0	0
Kaliophilite	wt%	0	0	0	0	0	0	0	0
Diopside	wt%	10.64	14.83	3.04	4.92	2.73	0	9.82	0
Hypersthene	wt%	14.55	11.8	0	0	0	9.4	11.24	3.57
Olivine	wt%	0	1.88	4.79	1.82	3.67	0	12.65	0
Magnetite	wt%	2.9	3.03	0.82	0.56	0.76	0.85	2.29	0.4
Ilmenite	wt%	9.5	10.83	0.38	0.57	1.52	1.33	8.22	0.38
Apatite	wt%	0	0	0	0	0	0	0.33	0
Sum	wt%	96.09	96.06	99.85	99.74	99.93	99.53	95.75	99.57

No.		9	10	11	12	13	14	15	16
sample_ID		AJMA-2017-150.1	AJMA-2017-151.1	AJMA-2017-164.1	AJMA-2017-184.1	AJMA-2017-192.1	AJMA-2017-197.1	AJMA-2017-201.1	AJMA-2017-203.1
Quartz	wt%	0	9.86	0	0	0	0	0	0
Corundum	wt%	0	3.43	0	0	0	0	0	0
Orthoclase	wt%	3.24	4.52	2.28	1.39	1.34	1.5	1.68	2.6
Albite	wt%	17.2	31.43	34.98	26.13	22.87	21.62	29.62	21.33
Anorthite	wt%	25.17	37.34	45.28	40.01	34.96	32.94	45.3	31.94
Nepheline	wt%	0	0	2.65	0	0	0	0	0
Kaliophilite	wt%	0	0	0	0	0	0	0	0
Diopside	wt%	13.35	0	5.21	1.96	8.75	9.31	6.01	11.96
Hypersthene	wt%	7.88	8.88	0	18.01	16.96	21.23	9.32	17.43
Olivine	wt%	16.19	0	6.76	4.47	9.76	7.79	3.49	8.86
Magnetite	wt%	2.6	0.54	0.47	1.15	0.96	1.04	0.71	1.15
Ilmenite	wt%	9.67	0.67	0.24	0.15	0.46	0.56	0.1	0.6
Apatite	wt%	0.26	0.4	0.25	0.15	0.17	0.15	0.14	0.22
Sum	wt%	95.56	97.07	98.12	93.42	96.23	96.15	96.37	96.08

No.		17	18	19	20	21	22	23	24
sample_ID		AJMA-2017-204.1	AJMA-2017-207.1	AJMA-2017-215.1	AJMA-2017-217.1	AJMA-2017-220.1	AJMA-2017-222.1	AJMA-2017-231.1	AJMA-2017-231.2
Quartz	wt%	0	5.65	2.61	2.13	0	2.31	0	14.37
Corundum	wt%	0	4.17	0.83	1.23	1.28	2.16	0	3.97
Orthoclase	wt%	2.34	2.95	5.18	3.96	5.32	5.32	7.09	2.36
Albite	wt%	21.19	42.02	38.97	39.37	38.41	41.86	32.08	40.57
Anorthite	wt%	31.84	36.06	40.53	40.52	46.14	40.19	47.26	35.22
Nepheline	wt%	0	0	0	0	3.53	0	6.25	0
Kaliophilite	wt%	0	0	0	0	0	0	0	0
Diopside	wt%	9.29	0	0	0	0	0	0.33	0
Hypersthene	wt%	16.33	7	9.08	8.81	0	5.54	0	2.64
Olivine	wt%	11.02	0	0	0	3.15	0	4.89	0
Magnetite	wt%	1.48	0.77	0.43	0.48	0.5	0.73	0.77	0.31
Ilmenite	wt%	0.76	0.57	0	0.52	2.09	1.71	1.14	0.38
Apatite	wt%	0	0.24	0.33	1.02	0	0	0	0
Sum	wt%	94.26	99.43	97.95	98.04	100.42	99.8	99.82	99.82

No.		25	26	27	28	29	30	31	32
sample_ID		AJMA-2017-233.1	AJMA-2017-238.1	AJMA-2017-260.1	AJMA-2017-281.1	AJMA-2017-283.1	AJMA-2017-298.1	AJMA-2017-306.1	AJMA-2017-312.1
Quartz	wt%	0	0	0	0	56.95	0	0	0
Corundum	wt%	1.3	0.53	0	0	4.9	0	0	0
Orthoclase	wt%	10.64	4.73	1.56	2.72	2.52	1.46	1.37	1.84
Albite	wt%	31.53	42.7	21.45	16.8	20.53	20.41	20.29	20.27
Anorthite	wt%	42.51	48.12	32.64	24.82	9.28	31.06	30.92	30.66
Nepheline	wt%	6.82	1.02	0	0	0	0	0	0
Kaliophilite	wt%	0	0	0	0	0	0	0	0
Diopside	wt%	0	0	11.06	14	0	8.77	14.5	12.18
Hypersthene	wt%	0	0	21.03	16.07	1.2	15.53	18.9	22.82
Olivine	wt%	5.77	2.27	6.77	11.52	0	16.18	8.02	6.11
Magnetite	wt%	0.82	0.35	0.94	2.78	0.1	1.4	1.12	1.23
Ilmenite	wt%	0.57	0.57	0.56	5.69	0	0.76	0.42	0.6
Apatite	wt%	0.24	0	0.15	0.94	0.33	0.23	0.28	0.2
Sum	wt%	100.18	100.3	96.17	95.35	95.81	95.79	95.82	95.91

No.		33	34	35	36	37	38	39	40
sample_ID		AJMA-2017-332.1	AJMA-2017-339.1	AJMA-2017-340.1	AJMA-2017-345.1	AJMA-2017-357.1	AJMA-2017-358.1	AJMA-2017-359.1	AJMA-2017-385.1
Quartz	wt%	0	0	0	0	4	0	3.54	0.36
Corundum	wt%	0	0	0	0	0	0	0	0
Orthoclase	wt%	1.17	2.3	3.04	0	3.6	6.74	4.16	2.38
Albite	wt%	23.94	21.37	24.96	23.09	16.6	15.28	16.01	35.36
Anorthite	wt%	36.71	32.15	37.36	35.97	24.07	20.44	22.87	39.98
Nepheline	wt%	0	0	0	0	0	0	0	0
Kaliophilite	wt%	0	0	0	0	0	0	0	0
Diopside	wt%	14.22	17.41	10.78	12.85	13.5	26.71	14.42	4.73
Hypersthene	wt%	4.26	11.95	0.81	10.79	28.99	10.99	29.41	13.76
Olivine	wt%	13.36	8.85	17.8	11.9	0	11.2	0	0
Magnetite	wt%	0.9	1.04	0.93	0.83	2.08	1.33	2.17	0.56
Ilmenite	wt%	0.5	0.68	0.64	0.48	1.95	1.53	1.89	0.27
Apatite	wt%	0.13	0.21	0.17	0.16	0.58	0.71	0.79	0.22
Sum	wt%	95.2	95.95	96.5	96.08	95.38	94.92	95.26	97.62

No.		41	42	43	44	45	46	47	48
sample_ID		AJMA-2018-1	AJMA-2018-2	AJMA-2018-65	MEM-1	MEM-4	MEM-4	ON-2	OTA-10
Quartz	wt%	0.11	0	0	0	0	0	0	0
Corundum	wt%	0	0	0	0	0	0	0	0
Orthoclase	wt%	2.52	2.67	3.08	0.95	1.54	1.8	1.47	5.73
Albite	wt%	29.92	11.88	16.69	28.63	31.69	38.97	21.86	12.18
Anorthite	wt%	47.19	18.67	25.49	38.14	46.12	44.47	33.33	24.31
Nepheline	wt%	0	0.26	0	2.97	3.14	0	0	0
Kaliophilite	wt%	0	0	0	0	0	0	0	0
Diopside	wt%	5.31	20.57	12.34	10.57	5.33	1.71	11.91	35.12
Hypersthene	wt%	10.34	0	6.89	0	0	1.73	18.22	4.67
Olivine	wt%	0	33.91	23.6	11.59	6.12	7.63	7.55	10.64
Magnetite	wt%	0.65	3.11	2.74	1.56	1.06	0.75	0.99	1.4
Ilmenite	wt%	0.91	4.58	5.36	3.36	2.96	0.51	0.58	1.94
Apatite	wt%	0.21	0.92	1	0.07	0.33	0.26	0.22	0.43
Sum	wt%	97.15	96.57	97.19	97.84	98.28	97.83	96.13	96.43

No.		49	50	51	52	53	54	55	56
sample_ID		OTA-1B	OTA-1B	OTA-2	OTA-2	OTA-3A	OTA-4	OTA-5A	RA-1B
Quartz	wt%	0	0	0	10.92	0	0	0	0
Corundum	wt%	0	0	0	1.83	0	0	0	0
Orthoclase	wt%	1.6	2.06	1.18	1.57	1.77	1.18	4.67	0
Albite	wt%	14.7	16.77	43.12	31.13	34.28	45.49	37.12	7.51
Anorthite	wt%	24.99	25.1	42.62	42.72	50.3	46.37	46.92	11.7
Nepheline	wt%	2.26	0	1.12	0	2.47	1.07	2.9	0
Kaliophilite	wt%	0	0	0	0	0	0	0	0
Diopside	wt%	24.21	17.42	5.22	0	5.16	0.7	2.21	31.69
Hypersthene	wt%	0	1	0	7.27	0	0	0	33.34
Olivine	wt%	15.09	19.65	2.58	0	2.51	2.24	2.45	6.66
Magnetite	wt%	2.67	2.6	0.49	0.35	0.39	0.28	0.36	1.38
Ilmenite	wt%	11.84	10.33	1.88	0.54	1.08	0.74	1.2	1.4
Apatite	wt%	0.01	0.3	0.4	0.61	0.09	0.12	0.21	0.25
Sum	wt%	97.37	95.22	98.62	96.95	98.06	98.19	98.05	93.94

No.		57	58	59	60	61	62	63	64
sample_ID		RA-2B	VUO-1	VUO-12	VUO-15	VUO-15	VUO-20	VUO-2A	VUO-2B
Quartz	wt%	0	0	3	0	0	0	0	0
Corundum	wt%	0	0	0.8	0	0	0	0.5	0
Orthoclase	wt%	1.3	2.95	7.45	3.01	3.4	1.77	5.97	9.93
Albite	wt%	32.01	29.64	37.93	15.7	17.43	15.4	37.07	31.57
Anorthite	wt%	48.91	45.61	38.27	24	25.45	28.6	47.24	45.48
Nepheline	wt%	2.1	1.45	0	1.67	0	0	1.65	3.39
Kaliophilite	wt%	0	0	0	0	0	0	0	0
Diopside	wt%	10.25	8.86	0	22.43	13.84	20.34	0	0.24
Hypersthene	wt%	0	0	8.19	0	6.28	9.65	0	0
Olivine	wt%	2.21	6.07	0	15.66	14.52	16.2	4.15	5.14
Magnetite	wt%	0.41	0.71	0.52	2.48	2.34	2.29	0.37	0.45
Ilmenite	wt%	0.55	2.68	1.16	12.05	11.8	2.83	0.51	0.65
Apatite	wt%	0.09	0.07	0.48	0.05	0.27	0.01	0.14	0.12
Sum	wt%	97.83	98.05	97.8	97.05	95.35	97.09	97.59	96.95

No.		65	66	67	68
sample_ID		VUO-4	VUO-4	VUO-5	VUO-5
Quartz	wt%	0	1.17	0	4.87
Corundum	wt%	0	0	0	0.22
Orthoclase	wt%	3.25	3.22	1.12	1.72
Albite	wt%	34.85	38.13	45.24	40.51
Anorthite	wt%	42.63	42.78	45.46	45.72
Nepheline	wt%	2.16	0	1.53	0
Kaliophilite	wt%	0	0	0	0
Diopside	wt%	8.02	1.7	2.49	0
Hypersthene	wt%	0	9.84	0	4.44
Olivine	wt%	4.76	0	1.38	0
Magnetite	wt%	0.79	0.61	0.22	0.24
Ilmenite	wt%	0.65	0.07	0.8	0
Apatite	wt%	0.01	0.24	0.07	0.29
Sum	wt%	97.12	97.76	98.32	98.01

APPENDIX 8. XRF/INAA/ICP-ES/DCP-ES analyses from Nykänen (1995). Sample and drill hole locations in Appendix 2.

No.		1	2	3	4	5	6	7	8	9
Sample ID		VUO 102 /90.85	VUO 97 /30.97	VUO 98 /78.30	VUO 101 /63.75	34-VMN-92	VUO 102 /74.55	125.2-VMN-92	VUO 98 /28.55	47-VMN-92
SiO2	wt%	50.81	51.92	53.08	49.16	51.57	50.22	51.58	50.23	51.63
Al2O3	wt%	14.21	28.04	24.11	11.19	17.66	16.88	13.10	7.62	19.91
FeOTOT	wt%	9.68	1.76	3.81	11.48	6.70	9.75	8.17	10.70	5.21
MgO	wt%	10.83	1.39	4.18	19.78	9.44	8.79	13.05	16.82	7.49
CaO	wt%	11.47	11.85	10.32	6.33	11.43	11.15	11.57	12.50	12.33
Na2O	wt%	1.96	4.32	4.08	1.19	2.28	2.28	1.56	0.88	2.56
K2O	wt%	0.20	0.53	0.13	0.09	0.18	0.20	0.12	0.10	0.20
TiO2	wt%	0.47	0.10	0.11	0.31	0.45	0.38	0.50	0.69	0.43
P2O5	wt%	0.01	0.02	0.02	0.02	0.02	0.02	0.02	0.02	0.03
MnO	wt%	0.15	0.02	0.10	0.20	0.12	0.12	0.16	0.22	0.10
Sum_ Oxides	wt%	99.79	99.95	99.94	99.75	99.85	99.79	99.83	99.78	99.89
V	ppm	142	30	68	88	116	114	152	178	99
Cr	ppm	389	0	88	483	499	429	701	784	451
Ni	ppm	1200	196	32	546	125	1623	156	258	100
Cu	ppm	892	643	9	215	49	1749	49	166	50
Zn	ppm	58	9	40	79	49	52	63	73	41
S	ppm	12350	3020	0	1890	110	20470	30	840	140
Nb	ppm	2	0	2	1	2	2	2	1	3
Rb	ppm	6	16	1	6	6	6	5	6	4
Sr	ppm	445	1618	974	293	571	550	376	181	740
Zr	ppm	36	34	37	18	16	28	10	33	51
Y	ppm	5	0	2	3	5	5	8	12	5
Ba	ppm	100	173	143	38	88	110	70	42	116
Sc	ppm	31	3	11	23	24	23	34	50	20
La	ppm	2	2	2	1	2	2	1	2	2
Ce	ppm	5	4	4	2	5	5	4	6	5
Nd	ppm	3				3		3	5	3
Sm	ppm	1	0	0	0	1	1	1	2	1
Eu	ppm	1	0	1	0	1	1	0	1	0
Tb	ppm	0				0		0	0	0
Yb	ppm	0	0	0	0	0	0	0	1	0
Lu	ppm	0			0	0	0	0	0	0

No.		10	11	12	13	14	15	16	17	18
Sample ID		VUO 97/ 73.30	VUO 97/ 36.15	VUO 97/ 85.30	VUO 99/ 86.85	VUO 102/ 22.20	VUO 100/ 91.4O	VUO 100/ 69.35	VUO 101/ 25.90	VUO 101/ 19.3O
SiO2	wt%	51.51	49.99	48.90	50.75	43.62	45.87	49.81	51.06	48.14
Al2O3	wt%	23.40	21.74	14.37	17.94	17.59	15.93	18.84	18.34	14.38
FeOTOT	wt%	3.73	4.49	8.50	6.77	11.84	10.28	7.84	6.08	9.29
MgO	wt%	4.35	7.25	12.89	11.22	19.68	15.05	8.81	10.55	0.14
CaO	wt%	12.56	13.36	12.23	9.44	4.32	10.27	10.78	10.75	10.86
Na2O	wt%	3.61	2.43	1.89	2.66	1.86	1.61	2.89	2.44	1.24
K2O	wt%	0.37	0.18	0.33	0.73	0.44	0.40	0.54	0.29	0.84
TiO2	wt%	0.31	0.38	0.53	0.21	0.17	0.21	0.21	0.26	0.32
P2O5	wt%	0.03	0.03	0.03	0.01	0.01	0.01	0.01	0.01	0.01
MnO	wt%	0.05	0.07	0.15	0.13	0.24	0.16	0.11	0.10	0.15
Sum_ Oxides	wt%	99.92	99.92	99.82	99.86	99.77	99.79	99.84	99.88	85.37
V	ppm	69	72	142	62	45	50	62	72	98
Cr	ppm	292	319	623	305	180	265	105	279	371
Ni	ppm	422	148	414	188	648	440	886	206	859
Cu	ppm	477	47	181	53	204	16	762	51	324
Zn	ppm	12	32	89	43	57	74	44	34	47
S	ppm	4350	0	2740	0	1770	0	9720	10	2910
Nb	ppm	2	4	3	0	1	2	2	1	0
Rb	ppm	6	1	7	30	20	7	17	11	35
Sr	ppm	1184	902	417	517	38	206	817	1014	205
Zr	ppm	60	48	31	47	23	35	31	37	9
Y	ppm	5	5	9	1	1	2	2	2	2
Ba	ppm	367	72	111	204	128	106	187	184	357
Sc	ppm	15	17	32	16	9	13	11	19	22
La	ppm	3	3	3						
Ce	ppm	7	7	7						
Nd	ppm	4	4	4						
Sm	ppm	1	1	1						
Eu	ppm	1	1	1						
Tb	ppm	0	0	0						
Yb	ppm	0	0	0						
Lu	ppm	0	0	0						

No.		19	20	21	22	23	24	25	26	27
Sample ID		VUO 99/ 77.45	VUO 101/ 58.75	VUO 101/ 36.50	VUO 101/ 24.40	VUO 101/ 23.80	VUO 102/ 34.25	VUO 99/ 25.40	VUO 101/ 71.20	VUO 101/ 55.10
SiO2	wt%	52.84	49.79	50.13	50.02	49.27	48.73	51.53	51.26	51.25
Al2O3	wt%	16.44	17.55	16.30	18.12	17.30	7.42	18.30	19.07	15.00
FeOTOT	wt%	6.47	10.43	9.73	7.65	6.68	14.35	6.27	6.51	8.70
MgO	wt%	9.47	11.02	11.37	11.28	12.97	23.66	8.83	8.56	14.40
CaO	wt%	10.68	8.21	9.53	9.92	11.17	4.09	11.60	11.34	8.08
Na2O	wt%	3.08	2.20	2.17	2.10	1.47	0.78	2.68	2.46	1.78
K2O	wt%	0.41	0.17	0.13	0.36	0.63	0.17	0.22	0.21	0.10
TiO2	wt%	0.37	0.28	0.29	0.27	0.25	0.31	0.31	0.35	0.33
P2O5	wt%	0.01	0.01	0.01	0.01	0.01	0.01	0.01	0.01	0.01
MnO	wt%	0.10	0.13	0.13	0.11	0.11	0.21	0.11	0.11	0.16
Sum	wt%	99.87	99.79	99.79	99.84	99.86	99.73	99.86	99.88	99.81
V	ppm	117	72	83	64	77	70	92	94	90
Cr	ppm	296	350	369	280	259	827	417	415	509
Ni	ppm	313	1999	1926	847	230	2149	117	642	467
Cu	ppm	373	1600	2421	571	26	800	36	405	201
Zn	ppm	55	54	40	36	41	80	44	42	62
S	ppm	2390	21380	21010	7310	0	4570	0	5640	2600
Nb	ppm	2	0	2	1	2	2	1	1	1
Rb	ppm	20	6	6	15	29	10	5	6	5
Sr	ppm	633	556	690	757	490	50	687	682	456
Zr	ppm	55	20	8	34	23	13	44	22	42
Y	ppm	3	3	3	3	3	3	4	4	4
Ba	ppm	92	77	63	191	212	45	74	109	69
Sc	ppm	28	18	20	16	16	22	23	20	22

No.		28	29	30	31	32	33	34	35	36
Sample ID		VUO 101/ 42.40	VUO 101/ 26.20	VUO 101/ 20.40	VUO 101/ 13.30	VUO 99/ 87.65	VUO 101/ 71.20	43.1-VMN-92	VUO 100/ 70.75	VUO 99/ 30.25
SiO2	wt%	51.38	50.36	49.95	52.04	49.73	51.25	52.17	50.61	51.02
Al2O3	wt%	10.26	14.88	11.50	17.20	9.75	19.13	16.60	7.86	18.19
FeOTOT	wt%	10.32	7.88	9.82	6.01	11.13	6.51	7.62	11.69	7.18
MgO	wt%	18.78	14.13	17.25	10.42	18.76	8.56	9.31	18.24	9.52
CaO	wt%	7.30	10.12	9.21	10.74	8.76	11.29	11.04	9.65	10.03
Na2O	wt%	1.00	1.72	1.17	2.59	0.92	2.46	2.36	0.81	3.24
K2O	wt%	0.11	0.25	0.38	0.43	0.17	0.20	0.20	0.10	0.25
TiO2	wt%	0.41	0.34	0.33	0.33	0.37	0.35	0.37	0.53	0.30
P2O5	wt%	0.01	0.01	0.01	0.01	0.01	0.01	0.01	0.01	0.01
MnO	wt%	0.20	0.14	0.18	0.10	0.18	0.11	0.15	0.25	0.11
Sum	wt%	99.77	99.83	99.80	99.87	99.78	99.87	99.83	99.75	99.85
V	ppm	118	100	96	103	116	94	134	157	84
Cr	ppm	685	479	469	368	331	415	111	931	260
Ni	ppm	402	234	351	280	703	641	102	364	137
Cu	ppm	212	18	32	481	529	405	91	69	30
Zn	ppm	68	48	63	31	59	41	56	85	48
S	ppm	1150	0	0	3460	8280	5670	720	280	0
Nb	ppm	2	1	1	2	2	2	2	1	1
Rb	ppm	7	11	16	18	9	5	4	6	6
Sr	ppm	340	595	144	668	47	680	569	14	621
Zr	ppm	27	33	15	22	19	26	0	27	42
Y	ppm	4	4	4	4	5	5	5	6	6
Ba	ppm	51	111	111	97	35	115	84	9	96
Sc	ppm	28	26	25	23	29	22	27	36	18

No.		37	38	39	40	41	42	43	44	45
Sample ID		VUO 101/ 32.85	VUO 101/ 31.95	VUO 101/ 23.40	VUO 101/ 21.25	VUO 102/ 20.40	VUO 98/ 52.00	VUO 98/ 3.80	VUO 99/ 85.55	VUO 99/ 102.25
SiO2	wt%	49.21	51.26	51.10	48.46	51.69	51.51	52.23	51.94	55.22
Al2O3	wt%	11.88	7.30	16.70	11.79	19.74	11.22	15.89	6.72	22.79
FeOTOT	wt%	9.20	12.11	6.92	10.56	7.95	8.89	7.08	8.70	3.26
MgO	wt%	16.84	19.33	11.30	17.91	7.60	14.11	10.06	18.89	3.72
CaO	wt%	10.70	8.23	10.58	9.40	8.55	11.86	11.42	12.00	7.64
Na2O	wt%	1.27	0.78	2.55	0.89	3.57	1.33	2.33	0.64	5.63
K2O	wt%	0.22	0.08	0.19	0.26	0.47	0.21	0.28	0.08	1.36
TiO2	wt%	0.32	0.41	0.43	0.33	0.15	0.51	0.42	0.70	0.22
P2O5	wt%	0.01	0.01	0.01	0.01	0.01	0.01	0.01	0.01	0.02
MnO	wt%	0.15	0.24	0.09	0.18	0.09	0.17	0.14	0.16	0.05
Sum	wt%	99.80	99.75	99.87	99.79	99.82	99.82	99.86	99.84	99.91
V	ppm	104	122	111	107	42	158	121	219	56
Cr	ppm	475	517	393	428	35	602	299	813	76
Ni	ppm	383	899	231	789	1069	147	93	293	297
Cu	ppm	109	493	60	490	732	46	36	112	145
Zn	ppm	59	69	37	48	37	72	58	50	20
S	ppm	770	4680	210	2020	11930	50	0	300	0
Nb	ppm	1	2	2	2	2	1	1	2	1
Rb	ppm	8	6	7	13	27	6	7	6	72
Sr	ppm	113	42	661	80	1622	244	881	17	1361
Zr	ppm	10	9	37	15	33	26	25	30	38
Y	ppm	6	6	6	6	6	6	8	10	0
Ba	ppm	82	14	74	69	287	45	92	13	323
Sc	ppm	24	32	24	23	8	33	31	49	11

No.		46	47	48	49	50	51	52	53	54
Sample ID		VUO 99/ 98.0S	VUO 102/ 39.55	VUO 102/ 27.50	VUO 102/ 12.3O	36-VMN-92	VUO 99/ 94.60	VUO 99/ 87.85	VUO 102/ 97.65	VUO 102/ 50.80
SiO2	wt%	53.85	45.67	50.91	46.57	48.47	48.48	52.70	51.86	46.60
Al2O3	wt%	24.22	12.29	21.39	17.93	21.80	22.29	3.37	20.66	20.04
FeOTOT	wt%	3.23	12.92	5.47	9.31	7.05	7.64	16.30	5.20	9.56
MgO	wt%	3.92	20.60	8.32	13.66	9.11	8.14	24.62	7.47	10.56
CaO	wt%	8.62	6.06	9.99	9.59	10.18	9.70	1.57	9.99	10.13
Na2O	wt%	4.58	1.17	2.88	1.93	2.61	2.80	0.14	3.30	2.16
K2O	wt%	1.29	0.76	0.57	0.48	0.33	0.58	0.05	1.03	0.50
TiO2	wt%	0.25	0.13	0.25	0.19	0.17	0.11	0.57	0.30	0.14
P2O5	wt%	0.02	0.02	0.02	0.02	0.02	0.02	0.02	0.02	0.02
MnO	wt%	0.05	0.13	0.09	0.13	0.11	0.07	0.32	0.08	0.09
Sum	wt%	100.03	99.75	99.89	99.81	99.85	99.83	99.66	99.91	99.80
V	ppm	48	30	56	42	30	18	106	82	32
Cr	ppm	88	94	308	344	61	9	472	313	83
Ni	ppm	585	1160	439	1196	1100	1664	1745	385	1624
Cu	ppm	101	627	612	1273	757	1643	1290	328	1573
Zn	ppm	18	35	83	61	109	36	88	32	148
S	ppm	0	8460	3120	6100	7690	17510	9500	3070	17190
Nb	ppm	1	2	0	2	2	1	2	1	2
Rb	ppm	59	28	36	34	10	18	7	45	29
Sr	ppm	1212	107	834	741	818	1099	4	1006	635
Zr	ppm	40	8	23	8	45	8	27	39	2
Y	ppm	0	0	0	0	1	1	1	1	1
Ba	ppm	314	178	180	125	123	725	14	286	122
Sc	ppm	11	10	12	12	7	7	40	15	6

No.		55	56	57	58	59	60	61	62	63
Sample ID		VUO 102/ 42.00	VUO 102/ 30.90	VUO 102/ 26.40	VUO 102/ 23.50	VUO 102/ 14.70	VUO 102/ 8.65	VUO 98/ 64.20	VUO 100/ 93.80	VUO 99/ 85.55
SiO2	wt%	46.70	44.53	48.44	48.02	45.60	46.08	53.05	48.73	49.86
Al2O3	wt%	21.23	14.46	10.42	24.42	6.85	17.23	19.07	16.84	18.28
FeOTOT	wt%	8.52	11.68	12.73	6.20	16.09	9.50	8.22	8.92	7.20
MgO	wt%	10.35	20.71	23.84	5.67	29.36	13.18	7.66	11.30	10.04
CaO	wt%	9.96	5.64	2.81	12.07	1.30	11.19	7.75	10.42	11.41
Na2O	wt%	2.47	1.82	0.91	3.03	0.05	1.93	3.56	2.39	2.45
K2O	wt%	0.39	0.50	0.14	0.27	0.01	0.32	0.16	0.86	0.26
TiO2	wt%	0.09	0.22	0.22	0.13	0.22	0.22	0.16	0.22	0.22
P2O5	wt%	0.02	0.02	0.02	0.02	0.02	0.02	0.02	0.02	0.02
MnO	wt%	0.10	0.20	0.23	0.06	0.18	0.13	0.17	0.14	0.11
Sum	wt%	99.83	99.78	99.76	99.89	99.68	99.80	99.82	99.84	99.85
V	ppm	14	50	53	20	53	54	91	70	55
Cr	ppm	8	135	518	64	558	432	390	73	115
Ni	ppm	837	861	1395	1621	1395	884	508	320	663
Cu	ppm	667	602	797	1478	836	756	424	28	373
Zn	ppm	78	91	53	12	91	55	88	55	38
S	ppm	7490	4570	6140	16490	7270	5540	11380	150	7300
Nb	ppm	1	2	2	2	1	1	1	1	2
Rb	ppm	11	20	9	12	6	18	3	20	9
Sr	ppm	801	117	31	1552	5	523	702	474	710
Zr	ppm	5	32	11	27	22	11	15	23	31
Y	ppm	1	1	1	1	1	1	1	2	2
Ba	ppm	164	190	36	172	10	136	194	353	78
Sc	ppm	6	15	15	6	16	15	19	12	15

No.		64	65	66	67	68	69	70	71	72
Sample ID		VUO 101/ 86.40	VUO 101/ 84.85	VUO 101/ 29.30	VUO 102/ 91.45	VUO 102/ 57.50	VUO 102/ 49.35	VUO 102/ 46.20	VUO 102/ 37.95	VUO 102/ 26.70
SiO2	wt%	51.19	51.24	51.52	50.51	49.51	48.49	46.92	50.15	44.42
Al2O3	wt%	18.68	22.90	19.64	16.57	22.29	22.66	20.65	17.46	17.38
FeOTOT	wt%	7.15	4.68	5.91	7.44	6.75	6.90	9.31	8.24	10.30
MgO	wt%	11.46	5.66	10.07	9.68	6.39	6.84	9.88	12.82	13.70
CaO	wt%	8.30	11.47	9.67	11.99	11.64	11.69	10.02	8.55	11.62
Na2O	wt%	2.32	3.35	2.49	2.75	2.65	2.64	2.46	2.01	1.82
K2O	wt%	0.37	0.29	0.18	0.38	0.32	0.33	0.33	0.16	0.22
TiO2	wt%	0.23	0.21	0.26	0.39	0.22	0.21	0.13	0.29	0.17
P2O5	wt%	0.02	0.02	0.02	0.02	0.02	0.02	0.02	0.02	0.02
MnO	wt%	0.12	0.07	0.12	0.12	0.07	0.07	0.10	0.13	0.13
Sum	wt%	99.84	99.89	99.88	99.85	99.86	99.85	99.82	99.83	99.78
V	ppm	59	51	57	110	58	48	32	69	38
Cr	ppm	352	135	237	534	244	155	151	512	184
Ni	ppm	157	429	246	213	1540	1679	2125	828	1112
Cu	ppm	27	300	136	126	1329	1542	1803	687	675
Zn	ppm	67	33	41	69	34	56	75	56	30
S	ppm	30	4650	1480	0	17100	18060	20960	6420	6670
Nb	ppm	1	2	2	1	1	2	1	2	2
Rb	ppm	9	7	7	17	11	13	16	8	7
Sr	ppm	672	959	1158	715	814	884	758	638	304
Zr	ppm	27	49	24	28	36	32	0	33	26
Y	ppm	2	2	2	2	2	2	2	2	2
Ba	ppm	134	189	107	203	140	152	136	66	68
Sc	ppm	16	13	12	23	11	9	4	15	10

No.		73	74	75	76	77	78	79	80	81
Sample ID		VUO 102/ 24.90	VUO 102/ 18.75	VUO 98/ 37.20	VUO 97/ 63.80	VUO 97/ 57.60	VUO 97/ 54.35	VUO 97/ 17.80	VUO 100/ 100.2	VUO 100/ 98.70
SiO2	wt%	51.11	43.52	46.14	44.89	51.88	47.97	51.22	52.35	51.03
Al2O3	wt%	23.25	16.44	9.93	17.14	21.16	19.94	25.07	19.20	22.76
FeOTOT	wt%	4.34	11.52	14.93	9.38	3.69	5.95	4.30	6.12	4.82
MgO	wt%	6.17	13.86	22.03	14.69	5.25	10.50	2.34	7.67	6.03
CaO	wt%	11.24	11.95	5.25	11.58	13.55	13.20	12.00	10.24	11.19
Na2O	wt%	3.22	1.96	0.90	1.37	2.71	1.38	4.07	3.65	3.54
K2O	wt%	0.25	0.22	0.09	0.43	1.34	0.66	0.66	0.25	0.28
TiO2	wt%	0.23	0.14	0.17	0.19	0.27	0.17	0.18	0.30	0.17
P2O5	wt%	0.02	0.02	0.02	0.02	0.02	0.02	0.02	0.02	0.02
MnO	wt%	0.06	0.15	0.25	0.13	0.06	0.09	0.03	0.08	0.07
Sum	wt%	99.89	99.78	99.71	99.82	99.93	99.88	99.89	99.88	99.91
V	ppm	48	31	40	36	78	42	58	70	42
Cr	ppm	268	160	166	3	298	146	39	88	69
Ni	ppm	282	945	1082	400	125	296	919	479	305
Cu	ppm	369	428	646	27	150	195	1454	205	59
Zn	ppm	16	57	320	52	18	39	26	37	31
S	ppm	1750	4320	5730	0	910	1580	4200	5820	1310
Nb	ppm	1	1	2	2	1	0	1	2	1
Rb	ppm	13	7	7	11	40	19	22	5	6
Sr	ppm	1182	101	126	337	915	606	1316	1127	1458
Zr	ppm	41	28	19	45	46	50	21	40	19
Y	ppm	2	2	2	2	2	2	2	3	3
Ba	ppm	103	30	18	85	437	218	184	97	169
Sc	ppm	11	10	12	8	17	10	8	11	10

No.		82	83	84	85	86	87	88	89	90
Sample ID		VUO 100/ 72.55	VUO 100/ 70.50	VUO 99/ 92.55	VUO 99/ 90.80	VUO 99/ 90.20	VUO 99/ 89.70	VUO 99/ 12.20	VUO 101/ 97.10	VUO 101/ 87.50
SiO2	wt%	49.73	51.92	48.48	47.18	46.67	50.14	52.55	51.36	51.83
Al2O3	wt%	17.82	21.17	10.59	12.26	14.81	12.85	19.15	16.26	18.30
FeOTOT	wt%	7.74	4.69	9.55	10.35	10.23	9.28	5.29	7.29	6.67
MgO	wt%	10.85	7.08	17.47	16.85	15.12	15.85	6.85	12.04	9.62
CaO	wt%	10.18	10.86	12.05	11.37	10.83	9.61	11.45	10.09	10.23
Na2O	wt%	2.59	3.52	1.22	1.23	1.44	1.45	3.40	2.18	2.48
K2O	wt%	0.55	0.35	0.14	0.13	0.30	0.16	0.69	0.18	0.26
TiO2	wt%	0.25	0.22	0.15	0.22	0.21	0.30	0.38	0.31	0.33
P2O5	wt%	0.02	0.02	0.02	0.02	0.02	0.02	0.02	0.02	0.02
MnO	wt%	0.12	0.08	0.14	0.18	0.16	0.16	0.10	0.13	0.12
Sum	wt%	99.85	99.91	99.81	99.79	99.79	99.82	99.88	99.86	99.86
V	ppm	69	58	50	70	60	89	93	90	90
Cr	ppm	256	239	205	221	156	333	331	428	291
Ni	ppm	430	146	944	410	669	320	102	288	154
Cu	ppm	225	50	396	57	442	127	43	134	53
Zn	ppm	57	37	61	60	67	64	36	51	54
S	ppm	2050	20	1310	0	5110	580	0	910	280
Nb	ppm	1	0	2	1	2	1	1	1	3
Rb	ppm	14	5	7	6	11	8	28	-6	8
Sr	ppm	650	1063	47	40	267	310	802	558	656
Zr	ppm	39	48	24	12	27	16	54	43	24
Y	ppm	3	3	3	3	3	3	3	3	3
Ba	ppm	200	149	21	26	110	49	157	68	138
Sc	ppm	17	12	16	20	18	25	19	22	22

No.		91	92	93	94	95	96	97	98	99
Sample ID		VUO 101/ 78.10	VUO 101/ 64.80	VUO 101/ 26.90	VUO 102/ 95.75	VUO 102/ 93.05	VUO 102/ 89.75	VUO 102/ 59.50	VUO 102/ 33.45	VUO 102/ 32.75
SiO2	wt%	50.31	51.67	47.23	50.76	51.01	51.52	51.33	50.65	46.69
Al2O3	wt%	13.21	18.54	13.00	15.06	16.81	20.26	22.90	19.06	11.10
FeOTOT	wt%	9.72	6.66	9.79	8.22	6.86	6.35	4.44	6.86	12.84
MgO	wt%	16.78	10.59	17.01	12.60	11.14	7.60	5.89	9.43	20.49
CaO	wt%	7.81	9.10	10.77	10.01	10.86	10.73	11.60	10.61	6.78
Na2O	wt%	1.22	2.66	1.30	2.21	2.29	2.74	3.54	2.39	1.24
K2O	wt%	0.24	0.19	0.25	0.46	0.40	0.28	0.27	0.41	0.19
TiO2	wt%	0.31	0.31	0.29	0.35	0.37	0.28	0.27	0.32	0.24
P2O5	wt%	0.02	0.02	0.02	0.02	0.02	0.02	0.02	0.02	0.02
MnO	wt%	0.19	0.12	0.16	0.13	0.11	0.10	0.08	0.11	0.16
Sum	wt%	99.81	99.86	99.82	99.82	99.87	99.88	100.34	99.86	99.75
V	ppm	83	78	84	97	95	76	53	79	54
Cr	ppm	475	370	320	514	478	323	245	574	154
Ni	ppm	369	182	310	886	339	494	163	1030	1328
Cu	ppm	112	67	49	666	461	502	74	943	727
Zn	ppm	73	51	49	49	48	45	45	39	135
S	ppm	410	250	190	5140	1180	5410	390	9470	9060
Nb	ppm	2	1	2	1	2	2	1	2	2
Rb	ppm	9	5	9	18	16	8	8	26	9
Sr	ppm	333	772	40	497	530	772	868	705	98
Zr	ppm	20	42	17	28	42	42	34	33	4
Y	ppm	3	3	3	3	3	3	3	3	3
Ba	ppm	65	142	71	124	199	132	108	154	54
Sc	ppm	23	19	21	22	19	18	9	17	13

No.		100	101	102	103	104	105	106	107	108
Sample ID		VUO 102/ 13.05	VUO 98/ 34.80	VUO 98/ 31.30	VUO 98/ 10.20	VUO 98/ 7.50	42-VW-92	VUO 97/ 23.40	VUO 100/ 101.0	VUO 100/ 95.10
SiO2	wt%	43.43	45.17	42.23	51.62	52.87	52.59	47.12	48.34	50.30
Al2O3	wt%	15.89	12.19	16.33	21.80	24.29	22.21	16.92	19.21	18.01
FeOTOT	wt%	11.67	13.59	12.80	4.91	3.19	4.77	7.72	7.68	7.85
MgO	wt%	15.04	19.89	14.19	6.43	3.72	4.47	12.79	9.53	10.33
CaO	wt%	11.42	7.03	11.52	11.12	11.59	11.95	13.38	11.80	10.02
Na2O	wt%	1.78	1.31	2.03	3.23	3.53	3.34	1.30	2.59	2.64
K2O	wt%	0.23	0.14	0.26	0.39	0.33	0.24	0.34	0.26	0.20
TiO2	wt%	0.17	0.18	0.19	0.29	0.33	0.25	0.14	0.31	0.32
P2O5	wt%	0.02	0.02	0.02	0.02	0.02	0.02	0.02	0.02	0.02
MnO	wt%	0.13	0.22	0.18	0.09	0.06	0.05	0.13	0.11	0.14
Sum	wt%	99.78	99.74	99.75	99.90	99.93	99.89	99.86	99.85	99.83
V	ppm	45	46	42	56	57	69	38	76	95
Cr	ppm	181	208	152	161	135	54	29	611	352
Ni	ppm	1799	864	755	82	56	268	586	284	205
Cu	ppm	1074	406	547	49	109	548	124	18	21
Zn	ppm	76	304	275	34	28	13	63	51	61
S	ppm	9140	3850	4650	0	820	5550	740	0	0
Nb	ppm	2	1	2	2	1	1	2	1	1
Rb	ppm	9	6	6	14	9	3	7	4	5
Sr	ppm	95	191	349	980	1144	930	389	1041	786
Zr	ppm	15	29	11	27	39	24	25	30	23
Y	ppm	3	3	3	3	3	3	3	4	4
Ba	ppm	41	26	56	145	166	123	99	159	86
Sc	ppm	7	16	14	13	13	14	8	16	19

No.		109	110	111	112	113	114	115	116	117
Sample ID		VUO 100/ 83.30	VUO 100/ 74.00	VUO 99/ 76.45	VUO 99/ 8.50	VUO 101/ 83.00	VUO 101/ 75.75	VUO 101/ 48.30	VUO 102/ 91.20	VUO 102/ 83.50
SiO2	wt%	49.87	52.26	54.86	51.78	51.10	50.13	49.21	51.47	51.41
Al2O3	wt%	18.30	4.17	13.05	18.38	18.74	13.10	11.52	20.34	18.91
FeOTOT	wt%	7.25	15.69	8.99	6.00	7.37	9.41	10.95	5.63	6.76
MgO	wt%	9.91	20.16	9.27	8.51	8.97	15.34	19.32	5.81	10.77
CaO	wt%	11.19	5.83	8.78	11.99	10.37	9.72	6.87	12.89	9.07
Na2O	wt%	2.74	0.43	3.66	2.54	2.70	1.41	1.29	2.90	2.31
K2O	wt%	0.18	0.05	0.71	0.16	0.19	0.14	0.09	0.40	0.18
TiO2	wt%	0.29	0.70	0.37	0.38	0.26	0.38	0.32	0.36	0.31
P2O5	wt%	0.02	0.02	0.02	0.02	0.02	0.02	0.02	0.02	0.02
MnO	wt%	0.11	0.36	0.12	0.11	0.12	0.15	0.19	0.08	0.12
Sum	wt%	99.86	99.67	99.83	99.87	99.84	99.80	99.78	99.90	99.86
V	ppm	75	104	119	108	60	104	87	100	77
Cr	ppm	233	323	276	456	219	505	519	267	414
Ni	ppm	170	485	157	131	253	758	414	662	268
Cu	ppm	28	204	688	80	61	580	85	767	134
Zn	ppm	48	109	111	45	57	54	77	32	51
S	ppm	0	1810	280	310	380	2920	190	8130	820
Nb	ppm	1	1	0	2	3	2	1	2	2
Rb	ppm	2	6	29	2	5	6	6	12	3
Sr	ppm	770	10	354	681	808	349	312	758	566
Zr	ppm	31	26	30	56	37	31	16	28	32
Y	ppm	4	4	4	4	4	4	4	4	4
Ba	ppm	52	1	214	84	107	77	42	150	91
Sc	ppm	14	32	28	22	13	28	26	22	17

No.		118	119	120	121	122	123	124	125	126
Sample ID		VUO 102/ 73.50	VUO 102/ 66.9O	VUO 102/ 64.65	VUO 102/ 25.90	VUO 97/ 115.70	VUO 99/ 84.75	VUO 99/ 20.90	VUO 99/ 5.40	35.1-VMN-92
SiO2	wt%	50.90	51.46	50.98	48.92	51.28	50.47	51.42	51.61	51.39
Al2O3	wt%	16.39	18.38	18.50	18.60	21.71	9.81	12.99	17.10	14.77
FeOTOT	wt%	7.74	6.54	7.22	8.68	4.50	10.85	8.90	6.64	7.00
MgO	wt%	11.63	10.47	10.41	9.90	6.63	17.53	13.28	9.68	11.88
CaO	wt%	10.69	10.23	9.93	10.65	11.60	9.38	10.50	11.81	12.18
Na2O	wt%	1.84	2.21	2.19	2.34	3.55	1.04	1.59	2.31	1.80
K2O	wt%	0.15	0.15	0.18	0.28	0.27	0.13	0.51	0.20	0.28
TiO2	wt%	0.36	0.32	0.31	0.33	0.27	0.34	0.44	0.36	0.40
P2O5	wt%	0.02	0.02	0.02	0.02	0.02	0.02	0.02	0.02	0.02
MnO	wt%	0.13	0.11	0.11	0.11	0.08	0.23	0.18	0.12	0.14
Sum	wt%	99.85	99.89	99.85	99.83	99.91	99.80	99.83	99.85	99.86
V	ppm	100	88	83	99	65	108	130	108	125
Cr	ppm	715	581	557	648	185	442	682	549	539
Ni	ppm	805	361	772	1752	114	369	167	168	169
Cu	ppm	679	245	679	1666	53	53	41	97	84
Zn	ppm	51	48	47	25	116	66	61	51	62
S	ppm	6990	2040	7540	15670	170	800	0	120	470
Nb	ppm	2	1	3	1	1	1	2	2	2
Rb	ppm	5	5	5	17	5	5	14	3	9
Sr	ppm	500	583	578	662	797	82	355	608	485
Zr	ppm	32	23	13	38	42	36	42	20	34
Y	ppm	4	4	4	4	4	5	5	5	5
Ba	ppm	75	82	80	124	144	24	272	95	125
Sc	ppm	24	18	18	21	13	28	28	24	28

No.		127	128	129	130	131	132	133	134	135
Sample ID		VUO 102/ 89.45	VUO 102/ 77.20	VUO 98/ 56.90	VUO 98/ 52.55	VUO 98/ 49.85	VUO 98/ 38.40	41-VMN-92	VUO 97/ 64.70	VUO 97/ 62.80
SiO2	wt%	51.31	51.08	52.51	52.53	52.31	47.79	52.62	51.44	51.81
Al2O3	wt%	17.68	12.23	16.33	20.24	19.38	8.32	19.91	17.98	20.62
FeOTOT	wt%	6.76	10.98	7.03	5.00	6.05	13.65	5.17	6.48	4.05
MgO	wt%	9.71	15.01	9.76	6.67	8.13	21.76	6.51	7.96	6.74
CaO	wt%	11.52	8.07	11.10	11.80	10.53	6.65	11.46	12.48	13.12
Na2O	wt%	2.20	1.50	2.41	2.76	2.69	0.82	3.48	2.57	2.95
K2O	wt%	0.16	0.14	0.18	0.20	0.31	0.10	0.28	0.38	0.19
TiO2	wt%	0.39	0.55	0.41	0.61	0.35	0.37	0.37	0.48	0.35
P2O5	wt%	0.02	0.02	0.02	0.02	0.02	0.02	0.02	0.02	0.02
MnO	wt%	0.12	0.19	0.13	0.08	0.12	0.25	0.08	0.08	0.06
Sum	wt%	99.87	99.77	99.88	99.91	99.89	99.73	99.90	99.87	99.91
V	ppm	110	129	113	96	81	91	99	135	101
Cr	ppm	536	555	232	257	189	342	155	718	396
Ni	ppm	312	927	108	78	122	804	60	408	98
Cu	ppm	274	687	42	36	102	642	30	361	73
Zn	ppm	49	91	46	43	56	57	27	26	26
S	ppm	550	8320	40	0	590	3120	90	3920	450
Nb	ppm	0	2	1	2	2	2	1	1	2
Rb	ppm	4	7	5	5	5	6	4	10	4
Sr	ppm	568	333	547	821	731	130	793	691	813
Zr	ppm	23	13	15	46	38	0	36	59	54
Y	ppm	5	5	5	5	5	5	5	5	5
Ba	ppm	97	69	68	97	160	24	136	130	90
Sc	ppm	24	28	22	20	19	27	25	27	22

No.		136	137	138	139	140	141	142	143	144
Sample ID		VUO 97/ 51.30	124-VMN-92	40-VMN-92	VUO 98/ 59.75	VUO 97/ 102.50	49.1-VMN-92	37-VMN-92	VUO 98/ 45.65	VUO 98/ 24.60
SiO2	wt%	50.82	51.60	52.01	52.58	50.21	51.68	51.71	50.99	52.41
Al2O3	wt%	19.54	15.24	17.27	17.88	19.05	15.57	17.29	14.23	15.98
FeOTOT	wt%	4.72	7.00	6.91	6.52	6.03	6.27	5.75	9.06	6.44
MgO	wt%	7.92	11.48	8.98	8.32	9.00	10.08	9.56	11.32	9.46
CaO	wt%	13.45	11.66	11.42	11.01	11.79	13.27	12.79	11.54	12.65
Na2O	wt%	2.73	2.06	2.47	2.72	2.76	2.13	2.06	1.85	1.62
K2O	wt%	0.21	0.22	0.25	0.31	0.54	0.19	0.17	0.18	0.60
TiO2	wt%	0.40	0.44	0.41	0.38	0.38	0.55	0.43	0.49	0.58
P2O5	wt%	0.02	0.02	0.02	0.02	0.02	0.02	0.02	0.02	0.02
MnO	wt%	0.08	0.14	0.13	0.13	0.10	0.12	0.11	0.15	0.12
Sum	wt%	99.89	99.86	99.87	99.87	99.88	99.88	99.89	99.83	99.88
V	ppm	105	131	111	131	100	163	121	140	120
Cr	ppm	517	589	208	424	309	942	720	354	409
Ni	ppm	129	139	115	105	318	125	127	768	108
Cu	ppm	42	50	109	31	163	37	21	956	54
Zn	ppm	31	53	39	55	96	48	57	62	44
S	ppm	80	140	170	10	1950	30	0	8100	850
Nb	ppm	1	1	1	1	1	2		2	2
Rb	ppm	3	5	5	7	12	4	4	6	13
Sr	ppm	722	481	581	649	604	496	610	449	308
Zr	ppm	54	43	27	24	54	33	19	23	31
Y	ppm	5	6	6	6	6	7	7	7	7
Ba	ppm	104	84	77	183	192	91	60	102	195
Sc	ppm	24	27	28	30	22	32	28	32	25

No.		145	146	147	148	149	150	151	152	153
Sample ID		VUO 98/ 20.60	VUO 98/ 18.00	VUO 97/ 12.20	VUO 100/ 100.8	VUO 100/ 87.75	VUO 98/ 2.00	43.2-VMN-92	VUO 98/ 6.20	VUO 98/ 40.40
SiO2	wt%	51.71	50.62	51.53	48.86	49.10	52.69	52.66	51.57	51.52
Al2O3	wt%	18.71	10.52	20.08	9.89	11.49	19.30	16.61	11.55	6.90
FeOTOT	wt%	5.47	9.56	5.85	10.61	10.24	5.67	7.92	9.43	11.91
MgO	wt%	8.01	14.62	6.17	16.86	14.65	6.87	8.83	13.23	18.06
CaO	wt%	12.74	12.15	12.05	11.38	11.79	11.82	10.46	11.53	9.55
Na2O	wt%	2.37	1.36	3.26	1.12	1.59	2.64	2.55	1.46	0.84
K2O	wt%	0.37	0.26	0.43	0.12	0.21	0.21	0.23	0.22	0.10
TiO2	wt%	0.40	0.51	0.42	0.74	0.55	0.56	0.40	0.62	0.64
P2O5	wt%	0.02	0.02	0.02	0.02	0.02	0.02	0.02	0.02	0.02
MnO	wt%	0.11	0.19	0.07	0.19	0.14	0.10	0.14	0.19	0.22
Sum	wt%	99.91	99.81	99.88	99.79	99.78	99.88	99.82	99.82	99.76
V	ppm	101	137	125	167	164	103	142	156	170
Cr	ppm	389	495	568	1976	496	205	99	341	649
Ni	ppm	131	232	109	336	239	93	74	124	530
Cu	ppm	97	101	25	18	25	45	97	68	775
Zn	ppm	54	75	27	77	71	48	55	83	58
S	ppm	0	120	0	0	0	80	20	230	2990
Nb	ppm	2	1	2	1	1	2	3	2	2
Rb	ppm	10	7	5	6	5	2	5	8	7
Sr	ppm	725	233	854	31	123	750	570	369	140
Zr	ppm	61	66	38	41	35	40	28	16	15
Y	ppm	7	7	7	8	8	8	8	9	10
Ba	ppm	185	68	112	13	43	98	86	84	35
Sc	ppm	22	36	23	45	42	23	20	34	47

No.		154	155	156	157	158	159	160	161	162
Sample ID		VUO 98/ 29.35	VUO 98/ 4.3o	VUO 98/ 3.50	VUO 98/ 6.90	44-VMN-92	VUO 97/ 90.40	VUO 99/ 82.15	VUO 98/ 84.20	VUO 97/ 93.40
SiO2	wt%	50.92	50.99	51.12	51.25	51.72	50.65	50.38	53.24	51.48
Al2O3	wt%	9.96	9.83	9.41	6.98	17.24	7.17	20.92	21.19	24.53
FeOTOT	wt%	9.13	10.01	10.51	11.87	7.83	9.19	7.25	6.44	4.66
MgO	wt%	14.00	14.81	14.80	16.14	8.10	17.39	7.57	6.40	3.19
CaO	wt%	13.87	11.90	11.64	11.67	11.52	13.30	9.92	8.21	10.68
Na2O	wt%	0.93	1.18	1.15	0.76	2.52	0.82	3.13	3.78	4.29
K2O	wt%	0.18	0.19	0.23	0.15	0.36	0.28	0.37	0.18	0.78
TiO2	wt%	0.62	0.66	0.68	0.68	0.41	0.82	0.20	0.24	0.22
P2O5	wt%	0.02	0.02	0.02	0.02	0.02	0.02	0.03	0.03	0.03
MnO	wt%	0.17	0.21	0.22	0.23	0.13	0.17	0.08	0.15	0.04
Sum	wt%	99.80	99.80	99.78	99.75	99.85	99.81	99.85	99.86	99.90
V	ppm	158	153	183	199	156	260	46	165	45
Cr	ppm	647	403	428	416	512	1288	87	339	112
Ni	ppm	188	117	149	417	84	294	1496	121	1627
Cu	ppm	64	12	32	437	29	92	987	65	1598
Zn	ppm	61	73	78	87	45	119	29	69	33
S	ppm	740	0	0	4310	0	250	18700	1060	19520
Nb	ppm	1	2	1	1	3	2	1	0	2
Rb	ppm	7	7	6	7	9	7	14	4	23
Sr	ppm	109	243	200	89	601	27	880	754	1382
Zr	ppm	38	28	32	34	19	51	32	28	34
Y	ppm	10	10	10	11	12	13	1	2	2
Ba	ppm	71	38	58	57	107	41	146	190	302
Sc	ppm	45	36	44	46	30	62	12	21	7

No.		163	164	165	166	167	168	169	170	171
Sample ID		VUO 97/ 79.70	VUO 97/ 25.50	VUO 97/ 2.40	45.1-VMN-92	VUO 101/ 17.70	VUO 97/ 103.80	VUO 97/ 41.65	VUO 97/ 31.30	VUO 97/ 29.50
SiO2	wt%	50.24	47.28	52.59	51.33	49.52	50.11	48.74	49.98	51.29
Al2O3	wt%	22.06	20.62	26.27	26.79	9.55	20.20	20.27	21.97	24.25
FeOTOT	wt%	5.28	8.48	2.20	2.75	12.03	5.83	5.89	5.63	3.59
MgO	wt%	c	8.35	1.68	2.64	17.98	7.65	9.39	6.18	4.15
CaO	wt%	9.07	11.87	11.93	12.07	8.91	12.06	12.68	12.88	12.48
Na2O	wt%	3.62	2.42	4.50	3.81	0.93	2.86	2.00	2.72	3.57
K2O	wt%	0.96	0.38	0.54	0.32	0.18	0.76	0.57	0.22	0.28
TiO2	wt%	0.20	0.32	0.20	0.18	0.43	0.29	0.22	0.21	0.25
P2O5	wt%	0.03	0.03	0.03	0.03	0.03	0.03	0.03	0.03	0.03
MnO	wt%	0.09	0.09	0.03	0.03	0.20	0.09	0.10	0.08	0.05
Sum	wt%	99.90	99.84	99.97	99.95	99.76	99.88	99.89	99.90	99.94
V	ppm	48	44	44	39	136	70	53	61	57
Cr	ppm	88	159	3	13	403	181	153	191	291
Ni	ppm	163	2349	29	842	1098	617	245	204	74
Cu	ppm	92	2187	19	838	522	586	16	35	37
Zn	ppm	64	37	0	1	51	68	31	27	28
S	ppm	350	20880	0	9120	17480	6100	0	50	0
Nb	ppm	1	5	3	2	2	2	2	1	1
Rb	ppm	30	11	13	8	10	17	19	1	4
Sr	ppm	1363	749	1414	1467	90	756	764	901	1195
Zr	ppm	58	37	44	40	8	52	38	33	33
Y	ppm	3	3	3	3	4	4	4	4	4
Ba	ppm	537	323	250	186	53	306	460	86	139
Sc	ppm	11	8	7	4	31	13	12	12	11

No.		172	173	174	175	176	177	178	179	180
Sample ID		VUO 97/ 28.95	VUO 97/ 10.50	VUO 99/ 13.60	VUO 97/ 44.80	VUO 97/ 28.30	VUO 100/ 58.80	35.2-VMN-92	VUO 97/ 77.80	VUO 97/ 68.00
SiO2	wt%	50.48	45.73	52.15	50.89	51.30	51.16	51.59	50.78	48.33
Al2O3	wt%	23.24	22.52	20.33	23.21	23.68	6.43	16.57	22.01	10.68
FeOTOT	wt%	3.67	6.37	4.97	3.60	3.58	10.73	6.31	4.95	10.64
MgO	wt%	6.06	4.12	6.24	5.97	4.99	17.62	10.13	4.67	15.35
CaO	wt%	13.30	19.20	12.44	12.72	12.54	11.88	12.44	12.35	12.54
Na2O	wt%	2.68	1.26	2.92	2.97	3.26	0.68	2.06	3.89	1.27
K2O	wt%	0.19	0.32	0.27	0.15	0.24	0.11	0.18	0.80	0.32
TiO2	wt%	0.23	0.25	0.46	0.32	0.28	0.94	0.45	0.33	0.45
P2O5	wt%	0.03	0.03	0.03	0.03	0.03	0.03	0.03	0.03	0.03
MnO	wt%	0.06	0.09	0.09	0.06	0.05	0.21	0.13	0.07	0.18
Sum	wt%	99.94	99.89	99.90	99.92	99.95	99.79	99.89	99.88	99.79
V	ppm	56	77	104	69	62	206	128	76	134
Cr	ppm	308	335	271	404	380	1464	500	295	801
Ni	ppm	144	642	76	215	639	774	145	446	763
Cu	ppm	124	496	38	120	714	737	85	439	403
Zn	ppm	21	36	45	18	15	71	48	38	51
S	ppm	0	7860	0	930	5330	5470	170	6640	3560
Nb	ppm	3	2	2	2	3	1	3	5	3
Rb	ppm	3	7	9	1	5	5	5	20	7
Sr	ppm	1074	1132	786	1167	1203	18	523	1801	72
Zr	ppm	25	16	51	52	34	47	20	45	28
Y	ppm	4	4	5	5	5	6	6	6	7
Ba	ppm	73	61	233	116	98	24	97	515	39
Sc	ppm	15	20	22	16	14	61	28	14	28

No.		181	182	183	184	185	186	187	188	189
Sample ID		48.1-VMN-92	VUO 102/ 75.90	VUO 98/ 16.10	VUO 97/ 21.40	VUO 97/ 108.80	48.3-VMN-92	48.2-VMN-92	VUO 97/ 13.85	VUO 100/ 92.85
SiO2	wt%	51,72	50,99	51,10	50,51	51,91	51,84	51,86	53,80	52,18
Al2O3	wt%	11,78	13,76	9,12	24,77	23,01	19,98	20,71	25,61	3,82
FeOTOT	wt%	7,63	8,51	11,30	5,03	3,77	5,56	4,97	2,23	17,00
MgO	wt%	12,57	8,97	14,44	3,12	4,86	6,88	6,30	0,84	21,39
CaO	wt%	13,75	14,47	11,26	12,03	11,76	11,73	12,07	11,58	3,81
Na2O	wt%	1,30	2,08	1,48	3,77	3,64	3,03	3,10	5,36	0,41
K2O	wt%	0,30	0,21	0,31	0,27	0,52	0,32	0,26	0,35	0,04
TiO2	wt%	0,61	0,67	0,55	0,32	0,32	0,40	0,49	0,12	0,58
P2O5	wt%	0,03	0,03	0,03	0,04	0,04	0,04	0,04	0,04	0,04
MnO	wt%	0,15	0,15	0,19	0,03	0,07	0,10	0,09	0,02	0,38
Sum	wt%	99,84	99,84	99,78	99,89	99,90	99,88	99,89	99,95	99,65
V	ppm	190	196	172	53	60	88	93	38	168
Cr	ppm	1046	319	475	217	122	330	357	7	288
Ni	ppm	177	830	545	2063	136	89	77	0	653
Cu	ppm	63	1803	589	1911	101	13	16	11	270
Zn	ppm	77	54	69	11	33	48	46	0	110
S	ppm	100	9710	3760	21190	1060	0	0	0	5670
Nb	ppm	2	2	2	3	4	5	4	3	2
Rb	ppm	9	6	10	6	9	6	4	7	6
Sr	ppm	315	445	145	1260	974	825	853	520	9
Zr	ppm	27	13	24	60	66	48	33	42	36
Y	ppm	8	9	12	3	4	5	6	6	7
Ba	ppm	198	131	33	116	293	133	125	141	0
Sc	ppm	39	39	44	11	10	19	19	5	50

No.			190	191	192	193	194	195	196	197
Sample ID			38-VMN-92	VUO 97/ 96.96	VUO 97/ 13.50	VUO 98 /55.00	VUO 97/ 15.00	VUO 99/ 13.85	VUO 97/ 88.80	49.2-VMN-92
SiO2	wt%		53,20	49,64	51,99	52,74	52,13	51,87	50,80	50,26
Al2O3	wt%		14,55	17,67	21,67	8,83	5,55	5,19	9,69	10,92
FeOTOT	wt%		9,04	6,45	4,67	9,99	11,04	11,18	8,73	7,73
MgO	wt%		9,17	10,07	5,36	14,68	15,12	16,53	13,09	11,57
CaO	wt%		10,45	13,28	11,75	11,41	13,32	12,68	14,75	14,33
Na2O	wt%		2,11	1,89	3,55	0,97	0,91	0,44	1,32	1,30
K2O	wt%		0,37	0,25	0,44	0,15	0,26	0,13	0,34	0,22
TiO2	wt%		0,74	0,45	0,36	0,79	1,20	1,46	0,87	3,09
P2O5	wt%		0,04	0,05	0,05	0,05	0,05	0,07	0,08	0,28
MnO	wt%		0,14	0,12	0,05	0,20	0,17	0,21	0,16	0,14
Sum	wt%		99,81	99,87	99,89	99,81	99,75	99,76	99,83	99,84
V	ppm		157	115	87	200	307	322	233	301
Cr	ppm		185	353	253	417	121	856	806	738
Ni	ppm		125	276	66	254	208	208	531	142
Cu	ppm		132	122	11	168	97	103	585	300
Zn	ppm		67	82	25	66	84	85	81	51
S	ppm		930	1070	0	2040	100	590	4930	1180
Nb	ppm		2	3	3	3	4	5	4	34
Rb	ppm		7	3	7	5	6	6	10	7
Sr	ppm		407	676	1001	114	45	20	338	319
Zr	ppm		27	47	21	29	47	34	37	126
Y	ppm		12	7	7	9	17	15	13	14
Ba	ppm		127	102	150	31	27	52	113	49
Sc	ppm		36	25	13	43	63	61	49	46

APPENDIX 9. XRF/ICP-MS oxide ore analyses by V. Nykänen.

No.		1	2	3	4	5	6	7	8	9
SampleID		VUO 114/ 33.80-33.87	VUO 114/ 146.45-146.55	VUO 78/ 588.20-588.30	VUO 114/ 47.30-47.40	VUO 112/ 81.00-81.10	VUO 78/ 489.00-489.10	VUO 112/ 72.30-72.40	VUO 112/ 64.45-64.55	VUO 112/ 70.00-70.10
SiO2	wt%	3,94	7,90	18,93	3,33	1,62	17,40	3,30	4,79	1,75
Al2O3	wt%	2,53	4,82	9,98	4,60	4,69	9,03	4,58	6,28	4,66
FeOTOT	wt%	63,41	60,66	44,10	67,14	66,18	44,40	65,79	61,46	67,64
FeTOT	wt%	49,29	47,15	34,28	52,19	51,44	34,51	51,14	47,77	52,58
FeO	wt%	57,07	54,59	39,69	60,43	59,56	39,96	59,21	55,31	60,88
Fe2O3	wt%	7,05	6,74	4,90	7,46	7,35	4,93	7,31	6,83	7,52
MgO	wt%	1,96	4,37	4,06	4,93	4,30	5,01	4,02	7,06	3,53
CaO	wt%	0,83	1,88	5,35	0,02	0,04	4,42	0,20	0,01	0,02
Na2O	wt%	0,20	0,10	1,60	0,05	0,04	1,38	0,06	0,05	0,04
K2O	wt%	0,02	0,01	0,18	0,00	0,00	0,55	0,00	0,00	0,00
TiO2	wt%	22,19	16,24	10,92	16,28	18,51	14,82	18,57	17,66	18,28
P2O5	wt%	0,01	0,01	0,01	0,01	0,01	0,02	0,02	0,02	0,02
MnO	wt%	0,31	0,32	0,22	0,26	0,28	0,27	0,30	0,28	0,27
Sum	wt%	95,40	96,31	95,35	96,62	95,67	97,30	96,84	97,61	96,21
V	ppm	4427	3421	2449	3564	4008	1728	3611	3405	3826
Cr	ppm	242	100	14	164	264	34	65	105	96
Ni	ppm	96	637	191	411	300	79	106	87	135
Cu	ppm	39	108	154	247	274	43	53	64	74
Zn	ppm	260	152	233	396	559	239	305	396	667
S	ppm	709	1144	134	958	1019	1165	773	899	303
Co	ppm	253	154	240	314	376	258	309	320	349
Sr	ppm	18	33	454	17	16	257	8	24	11
Zr	ppm	52	29	52	4	46	130	43	67	74
Y	ppm	4	0	4	0	4	0	0	0	0
Ba	ppm	2	7	92	3	0	313	11	4	3
Sc	ppm	9	16	15	15	22	17	15	15	18

No.		10	11	12	13	14	15	16	17	18
SampleID		VUO 78/ 601.50-601.60	VUO 92/ 345.10-345.20	VUO 78/ 632.00-632.10	VUO 112/ 60.90-61.00	VUO 78/ 641.00-641.10	VUO 93/ 218.00-218.10	VUO 78/ 613.00-613.10	VUO 93/ 179.80-179.90	VUO 93/ 199.74-199.82
SiO2	wt%	23,05	18,33	22,18	3,97	37,07	20,58	30,41	4,58	9,51
Al2O3	wt%	12,08	9,31	13,26	4,62	17,58	3,55	12,70	5,64	6,37
FeOTOT	wt%	39,75	41,38	39,55	63,74	23,32	42,07	31,95	62,70	55,72
FeTOT	wt%	30,90	32,16	30,74	49,55	18,13	32,70	24,83	48,74	43,31
FeO	wt%	35,78	37,24	35,60	57,37	20,99	37,86	28,76	56,43	50,15
Fe2O3	wt%	4,42	4,60	4,40	7,08	2,59	4,68	3,55	6,97	6,19
MgO	wt%	4,38	6,68	3,39	4,94	2,51	13,93	5,67	3,98	5,41
CaO	wt%	6,54	5,32	5,27	0,09	8,19	5,09	7,91	0,35	1,83
Na2O	wt%	1,88	1,20	1,87	0,05	3,17	0,18	2,19	0,09	0,41
K2O	wt%	0,18	0,22	0,58	0,00	0,23	0,02	0,33	0,39	0,41
TiO2	wt%	9,80	13,78	10,74	18,75	5,73	14,49	8,16	18,43	16,81
P2O5	wt%	0,02	0,02	0,02	0,02	0,02	0,02	0,02	0,02	0,02
MnO	wt%	0,22	0,31	0,25	0,30	0,14	0,30	0,21	0,31	0,29
Sum	wt%	97,90	96,55	97,11	96,48	97,96	100,23	99,55	96,49	96,78
V	ppm	1811	2049	2436	3301	1382	1952	1658	3015	1949
Cr	ppm	12	38	38	9	43	40	21	60	27
Ni	ppm	184	79	180	44	134	150	82	42	44
Cu	ppm	77	82	87	88	98	111	129	161	173
Zn	ppm	199	238	179	360	124	173	165	439	160
S	ppm	1197	1049	853	1087	1784	1009	1016	1330	2367
Co	ppm	244	264	200	284	115	341	196	325	221
Sr	ppm	447	41	496	25	971	19	351	31	93
Zr	ppm	44	86	45	85	51	100	83	87	145
Y	ppm	0	0	1	0	1	3	7	0	4
Ba	ppm	90	37	384	5	155	13	95	95	66
Sc	ppm	17	20	12	19	10	41	19	15	35

No.		19	20	21	22	23	24	25	26	27
SampleID		VUO 114/ 32.80-32.90	VUO 85/ 296.90-289.05	VUO 112/ 50.65-50.80	VUO 114/ 108.00-108.10	VUO 114/ 103.00-103.15	VUO 93/ 182.85-183.00	VUO 93/ 189.35-189.45	VUO 85/ 269.40-269.50	VUO 78/ 501.75-501.90
SiO2	wt%	5,16	7,22	21,77	25,17	30,82	35,10	24,28	16,78	9,65
Al2O3	wt%	5,78	6,85	13,65	2,64	7,65	10,34	8,62	9,11	7,31
FeOTOT	wt%	61,63	58,90	38,46	35,66	27,61	23,79	34,54	45,18	54,26
FeTOT	wt%	47,91	45,78	29,90	27,72	21,46	18,49	26,85	35,12	42,18
FeO	wt%	55,47	53,01	34,61	32,09	24,85	21,41	31,09	40,66	48,83
Fe2O3	wt%	6,85	6,55	4,27	3,96	3,07	2,64	3,84	5,02	6,03
MgO	wt%	6,37	7,18	3,50	12,80	11,89	6,86	5,94	5,58	4,54
CaO	wt%	0,04	0,54	7,36	6,72	9,44	11,21	7,63	4,37	2,62
Na2O	wt%	0,05	0,18	0,57	0,40	1,10	1,04	1,01	0,91	0,12
K2O	wt%	0,01	0,21	1,03	0,03	0,17	0,32	0,36	0,65	0,48
TiO2	wt%	17,25	15,86	9,34	15,24	11,12	6,77	14,33	14,44	17,43
P2O5	wt%	0,02	0,02	0,02	0,02	0,02	0,03	0,03	0,03	0,03
MnO	wt%	0,27	0,24	0,17	0,28	0,25	0,20	0,31	0,27	0,31
Sum	wt%	96,58	97,20	95,87	98,96	100,07	95,66	97,05	97,32	96,75
V	ppm	3693	3441	1493	1261	1052	1073	2560	1966	2441
Cr	ppm	124	78	38	71	3	40	45	32	32
Ni	ppm	386	390	62	253	144	29	32	1	40
Cu	ppm	236	238	267	313		43	60	82	113
Zn	ppm	218	322	134	144	140	141	337	264	239
S	ppm	959	1009	2182	1205	1135	3268	1068	1051	1067
Co	ppm	313	328	187	317	204	152	330	270	287
Sr	ppm	10	34	763	34	91	420	42	189	208
Zr	ppm	39	44	79	107	65	105	72	76	251
Y	ppm	0	0	0	3	13	10	1	1	0
Ba	ppm	8	80	568	8	22	62	111	178	127
Sc	ppm	18	14	14	59	45	34	16	18	15

No.		28	29	30	31	32	33	34	35	36
SampleID		VUO 114/ 105.40-105.50	VUO 85/ 288.95-289.05	VUO 112/ 55.90-55.95	VUO 85/ 261.80-261.90	VUO 112/ 40.95-41.05	VUO 78/ 413.00-413.10	VUO 78/ 581.50-581.60	VUO 78/ 559.13-559.23	VUO 78/ 567.88-567.90
SiO2	wt%	32,35	3,59	24,08	16,94	42,76	32,89	32,57	43,49	28,08
Al2O3	wt%	5,97	2,68	8,86	8,56	21,02	10,92	10,62	19,90	8,25
FeOTOT	wt%	25,27	66,93	35,99	44,92	19,12	24,08	26,70	17,26	29,43
FeTOT	wt%	19,64	52,02	27,98	34,92	14,86	18,72	20,75	13,42	22,88
FeO	wt%	22,74	60,24	32,39	40,43	17,21	21,67	24,03	15,53	26,49
Fe2O3	wt%	2,81	7,44	4,00	4,99	2,12	2,68	2,97	1,92	3,27
MgO	wt%	12,42	2,28	7,78	5,36	1,43	4,44	8,97	1,65	7,91
CaO	wt%	10,92	0,82	6,61	4,48	8,77	7,59	8,93	9,01	8,70
Na2O	wt%	0,83	0,19	1,29	1,17	3,48	2,21	1,44	3,43	0,90
K2O	wt%	0,12	0,13	0,15	0,55	0,53	0,37	0,21	0,28	0,43
TiO2	wt%	11,92	18,82	13,05	14,55	4,33	14,93	5,73	4,28	11,92
P2O5	wt%	0,03	0,03	0,04	0,04	0,05	0,06	0,06	0,07	0,07
MnO	wt%	0,26	0,36	0,29	0,28	0,11	0,32	0,21	0,12	0,35
Sum	wt%	100,09	95,83	98,14	96,85	101,60	97,81	95,44	99,49	96,04
V	ppm	1031	3753	1565	1914	580	677	1342	771	1445
Cr	ppm	43	48	42	52	56	16	29	48	30
Ni	ppm	46	115	25	30	23	15	48	21	69
Cu	ppm	117	253	120	156	73	45	258	50	159
Zn	ppm	113	271	164	218	103	119	162	85	159
S	ppm	1070	1342	1122	1211	2168	1780	1315	2279	114
Co	ppm	192	306	245	264	91	187	304	98	191
Sr	ppm	93	26	67	116	959	478	139	828	88
Zr	ppm	88	77	144	111	75	335	73	87	197
Y	ppm	13	0	13	0	0	7	10	3	14
Ba	ppm	28	67	9	213	341	128	49	198	60
Sc	ppm	54	15	39	21	6	25	43	8	28

No.		37	38
SampleID		VUO 78/ 531.00-531.15	VUO 112/ 46.70-46.85
SiO2	wt%	33,19	45,70
Al2O3	wt%	7,96	21,10
FeOTOT	wt%	26,57	15,32
FeTOT	wt%	20,65	11,91
FeO	wt%	23,91	13,79
Fe2O3	wt%	2,95	1,70
MgO	wt%	9,96	1,07
CaO	wt%	9,28	8,37
Na2O	wt%	1,10	3,80
K2O	wt%	0,28	0,62
TiO2	wt%	9,42	3,72
P2O5	wt%	0,09	0,10
MnO	wt%	0,25	0,11
Sum	wt%	98,10	99,91
V	ppm	682	434
Cr	ppm	8	72
Ni	ppm	51	16
Cu	ppm	32	48
Zn	ppm	176	69
S	ppm	962	1926
Co	ppm	171	66
Sr	ppm	107	937
Zr	ppm	133	127
Y	ppm	13	4
Ba	ppm	64	334
Sc	ppm	40	4